

PhD Thesis

**METHODOLOGY FOR HYBRID MANUFACTURING OF  
TURBOMACHINERY INTEGRAL ROTARY COMPONENTS IN  
THERMORESISTANT SUPER ALLOYS**

Presented by

**Ms. Haizea González Barrio**

At

**The Department of Mechanical Engineering**

Belonging to

**Universidad del País Vasco  
Euskal Herriko Unibertsitatea**

Presented to obtain the degree of

**Doctor in Mechanical Engineering**

Directed by

**Dr. Dña. Amaia Calleja Ochoa  
Dr. D. Aitzol Lamikiz Mentxaka**

**October 2019, Bilbao**



PhD Thesis

**METHODOLOGY FOR HYBRID MANUFACTURING OF  
TURBOMACHINERY INTEGRAL ROTARY COMPONENTS IN  
THERMORESISTANT SUPER ALLOYS**

Presented by

**Ms. Haizea González Barrio**

At

**The Department of Mechanical Engineering**

Belonging to

**Universidad del País Vasco  
Euskal Herriko Unibertsitatea**

Presented to obtain the degree of

**Doctor in Mechanical Engineering**

Directed by

**Dr. Dña. Amaia Calleja Ochoa  
Dr. D. Aitzol Lamikiz Mentxaka**

**October 2019, Bilbao**





*Mirando al cielo...*

*Over the rainbow...*



## Agradecimientos/Aknowledgments

Me gustaría dedicar estas líneas a todas aquellas personas que, con su colaboración y apoyo, han hecho posible la realización de la presente tesis doctoral. De manera especial quiero destacar el apoyo recibido por mis directores de tesis Aitzol Lamikiz Mentxaka y Amaia Calleja Ochoa, así como de Luis Norberto López de Lacalle Marcaide; puesto que de ellos nació la idea inicial de este trabajo y la motivación para iniciar mi camino en la investigación con ilusión. Quiero agradecer también al resto de profesores del Grupo de Fabricación de Alto Rendimiento, por ser un referente del bien hacer.

En primer lugar, me gustaría destacar que esta tesis no es resultado de un trabajo individual, sino fruto de la colaboración prestada por todos mis compañeros del taller a lo largo de estos años. Gracias Amaia por haber sido mi apoyo desde que era estudiante, por estar a mi lado en todo momento, incluso cuando no se acababa de vislumbrar el final del túnel. Gracias a todos los que fueron, los que somos y los que serán parte de esta pequeña familia que llamamos “el taller de la uni”; (Asier, Adrián, Álvaro, Izaro, Iker, Rober, Silvia, Gorka, Olatz, Aintzane, Jonan), las dos peceras pequeñas (Egoitz, Iñaki) y la pecera grande (Leire, Mario, Mada, Exe, Marta, Iker, Iñigo) y muchos más que seguramente olvido. Finalmente, no puedo dejar de hacer mención especial al *Chip team* que hemos ido creando poco a poco, junto con Octavio y todos “mis niños”: con Gaizka, Pablo, Ander y Mikel empezó todo...y ahora no puedo olvidarme de que seguimos creciendo: Gonzalo, Del Olmo, Olaia, Aner, Andoni, Andrea, Jonan, Arkaitz y Ainhoa R. y C.

En el terreno personal, el apoyo de mi familia ha sido imprescindible, gracias por aguantarme y estar ahí siempre, no sólo en los buenos, sino también en los malos momentos: Aita, Ama, Adonay y Saday, todos mis logros son también los vuestros. También por supuesto a L@s Gonzalez y Los Barrio y CIA (y a mi ojito derecho Hodei) por ser una familia maravillosa y darme siempre ánimos a luchar por lo que quiero.

Por supuesto, aquí no pueden faltar todas aquellas personas especiales que han pasado por mi vida a lo largo de los años y que me han enseñado tanto. En primer lugar, mi *tata* Janire juntas desde pequeñas, gracias por todos tus consejos y estar siempre ahí. Lore y Aintza, un viaje en el que construimos algo mágico juntas y que jamás se va a poder deshacer. Galder y Alexia, al final este no es el libro que me habéis sugerido....pero es un libro. Nuria, compañera de batallas (¡y no sólo en la uni!). Y por supuesto toda esa gente que está ahí y me aguanta cuando ni siquiera yo puedo: *XoXos*, *Cuatro culeros*, *Cansinitos*. ¡Mil gracias a todos!

Finally, this could not have been possible without the acknowledgment to everybody from the AMRC (Sheffield), thanks to my airfoils team for making me feel as at home and giving me the opportunity of learning from a great group. Particularly, thanks to Dennis Fretwell (Carl from Up) to give me a great support and being a great friend and Rezleen Sheikh because you have become my family, my home and my safe place.

## Summary

The main objective of this thesis dissertation is focused on the different stages inside the production chain for the hybrid manufacturing (additive/subtractive manufacturing) of high-added value components, more specifically aeronautical turbomachinery integral rotary components (IBRs). For that purpose, a schematic methodology was developed, fully correlating the different stages of additive manufacturing, subtractive manufacturing and control. Moreover, these stages were integrated at the same CAD/CAM/CAE software environment to reduce the use of resources and facilitating a user-friendly interface for the final operator.

The optimization of additive and machining strategies with the aim of presenting a more robust and productive process is considered one of the trending topics inside the scientific community. Because of that, at the present work it is addressed some keys and challenges for different stages inside the hybrid manufacturing process; both of them related to different strategies or alternatives to fabricate and repair aeronautical turbomachinery monolithic components. Regarding additive manufacturing, this study was focused on the process known as Laser Metal Deposition (LMD). Facing the necessity of CAM software to define LMD strategies, mainly when it is used for the repair or creation of complex geometries that require 5 simultaneous axes. For this purpose, it was presented the development of a complete CAM module specific for LMD that offers the possibility of defining three types of operations: layer by layer, 3 axes and 5 simultaneous axes. In addition, this module implements a geometric model that predicts the final part obtained according to the selected material and the process parameters; in this way, this prediction could be used as a starting point for the following machining stages, reducing non-cutting movements (avoiding downtime).

Besides that, this work presents some advances in the field of machining. Two different lines are covered, one related to the optimization of machining strategies and the other one related to new processes as a complement or alternative to current conventional processes. To do that, the use of mathematical algorithms is extended for complex surfaces machining strategies optimization; acquiring special importance in order to reduce manufacturing times and costs. In this line, the development of an algorithm and its validation were presented, allowing the use of the flank machining technique (taking advantage of the entire effective cutting length of the tool) in the machining of non-developable surfaces; conventionally machined using point milling strategy. Regarding to new machining processes, experimental tests and results were presented on full slotting to analyse the feasibility of the process known

as Super Abrasive Machining (SAM) as an alternative to conventional milling for IBRs made of low machinability alloys.

## Resumen

El principal objetivo para el desarrollo de esta tesis doctoral consiste en abordar de manera conjunta las diferentes etapas dentro de la cadena de producción de fabricación híbrida (aditiva y sustractiva) de componentes de alto valor añadido, más concretamente componentes rotativos integrales (IBRs) dentro del sector aeronáutico. Siguiendo dicho propósito, se ha desarrollado una metodología esquemática que correlaciona dichas etapas: fabricación aditiva, fabricación mediante el arranque de viruta y medición y control. Además, se presenta la implementación de todas ellas dentro del mismo entorno de fabricación (software CAD/CAM/CAE), reduciendo de este modo el uso de recursos y acercándose de manera más utilitaria al usuario final.

La optimización de las diferentes estrategias de aporte y mecanizado para la obtención de un proceso más productivo y robusto se considera uno de los temas de investigación más presentes en la comunidad científica. Por esta razón, en este trabajo se abordan aspectos claves y desafíos presentes en las etapas descritas dentro de la fabricación híbrida, ambos relativos a las diferentes estrategias o alternativas para la fabricación y reparación de componentes monolíticos de turbomaquinaria aeronáutica. En lo que respecta a la fabricación aditiva, este estudio se ha centrado en el proceso *Laser Metal Deposition (LMD)*. Ante la necesidad de software CAM para la definición de estrategias de LMD, principalmente cuando se utiliza para la reparación o creación de piezas de geometría compleja que requieren de aporte en 5 ejes simultáneos. Para ello, se presenta el desarrollo de un módulo completo de CAM específico para LMD que ofrece la posibilidad de definir tres tipos de operaciones: capa a capa, 3 ejes y 5 ejes simultáneos. Además este módulo implementa un modelo geométrico que predice la pieza final obtenida acorde al material seleccionado y los parámetros del proceso; de este modo, permite utilizar dicha predicción como tocho de partida para las siguientes etapas de mecanizado, reduciendo las trayectorias en vacío (evitando tiempos muertos).

Por otra parte, también se ha trabajado en el campo del mecanizado por arranque de viruta. En dicho campo se abordan dos líneas diferentes, una relacionada con la optimización de las estrategias de mecanizado utilizadas y la otra relativa a nuevos procesos como complemento o alternativa a los procesos convencionales actuales. La utilización de algoritmos matemáticos para la optimización de estrategias de mecanizado de superficies complejas está adquiriendo especial importancia para reducir tiempos y costes de fabricación; en esta línea se plantea el desarrollo de un algoritmo y la validación del mismo que permite utilizar la técnica de mecanizado de flanco (aprovechando toda la longitud de corte efectiva de la herramienta) en

el mecanizado superficies no desarrollables que convencionalmente se mecanizan mediante la técnica *point milling* o copiado con bola. En lo que se refiere a nuevos procesos de fabricación por arranque de viruta, se han presentado una serie de resultados sobre ensayos de ranurado para analizar la viabilidad del proceso como una alternativa al fresado convencional para componentes integrales rotativos de aleaciones de baja maquinabilidad conocido como *Super Abrasive Machining (SAM)* o Mecanizado Súper Abrasivo.



## Laburpena

Doktorego tesi honen helburua, balio altuko osagaien fabrikazio hibidorako (gehigarria eta kentzaile) produkzio kateak biltzen dituen etapa guztien aldibereko garapenean datza. Hain zuzen ere, aeronautika sektoreko biraketazko elementu integralena (IBRs). Jomuga hori lortzeko, metodologia eskematiko bat garatu da etapa ezberdinak erlazionatzeko: fabrikazio gehigarria, txirbil-harroketa bidezko fabrikazioa eta neurketa eta kontrola. Gainera, dokumentu honek, fabrikazio ingurune berdineko aipatutako etapa guztien inplementazioa aurkezten du (CAD,CAM,CAE softwarea), modu honetan, baliabideen erabilpena murriztuz eta azkeneko kontsumitzaileari modu erabilgarrian hurbilduz.

Gaur egun, prozesu sendoago eta emankor bat lortzeko, mekanizazio eta gehitze fabrikazio estrategia ezberdinen optimizazioa, zientzia elkarteko ikerkuntza gairik garrantzitsuenetarikoa da. Hori dela eta, lan honetan fabrikazio hibrido barnean deskribatutako etapen funtsezko aspektuak eta uneko erronketaz hitz egiten da, biak aeronautikako turbomakinen osagai monolitikoen fabrikazio eta konponketarako estrategia zein aukera ezberdinekiko erlatiboak izanik. Gehitze fabrikazioaren ildotik, ikerketa hau *Laser Metal Deposition (LMD)* prozesuan ardatzu da. LMD estrategiari dagokionez, hauek definitzeko CAM software-aren beharra dago batez ere, geometria konplexuko piezen konponketarako edo sorkuntzarako, izan ere, honek 5 ardatzen aldi bereko lanaren beharra dute. Helburu horrekin, LMD prozesuan oinarritutako CAM modulu espezifiko bat aurkezten da, hiru operazio ezberdin definitzeko gai dena: geruzageruzakoa, aldi bereko 3 ardatz eta 5 ardatz. Bestalde, modulu honek modelo geometriko bat barneratzen du, zeinek azkeneko pieza aurreikusi dezake aukeratutako materialaren eta prozesuaren parametroen arabera; honela, aurreikuspen hori erabili daiteke hasierako totxo gisa hurrengo mekanizazio etapentzako, hutseko ibilbideak murriztuz (denbora hilak ekidin).

Bestaldetik, ikerkuntza honetan txirbil-harroketako mekanizazio arloan ere lan egin da. Aipatutako esparruan bi ildo ezberdin lantzen dira, bata erabilitako mekanizazio estrategien hobekuntzarekin erlazionatua eta bestea gaur eguneko prozesu tradizionalen osagarri edo ordezkapen izango diren prozesu berriekin lotutakoa. Algoritmo matematikoen erabilpena garrantzia lortzen doa gainazal konplexuen mekanizazio estrategiak hobetzeko, fabrikazio denbora eta kostuak murriztuz: ildo honetatik abiatuta, algoritmo berri baten garapena eta balioztatzea proposatzen da, garagarriak ez diren gainazalen mekanizazioan, albo mekanizazio teknika (erremintaren ebaketa luzera eraginkor osoa baliatzea mekanizatzeke) erabili ahal izateko, gaur egun erabiltzen den *point milling* edo bola bidezko mekanizazio teknika beharrez.

Txirbil-harroketazko fabrikazio prozesu berriei dagokienez, artekaketa entseguen emaitzak aurkeztu dira zeinetan prozesuaren bideragarritasuna aztertu dan. Zehazki, makinabilitate baxuko aleazioen biraketazko elementu integralen ohiko fresaketa prozesuaren alternatiba lez, hain zuzen ere, Super Abrasive Machining (SAM) edo mekanizazio urratzaile deritzona.

## Table of Contents

|  |           |
|--|-----------|
| <b>Chapter I. Introduction.....</b>  | <b>5</b>  |
| I.1. Introduction.....   | 5         |
| I.2. Objectives.....   | 7         |
| I.3. Thesis organization.....  | 8         |
| <b>Chapter II. Evolution of design, manufacturing and repairing techniques for turbomachinery integral rotary components ...</b> | <b>12</b> |
| II.1. Introduction.....  | 12        |
| II.2. Aircraft engines .....   | 13        |
| II.2.1. Turbojet.....  | 15        |
| II.2.2. Turbofan.....  | 16        |
| II.2.3. Turboshaft.....  | 16        |
| II.2.4. Turboprop .....  | 17        |
| II.2.5. Propfan.....   | 18        |
| II.2.5. New engines.....   | 19        |
| II.3. Turbomachinery Rotary Components.....  | 20        |
| II.3.1. Terminology and operational behavior.....  | 21        |
| II.3.2. Material composition .....   | 23        |
| II.3.3. Complex surfaces: Developable and non-developable surfaces.....  | 25        |
| II.3.4. IBRs requirements.....   | 26        |
| II.4. IBRs manufacturing processes .....   | 28        |
| II.4.1. Monolithic components manufacturing processes.....   | 30        |
| II.4.1.1 Casting.....  | 30        |
| II.4.1.2 Electro Discharge Machining (EDM).....  | 31        |
| II.4.1.3 Electro Chemical Machining (ECM) / Precise Electro Chemical Machining (PECM).....                                       | 32        |
| II.4.1.4 Additive Manufacturing (AM) .....   | 33        |
| II.4.1.5 Conventional Machining Process: 5-axis Milling.....   | 35        |

|   |    |
|---|----|
| II.4.1.6 Super Abrasive Machining (SAM).....  | 41 |
| II.4.2. Algorithms to optimise manufacturing processes .....  | 47 |
| II.5. Hybrid manufacturing systems and multitasking machines .....  | 51 |
| II.5.2. Hybrid manufacturing systems inside the Industry 4.0 context .....                                | 53 |
| II.5.2. Process integration and digitalization: Digital twins .....                                       | 55 |
| II.6. Repairing processes.....  | 56 |
| II.6.1. Industrial Applications.....  | 59 |
| II.6.1.1 Moulds and dies sector .....   | 60 |
| II.6.1.2 Aeronautical sector .....  | 61 |
| II.6.2. Repairing strategies and process control.....   | 62 |
| II.7. Specific CAD/CAM systems for IBRs manufacturing .....   | 65 |
| II.7.1. CAD/CAM systems for hybrid manufacturing (AM/SM) .....  | 66 |
| II.7.2. Virtual verification systems.....   | 67 |
| II.8. Summary of the manufacturing and repair methods for turbomachinery integral rotary components ..... | 68 |

## **Chapter III. Complete methodology for hybrid manufacturing and repairing of turbomachinery rotary components .....72**

|  |    |
|--|----|
| III.1. Introduction.....                                   | 72 |
| III.2. Design process.....                                 | 72 |
| III.3. LMD process integration .....                       | 73 |
| III.4. Machining process integration.....                  | 75 |
| III.5. Measurement and control .....                       | 77 |
| III.6. Main benefits of process stages co-integration..... | 79 |

## **Chapter IV. API development for hybrid manufacturing using Laser Metal Deposition .....84**

|                                      |    |
|--------------------------------------|----|
| IV.1. Introduction .....             | 84 |
| IV.2.API 1: CAM module for LMD ..... | 85 |

|  |     |
|--|-----|
| IV.2.1. User-interface .....   | 86  |
| IV.2.1.1 LMD CAM Module label at the initial window .....                              | 87  |
| IV.2.1.2 Specific LMD CAM template .....   | 88  |
| IV.2.2. Process parameters and tool definition.....                                    | 90  |
| IV.2.3. Tool-paths generation.....   | 92  |
| IV.2.4. Main LMD operations definition.....  | 94  |
| IV.2.4.1 Planar LMD.....   | 94  |
| IV.2.4.2 3-axis LMD.....   | 95  |
| IV.2.4.3 5-axis LMD.....   | 96  |
| IV.3. API 2: development for added material geometry generation .....                  | 97  |
| IV.3.1. Added material resulting solid .....   | 99  |
| IV.3.2. Mass-balance based algorithm for the estimation of the added clad geometry ..  | 101 |
| IV.3.3. API 2 integration into API 1.....  | 102 |
| IV.4. Integration of the virtual machine for a complete simulation of the process..... | 106 |
| IV.5. Validation of the defined methodology in single tracks .....                     | 108 |
| IV.5.1. Definition of used equipment .....   | 108 |
| IV.5.2. Material selection .....   | 111 |
| IV.5.3. API 2 estimation: single tracks and single blade .....                         | 112 |
| IV.6. Case of study: Blisk LMD .....   | 116 |

## **Chapter V. New processes for manufacturing and repairing turbomachinery integral rotary components ..... 124**

|   |     |
|---|-----|
| V.1. Introduction .....   | 124 |
| V.2. Surface approximation algorithm for operations optimization..... | 126 |
| V.2.1. Conical tool flank approximation for surface finishing .....   | 127 |
| V.2.2. Validation of developed algorithm .....                        | 130 |
| V.3. New manufacturing processes: Super Abrasive Machining (SAM)..... | 134 |
| V.3.1. Description of the equipment.....                              | 136 |

|   |            |
|---|------------|
| V.3.2. Choice of material.....                                  | 139        |
| V.3.3. Slotting strategy: experimental set-up.....              | 140        |
| V.3.4. Obtained results.....                                    | 143        |
| V.3.4.1 Roughness.....  | 143        |
| V.3.4.2 Cross-section and white layer.....                      | 146        |
| V.3.4.3 Residual stress.....                                    | 147        |
| V.3.4.4 Microhardness.....                                      | 148        |
| V.3.4.6 Tool wear.....  | 150        |
| V.3.4.6 Summary of obtained results and conclusions.....        | 151        |
| <b>Chapter VI. Contributions and future research lines.....</b> | <b>155</b> |
| VII.1. Introduction.....  | 155        |
| VII.2. Thesis contributions.....                                | 155        |
| VII.3. Publications.....  | 157        |
| VII.3.1. Indexed publications.....                              | 157        |
| VII.3.2. National and international congresses.....             | 158        |
| VII.4. Future research lines.....                               | 160        |
| <b>Bibliography</b>   | <b>163</b> |

## Figure index

|  |    |
|--|----|
| Figure II.1 Comparison between OTTO cycle (piston engine principle) and Brayton cycle (reaction engine principle) .....  | 14 |
| Figure II.2 Diagram of a turbojet engine airflow and working conditions (top) (pplc, 1986), an axial flow turbojet form General Electric which production ended in 1988 (GE J85) ..... | 15 |
| Figure II.3 Diagram of a turbofan engine operation (top) (pplc, 1986) and a turbofan GE trent7000 .....  | 16 |
| Figure II.4 Diagram of turboshaft engine operation (top) (pplc, 1986) and a turboshaft GE XT700 ..   | 17 |
| Figure II.5 Diagram of a turbopropeller engine (top) (pplc, 1986) and a turbopropeller GE T64 with a gearbox at the middle and a turbine core at the right .....                       | 18 |
| Figure II.6 Diagram of a propfan and an open rotor mockup from Safran, 2017 .....  | 19 |
| Figure II.7 Rolls-Royce engine evolution (Rolls-Royce, 2019).....  | 19 |
| Figure II.8 Rolls-Royce testing in Derby (UK) a key component of the UltraFan® (Rolls-Royce, 2019)   | 20 |
| Figure II.9 Turbomachinery rotary components: (a) Blisk, (b) Turbine blades and fir-trees, (c) Impeller .....  | 20 |
| Figure II.10 Turbine blades and mounting disc, blisk and impeller terminology and designation.....   | 21 |
| Figure II.11 Jet Engine common material distribution (Campbell, 2006) .....  | 23 |
| Figure II.12 Examples of different type of surfaces: (a) ruled surface: cone, (b) double curved surface: sphere, (c) free form surface: impeller .....                                 | 25 |
| Figure II.13 3D passive flow-driving numerical model (Y. Cui, 2019): (a) Mesh structures and boundary conditions; (b) Streamlines through guide vanes and rotor blades.....            | 27 |
| Figure II.14 IBRs manufacturing methods subjected to material resistance and geometry (M. Bußmann J. K., 2005) .....   | 28 |
| Figure II.15 Production costs of 20 process chains for impeller manufacturing; (P18) is considered the conventional reference process chain (A. Klink, 2018) .....                     | 30 |
| Figure II.16 Examples of casting impellers: a) Turbocharger (Chevrolet, 2016), b) Centrifugal pump (ScottTech, 2017).....  | 31 |
| Figure II.17 Material removal rates for WEDM and SEDM manufacturing process on thermoresistant superalloys (F.Klocke, 2013) .....  | 32 |
| Figure II.18 Generated optimal tool-paths and a shrouded blisk manufacturing by EDM (I.Ayesta, 2016).....  | 32 |
| Figure II.19 a) ECM method definition for a blisk and b)Blades in Ti60 blisk using ECM (Chen Xuezheng, 2016) .....   | 33 |
| Figure II.20 a) Schematics from Boeing patent application and b) Airbus A380 first 3D printed manifold flying.....   | 34 |
| Figure II.21 Impeller blades repairing process through hybrid manufacturing (Zelinski, 2015) .....   | 35 |

|  |    |
|--|----|
| Figure II.22 High pressure compressor generic blisk specifications (F. Klocke R. S., 2015) and Ti and Ni alloys material removal rates and cutting conditions (F.Klocke, 2013) ..... | 36 |
| Figure II.23 Sandvik and Emuge-Franken milling cutting tool forms for IBRs manufacturing .....   | 38 |
| Figure II.24 IBRs roughing strategies: slotting, trochoidal and plunge milling.....  | 39 |
| Figure II.25 Point milling and flank milling applied to a single blade .....   | 39 |
| Figure II.26 Error estimation by (J. Senatore, 2008) : (a) tool cut position and principle of error and (b) a case study for this error estimation .....                             | 41 |
| Figure II.27 A variety of SAM tools geometries (D.K. Aspinwall S. S., 2007).....   | 43 |
| Figure II.28 Bladed disc fir-trees manufacturing using SAM .....   | 43 |
| Figure II.29 IBR flank SAM: (a) Final tool paths using iteration and shaped tool and (b) surface finishing estimation and obtained final component (Wu, 2012).....                   | 45 |
| Figure II.30 Traditional tool-paths generation methods: iso parametric, iso planar and iso scallop (N. SHOKROLLAHI, 2014).....   | 48 |
| Figure II.31 (left) C-space method & (right) Rolling Ball method.....  | 49 |
| Figure II.32 5-axis free-form surface approximation algorithm (Bo P., 2016): (a) Differences between the number of patches (b) different tool positions and geometries .....         | 50 |
| Figure II.33 Global approach for manufacturing processes, considering modelling and monitoring (Gonzalez-Barrio, 2018).....  | 51 |
| Figure II.34 Lasertec 65 Additive Manufacturing model from DMG MORI SEIKI AG .....   | 53 |
| Figure II.35 Digital compass for Industry 4.0 philosophy application (D. Baur, 2015).....  | 54 |
| Figure II.36 Digital twin 8-dimension model (Stark R., 2019) .....   | 56 |
| Figure II.37 Different steps for IBRs tips repairing operation (Fraunhofer IPT, 2015) .....  | 58 |
| Figure II.38 Mould repair operation using LMD process (OR Laser News, 2017) .....  | 60 |
| Figure II.39 Repair of turbomachinery components (Fraunhofer Institute for Laser Technology ILT, 2019).....  | 62 |
| Figure II.40 Different multi-axis LMD strategies applied to a spherical geometry: a) Programmed strategies, b) coated part, c) final part (A. Calleja, 2014).....                    | 64 |
| Figure II.41 Machine tool simulation module from NX® Siemens, a) machine kinematics, b) axis definition window and c) machine design .....   | 67 |
| Figure III.1 Diagram of the methodology for turbomachinery integral rotary components design in hybrid manufacturing.....  | 73 |
| Figure III.2 Integration of additive manufacturing process into turbomachinery integral rotary component hybrid manufacturing methodology.....                                       | 75 |
| Figure III.3 Integration of subtractive manufacturing process into turbomachinery integral rotary component hybrid manufacturing methodology.....                                    | 77 |
| Figure III.4 Integration of measurement and control stages into turbomachinery integral rotary component hybrid manufacturing methodology.....                                       | 78 |
| Figure IV.1 Flowchart for developed APIs integration for LMD CAM solution .....  | 85 |



|  |     |
|--|-----|
| Figure IV.2 Accessibility to LMD CAM module: a) software initial window, b) inside machining module.....                           | 86  |
| Figure IV.3 LMD module template and the relation with the code of the installed archive ugs_LMD_template.pax .....                 | 87  |
| Figure IV.4 Required archives and their co-relation to implement the defined LMD module in the CAM environment.....                | 88  |
| Figure IV.5 Laser_Metal_deposition.prt: Operations definition, Menu description and Master model .....                             | 89  |
| Figure IV.6 UPV/EHU Coaxial nozzle and beam modelling for the LMD CAM module .....   | 91  |
| Figure IV.7 Implementation of LMD tool definition menu in the programmed CAM module for LMD .....                                  | 92  |
| Figure IV.8 Parameters considered for LMD tool-paths generation .....  | 93  |
| Figure IV.9 API Planar LMD operation: a) User menu, b) description and c) example of complete layer generation .....               | 94  |
| Figure IV.10 API 3-axis LMD operation: a) User menu, b) description and c) example of a developable single blade generation .....  | 95  |
| Figure IV.11 API 5-axis LMD operation: a) User menu, b) description and c) example of a blisk blade generation .....               | 97  |
| Figure IV.12 a) API 1 resulting tool-paths, b) API 2 resulting added geometry .....  | 98  |
| Figure IV.13 API 2: flowchart for final added geometry generation.....   | 99  |
| Figure IV.14 Calculation of LMD clad diameter according to Mass Balance algorithm.....   | 101 |
| Figure IV.15 Developed API menu for LMD clad generation and LMD operation selection.   | 103 |
| Figure IV.16 Block UI Styler and menus editor.....   | 104 |
| Figure IV.17 Visual Studio 2010® programming window .....  | 104 |
| Figure IV.18 Operation selection C# fragment from the API code.....  | 105 |
| Figure IV.19 Operation selection C# fragment from the API code.....  | 106 |
| Figure IV.20 Digitalization of retrofitted Kondia B-500 and single-blade real process verification (UPV/EHU).....                  | 107 |
| Figure IV.21 Microstructure from LMD Inconel®718 clad generation (UPV/EHU) .....   | 111 |
| Figure IV.22 a) Hastelloy®X performed 12 test (UPV/EHU), b) clad geometrical parameters (Toyserkani E. K. A., 2004) .....          | 113 |
| Figure IV.23 a) single blade demonstrator and LMD strategy design, b)LMD process and c) final blade generated by LMD process ..... | 114 |
| Figure IV.24 a) LMD blade intermediate height measurements and different issues observed in 5-axis LMD process .....               | 115 |
| Figure IV.25 a) defined blisk geometry and b) API 1 LMD 5-axis strategy programing.....  | 116 |
| Figure IV.26 a) LMD nozzle virtual verification and b) final geometry obtained with the mass-balance algorithm .....               | 117 |

|  |     |
|--|-----|
| Figure IV.27 Individual blades order of generation .....   | 117 |
| Figure IV.28 a) LMD process for blisk generation, b) Obtained blisk geometry, c) Optical scanning process, d) General overview of dimensional deviation results, e) Blade 1 results from the front and the top point of view ..... | 118 |
| Figure IV.29 Blade 1 height measurements.....  | 119 |
| Figure IV.30 a) LMD obtained blades and b) Machined blades.....  | 120 |
| Figure V.1 IBRs manufacturing process and presented developments applicability .....   | 125 |
| Figure V.2 Graphical example for the auxiliary surface calculation (Bo P., 2016).....  | 126 |
| Figure V.3 Auxiliar surface calculation for the conical tool and the tangential movability definition .....  | 127 |
| Figure V.4 Fitting conical envelopes to the final desired surface: a) random tool positioning for covering entire surface and b) feasible motion position for the tool to be adapted to the final surface .....                    | 128 |
| Figure V.5 Motion optimization for the conical tool.....   | 128 |
| Figure V.6 a) Demonstrator single blade design for algorithm validation and b) selected cutting tool .....   | 130 |
| Figure V.7 concave (top) and convex (bottom) 3 patches division for algorithm validation .....   | 131 |
| Figure V.8 Surface finishing approximation for T3 comparing the results obtained with the algorithm (blades) with CAM software results (bottom of each picture).....   | 133 |
| Figure V.9 Final obtained components using the default (left) and the algorithm (right) .....  | 134 |
| Figure V.10 Medium-sized IBRs conventional manufacturing process.....  | 135 |
| Figure V.11 Microstructure of selected material Inconel <sup>®</sup> 718.....  | 139 |
| Figure V.12 Full slotting definition.....  | 140 |
| Figure V.13 Selected milling cutting tool .....  | 140 |
| Figure V.14 Selected grinding tool and grain distribution pattern and profile .....  | 141 |
| Figure V.15 Grinding process parameters definition .....   | 142 |
| Figure V.16 Slot 1 surface profile and 2D topography.....  | 145 |
| Figure V.17 3D topography for flank milling and flank SAM respectively .....   | 145 |
| Figure V.18 Cross-section of the Inconel <sup>®</sup> 718 surface after flank milling and flank SAM .....  | 146 |
| Figure V.19 Residual stresses obtained for flank milling on Inconel <sup>®</sup> 718.....  | 147 |
| Figure V.20 Residual stresses obtained for flank SAM on Inconel <sup>®</sup> 718 .....   | 148 |
| Figure V.21 Measuring sections and slot performance direction definition .....   | 149 |
| Figure V.22 Microhardness obtained values for material base, flank milling and flank SAM .....   | 150 |
| Figure V.23 Abrasive tool wear types presented during the performed tests .....  | 151 |

## Table index

|  |            |
|--|------------|
| <i>Table II.1 Patents related to super abrasive machining .....</i>  | <i>45</i>  |
| <i>Table IV.1 Kondia Aktinos-500 machine working characteristics .....</i>   | <i>109</i> |
| <i>Table IV.2 Fiber laser Rofin FL010 characteristics .....</i>  | <i>109</i> |
| <i>Table IV.3 Sulzer Twin-10C powder feeder characteristics .....</i>  | <i>110</i> |
| <i>Table IV.4 Continuous coaxial nozzle design and characteristics .....</i>   | <i>110</i> |
| <i>Table IV.5 Inconel®718 composition, mechanical and physical properties (Kitagawa, Kubo, &amp; Maekawa, 1997).....</i> | <i>112</i> |
| <i>Table IV.6 Hastelloy®X composition, mechanical and physical properties (International, 2018).....</i>                 | <i>112</i> |
| <i>Table IV.7 Hastelloy®X experimental tests to obtain adequate LMD parameters.....</i>                                  | <i>113</i> |
| <i>Table IV.8 Validation of API 2 clad diameter calculation.....</i>   | <i>114</i> |
| <i>Table IV.9 LMD process parameters for Inconel®718 single blade generation .....</i>                                   | <i>115</i> |
| <i>Table IV.10 LMD process parameters for Inconel®718 blisk generation .....</i>   | <i>116</i> |
| <i>Table IV.11 Machining process defined parameters .....</i>  | <i>120</i> |
| <i>Table V.1 Tool 1 comparison of the obtained results .....</i>   | <i>131</i> |
| <i>Table V.2 Tool 2 comparison of the obtained results .....</i>   | <i>132</i> |
| <i>Table V.3 Tool 3 comparison of the obtained results .....</i>   | <i>132</i> |
| <i>Table V.4 Ibarria® ZV-25/U600 main characteristics.....</i>   | <i>136</i> |
| <i>Table V.5 Optical confocal microscope characteristics.....</i>  | <i>137</i> |
| <i>Table V.6 Mitutoyo TM-505 microscope main characteristics .....</i>   | <i>137</i> |
| <i>Table V.7 Microhardness Tester FM-800 main characteristics.....</i>   | <i>138</i> |
| <i>Table V.9 Inconel 718 chemical composition (%), mechanical and physical properties .....</i>                          | <i>139</i> |
| <i>Table V.10 Definition of the cutting conditions for the experiments.....</i>  | <i>141</i> |
| <i>Table V.11 In-situ obtained roughness values for FSAM and Fmilling.....</i>   | <i>144</i> |



## Nomenclature

|                            |  |
|----------------------------|--|
| <b>2D</b>                  | Two dimensions   |
| <b>3D</b>                  | Three dimensions   |
| <b>API</b>                 | Application Program Interface  |
| <b>CAD</b>                 | Computer Aided Design  |
| <b>CAM</b>                 | Computer Aided Manufacturing   |
| <b>LMD</b>                 | Laser Metal Deposition   |
| <b>TEDAE</b>               | Spanish Association of Defence, Aeronautics and Space Technology Companies |
| <b>EDM</b>                 | Electro Discharge Machining  |
| <b>WEDM</b>                | Wire Electro Discharge Machining   |
| <b>SEDM</b>                | Sinking Electro Discharge Machining  |
| <b>UAV</b>                 | Unmanned Aerial Vehicle  |
| <b>NASA</b>                | National Aeronautics and Space Administration                              |
| <b>IBR</b>                 | Integral Bladed Rotor  |
| <b>R&amp;D</b>             | Research and Develop   |
| <b>NURBS</b>               | Non-Uniform Rational B-Splines   |
| <b>CFD</b>                 | Computational Fluid Dynamic  |
| <b>ECM</b>                 | Electro Chemical Machining   |
| <b>PECM</b>                | Pulse/Precise Electro Chemical Machining                                   |
| <b>LFW/IHFP</b>            | Linear Friction Welding/ Inductive High Frequency Pressure Welding         |
| <b>AWJC</b>                | Abrasive Water-Jet Cutting   |
| <b>HSC</b>                 | High Speed Cutting   |
| <b>AM</b>                  | Additive Manufacturing   |
| <b>SM</b>                  | Subtractive Manufacturing  |
| <b>SAM</b>                 | Super Abrasive Machining   |
| <b>HIP</b>                 | Hot Isostatic Pressing   |
| <b>MJ</b>                  | Material Jetting   |
| <b>BJ</b>                  | Binder Jetting   |
| <b>PBF</b>                 | Powder Bed Fusion  |
| <b>EBM</b>                 | Electron Beam Melting  |
| <b>SLM</b>                 | Selective Laser Melting  |
| <b>CNC</b>                 | Computer Numerical Control   |
| <b><math>a_p</math></b>    | Axial depth of cut   |
| <b><math>a_e</math></b>    | Radial depth of cut  |
| <b><math>\rho_i</math></b> | Radius of curvature  |

|                |  |
|----------------|--|
| $\alpha_i$     | Twist angle  |
| <b>CFG</b>     | Creep Feed Grinding  |
| <b>CBN</b>     | Cubic Boron Nitride  |
| <b>UTC</b>     | United Technologies Corporation                                |
| <b>C-space</b> | Configuration space methods                                    |
| <b>RBM</b>     | Rolling Ball Method  |
| <b>DT</b>      | Digital Twin   |
| <b>DMD</b>     | Direct Metal Deposition  |
| <b>GE</b>      | General Electric   |
| <b>NC</b>      | Numerical Control  |
| <b>API</b>     | Application Programming Interface                              |
| <b>UPV/EHU</b> | Universidad del País Vasco/ Euskal Herriko Unibertsitatea      |
| $m_i^i$        | Powder mass injected on i point [Kg]                           |
| $m_p^i$        | Mass discrete element of material added on i point [Kg]        |
| $\Delta x$     | Base of the discrete element on x axis [mm]                    |
| $\Delta y$     | Base of the discrete element on y axis [mm]                    |
| $\phi_i$       | Powder mass flow on i point [g/mm <sup>2</sup> *min]           |
| $\phi$         | Powder mass flow [g/ min]                                      |
| $t_{iny}$      | Powder injection time [s]                                      |
| $\Delta s$     | Trajectory discretization distance step [mm]                   |
| $v_f$          | Process Feed rate [mm/min]                                     |
| $\rho_{mat}$   | Material density [Kg/m <sup>3</sup> ]                          |
| $H_i$          | LMD Clad height in i point [mm]                                |
| <b>H</b>       | LMD Clad height  |
| <b>W</b>       | LMD Clad width   |
| $\Delta z$     | Distance between LMD clads                                     |
| <b>R</b>       | Ruled surface  |
| <b>pq</b>      | Motion of the conical axis                                     |
| $d_i$          | Family of spheres  |
| $\mu_i$        | Constant values for point-surface proximity                    |
| $F_{motion}$   | Function to obtain ruled surface approximation                 |
| $F_{plane}$    | Function that represents plane for proximity                   |
| $F_{fair}$     | Function that represents the fairness of two boundary curves   |
| $F_{point}$    | Function that represents point for proximity                   |
| $F_{rigid}$    | Function that controls the rigidity                            |
| $F_{ortho}$    | Function that maintains the tool motion orthogonal to the axis |

|                       |  |
|-----------------------|--|
| <b>p</b>              | Boundary cubic B-spline 1 <sup>st</sup> curve          |
| <b>q</b>              | Boundary cubic B-spline 2 <sup>nd</sup> curve          |
| <b>T<sub>i</sub></b>  | Conical tool definition                                |
| <b>r<sub>i</sub></b>  | Conical tool radius                                    |
| <b>l</b>              | Conical tool cutting length                            |
| <b>V<sub>c</sub></b>  | Cutting Speed [m/min]                                  |
| <b>N</b>              | Spindle Speed [rpm]                                    |
| <b>AFM</b>            | Abrasive Flow Machining                                |
| <b>ASTM</b>           | American Society for Testing and Materials             |
| <b>HRC</b>            | Rockwell C Hardness                                    |
| <b>h<sub>eq</sub></b> | Equivalent chip thickness [μm]                         |
| <b>Q'</b>             | Specific material removal rate [mm <sup>3</sup> /mm*s] |
| <b>V<sub>s</sub></b>  | Grinding speed [m/s]                                   |
| <b>V<sub>w</sub></b>  | Grinding feed rate [mm/min]                            |
| <b>R<sub>a</sub></b>  | Average roughness                                      |
| <b>R<sub>z</sub></b>  | Five consecutive maximum heights between peak-valley   |
| <b>D</b>              | Hole diameter for hole drilling technique              |
| <b>Z</b>              | Maximum depth for hole drilling technique              |





---

## **Chapter I. Introduction**

---



# Chapter I. Introduction

*This chapter presents the background of this work application considering the industrial environments and requirements. Afterwards, the main objectives for the proposed work are cited in detail and, finally, the document structure is described.*

## I.1. Introduction

This thesis presents the result of a researching work about a methodology for high-added value components combining multi-axis additive manufacturing and machining processes. This work, carried out at the Department of Mechanical Engineering from the University of the Basque Country (UPV/EHU), pretends to complement the current knowledge of both processes through experimental studies and processes modelling. Therefore, it is provided a reliable method for manufacturing these complex and valuable components.

The globalization has led the air transport to suffer from a progressive stage of growth during the last decades. In spite of being influenced by many factors such as the world economy or the fuel price, the predictions point to a growing continuity in the next two decades. For example, in the case of the market analysis performed by Boeing that previews an increase in the air traffic of 5% per year, this will imply the duplication of the last 30 years growth rate (Boeing, 2017). Another industrial giant of this sector, Airbus, carried out the prediction study prognosticating a similar sector evolution (Airbus, 2017). Both agree that around the 70% of manufactured aircrafts will be single aisle, and almost the 40% will be for intercontinental flights, i.e. Asia and the Pacific. This trend is reflected on the demand of different improvements in turbomachinery components.

Moreover, it should be considered that an aircraft engine has about 700 compressor blades and the price of a single blade is approximately 300 dollars compared with the repairing costs that amount to 120 dollars; it is highly profitable to repair them instead of replacing them for new ones. The tip is susceptible to be repaired up to 4 times before declaring that blade as *scrap* (useless). Additionally, the 20% of the production is declared as *scrap*; this means that in one year nearly 40,000 blades go through Iberia's Engine Workshop, corresponding to 190 engines. The possibility of repairing them and increasing their life cycle contributes directly to the reduction of costs (Iberia, 2014). Therefore, it is a direct entry in the profits. This gives rise

to the demand of improved and new manufacturing technologies, where the additive manufacturing takes on great importance for repairing operations.

Among different additive manufacturing technologies, laser metal deposition or laser cladding stands out as a result of the main advantages it presents. The high energy density provided by laser sources is used to melt part of the base material where a material is injected, it allows to generate a high quality bonded clads and a minimal heat affected zone. The consecutive union of several clads generates the coating of a part or even leads to a complete manufacture of a part using this technology. In this respect, researching efforts are directed towards the necessity and implementation of 5-axis simultaneous movements operations for this technology, the complexity of tool-paths generations and different machine and process limitations. These operations offer many advantages in terms of added material directionality and adaptability for complex geometries. The presented work is carried out precisely within this framework, developing a CAM module specifically oriented to this technology for different operations (including 5-axis operations) implementing a geometry prediction model based on the process parameters and the material selected with the aim of optimising these strategies and becoming them more accessible on the market. Moreover, this work addresses methods for optimising repairing operations for monolithic turbine rotary components.

In addition, the great level of competence achieved in this sector leads industrial manufacturers to the continuous search for manufacturing processes improvements that allow reducing manufacturing costs and times so, at the same time, increase the productivity and the production. In particular, the machining process is one of the most studied with the aim of improving its efficiency by reducing machining times and therefore manufacturing costs. In this sense, along this dissertation it is covered a mathematical algorithm verification for tool-paths optimization; offering a solution for flank milling strategies applied to non-developable complex surfaces (commonly presented in turbomachinery integral rotary components). Concurrently, in line with the search for new technologies, a new manufacturing process is studied as a complement or alternative to the conventional milling process, known as super abrasive machining.

All in all, with the aim of facing the growing demand for turbomachinery components in compliance with the current regulations, it is necessary to introduce improvements in the manufacturing processes of aeronautical engines. These design and manufacturing improvements present new challenges for the aeronautical industry. In order to face these challenges, it is necessary to optimise existing manufacturing processes and develop new

processes. In this sense, in this work, researching advances are directed towards the broadening of knowledge on the process of additive manufacturing in 5 continuous axes and its subsequent machining. The combination of manufacturing processes based on machining and laser results into a methodology for optimising the manufacturing process of monolithic turbine components using this hybrid approach.

## **I.2. Objectives**

At the presented work it is raised a developed methodology for the new trend of hybrid manufacturing, combining additive and subtractive manufacturing technologies. This hybrid manufacturing tendency is directly related to sustainability principles of recycling, repairing and reducing resources waste. One of the main targets in the industry for this methodology consists on the repairing and manufacturing of aeronautical turbomachinery integral rotary components, due to their geometrical complexity, their tough mechanical requirements and the avoidance of complete component discard. Hence, this work pretends to improve and broaden knowledge about the integration of both technologies, additive and subtractive, in the global hybrid manufacturing concept, taking into account the challenges that are still subject matter of international researches. On the one hand, additive manufacturing is completed with a CAM module oriented to the process specifications and a final added geometry prediction. On the other hand, an initial approach to super abrasive machining is presented, considered as a possible alternative to conventional manufacturing processes for these complex and strict turbomachinery components. In sum, the pursued aims of this thesis are detailed in the following points:

- a) A feasible and integral methodology development for hybrid manufacturing, combining additive and subtractive process, with the aim of give a global vision for the repairing and manufacturing of high-added value components.
- b) A CAM module development specifically oriented to additive manufacturing process. This module would consider, not only planar strategies but also complex geometries generations through 5-axis simultaneous. Moreover, this module will be implemented into a commercial CAD/CAM software with a pleasant and intuitive user-friendly interface.
- c) An API will be developed, implementing in the CAM module the possibility of predicting the final geometry obtained through the additive manufacturing process.

For this prediction it will be offered two options, one is introducing the clad size manually (based on operator experience and knowledge) and the other one is based on a mass-balanced algorithm, considering the material and process parameters. A complex turbomachinery integral rotary component is selected as a case study for the CAM module and predicted geometry validation.

- d) An algorithm-based solution for flank milling non-developable complex surfaces. The proposed algorithm will be validated with a complex geometry that consists on a single blade from aeronautical turbomachinery component.
- e) Related to the subtractive manufacturing processes, it is performed an initial approach for super abrasive machining, comparing this new process to the conventional milling process used for these turbomachinery components. As a novelty, a serial of experiments are performed for roughing stage, analysing the process behaviour with thermoresistant superalloys.
- f) Analysis of the feasibility of super abrasive machining implementation into conventional milling machines, in spite of not fulfilling this technology machines requirements.

It is a reality that additive manufacturing and machining are called to work together dependently in many manufacturing and industrial sectors. Consequently, the holistic vision of this relation provided by this thesis is enclosed in the real industry in the interest of being applied in a near future.

### **I.3. Thesis organization**

After the contextualization of this thesis application and the issues to deal with, the presented work was organized following a serial of chapters that are described below.

In the **Chapter I** it is described, in brief, the background of repairing and manufacturing processes of high-added value turbomachinery components. In this chapter, it is considered the industrial sector target and needs, the main objectives for the proposed work and the document structure.

Likewise, in the **Chapter II** it is presented the study of the art for the evolution of design, manufacturing and repair techniques for aeronautical turbine monolithic components. First of

all, the general criteria to be taken into account in the design phase of this type of parts are described. It also includes a classification of the aeronautical engines according to their application and their components. Secondly, a summary of the different manufacturing processes of turbine rotor manufacturing parts depending on their application is presented. As far as the machining process of the parts is concerned, the different algorithms developments for optimising manufacturing processes are presented. Finally, it describes the process of repairing monolithic parts of turbine rotors through the process of material input by LMD and the CAD/CAM software available in the market. In this way, the different applications and the industrial implantation are exposed.

**Chapter III** presents a comprehensive methodology for the hybrid manufacture and repair of high value-added components. In a first stage, a diagram is presented with the complete methodology through different stages inside the hybrid manufacturing process, all stages interconnected. Afterwards, each stage is completed with specific module development and every stage was implemented inside the same CAD/CAM manufacturing software.

**Chapter IV** is dedicated to the development of a specific CAD/CAM module completely oriented to LMD process for planar, 3-axis and 5-axis LMD operations. With the aim of programming this module, two APIs were developed implemented inside the same CAD/CAM environment. This chapter describes the two APIs, step by step, for different operations definition and generated clad geometry estimation based on a mass-balanced model. Moreover, this chapter shows the integration of these APIs inside the CAD/CAM environment. To this end, it is presented the programming steps carried out to integrate into the CAM environment. Finally, the validation of the model is presented with three real application cases such as single tracks, a single blade and an entire blisk generation.

**Chapter V** describes new advances for turbomachinery integral rotary components made of difficult-to-cut thermoresistant superalloys. On the one hand, this chapter presents an algorithm development and validation for adapting flank milling strategy to manufacture non-developable freeform surfaces. On the other hand, the feasibility of SAM process is evaluated, performing a serial of experiments full slotting Inconel®718. Moreover, surface integrity is evaluated in terms of roughness, residual stresses, microstructure and microhardness.

Finally, **Chapter VI** presents the main contributions derived from the developed work, as well as the possible future lines that have arisen from this work that will allow deepening even more in the knowledge of this process.





---

**Chapter II. Evolution of design, manufacturing and  
repairing techniques for turbomachinery integral  
rotary components**

---



# Chapter II. Evolution of design, manufacturing and repairing techniques for turbomachinery integral rotary components

*This chapter presents a literature review of the state of the art for the evolution of turbomachinery integral rotary components design, manufacturing and repairing techniques. For this purpose, a brief introduction of technological and industrial point of view related to this kind of components is stated. Additionally, aircraft engines are described more in detail, distinguishing different types of turbines, applications and requirements. Furthermore, manufacturing processes and challenges for this kind of components are analysed (conventional, non-conventional and new feasible processes). Moreover, inside the hybrid-manufacturing field, an analysis of the state of the art for these turbomachinery components repairing techniques is presented. Finally, a detailed study is conducted on the Industry 4.0 concept and the influence on this hybrid manufacturing process.*

## II.1. Introduction

The aeronautical industry is considered one of the strategic sectors of the global market. According to the Spanish Association of Defence, Aeronautics and Space Technology Companies (TEDAE), this sector generates a total revenue of 7.8 billion Euros, which 11% is assigned to R&D+i activities. This investment stems from the need to face the global competitiveness; not only related to the design of new components, but also related to mechanical properties during the life cycle and manufacturing processes optimization to obtain the final component requirements (Asociación Española de Empresas Tecnológicas de Defensa).

Turbomachinery rotary components in aircraft engines, mainly in the compressor and the turbine, present a complex geometry composed of a serial of blades distributed along the same rotor. In some cases, when the turbomachinery presents a big size, these components are an assembly of smaller pieces, mounting single blades in some rotor section, which in turns it is mounted on the final rotor. Nevertheless, in the last decades, there is a new trend to integrate blades and the rotor in a monolithic component. With the aim of achieving this purpose, blades are manufactured directly over a revolution body. Thus, it is obtained a

compact component with more complex geometries because original assembly junctions are avoided. However, turbomachinery integral rotary components manufacturing presents some difficulties, such as accessibility and geometrical complexity, among others.

The manufacturing process optimization of this kind of components is the principal target for large aeronautic engines manufacturers; this is the case of one of the global leader in blisk manufacturing: MTU engine that in 2014 they opened a new center oriented to blisk manufacturing in Munich (Germany), expecting blisk manufacturing up to 3500 per year. (MTU Power, 2019).

In relation to different manufacturing processes, there are many challenges related to these type of components. Due to the working conditions and critical functioning requirements, they are composed of difficult-to-cut materials, concretely thermoresistant superalloys (Ti and nickel-based alloys). They are characterized by the combination of high hardness values with low thermal conduction values. On the contrast, they imply tool wear and early breakage and elevated cutting forces (Pereira, Rodríguez, Barreiro, Fernández-Abia, & López de Lacalle, 2017). Some manufacturing technologies, such as *electro discharge machining* (EDM), presents a great behaviour against cited challenges; however, manufacturing times and costs are higher (Torres, Arbizu, & Pérez, 2017). Here is where new trends of manufacturing processes and conventional manufacturing process optimization play critical roles to offer an efficient production, in terms of not only part quality but also reducing manufacturing chain times and material/tool consumption.

In connection with the philosophy of Industry 4.0 and the concept of circular economy, it is promoted the recycling, remanufacturing, reusing and refurbishing of materials and components (Shanshan Yang, 2018). It should be pointed out that hybrid manufacturing processes combining additive and subtractive manufacturing technologies, commonly studied to repair damaged turbomachinery rotary components, are at early stages and present many industrial and scientific challenges to be addressed.

## **II.2. Aircraft engines**

There are different types of aircraft engines configurations depending on the final application. Nevertheless, there are some monolithic complex pieces presented in most aircraft engines, such as blisk and impellers. Thus, the design and manufacturing optimization of this type of parts has a direct influence on the final engine performance.

The aircraft engine is part of the propulsion system that generates mechanical power. The aircraft engine is divided into the following major types: piston engines, reaction engines and electrically powered engines. Electrically powered engines are used for small multirotors or multicopter, which their main applications are radio control aircrafts or UAVs; also, there is a new trend for electric or semi electric powered aircrafts. Piston engines are mainly used for sport and leisure aviation and small aeroplanes that require low power and reduced weight. This type of engines specifications of low weight implies not feasibility of supplying big aircraft and high cruising speed power requirements. Hence, nowadays reaction engine or jet engine is the type more common presented in the propulsion for civil and military aircrafts because they offer higher power-to-weight ratio than piston engines.

The difference between piston engines and jet engines is the functioning principle. Piston engines follow the OTTO cycle and jet engines the BRAYTON cycle. Both, piston and jet engines are divided into four stages: air/fuel intake, compression, combustion and exhaust. Nevertheless, the main difference lies in the combustion stage, being at constant volume for piston engines and at constant pressure for reaction engines (Figure II.1).

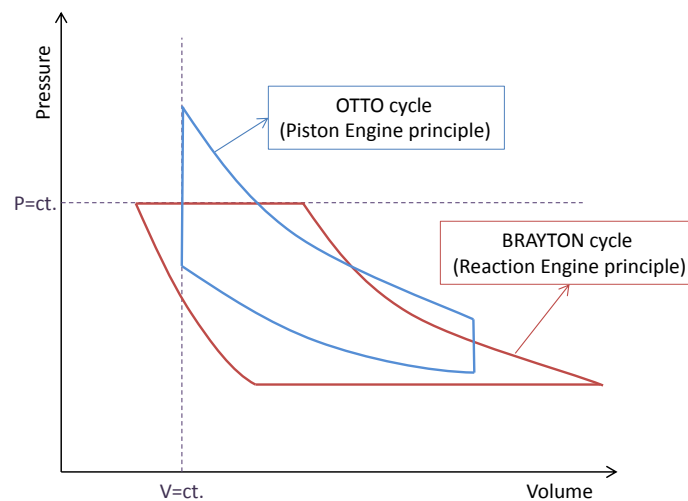


**Figure II.1** Comparison between OTTO cycle (piston engine principle) and Brayton cycle (reaction engine principle)

Theoretically, maintaining the volume constant (OTTO cycle) instead of the pressure constant (BRAYTON cycle) it is achieved higher performance. However, valves and chamber input/output deflectors are needed to run this process, implying a complexity of engine manufacturing, weight increment and decreasing functioning safety (Díez, 2002). This is the main reason why nowadays the reaction engine is more extended among civil and military aircrafts (NASA, 2007). Inside reaction engines classification, the following configurations that

require of blisk/impeller components are distinguished: turbojet, turbofan, turboprop, turboshaft and propfan.

### II.2.1. Turbojet

The turbojet engine was the most popular engine of high-speed aircraft, despite the high fuel consumption. Nonetheless, currently it is just part of old and vintage aircrafts, some military aircrafts, as well as, rocket engines.

The operation principle of the turbojet is based on a continuous gas turbine with the four stages stated before: intake, compression, combustion and exhaust (Figure II.2). Firstly, the air is introduced into the engine through the front intake. Then, at the compression stage a high quantity of air is compressed to be pushed to the combustion stage. In order to perform the compression stage, it is possible to use or axial (*blisk*) or centrifugal compressors (*impeller*). Once the air pressure is the adequate, it is introduced into the combustor where the fuel is burned continuously. At this point, it starts the expansion stage, the air at elevate temperature and pressure is conducted to the turbine (Figure II.2). Finally, the air goes through the propelling nozzle where the speed increases decreasing the pressure to the output pressure; this process transforms the pressure into speed (Springer, 2001).

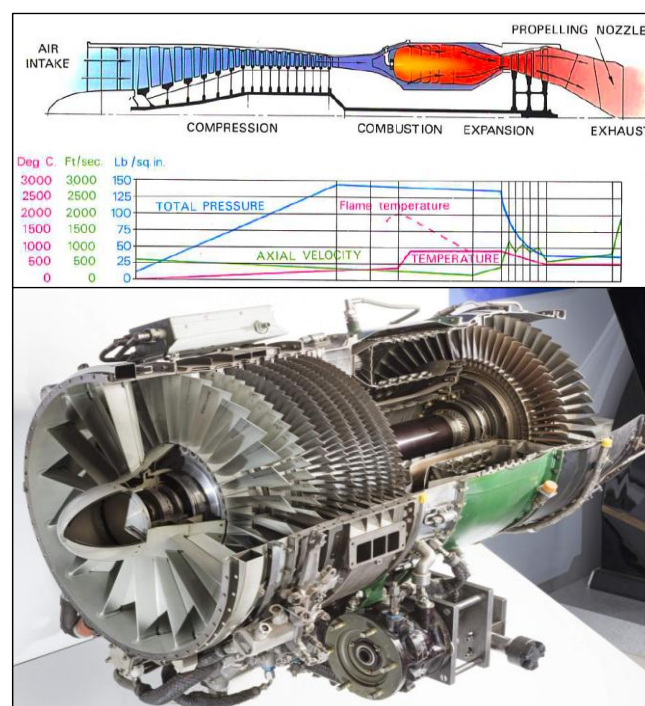


Figure II.2 Diagram of a turbojet engine airflow and working conditions (top) (pplc, 1986), an axial flow turbojet form General Electric which production ended in 1988 (GE J85)

The replacement of the majority of this type of jet engines is due to the fact that the elevated speed at the exhaust stage implies an increment of fuel consumption, additionally it should be pointed that they are also very noisy (pplc, 1986). At the present, modern aircrafts use turboprops for low speeds or turbofans for high speeds because their fuel consumption is lower and they have a more quiet operation.

### II.2.2. Turbofan

Nowadays, most of modern jet aircrafts contain this type of engine due to the fact that they present a high performance ratio combined with an acceptable fuel consumption compared with turbojets.

The operation principle of the turbofan consists of two different air flows through the engine (Figure II.3). The main characteristic of this type of engine is that includes a big external fan at the air intake stage. The main air flow performs the same stages as the turbojet engine: intake, compression, combustion and exhaust. The secondary air flow avoids the combustion stage, accelerating the air flow directly from the fan and mixing with the primary air flow at the exhaust stage. Thus, this fan system generates most of the thrust required by the engine, letting to the escape gases approximately the 30% of the work (C. Kling, 2011).

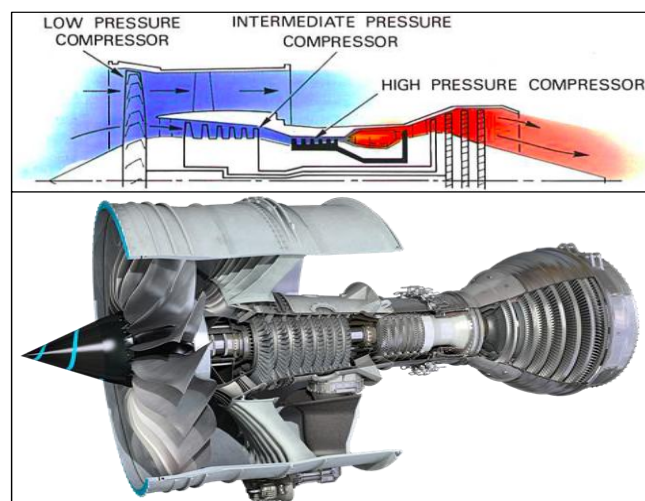
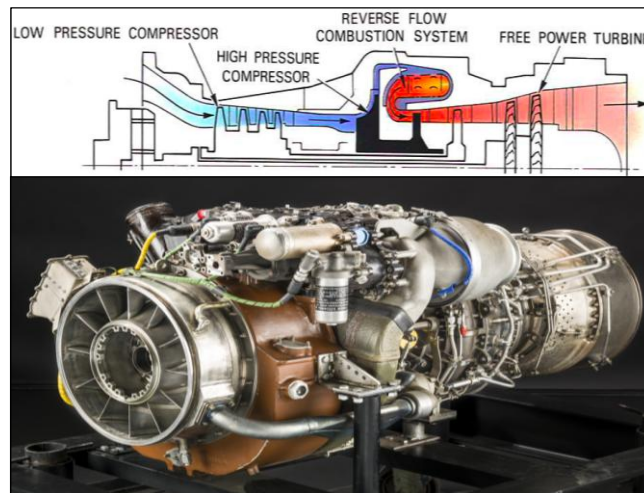


Figure II.3 Diagram of a turbofan engine operation (top) (pplc, 1986) and a turbofan GE trent7000

### II.2.3. Turboshaft

Turboshhaft engines are mainly used for helicopters and auxiliary energy unities. This engine configuration is single-spool or multi-spool, but normally the single-spool is employed to minimize weight; what makes it suitable for light weight helicopters (P.P. Walsh, 2004).

The operation of this type of engine consists of a gas turbine that transmits the power through a shaft (Figure II.4). The main difference between turboshaft and turbojet is that gases from escape stage in turboshaft engines have not enough energy to produce a significant thrust. In the case of turboshaft engines, the engine is connected to a fixed transmission structure; so it is designed in a manner that the speed of the helicopter rotor is independent of the gas generator rotating speed (Bellis).



**Figure II.4** Diagram of turboshaft engine operation (top) (pplc, 1986) and a turboshaft GE XT700

#### ***II.2.4. Turboprop***

Turboprop engines are used for aircrafts that require not very high-speed, as in the case of military or civil aircrafts for covering not very long distances. Figure II.5 shows an example of turbopropeller GE T64).

The turboprop main characteristic is that the power produced by the engine is used to move a propeller. The propeller is the component that generates the thrust necessary to impulse the aircraft, generating the 90% of the actual thrust. In order to carry out that function, a speed reduction gearbox is used connecting the engine to the propeller. The gears are necessary to keep the propeller from going to supersonic and losing efficiency (NASA, 2007). Related to a concrete engine weight, the turboprop accelerates more air than the turbofan at lower speed, generating more thrust at the same fuel consumption. However, at higher speeds and altitudes the thrust decline rapidly.



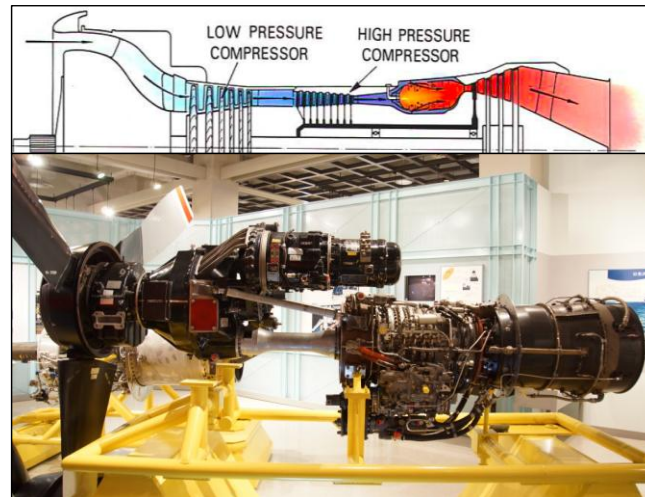


**Figure II.5** Diagram of a turbopropeller engine (top) (pplc, 1986) and a turbopropeller GE T64 with a gearbox at the middle and a turbine core at the right

### ***II.2.5. Propfan***

The propfan engine concept was born in 70's-80's with the aim of offering a cost-effective alternative to the existing engine models. Nevertheless, the excessive noise and the risk of using exposed propellers and supported by the fuel price decline led to avoid this engine for civil aircrafts, but not for military service. The Antonov AN-70 was the first high dimension aircraft for military purposes using a propfan engine, designed in 90's (Air Force Technology).

This type of engine was designed as a hybrid engine between a turbofan and a turboprop, offering the turbofan performance with the turboprop fuel saving (H.D. Perkins, 2015). This engine consists of a turbofan with two opposite rotational propellers mounted on the backside of the engine, allowing balancing the output flux direction and increasing generated energy (Figure II.6).

Nowadays, the interest on this engine configuration is re-emerging out due to the increment of fuel costs (the fuel consumption is 20% less than in turbofan (Change, 1999)) and, additionally, the necessity of using more eco-friendly and sustainability solutions, reducing CO<sub>2</sub> emissions (Åkerman, 2005).

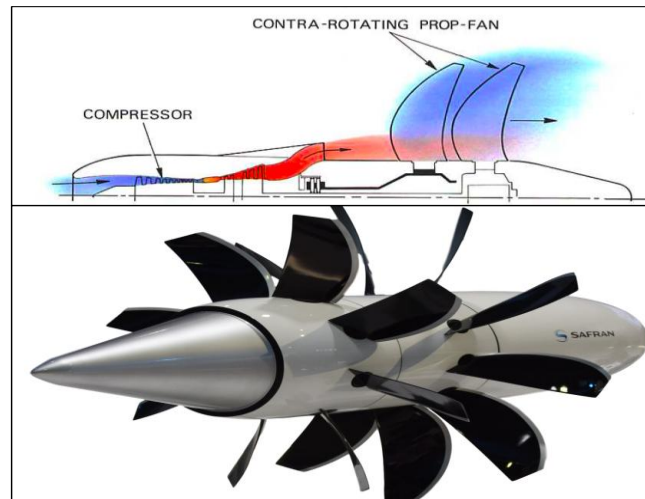


Figure II.6 Diagram of a propfan and an open rotor mockup from Safran, 2017

### II.2.5. New engines

The last generation of direct transmission engines are still competitive in terms of global performance compared, i.e. LEAP (CFM international) or GE9X (General Electric) (D.E. Van Zante, 2016). Nonetheless, the reduction of rotational speed and the ratio of the fan pressure in this type of engines imply the necessity of decreasing engine noise. In order to give a solution to this issue, Pratt & Whitney and the NASA developed a new engine called Geared Turbofan (GTF). The GTF configuration consists of a turbofan where the low-pressure shaft and the fan are assembled through a reduction gearbox, making possible that the low-pressure shaft rotates at higher speed than the fan. This engine decreases the number of stages between the compressor and the turbine, leading to a weight reduction and engine total length. In 2016s first Geared turbofan (PW1000G) were implemented in some commercial and civil aircrafts. Therefore, it is decreased the complexity of this configuration, reducing costs and increasing engine performance. Moreover, this solution is more environmentally friendly because the fuel consumption decreases, so the pollution.

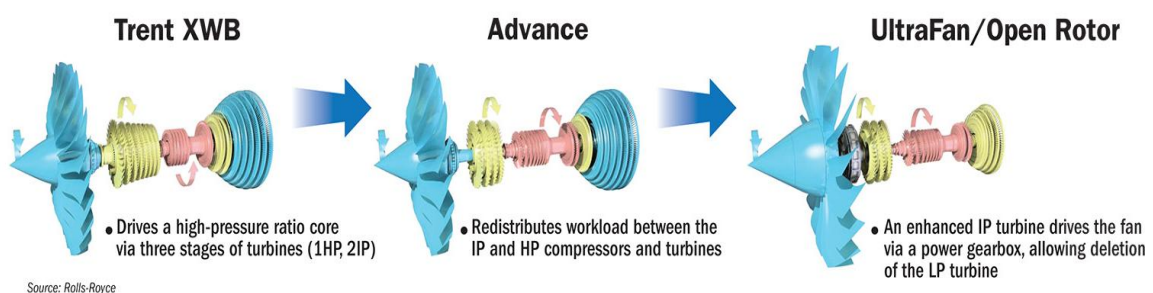


Figure II.7 Rolls-Royce engine evolution (Rolls-Royce, 2019)

Currently, Rolls-Royce is developing the UltraFan® (Figure II.7) engine design using a gearbox to reduce fan rotational speed. Figure II.8 shows a successful test carried out in Derby (UK) of a key component of the UltraFan®; it is expected the full implementation in the market throughout the 2025s. It is a promising design in terms of fuel, weight and noise reduction, estimating an increase of the efficiency in 25% compared with a first-generation Trent engine (Rolls-Royce, 2019).



**Figure II.8** Rolls-Royce testing in Derby (UK) a key component of the UltraFan® (Rolls-Royce, 2019)

### II.3. Turbomachinery Rotary Components

Turbomachinery rotary components acquire especial relevance for aeronautical jet engines reliability and security. Among them, noteworthy components are axial/centrifugal compressors and turbines in civil aviation. Figure II.9 shows the three main different geometries presented in this type of components: Blisk, Turbine with assembled blades on fir-trees and impellers. Traditionally, axial rotors were composed by the assembly of single blades into the disc, manufacturing both of them separately. Nevertheless, there is a clear trend towards monolithic components fabrication.

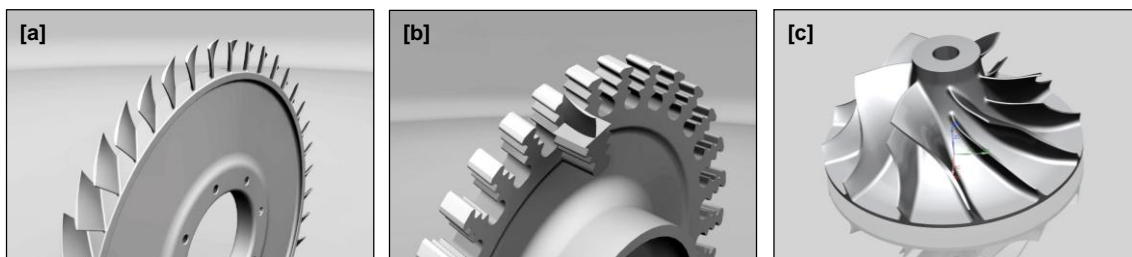


**Figure II.9** Turbomachinery rotary components: (a) Blisk, (b) Turbine blades and fir-trees, (c) Impeller

### II.3.1. Terminology and operational behavior

Jet engine compressors and turbines consist of a long shaft with rotary bladed discs along the entire perimeter, interleaved with stator fixed blades situated in the engine cover. The main function of the compressor is to elevate the pressure of the air that travels through it, leading to a more efficient combustion and exhaust processes. The turbine expands the combustion resultant gases before being sent back to the atmosphere; in this case the energy derived from the expansion rotates the shafts, which in turn, moves compressors and the fan (J.D. Mattingly, 2016).

Figure II.10 shows common geometries of turbomachinery rotary components, defining the constitutive surfaces. Assembled discs, blisks and impellers present complex non-developable warped surfaces jointed to a rotary disc that is connected to the turbine shaft. The fluid is introduced through the blades embracing the rounded edge named leading edge and comes out of the blade from the trailing edge. The internal surface of revolution is denominated hub and the external surface of revolution shroud. In the cases in which the rotary component is composed of a disc and single blades mounted along it, there is a surface called blade root that matches with the disc junction surface known as fir-tree. The pressure surface is the blade concave surface where the fluid pressure values are higher whereas the suction surface is the blade convex surface where fluid velocities are higher. In the case of the impeller design, it could be found some secondary blades situated in alternance with the main blades, denominated splitters. The main function of these splitters is the avoidance of pressure fluctuations derived from the differences between entry and exit blade distance, improving compressor performance (Pranit M. Patil, 2013).

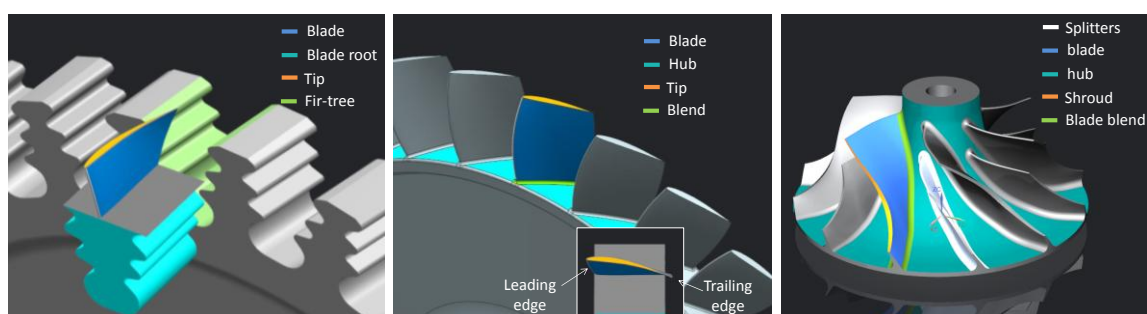


Figure II.10 Turbine blades and mounting disc, blisk and impeller terminology and designation

There is a new trend to fabricate these turbomachinery components as a monolithic part. They are known as Integral Bladed Rotors (IBRs), consisting on rotary bladed discs manufactured from a single piece. Inside IBRs definition, there are two main turbomachinery components: impeller and blisk. Monolithic rotary components present many advantages compared with

assembled components; the first one is the avoidance of junction, so any issue derived from union systems (Mateo, 2014). Additionally, they offer total weight reduction around 30%, improvement of aerodynamics reducing friction issues and fluid leakages, fuel consumption and emissions/noise reduction presenting a more green solution (M. Bußmann J. K., 2005) (Kumar, 2013). Nonetheless, there are some drawbacks derived from these integral designs, i.e. manufacturing processes present more difficulties requiring solutions that are more complex (accessibility issues, tool adaptability, machine kinematics limitations...). Moreover, assembled bladed discs main advantage is that the separate components are performed by hot forging process allowing the optimal material fibres orientation, so leading to more resistant components. In these cases two more advantages are presented, one is the material waste reduction and the other one is, in case of any blade wear or damage, each blade can be replaced individually instead of discarding the whole component.

Reached temperatures in some turbine stages are elevate so the use of an integral component (blisk) is, at this moment, trending topic for R&D. It is becoming a handicap achieving blades complex geometries with internal cooling ducts or the combination of different materials and microstructures for the disc and blades with the aim of improving/optimising mechanical properties (M. Bußmann E. B., 2009).

Conversely, centrifugal compressors are composed of one or two compression stages using impellers. The impeller is a compression rotary disc that changes flux direction from axial to radial. The operational principle consists on the following steps: the fluid entries axially through the centre of the impeller, and after being pushed by the blades, it flows radially at higher pressure and velocity than the initial. Blades are commonly designed as non-developable ruled surfaces, with small curvature at the beginning and the end of them but high at the intermediate zone. Furthermore, blades overhang has a small size achieving higher rotational speeds than other turbomachinery components. On the contrast, axial compressors offer higher thrust compared with centrifugal compressors for the same frontal area. Moreover, there is a possibility of enhancing achieved pressure including more stages inside the axial compressors. This is why axial compressors are more popular for most of turbofan engines. Centrifugal compressors present more robustness for small-medium turbofan engines and turboshaft or turboprop engines (El-Sayed, 2016).



### II.3.2. Material composition

Due to the fact that IBRs components are exposed to extreme working conditions during their entire lifetime, some parts of the engine require high heat resistant superalloys, such as titanium and nickel-based alloys, that present stability of material properties working under temperatures up to 400°C and 600°C, respectively (Campbell, 2006). Additionally, with the aim of standing those extreme working conditions, materials should fulfil some extra requirements such as a good resistance to impact loads, fatigue and erosion and a high ratio between mechanical resistance and material density (Rao, 2011).

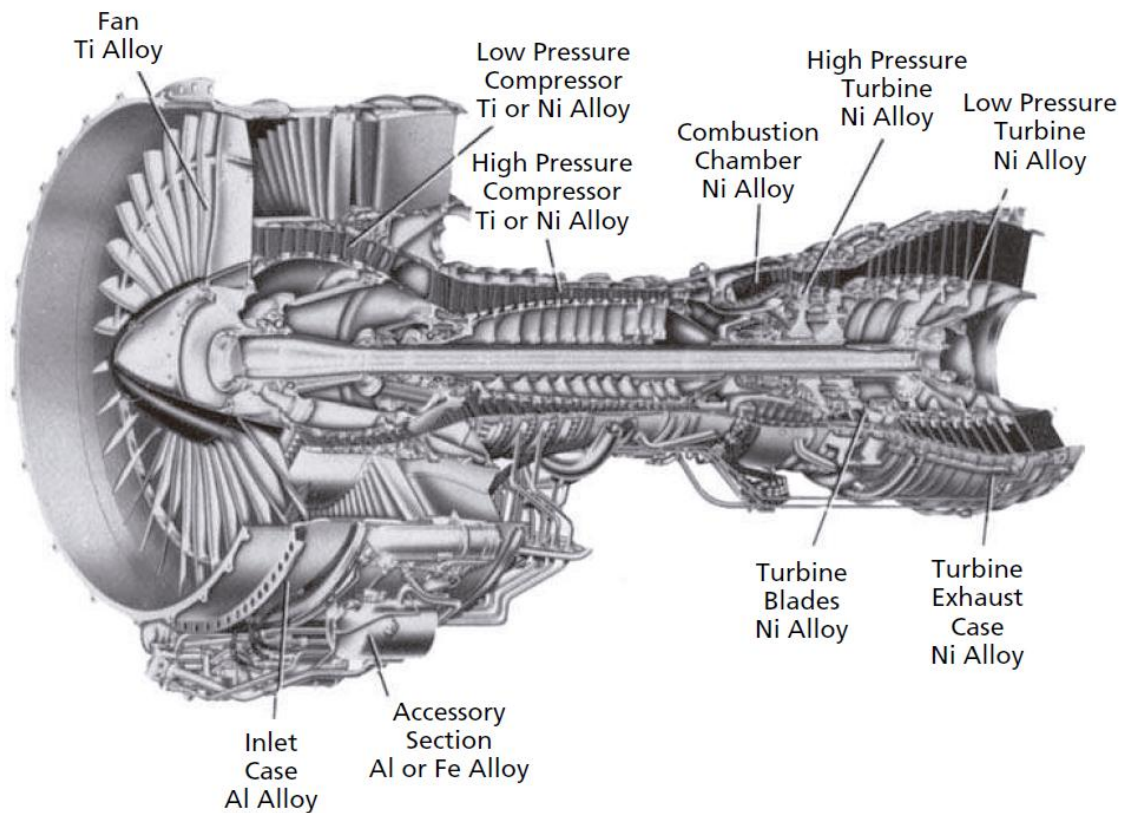


Figure II.11 Jet Engine common material distribution (Campbell, 2006)

Figure II.11 shows different materials presented in engine turbomachinery components, distributed depending on thermal and pressure stresses. Concretely, nickel-based alloys are mainly used for hot sections (combustion chamber, and the turbine rotary components) and titanium alloys are commonly used for cold sections (fan and compressor components). Titanium and nickel-based alloys main applications and advantages for engine components are described more in detail hereafter.

· **Titanium alloys**

Titanium alloys present good relation between mechanical properties and weight reduction due to their low density, approximately 40% lower than steel and 50% lower than nickel-based alloys (R.Padmanabhan, 2011). Titanium alloys classification is based on the percentage of alpha and beta phases presented in their structure at room temperature. On the one hand, the alloys close to alpha phase present highest creep and oxidation properties, as well as retain their strength working at elevated temperatures; however, among Ti alloys, they have the lowest formability. On the other hand, the beta Ti alloys present better formability, even offering the capability of being formed at room temperature, by contrast, the density increases and the ductility decreases leading to limited weldability after heat treatments. Finally, alpha-beta alloys present more proportioned characteristics: good strength at room temperature and admissible for short times at high temperatures (Campbell, 2006).

One of the most used alpha-beta alloys is Ti6Al4V, characterized by high resistant to tensile strength, corrosion and fatigue, coupled with intermediate fracture toughness that remain up to 350°C. Another Ti alloys are more common for engine stages that require higher temperature working conditions (500°C-600°C), i.e. Ti6242, Ti6246 or Ti17 (G. Lütjering, 2007).

· **Nickel/ Iron-Nickel based alloys**

Nickel based alloys contain at least 50% of nickel and they are commonly used for the hottest components inside aircraft engines where the temperature overpasses 500°C-600°C. These superalloys present hardness, low thermal conductivity and good ductility (F., Krämer, Sangermann, & Lung, 2012) (Moussaoui, Mousseigne, Senatore, Chieragatti, & Lamesle, 2015). Inside this group, it could be found Udimet®720 and Hastelloy®X. The Hastelloy®X is a solid strengthened solution that offers an excellent combination of outstanding oxidation resistance, what makes it appropriate for corrosive environments (T.-K. Yeh, 2013).

Iron-Nickel based alloys contain at least 25% of Nickel (common range: 25%-45%) and 15-60% of iron. Inconel®718 (53% Ni) is the most widely used since its development in the 60s, it offers a good combination between good mechanical properties and high corrosion resistance at 600°C working conditions, considered one of the strongest alloys at low temperatures, but this characteristic decreases rapidly at higher temperatures, 650°C-850°C (Reed, 2006).

### II.3.3. Complex surfaces: Developable and non-developable surfaces

A surface could be defined as the common part of two adjacent areas in the space. Surfaces contain two faces, but from the representative point of view, they are considered as a thin film that covers any solid body or splits two regions in the space. Hence, it is defined as *geometrical body* when material bodies are separated from all its properties, except of their form and extension (E. Zorrilla, 1986). Surfaces are classified as ruled, non-ruled/curved and free-form/sculptured surfaces.

Ruled surfaces are described as the movement of one straight line (generatrix) along one or various curves (guidelines). That is, it is considered a ruled surface when for each point there is a straight line lying on the surface (do Carmo, 1976). At the same time, ruled surfaces are divided into developable or warped surfaces. In the case of developable surfaces, the plane tangent to the surface is unique for all the points in generatrix line, allowing to be transformed into a flat segment. The main difference for warped surfaces is that there is also a plane tangent that contains the generatrix but in this case, it is variable for each generatrix point; what makes it impossible to be adapted to a flat plane without a deformation or breakage.

Non-ruled, curved or double curved surfaces are those that are generated by a curved generatrix. There are many different geometries inside this group, depending on the curve nature, movement law and form variability.

Duncan and Mair (J. P. Duncan, 1983) defined free form or sculptured surfaces as surfaces that are not generated in a continuous manner and present an arbitrary form as that generated by sculptors. Actually, this group involves forms that are not adjusted to simple mathematical expressions. Figure II.12 shows some example of ruled surface, double curved surface and a free form surface.

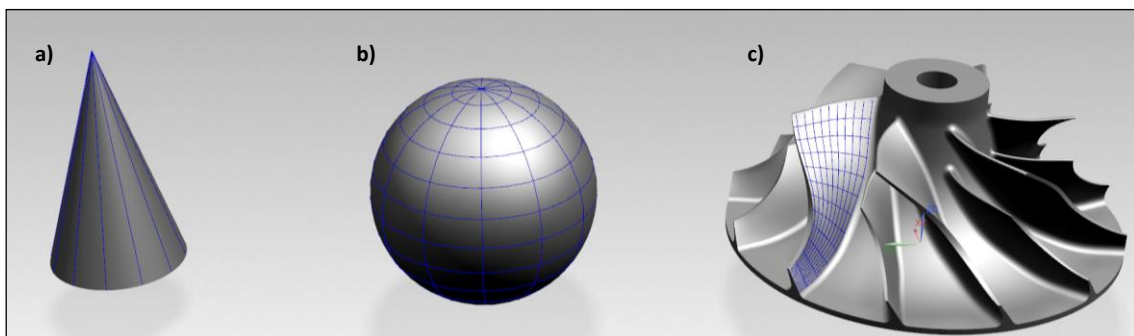


**Figure II.12** Examples of different type of surfaces: (a) ruled surface: cone, (b) double curved surface: sphere, (c) free form surface: impeller



IBRs are commonly composed by free form or sculptured surfaces. In general, these surfaces are designed with finite elements software, under fluid mechanics principles, obtaining a final surface formed by small patches. Coons surfaces, Bezier surfaces, B-Splines or NURBS are encompassed among different existing methods for free form surfaces generation (Forrest, 1972) (Onur Rauf Bingol, 2019).

Nevertheless, from an industrial point of view, it is considered as a complex geometry the surface that is not created from a developable primitive surface (cylinder, cube, cone, etc.). Non-developable ruled primitive surfaces are not considered inside this group, such as paraboloids and hyperboloids, along with non-ruled and free form surfaces. Developable surfaces fit with the machining strategy denominated flank milling. This strategy offers optimal machining times and surface quality, using the total cutting length of the tool (R. F. Harik, 2013). By contrast, complex surfaces present a big challenge for manufacturing strategies, being the most popular for these surfaces the point milling strategy that consists on a combination of tool path that reproduces desired surface in different steps, generating a scallop between defined steps. These scallops frequently require polishing operations, what increases manufacturing times and costs (Julien Chaves-Jacob, 2012).

#### ***II.3.4. IBRs requirements***

The use of gas turbines requirements for aeronautical applications has evolved severely in the last 50 years in respect to fuel consumption reduction, improvements of resistance-weight ratio, noise and emissions reduction and reliability. With the aim of supplying cited requirements, it was necessary to design turbines with higher loads in each stage, higher pressures, less axial backlashes, increase temperature profiles, improve cooling process, new material developments, etc. (G. Modgil, 2013).

The reliability of turbomachinery rotary components depends on their structural integrity. This is the reason why the design and analysis of different stages along the product development process must be rigorous to ensure the accomplishment of manufacturer requirements. For this purpose, it is necessary to consider aerodynamic, thermodynamic and tensional behaviour. It is necessary a fluid simulation to obtain velocity, pressure and temperature values in order to acquire relevant information to optimise blades geometries and maximize kinematic-thermodynamic cycle effectiveness. Numerical methods have been applied to turbomachinery rotary components designs since 1940s, however it was around 80s, with the evolution of computer characteristics, when fully three-dimensional methods (3D) replaced to

single calculation methods (Dawes, 1999). The use of Computational Fluid Dynamic (CFD) provides detailed information about the fluid behaviour depending on the 3D studied geometry. Nevertheless, it should be pointed out that this computational tool is directly dependent of the mesh generator and resolution. Moreover, the good quality of generated mesh depends on, not only generator resolution, but strongly on user knowledge (J. S. Anagnostopoulos, 2006). One of the main reasons to the common used of CFD for turbomachinery integral rotary components design is derived from the elevated cost of experimental prototyping (Hornsby, 2002) (R. Biollo, 2011) (C. Robinson, 2012), reducing significantly the cost of these components design up to 65% in 2005 (J. Spann, 2006). Y.Cui et al. 2019 performed a review of the evolution and different CFD studies on axial-flow self-rectifying turbines (YingCui, 2019). Figure II.13 shows a numerical model of the unsteady behaviour of impulse turbine under various constant-flow conditions (Y. Cui, 2019).

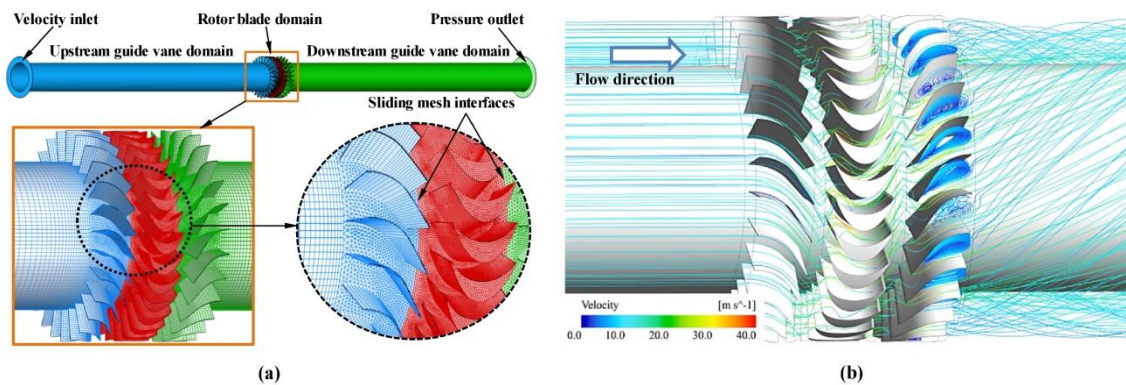


**Figure II.13** 3D passive flow-driving numerical model (Y. Cui, 2019): (a) Mesh structures and boundary conditions; (b) Streamlines through guide vanes and rotor blades.

Besides, there are strict regulations and goals from International Institutions in terms of emissions and noise reductions, along with airlines costs reduction, so technological improvements are required constantly. Another main objective is the fuel consumption reduction; one way to get this reduction consists of optimising thermal efficiency (Kyprianidis, 2011). For this purpose, it is required to increase pressure ratio in the cycle, implying higher temperatures for compression stages and loads (Spittle, 2003). Furthermore, there are extra control analyses to be done related to the following mechanical loads: (1) Radial loads caused by centrifugal forces intervening on the blades, (2) Bending stresses generated when the fluid compresses the blade and (3) Thermal loads derived from the unequal expansion/contraction along the blade surface.

The combination of defined loads and blades vibrations could lead to crack formations, so components breakages. Consequently, IBRs complex geometrical designs, extreme working

conditions/requirements and difficult-to-cut materials imply numerous manufacturing challenges referred in the following sections.

## II.4. IBRs manufacturing processes

The classification of manufacturing processes is conditioned by component characteristics, sector of applications, material requirements and geometrical definition. Among IBR definition, the geometry is divided into two main groups based on the relation between the length or blades areas and the diameter of the disc. Figure II.14 presents IBRs manufacturing processes in accordance with this relation, which shows the use of monolithic manufacturing processes for small-medium diameters and union processes for big diameters (M. Bußmann J. K., 2005).

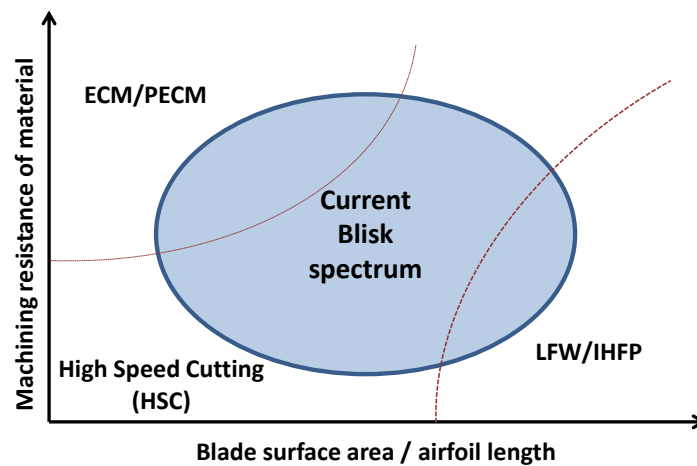


Figure II.14 IBRs manufacturing methods subjected to material resistance and geometry (M. Bußmann J. K., 2005)

The first group, where the component size is elevated, involves geometries as the fan and first stages of low-pressure compressors. These components are commonly made by forging and manufactured by union processes; applying a welding process between single blades and the main disc. Among welding processes, *Linear Friction Welding (LFW)* and *Inductive High Frequency Pressure Welding (IHFP)* are found (M. Bußmann E. B., 2013).

The LFW process consists on fixing strongly the disc while single blades are oscillating along a linear movement; the generated friction leads to the necessary heat to obtain a welding clad between both components. Finally, a milling process is performed to remove the remained extra material (Kumar, 2013). At the present time, this technique obtains welding results with high integrity, low distortions and fine grain microstructure in the thermal affected zone (Mateo A. , 2011). The IHFP process uses a high frequency alternating current that generates an elevate electromagnetic field heating the materials up to the required temperature (M.

Bußmann E. B., 2009). Inside this group, the *Abrasive Water-Jet Cutting* (AWJC) is presented as an alternative for blisk roughing strategies with blades length over 150 mm and cutting widths of 100 mm (Snecma, 2009).

The second group encompasses IBRs geometries with small blades size compared with the component diameter, such as high-pressure compressor stages. Currently these components are manufactured using *High Speed Cutting* (HSC) of a monolithic piece due to the process flexibility and the wide knowledge of this conventional process. Among material removal processes of these components, they are cited: *Casting*, *Pulse/Precise Electro Chemical Machining* (PECM), *Electro Discharge Machining* (EDM), *Additive Manufacturing* (AM), *Grinding* and *Super Abrasive Machining* (SAM). The subsection II.4.1 will focus on monolithic manufacturing processes.

Additionally, with the aim of reducing material waste and manufacturing times, near-net-shape processes are becoming an alternative as a primary process: *Additive Manufacturing* (AM), *Casting* and *Sintering*. Nonetheless, the high complexity of these components is still a *handicap* compared with the forging preforms that achieve good mechanical properties and higher resistances due to the optimal fibre orientation (Boddenberg, 1966) (C. Leyens, 2003) (A. Bhattacharjee, 2017). One of the most popular post-treatment to optimise these primary processes is known as *Hot Isostatic Pressing* (HIP). The HIP consists on applying elevate temperature (482°C for aluminium to 1320°C for nickel-based superalloys) and pressure (range: 50.7 MPa – 310 MPa, being 100 MPa the most common pressure) simultaneously on the part, removing porosity and improving mechanical properties (J. M. de Monicault, 2008). Considering those new alternatives and their combination in order to obtain the optimal IBR manufacturing process, Klocke et al. (F. Klocke R. S., 2015) performed an technological and economic analysis determining 7 different process chains combining milling, PECM, ECM and AM, establishing complete machining process as the referent process. Following the same objective of finding the optimal IBR manufacturing process chain, Figure II.15 shows a comparative chart between 20 reliable process chains, based on a previous technological analysis, defined for a Ti based impeller manufacturing (A. Klink, 2018).

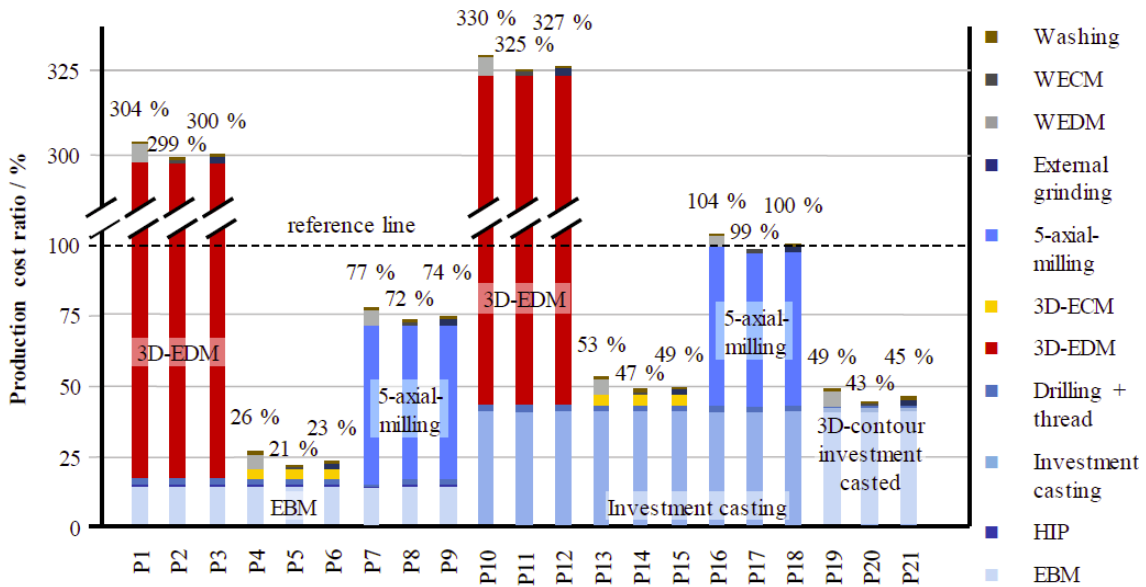


Figure II.15 Production costs of 20 process chains for impeller manufacturing; (P18) is considered the conventional reference process chain (A. Klink, 2018)

### II.4.1. Monolithic components manufacturing processes

Hereafter, manufacturing processes for monolithic components (small-medium size IBRs) are described more in detail, with their main advantages, drawbacks and applications.

#### II.4.1.1 Casting

*Sand Casting* is used for medium-small impellers that do not require elevate finishing accuracy and mechanical properties. Figure II.16.a shows an example of these applications: automotive turbocharger. This type of impeller does not require tough tolerances and it is generally manufactured in big batches. These components are widely used for automotive reciprocating internal combustion engines, particularly for diesel cycles. These engines consist on a turbine and a compressor, where the impeller is installed, connected coaxially. The turbine is activated with the motor exhaust gases, empowering in turn the centrifugal compressor. This centrifugal compressor squeezes the engine intake air. The air gets into the cylinder with higher density and oxygen mass, obtaining more power for the same piston displacement.

Casting impellers are used, in usual manner, for centrifugal pump impellers (Figure II.16.b). In these cases, the impeller is empowered by a motor, so the liquid enters axially through the impeller eye (*suction side*), goes through the blades and is driven out radially with higher pressure and velocity. Impellers fabricated by sand casting are commonly made of steel, bronze, brass, aluminium or plastic.

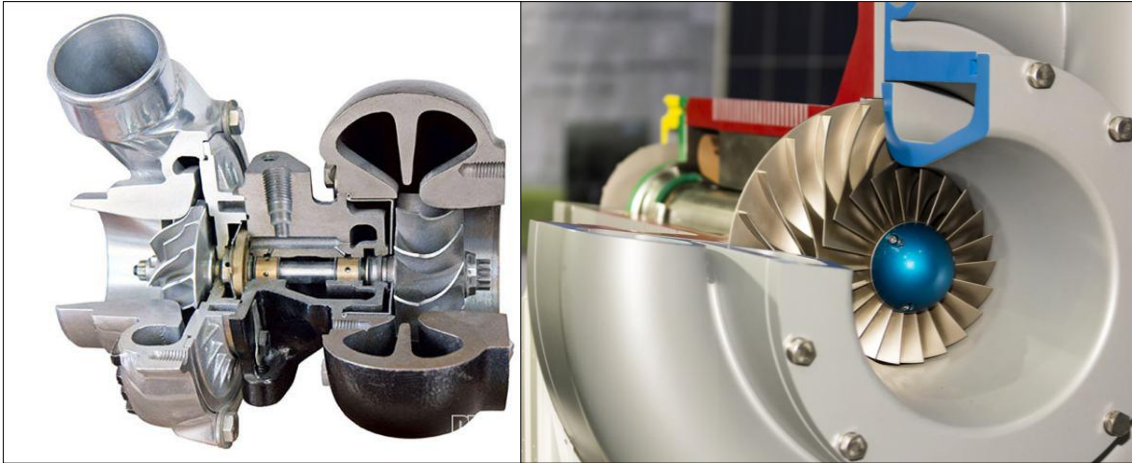


Figure II.16 Examples of casting impellers: a) Turbocharger (Chevrolet, 2016), b) Centrifugal pump (ScottTech, 2017)

#### II.4.1.2 Electro Discharge Machining (EDM)

The *Electro Discharge Machining* (EDM) is based on an electro-thermal machining process; an electric discharge is generated between an electrode and the desired part immersed in a dielectric medium, requiring both materials to be conductive. The heat generated by the discharge melts and evaporates part material and to a lesser extent the electrode. Despite of being a manufacturing process adequate to obtain complex geometries with tough tolerances, which cannot be achieved with other manufacturing process, the main drawback lies on the reduced material removal rates. Moreover, the thermal nature of this process causes a molten metal superficial layer (with different properties than base material) that affects to the fatigue response (J.P. Kruth, 1995). Nevertheless, this technology evolved to eliminate this surface integrity issues for thermoresistant superalloys such as Ti6Al4V and Inconel®718 (D.K. Aspinwall, 2008).

This technology is commonly used for low-machinable materials as titanium and nickel-based superalloys (Figure II.17) due to the fact that there is no direct contact between the tool and the desired part, the effect of material properties does not cause cutting forces and do not have influence on the erosion process (I.Ayesta, 2016). Klocke et al., 2013 performed a technological and economical comparison of roughing via milling, WEDM and SEDM for titanium and nickel-based blisk concluding to consider EDM as the most economical roughing process and a real alternative for large batches, up to 400 blisk per year (F.Klocke, 2013).



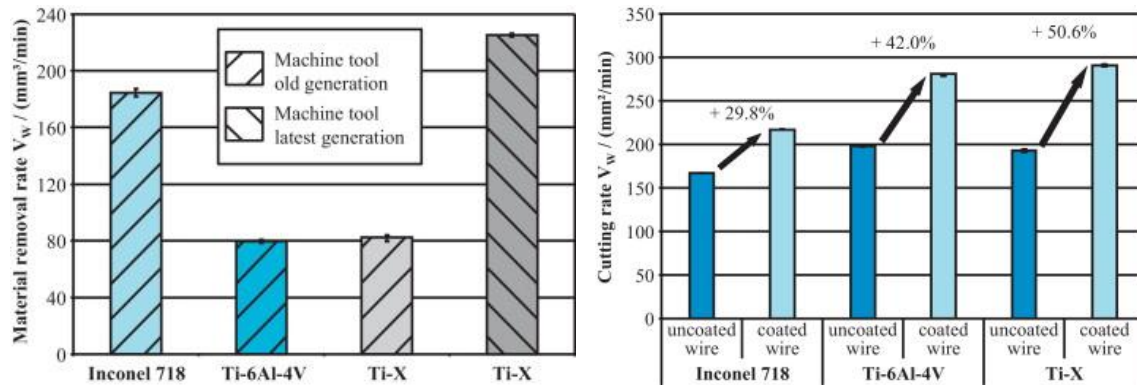


Figure II.17 Material removal rates for WEDM and SEDM manufacturing process on thermoresistant superalloys (F.Klocke, 2013)

This manufacturing process is a feasible alternative for closed-type blisk and impellers (Figure II.18), known as *shrouded blisk*, *integrated impeller* and *hooded impeller*. This type of geometry presents tool accessibility inconveniences for the conventional milling process to be manufactured from a monolithic part. The main challenges for EDM-ing these blisk and impeller components consist on optimising electrode design and tool-path programming for the cavity performance (L. I. Gang, 2007).

Furthermore, these applications require the use of a machine with more than 3-axis and the difficulties of their interpolation. Additionally, it is necessary various electrodes to achieve the final desired form (D. Y. Yang, 2013). At the present time, there are highlighted many technical studies about blisk/impeller manufacturing with cylindrical and complex form electrodes using multi-axes numerical control strategies (I.Ayesta, 2016) (Xiaoming Kang, 2018).

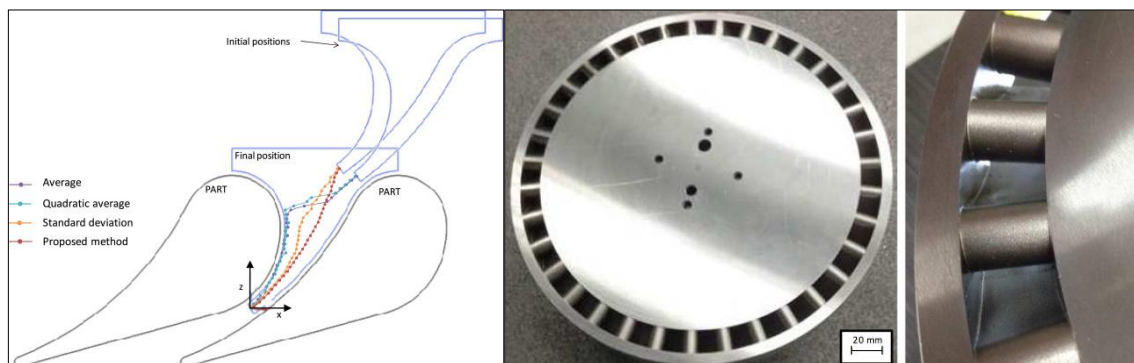


Figure II.18 Generated optimal tool-paths and a shrouded blisk manufacturing by EDM (I.Ayesta, 2016)

#### II.4.1.3 Electro Chemical Machining (ECM) / Precise Electro Chemical Machining (PECM)

The *Electro Chemical Machining* (ECM) is a non-conventional material removal machining process by electrolysis where a voltage is applied between a form electrode (cathode) and the

part to be manufactured (anode) through an electrolytic liquid (K.P. Rajurkara, 2013) (G. Srinivas, 2018). The removed material precipitates in the electrolytic solution as metallic hydroxide. The machining process is performed without thermal and mechanical stress, thus material properties are not disturbed, so there is no presence of white layer. It is presented as a good alternative for big batches and very low machinable materials because the electrode presents a reduced wear but the machine investment is elevated. In the classical process it is applied a direct current voltage between 5 V and 10 V, achieving feeds up to 10 mm/min. Figure II.19 shows a diagram of ECM methodology and the application of this technique under different process parameters with the aim of determining optimal ECM parameters for Ti60 related to the surface roughness (Chen Xuezhen, 2016).

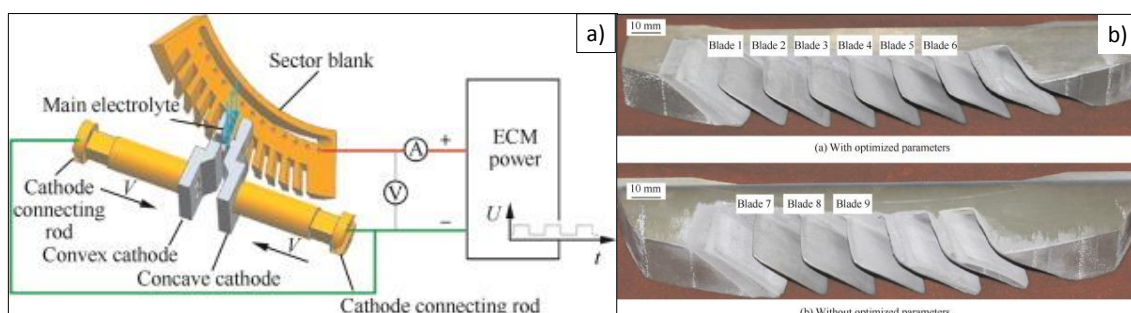


Figure II.19 a) ECM method definition for a blisk and b) Blades in Ti60 blisk using ECM (Chen Xuezhen, 2016)

The *Pulse/Precise Electro Chemical Machining* (PECM) is a variant of ECM that combines a pulsed voltage with an oscillate movement of the cathode, obtaining a better finishing accuracy. The main inconvenience presented by this process is that the machine investment is higher and cutting feeds are lower, around 0.5 mm/min (F. Klocke, 2014) (J. Zhang, 2016).

One of the main applications for these ECM and PECM techniques are the blisks located in the high-pressure turbines compressors. For aeronautical turbines the material resistance and hardness are crucial to withstand the extreme working temperatures, thus it directly impacts on material machinability, so leading to the necessity of difficult-to-cut thermoresistant superalloys, nickel forged parts, sintering materials, nickel-based alloys, among others.

#### II.4.1.4 Additive Manufacturing (AM)

Over the last three decades, the *Additive Manufacturing* (AM) has become a competitive alternative or complement in such a strict sector as the aeronautical or the automotive. This technology is still in early stages; however, it presents many new opportunities in terms of material waste and sustainability. By the end of 80s, it was developed the first generation of *Material jetting* (MJ) commercial 3D system rapid prototyping machine. During the early 90s,



The Massachusetts Institute of Technology developed the first *Binder Jetting* (BJ) methods with a powder bed similar to the actual *Powder Bed Fusion* (PBF) processes (Ian Gibson, 2015).

At the beginning, this technology was utilized for prototyping and small fixtures, but little by little, it has been expanding and replacing to other manufacturing processes for small batches. Among different AM processes, processes most commonly used for entire part creation consists on placing a flat powder layer of the part material and it is heated and solidified using electron beam (*Electron Beam Melting* or EBM) or laser (*Selective Laser Melting* or SLM) (Lawrence E. Murr, 2012). Thus, the final desired form is generated by overlapping of single layers.

The main challenges for these technologies reside on good heat dissipation generated during the process and reducing originated distortions. On the contrary, these technologies offers advantages as the good powder utilization reducing material waste and the possibility of generating impossible geometries for other technologies. The achieved tolerances for Ti and Ni based superalloys aeronautical components using AM in the order of 100  $\mu\text{m}$  or higher (F. Klocke, 2014). It should be pointed that, in the case of using AM for Ti alloys, it is necessary to consider this material tendency to oxidation; that is why the EBM technology is performed helped by an inert gas (J. Karlsson, 2014) (Shunyu Liu, 2019). Overall, the process has not the capability of achieving the tough finishing dimensional requirements, being needed a finishing stage through a material removing manufacturing process (A.L. Cooke, 2010).

In 2015, The Boeing Company filed a patent application for defining airplanes components that are going to be produced by AM, covering 300 part numbers on 10 different aircrafts; Figure II.20.a shows the components determined by Boeing patent (Koreis & Robert, 2015). Airbus is also promoting AM components in their aircrafts; the 30<sup>th</sup> March 2017 the first fully 3D printed hydraulic spoiler manifold flew in an A380 shown in Figure II.20.b (Sander, 2017).

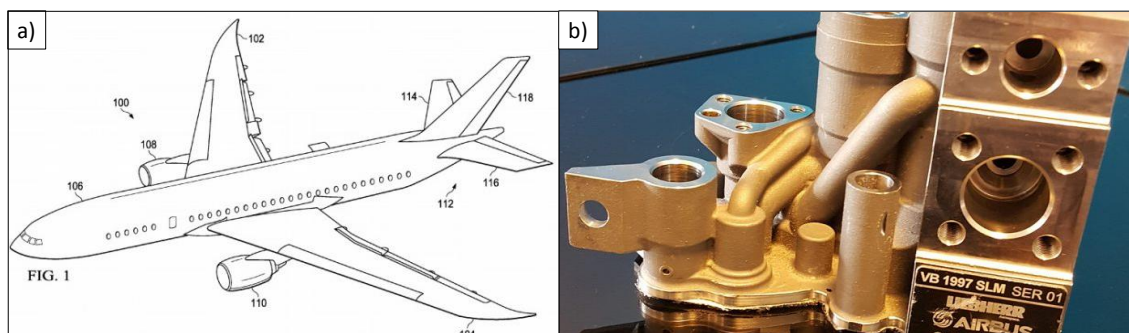


**Figure II.20** a) Schematics from Boeing patent application and b) Airbus A380 first 3D printed manifold flying

Another AM technology that is outstanding process in the aeronautical sector is the *Laser Metal Deposition* (LMD). In this technology, a laser is in charge of melting the substrate meanwhile, a nozzle injects the metallic powder to be added in the area of the melting pool. During the process performance, it is protected by inert gas streams to avoid interactions between melted materials and the oxygen (Toyserkani E., 2004). Creating consecutive clads, a layer or coating is generated and, consequently, when overlapping layer over layer it results into the 3D final desired geometry.

The LMD main applications are direct blades fabrication for small blisks and for damaged areas repairing process (Figure II.21). For repairing operations, LMD process requires previous stages: component damaged areas inspection, repairing tool-path strategies definition, studying repairing necessities and feasibility and, finally, a measuring and control stage for final obtained geometry and the material properties (J. Aschenbruck, 2014). In both the direct blades manufacturing and damaged components repair through LMD, it is required a posterior stage of machining to achieve the blades final desired geometry fulfilling tolerances requirements. Hence, this additive manufacturing process provides an initial geometry closer to the final geometry, so it is addressed inside the “Near-Net-Shape” concept. This technology is detailed in depth in the section II.5.

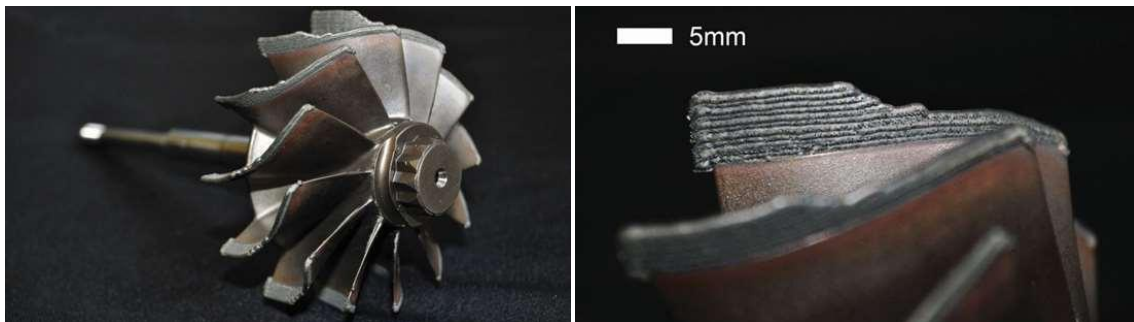


**Figure II.21** Impeller blades repairing process through hybrid manufacturing (Zelinski, 2015)

#### ***II.4.1.5 Conventional Machining Process: 5-axis Milling***

The conventional milling process consists on a rotary cutting tool that removes material from the workpiece surface until achieving final desired geometry (Brown & Sharpe Manufacturing Company, 1935). It was in 1795 when Eli Terry used the first milling machine for the clock industry (Roberts, 1994), but it was not until around 1810 when milling concept was considered independent from turning technology (Woodbury, 1972). This process suffered a drastically evolution thanks to Computers and CNC improvements by the 80s (Noble, 1984).

Nowadays, milling process embraces a numerous capabilities for complex geometries generation and multiple materials, offering flexible solutions.

Related to IBRs manufacturing processes, for medium sized impeller and blisk manufacturing, 5-axis milling is the conventional material removal process most commonly used. Thus, a complete component is machined from a solid block, obtaining a monolithic part without discontinuities between the different elements, so junctions are avoided and it is obtained superior mechanical properties. These advantages are critical for turbomachinery rotary components because they are exposed to elevated temperatures from exhaust gases (900°C-1400°C) and extreme working conditions; so heat resistant superalloys are required, such as Inconel®718 or Inconel®615. Comparing blisks with assembled disks, the component weight is reduced up to 20%, increasing the efficiency considerably, reducing at the same time the fuel consumption and gas emissions. Nonetheless, this process presents some difficulties: elevated machining times, tool costs and a surface integrity dependent on machine kinematics.

As it was mentioned previously, Ti and Ni alloys are the materials used for these type of components and they are characterized by their low machinability, so Figure II.22 shows the expected material removal rates and used cutting conditions ranges recommended for these materials and components (F.Klocke, 2013) (F. Klocke R. S., 2015).

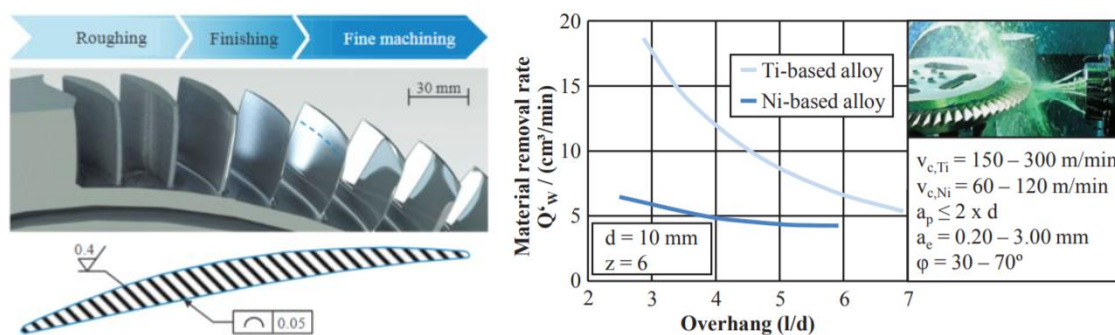


Figure II.22 High pressure compressor generic blisk specifications (F. Klocke R. S., 2015) and Ti and Ni alloys material removal rates and cutting conditions (F.Klocke, 2013)

Even though the principal impeller application manufactured by this process is the aeronautical engine, there are many applications not that popular that should be highlighted: High-speed watercrafts and motor boats, washing machines, hoovers, water propellers from firefighting trucks and ventricular assist devices.

In the case of medium-sized blisks, milling is the most usual manufacturing process, especially for titanium alloys and Inconel®718. These components are commonly placed in the medium and high-pressure turbines compressors for aeronautical engines. Being located in the

compression areas, both the high and the low pressure zones from the engines, materials need to present good resistance properties to high temperature and pressure, so once again they are made of difficult-to-cut materials, such as forged materials, casted blades, monocrystalline materials, etc. At the present time, new challenges are presented related to materials because the traditional Ti6Al4V tends to be replaced by Ti6242 and Ti6246 alloys, as well as the Inconel®718 by the DA718.

· **Cutting tools and tool holders**

One of the main advantages of the conventional milling process is the great adaptability for a huge variety of geometries and range of tool size and form that could be found in the market for many different applications. Usually, solid coated carbide mills are the tool type recommended for blisk and impeller manufacturing processes. Solid carbide mills are standardized in a range of diameters from 2-16mm; moreover, carbide tools present good tenacity and heat resistance for machining Ti and Ni superalloys (Sandvik Coromant, 2019). Besides that, indexable milling cutters are an economical alternative for some specific operations, concretely roughing operations, though their use is not very extended for these components manufacturing. Furthermore, coatings (TiAlN, TiN, AlCrN, AlCr and CrN) add real advantages to these cutting tools improving friction, temperature, oxidation and corrosion resistance.

From the tool forms point of view, frontal, frontal with corner radius and spherical are the most popular for IBRs manufacturing (Figure II.23). Frontal mill is indicated for roughing because the cutting speed depends on the tool diameter, so, in this case, it does not decrease at the tool tip. Frontal with corner radius is one alternative to the excessive cutting edges wear with 5-axis movements. Moreover, these corner radiuses are also adaptable to the blades blend so making them an option for semifinishing operations. However, conical tools are normally selected for semifinishing and finishing operations, more specifically they adapt with the entire cutting length in those cases that the surfaces are ruled. Spherical tools are used for finishing strategies. Moreover, in some cases that are concaves surfaces with small curvatures radius, spherical tools are the only feasible solution. Finally, there is a new trend to barrel shape tools, some studies around this form led to the conclusion that they are a real alternative for semifinishing and finishing non-extremely curved blades (emuge high performance tools, 2017). The main advantage of this cutting tool form resides in the curvature radius that allows to reduce the number of passes, so the machining time (E. Artetxe, 2016) (G. Urbikain, 2017).



**Figure II.23** Sandvik and Emuge-Franken milling cutting tool forms for IBRs manufacturing

In addition to the foregoing, the adequate choice of the tool holder has also influence on the milling process. On the one hand, each holder type presents different characteristics in terms of accuracy, clamping forces or lubricooling systems. On the other hand, milling strategies closer to blades blends require a holder with smaller body to avoid collisions. Hence, thermal tool holders fit with these requirements.

#### · **Manufacturing strategies**

By now, manufacturing processes for complex geometries are still a subject matter for many researchers related to the number of aspects involved. In the first instance, it should be outlined that the programming of these complex geometries machining strategies it is commonly performed supported by CAM software, since manually programming is practically impossible. It is true that finishing strategies are the ones that have more influence on the final geometry and surface tolerances. Nevertheless, Roughing and semifinishing strategies, previous to finishing stages, require special attention because it is at those stages the machining process productivity can be optimised (K. Morishige, 1997) (E. Abele, 2017).

IBRs manufacturing processes optimization is focused on prioritising the productivity for roughing strategies and accuracy for semifinishing and finishing strategies. Productivity mainly depends on the machining times and tool cost. Despite of the great technological advances related to milling cutting tools, the IBRs manufacturing is still requiring the use of a lot of milling tools due to the tool wear and breakage. In addition, the increase of the productivity with aggressive cutting conditions and strategies implies the rise of tool wear. Therefore, the main objective for roughing stage is achieving a balance between productivity and process costs.



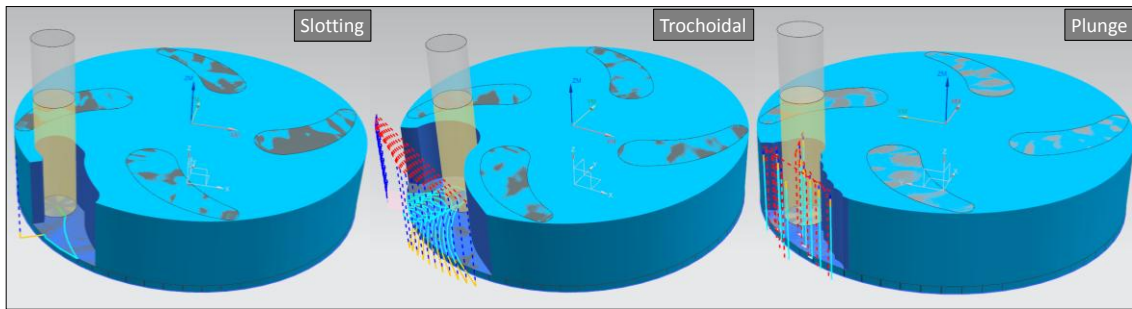


Figure II.24 IBRs roughing strategies: slotting, trochoidal and plunge milling

Figure II.24 shows three of the most applied roughing strategies: *slotting*, *trochoidal milling* and *plunge milling*. *Full slotting* strategy consists on using the complete diameter as the radial depth of cut ( $a_e$ ). The main advantages of this strategy are the high material removal rates in steady state and the simplicity of the required tool-path. Nevertheless, this strategy causes elevated radial cutting forces so in some cases the axial cutting depth needs to be performed in many passes. *Trochoidal milling* combines the tool linear movement with circular trajectories, implying less tool wear compared with slotting (A. Pleta, 2018). Moreover, radial cutting forces are smaller what offers the option to use higher cutting speed and axial depth of cut. The main drawback of trochoidal milling is that requires higher machine dynamic capabilities to perform the continuous circular movements (G. Kappmeyer, 2012). At the *plunge milling*, the tool moves along the tool axis (z-axis), the machining is performed with the secondary edge and lateral vibrations are avoided. Some plunge applications are cited hereafter: deep slots, insufficient stability and materials with low machinability (L.N. López de Lacalle, 2011). Finally, General Electric patented an alternative for roughing curved slots using indexable milling cutters instead of solid carbide tools (GE International Inc, 2013).

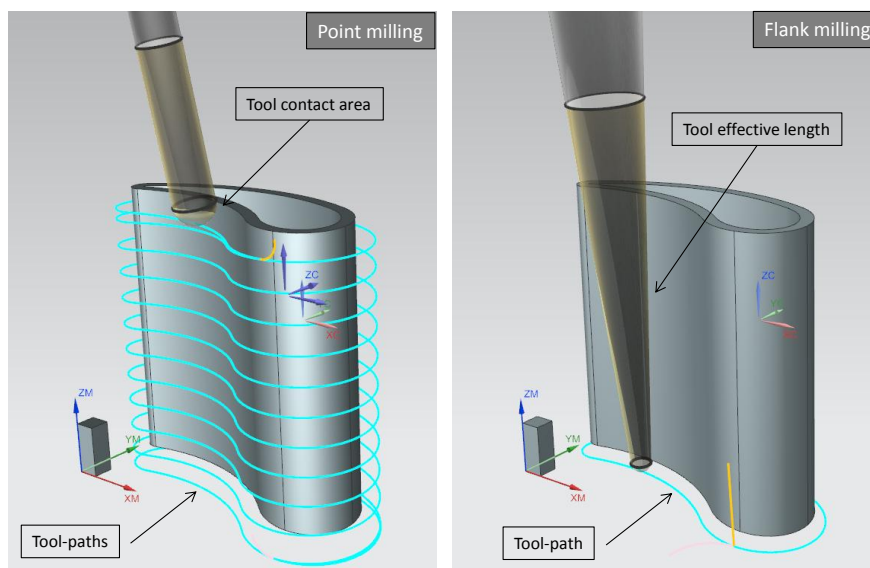


Figure II.25 Point milling and flank milling applied to a single blade

On the other side, semifinishing and finishing strategies define final geometry, dimensional tolerances and surface finishing requirements. Milling strategies are categorized as a function of the tool contact surface during the machining, differing two types for complex geometries: *point milling* and *flank milling* (Figure II.25). The *point milling* strategy is performed with ball-nose cutting tools and the material removal is conducted with the spherical side of the milling tool. This strategy main drawback resides on high machining time and the extreme tool wear because it is constantly cutting with the same tool region. On the contrary, at *flank milling* strategy, the machining is performed with the total effective length of the tool, so the productivity of this strategy is higher than the *point milling*; reducing machining times and making the maximum use of tool cutting edges. Nonetheless, this is not always a useful option for complex geometries because the accuracy of this strategy depends on the surface type, being necessary a developable ruled surface for its adequate application. Moreover, another inconvenient of this strategy is found in the operation stability, since it is much influenced by the defined cutting parameters; if they are not the appropriate ones, there is a possibility of vibrations appearance; leading to inadmissible finishing requirements. On top of that, for difficult-to-cut materials it should be pointed out that the bigger the contact between tool and part is, the higher power, stability, chip evacuation and machine capabilities are required.

In those cases that the geometries to be machined are developable ruled surfaces, the tool flank is maintained tangent to the surface along the entire tool axis. Therefore, *flank milling* strategies keep that tangential contact between the tool axis and the surface along each generatrix that defines the surface, permitting the use of the total effective tool length as the axial depth of cut ( $a_p$ ). This leads to a more productive process, with higher material removal rates and a machine time and cost reduction. Nevertheless, to ensure the process stability and efficiency it is required the use of tools with big dimensions, reducing bending risks and vibration appearances inherent to this strategy.

It is important to emphasize the differences between developable and non-developable ruled surfaces, because the use of *flank milling* for non-developable surfaces implies an error studied by Senatore et al. (J. Senatore, 2008). The error expression was reduced analytically to an expression that relates the radius of the tool and the angle between the tangent planes at both extremes of the surface isoparametrics. Additionally, Senatore considered three special cases: (1) the radius of curvature  $\rho_i$  is larger than the tool radius, (2) when the twist angle ( $\alpha_i$ ) is small and (3) a combination of both,  $\rho_i$  larger than the tool radius and a small twist angle; being this last case, the one that fits with the ruled surfaces used for turbine blades. Figure II.26

shows the tool cut into cross sections and the principle for error estimation (Figure II.26.a) and a case of application for error calculation where the grazing curve was calculated for tool positions and the error is plotted below (Figure II.26.b).

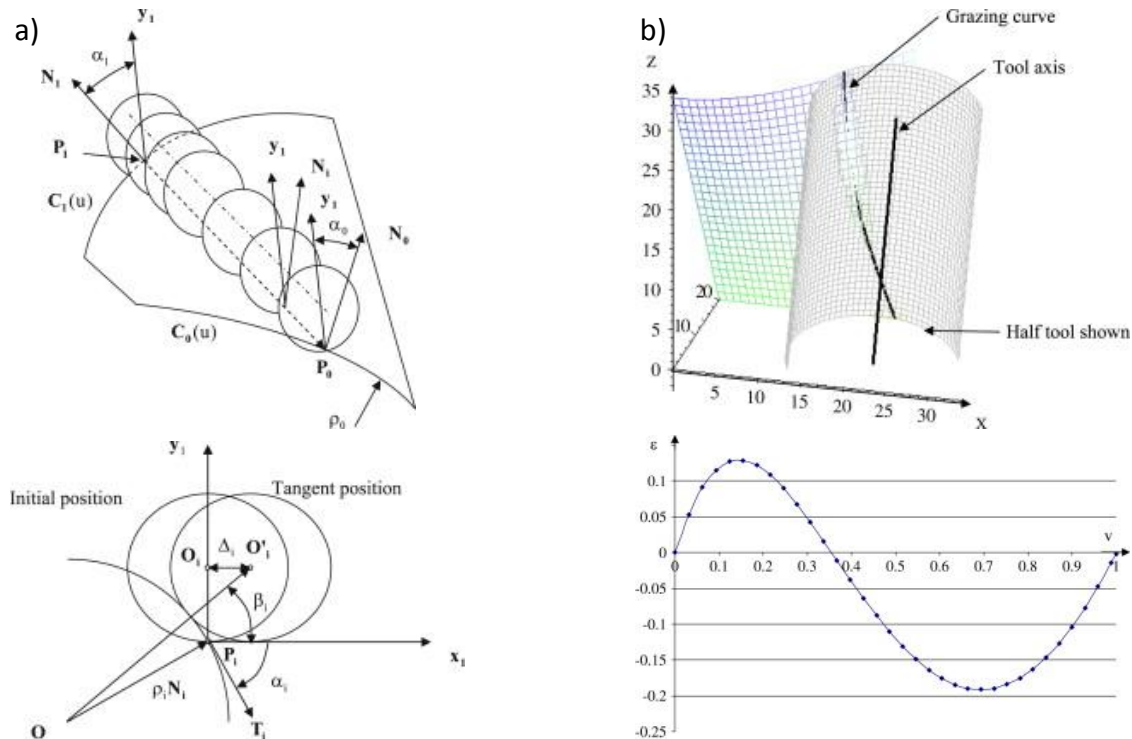


Figure II.26 Error estimation by (J. Senatore, 2008) : (a) tool cut position and principle of error and (b) a case study for this error estimation

For that reason, if the ruled surface is developable both tangent planes to the isoparametric are coincident, leading to a null error. It is noteworthy that there are numerous researches about *flank milling* optimization algorithms. Some of them are based on a surface approximation to the tool envelope and tool axis position optimization for each point in the surface to be machined. These algorithms for strategies optimization are described more in detail in the subsection II.4.2.

#### II.4.1.6 Super Abrasive Machining (SAM)

As it was mentioned previously, IBRs present many challenges related to the low machinability combined with difficult geometries and finishing requirements. These issues lead to optimising traditional manufacturing processes, improving cutting strategies, new tools design, and cooling techniques. Along this chapter, many manufacturing processes, commonly used for manufacturing those components, were detailed. On the one hand, traditional or conventional manufacturing processes were explained; this is the case of milling. On the other hand, non-



conventional manufacturing technologies were considered as an alternative, i.e. *electrochemical machining* (ECM) or *electro-discharge machining* (EDM).

Notwithstanding, abrasive processes need to be considered as a possible alternative for IBRs manufacturing. There are some non-conventional abrasive technologies (*Abrasive flow machining, magnetic abrasive finishing* or *magneto-rheological abrasive flow finishing*) characterized by their good performance for complex geometrical cavities with limited accessibility for conventional processes, achieving great dimensional accuracies and finishing surface quality requirements (Dehghan Ghadikolaei, 2014). However, at the same time, these processes present low material removal rates, implying less productivity in terms of machining time and costs (Flaño O., 2018).

In the last decade, a new abrasive process was born, known as *Super Abrasive Machining* (SAM), on the path of finding innovative technologies to cover these productivity issues. R. Petrilli (Petrilli, 2012) defined this process as “grinding at machining rates”. Therefore, this technology provides, under similar cutting conditions of single point machining, a finishing precisions closer to grinding technology, what makes this process more versatile than grinding or milling techniques. The main difference between the conventional grinding and SAM is that grinding is commonly used for low material removal rates oriented to achieve final size and finishing requirements; in contrast, SAM is more adaptive for a variety and complex geometries and higher material removal rates, offering as well, elevated accuracy and surface quality. A notable difference between both processes resides on the type of abrasive tools used; SAM abrasive tools (see Figure II.27) covers a wide range of small geometries - diameters  $\leq 25\text{mm}$  - and they consists on single layer electroplated superabrasive grinding wheels. Nonetheless, it also needs to be stressed that rotational speeds required to obtain the adequate peripheral cutting speeds are very high, in most of the cases over 50,000 rpms (D.K. Aspinwall S. S., 2007). Additionally, it is noteworthy that using these kinds of tools, due to process temperature and extreme cutting conditions, cutting fluids are required, particularly cutting oil (Caggiano A., 2009) (Sinha M.K., 2017).

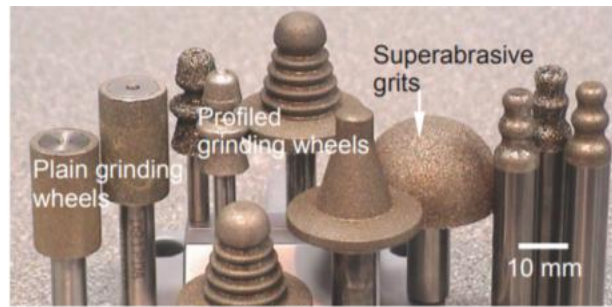


Figure II.27 A variety of SAM tools geometries (D.K. Aspinwall S. S., 2007)

The grinding technique considered as the closest rival to SAM is *creep feed grinding* (CFG), characterized by large cutting depths ( $a_p = 0.1-30$  mm) and high cutting speeds ( $v_c = 20-30$  m/s). Comparing both techniques, SAM achieves the equivalent amount of material removed at higher speeds, with lower workpiece loads, and more accurate dimensional tolerances (Włodzimierz Wilk, 2008); since these advantages make SAM a suitable and efficient alternative to manufacture IBRs nickel-based superalloys (Erickson, 2011).

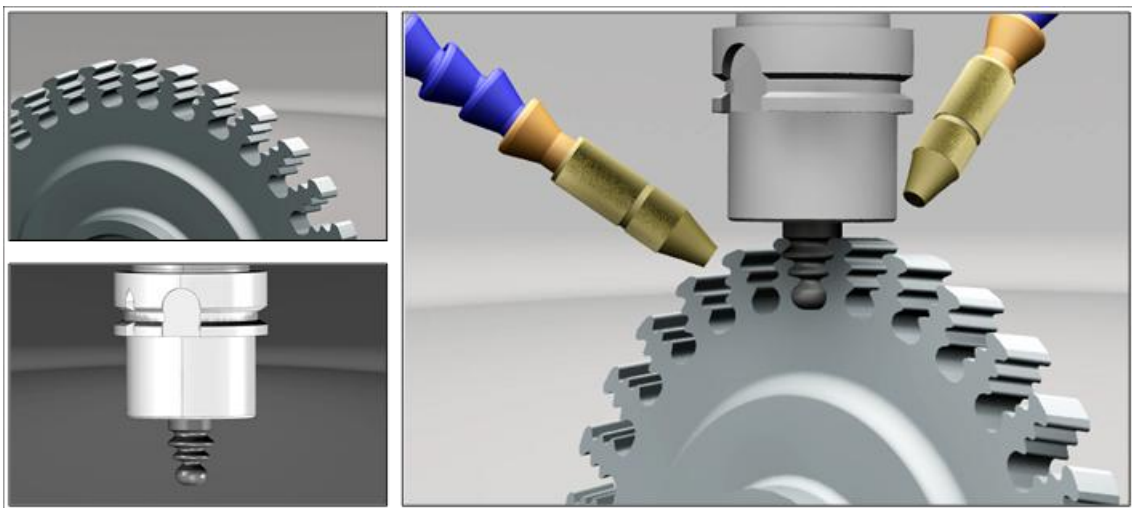


Figure II.28 Bladed disc fir-trees manufacturing using SAM

The use of SAM is recommended for three main application groups: (1) there are some manufacturing processes divided into different stages of machining, grinding and heat treatments, so in these cases, SAM could reduce all stages into only one. (2) The use on components from other near net shape processes. (3) Formed slots and flat surfaces finishing operations. Figure II.28 shows some of the initial target for SAM application: fir-trees that are the junction area between the disc and single blades. Traditionally, these components are manufactured by broaching, however this process is considered not cost effective and a time consuming. Therefore, (D.K. Aspinwall S. S., 2007) performed a set of experiments with single layer electroplated CBN and diamonds wheels to manufacture fir tree roots using SAM process. For the same application field, Curtis et al. (Curtis D.T., 2009) performed

electrochemical SAM experiments on finishing fir trees analysing roughness and overcut, observing low forces (37 N) with an average depth of cut of 0.92 mm.

Furthermore, SAM was presented in (Włodzimierz Wilk, 2008) as a solution to increase machining efficiency during the production of blades and turbine disks. Moreover, it was tested with other more complex geometries, such as the blades from IBRs or impellers. In fact, Rolls-Royce claims, under the correct performance, that the process is capable of stock removal at a rate of 80 cubic millimetres per second per millimetre of wheel width. That is, eight times the achievable rate using plated CBN wheel technology for super abrasive machining of nickel alloys on a conventional grinding machine (Fritz Klocke, 2015).

In a similar manner to the tendency of *flank milling*, *flank SAM* is also considered as a more productive and effective process. Hence, Wu presented in (Wu, 2012) a solution for obtaining Pratt and Whitney non-developable blisk geometry through *flank SAM*. As it was mentioned before, non-developable surfaces are not suitable for flank techniques, so this author proposed a surface modification, preserving aerodynamics and structural properties, and supplement the manufacturing process with new tool paths and shaped cutting tools (Figure II.29.a). The results shown in Figure II.29.b a successful process in which the combination of flank SAM technology with the shaped cutting tools open the possibility of new surface designs more efficient aerodynamically. For that purpose, the developed method follows these steps: (1) redesigning blade surface for improving the performance; (2) adapting the designed surface to make feasible *flank SAM* technique, iterating mechanical, aerodynamic and structural simulations; and finally, (3) blade manufacturing using two CBN electroplated abrasive tools, one for suction surface and another one for pressure surface (Figure II.29.a).

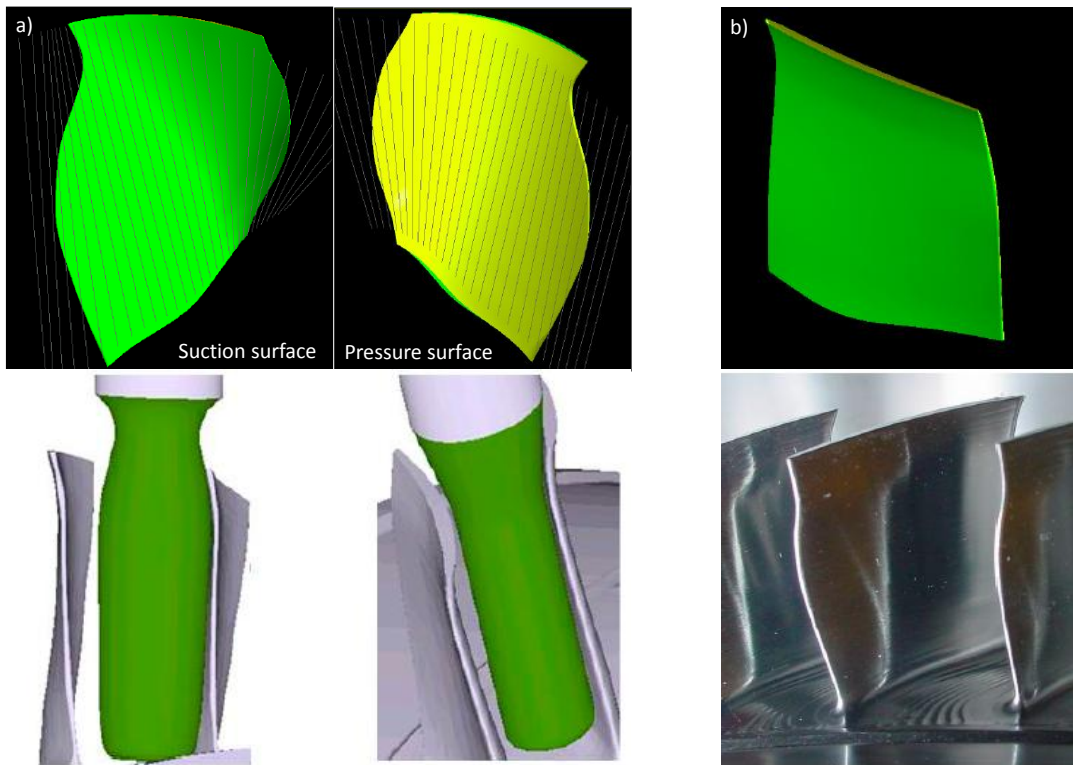
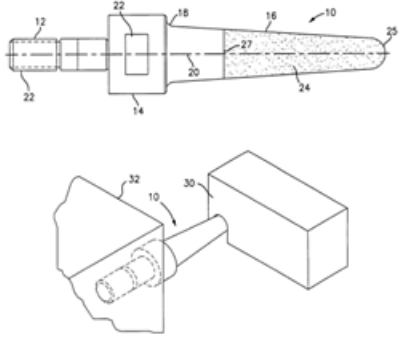
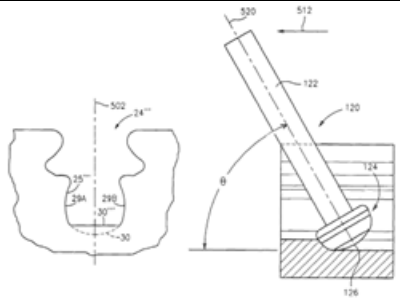
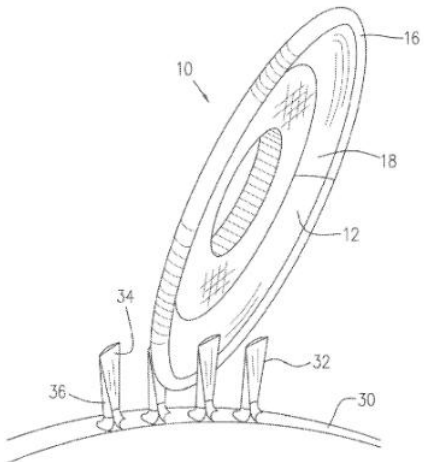
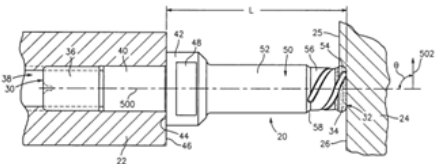


Figure II.29 IBR flank SAM: (a) Final tool paths using iteration and shaped tool and (b) surface finishing estimation and obtained final component (Wu, 2012)

Finally, Table II.1 shows a summary of the most significant patents related to super abrasive tools and main applications, frequently developed by the main turbine manufacturer as Pratt and Whitney, General electric and United Technologies Corporation (UTC), among others.

Table II.1 Patents related to super abrasive machining

| Patent Number & Title   | Description   | Figures |
|---|---|---------|
| <p>US 7144307 Point abrasive machining of nickel alloys. UTC. (Brian J. Schwartz, 2006)</p> | <p>This patent develops a superabrasive manufacturing process similar to point milling strategy for nickel-based alloys. The used tool consists on a specific tool coated with abrasive material.</p> |         |

|  |  |  |
|--|--|--|
| <p>US 7101263 Flank superabrasive machining. <b>UTC.</b> (Brian J. Schwartz B. D., 2006)</p>                             | <p>This patent develops a new superabrasive conical tool for using flank SAM on complex geometries as turbine blades.</p>  |    |
| <p>US 7007382 Slot machining. <b>UTC.</b> (Mantel, 2006)</p>   | <p>This patent presents a methodology for initial slots in fir-trees in three different stages. (1) Slot base, (2) right lateral side and (3) left lateral side.</p> |    |
| <p>US7303461B1 Method of machining airfoils by disc tools. <b>Pratt and Whitney.</b> (Marc Lorenzo Campomanes, 2007)</p> | <p>This patent develops a grinding peripheral strategy to remove material on airfoils discs using multi-axis simultaneous motions.</p>                               |   |
| <p>US 7789732 Superabrasive tool. <b>UTC.</b> (Daniel F. Grady, 2010)</p>  | <p>A special abrasive machining tool for point machining in different steps. The body is composed of a tool tip abrasive coating.</p>                                |  |

|   |  |  |
|---|--|--|
| <p>US 7896728 Machining methods using superabrasive tool.<br/><b>UTC.</b> (Brian J. Schwartz D. F., 2011)</p>                             | <p>A tool for abrasive machining with a concave abrasive coated protuberance at the tip end and a radial span at least 20% of the protuberance radius.</p> |  |
| <p>EP 2705926 A1 Finishing process for making blade slots in a rotor disc. <b>Fidia SpA &amp; GE Avo SRL.</b> (Marco Cherubini, 2014)</p> | <p>This patent filed a finishing process for fir trees manufacturing using a grinding tool along trochoidal paths.</p>                                     |  |

#### II.4.2. Algorithms to optimise manufacturing processes

The generation of 5-axis simultaneous tool paths for manufacturing free form surfaces has been a growing field of research in recent years and covers multiple areas derived from the large number of factors involved in manufacturing processes. In particular, many algorithms are developed with the aim of improving machining strategies and obtaining a more productive process. These algorithms are programmed around three main crucial aspects: tool-paths generation, optimal tool position and the avoidance of collisions (T.D., 2014). Nevertheless, the three aspects are correlated between them, thus the global solution to optimal strategies programming is divided in turn into the following stages: (1) Tool definition or selection, (2) tool-path pattern and direction definition, (3) surface contact points specification and finally, (4) local and global collisions free verification to obtain tool axis orientation. The provided solution must meet the requirements of being free of collisions, fulfilling defined tolerances and minimizing machining time. Moreover, developed algorithms need to be efficient in terms of computational costs, memory usage and be adaptive to a spread range of surfaces.

Related to IBRs, there is a common issue presented during the machining of warped surfaces consisted on the appearance of machining marks because of the sudden movements between free collision positions. With the aim of facing this issue, Chen et al. (Chen H.P., 2009) proposed a solution smoothing the tool paths performed by a ball end mills, modifying and adapting rotational positions inside the collisions free zone. In line with this solution and oriented to blisk geometries, Tung et Tso (Tung C., 2011) used boundary surfaces to prevent extreme tool orientation changes between two points.

The traditional tool-paths generation methods are iso-parametric, iso-planar and iso-scallop (Figure II.30). The iso-parametric consists on generating the tool-paths maintaining constant one parameter of the parametric surface (Loney G.C., 1987). The iso-planar, instead, generates the tool-paths dividing the surfaces into parallels planes in the Cartesian space, constraining it by the finishing required scallop. However, the defined constrain could offer a conservative solution not very productive and with excessive surface quality (Han Z.L., 1999). Finally, the iso-scallop method is based on keeping the scallop height constant along the entire surface, optimising the successive stages from an initial pattern (Lin R.S., 1996). Shokrollahi and Shojaei (N. SHOKROLLAHI, 2014) performed an experimental comparison between the three different methods machining an sculptured surface, concretely a double curvature surface, concluding that for this type of surfaces the optimal method is the iso-scallop in terms of finishing tolerances and balanced with machining time.

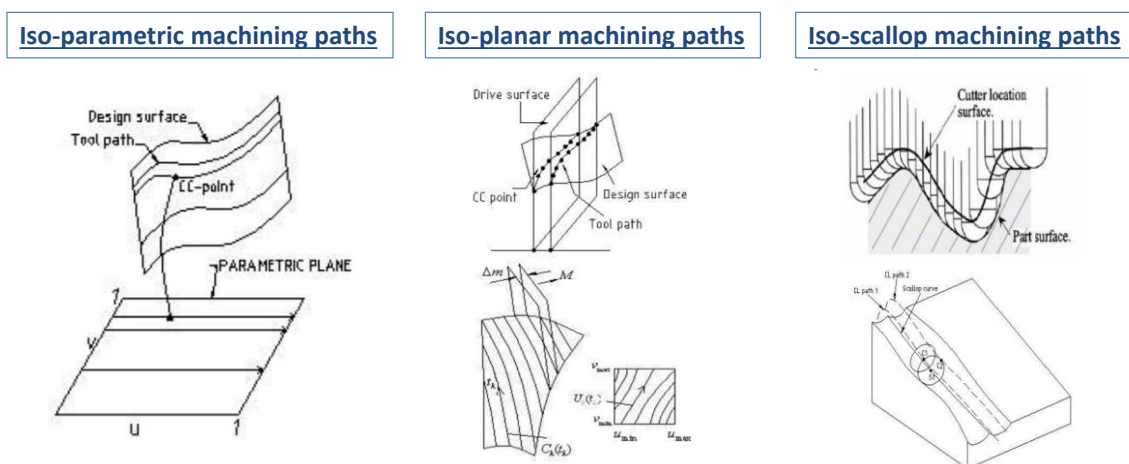


Figure II.30 Traditional tool-paths generation methods: iso parametric, iso planar and iso scallop (N. SHOKROLLAHI, 2014)

Among the most recent developments in tool-paths definition methods, it is found the *C-space* (*Configuration space methods*) presented by Choi et al. (Choi B.K., 1997) and Morishige et al. (Morishige K., 1997). This method analyses possible configuration for a solid/rigid component with a determined levels of freedom and represented as points in a C- space. These points



depend on the levels of freedom and the obstacles position. Thus, it offers the chance to know which combinations are free of collisions. Figure II.31 shows the C-space method applied and the analysis of the feasible regions to be machined (Cha-Soo Jun, 2003). Another technique for tool orientation definition avoiding local collisions is known as *Rolling Ball Method* (RBM) (Yuan-Shin Lee, 2000). This method calculates different tool adjusting the contact point in curve sections avoiding local collisions, Figure II.31 shows a tool-path calculated through RBM where  $P_i$  are the tool contact points and it is also marked a critical region to be machined with smaller radius tool.

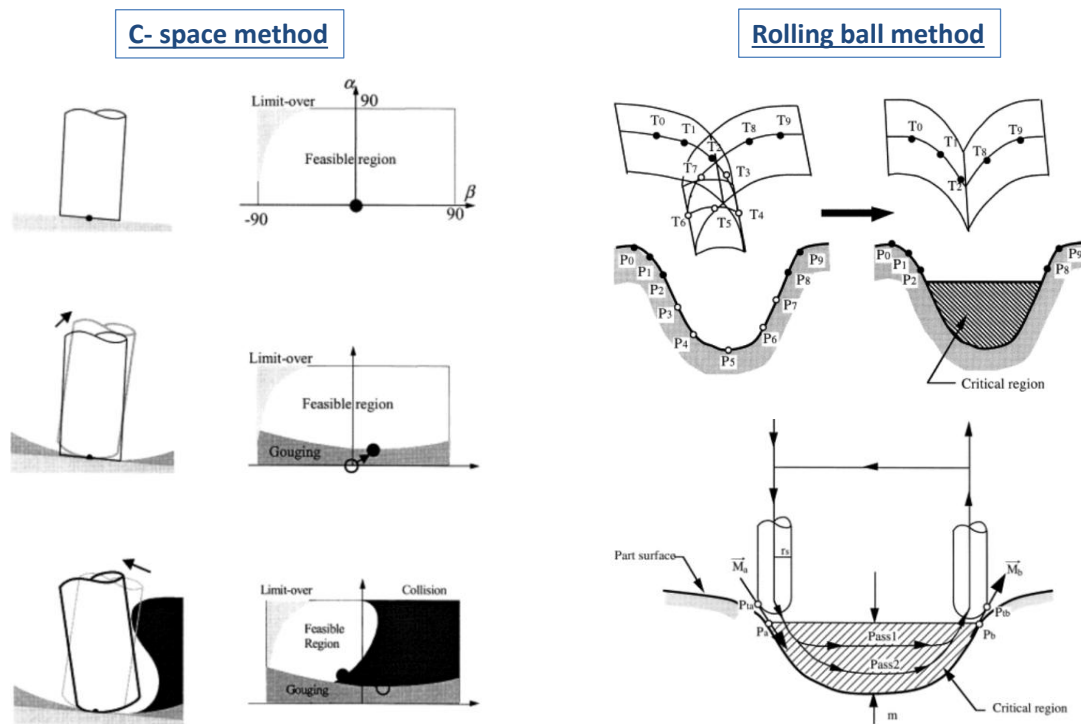


Figure II.31 (left) C-space method & (right) Rolling Ball method (Cha-Soo Jun, 2003)

By following the same objective and related to roughing strategies for non-ruled complex geometries, Fan et al. (Fan H.Z., 2013) developed a solution calculating a ruled surface around the original non-ruled surface, simplifying calculus and tool-paths. Heo et al. (Heo E.Y., 2008) proposed a methodology dividing impeller roughing into 3+2 axes operations, calculating free of collisions regions for tool-paths. Qi et al. (Qi R., 2009) also analysed the possibility of roughing strategies optimization for these types of components using an algorithm that calculated the optimal tool diameter. Additionally, for 5-axis machining, the process is composed of two surfaces, the guiding surface and the orientation surface; the guiding surface is the one that ensure the geometrical compliance and the orientation surface provides the tool orientation (Lavernhe S, 2008).



As it was mentioned previously, *flank* strategies present the most productive solution in terms of machining times and costs; that is why in recent years many studies were developed to reduce the tool positioning error relative to the generatrix of the non-developable ruled surfaces. Tool repositioning methods are mainly divided into two different types, analytics and numerical; the first ones are easier to be implemented but obtained errors are bigger than numerical ones (Senatore J., 2012). Some of these published works were focused on obtaining a surface to be machining using *flank milling* strategies preserving aerodynamic properties and structural integrity near to the original surface (Li C., 2007) (Gong H. W. N., 2009), another ones developed flank milling multistage techniques or tool geometry customization according to the surface (Wu C.Y., 1995).

Bo et al. (Bo P., 2016) presented an algorithm that contemplated all defined stages, the approximation using envelopes to the free-form surface, a method that offers the optimal tool geometry and tool axis position (Figure II.32.b) and the differences presented in terms of accuracy for single patch or multipatches (Figure II.32.a). These types of algorithms allows to achieve a balance between optimal tool shape and position combined with the most productive tool-path. Following this line, Bo and Barton (Bo Pengbo, 2019) presented an initialization algorithm for initial 5-axis milling paths of general tools easily found in standard tools manufacturers.

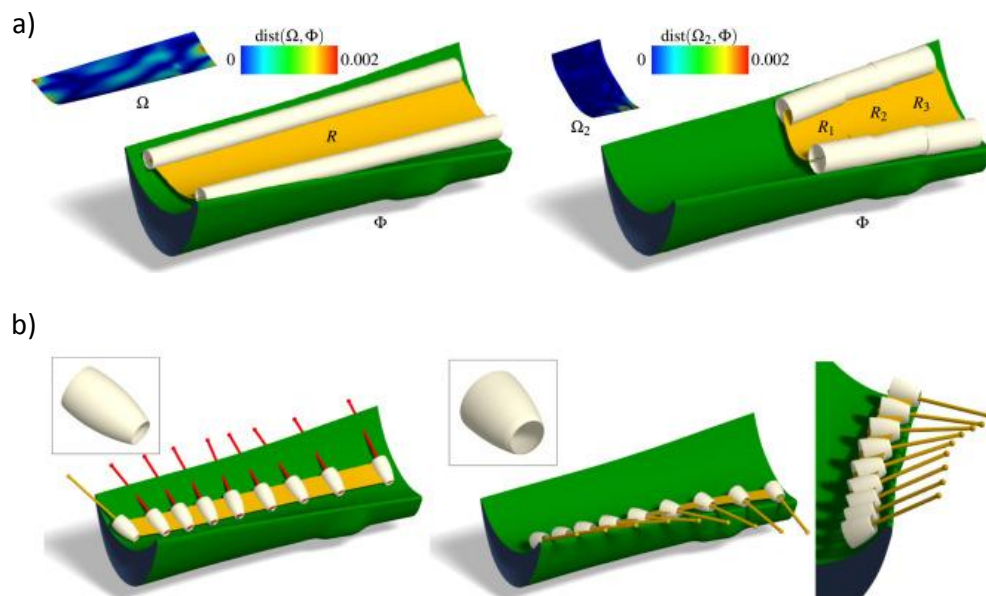


**Figure II.32** 5-axis free-form surface approximation algorithm (Bo P., 2016): (a) Differences between the number of patches (b) different tool positions and geometries

## II.5. Hybrid manufacturing systems and multitasking machines

On the path of optimising manufacturing processes, it should be pointed out that achieving a complete and reliable manufacturing process of complex geometries requires considering all factors involved in the entire manufacturing chain. For that purpose, Gonzalez-Barrio et al. presented a holistic approach diagram that collects critical variables for the majority of productive processes (Figure II.33). Finally, this global approach was applied to a single blade initially manufactured by additive manufacturing and going through the defined sets: inputs, machine, modelling & process, monitoring & control and obtained outputs. (Gonzalez-Barrio, 2018).

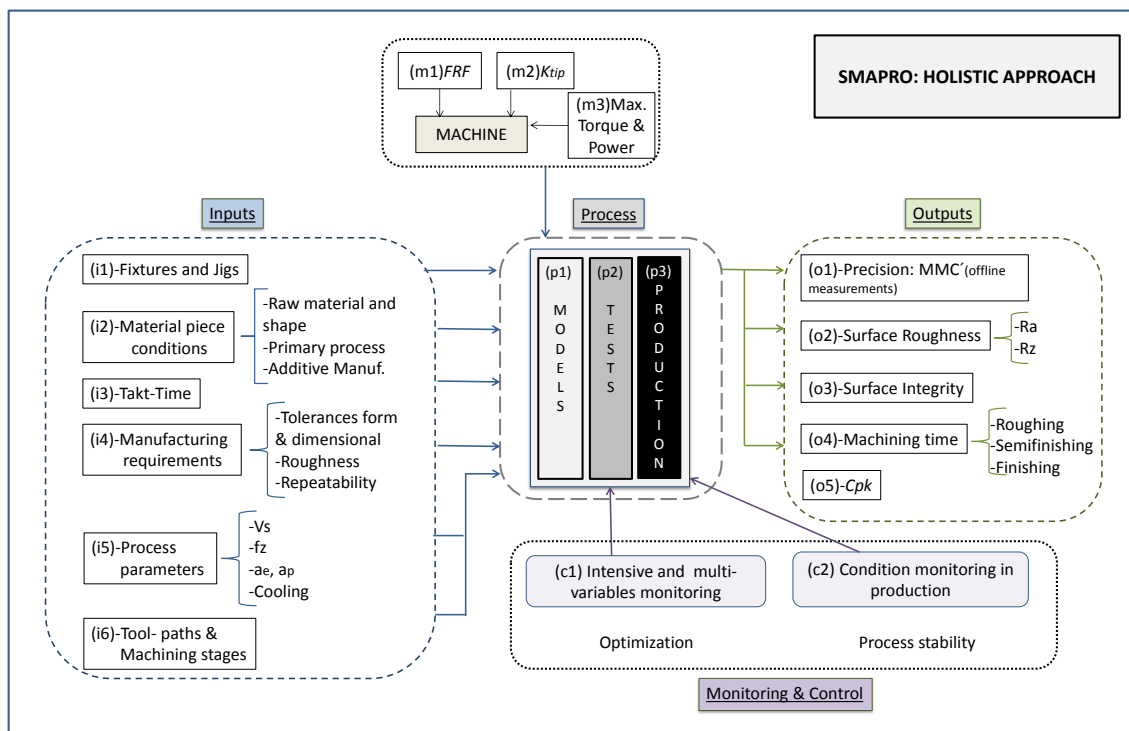


Figure II.33 Global approach for manufacturing processes, considering modelling and monitoring (Gonzalez-Barrio, 2018)

With the main objective of addressing these aspects, the machine-tool sector has evolved to adequate to industrial requirements of the time. Traditionally, there were two main machine-tool typologies: milling and turning. Notwithstanding, it was by the end of 90s when both technologies appeared integrated in the same machine, giving rise to the concept of multitasking machining. These evolutions are derived from the necessity of optimising entire product manufacturing chains, combining different manufacturing process, reducing material waste, machining times and machine/tools costs (Nagae A, 2012). In addition, one of the main

advantages presented by the multitasking concept is the reduction of human resources, batching various processes inside the same machine. Chronologically, there are some advances considered key milestones in the multitasking evolution history and main machine-tools developers: (1) in 1982 WFL<sup>®</sup> presented the machined WNC 500S Millturn, (2) in 2000 Nakamura Tome<sup>®</sup> presented Super Multi-tasking machine STW-40, (3) in 2001 Mazak<sup>®</sup> developed the INTEGREX multitasking machines family, (4) in 2005 DMG/MORI<sup>®</sup> presented the NT Series, (5) in 2007 GMTK<sup>®</sup> and Ibarmia<sup>®</sup> designed GEMINIS VL the ZVH multiprocess family respectively, (6) in 2011 Soraluca<sup>®</sup> presented the F-MT mill turning centre and (7) in 2014 DMG/MORI<sup>®</sup> burst into the market the new hybrid manufacturing machine LASERTEC 65D combining additive manufacturing and subtractive manufacturing.

The need of multitasking developments is a reality to embrace new horizons derived from the globalization challenges as mass customization or global market competitiveness. Accordingly, the combination of different processes opened its doors to new process and mix conventional and non-conventional processes with the aim of offering a more flexible solution for industrial requirements; i.e. super abrasive machining (SAM), deep boring, taper boring with U-axis tool, hobbing, different grinding processes, electro discharge machining (EDM), turning or additive manufacturing (Calleja-Ochoa A., 2017). Among multitasking machines configurations, the mix of additive and subtractive manufacturing processes is a combination of processes that stands out with special interest. This new concept of hybrid AM/SM led machine tool manufacturers to develop hybrid machines, giving a solution to this new era and fulfil industrial expectations. Related to multitasking machines, DMG MORI SEIKI AG is considered one of the pioneers; presenting the Lasertec 65 Additive Manufacturing model (Figure II.34), a hybrid machine combining LMD with milling (DMG MORI, 2014). Moreover, following this line of hybrid manufacturing; other machine tools suppliers joined that initiative, for example IBARMIA<sup>®</sup> presented in the EMO 2015 (Milan) IBARMIA<sup>®</sup> ADD+PROCESS ZVH, combining AM with turning and milling operations (IBARMIA INNOVATEK, 2015). MAZAK presented the INTEGREX i-400AM able to change the cladding nozzles adapting to different needs (Mazak, 2015), WFL developed M80 MILLTURN multitasking machine with 6Kw laser integration (Allcock, 2015) and, in the same line, HERMLE presented the model MPA 40 that integrates AM in a 5-axis machining centre thought for large components (Hermle, 2016). Finally, It should be pointed that AM is not only combined with milling/turning technologies, ELB Eib-Schliff WZM developed a machine called MILLGRIND that combines AM with milling and grinding technologies (Elb-Schliff, 2016).



Figure II.34 Lasertec 65 Additive Manufacturing model from DMG MORI SEIKI AG

### ***II.5.2. Hybrid manufacturing systems inside the Industry 4.0 context***

A fundamental key to understand the hybrid manufacturing (AM/SM) success is the present industrial contextualization. The fourth industrial revolution, known as Industry 4.0, was born originally at the Hannover Messe in Germany in 2011 and it has become one of the most popular issues for industrial and academic fields (V. Roblek, 2016) (F. Chiarello, 2018). Last digital advances and technologies support this era and brought new concepts such as digitalization, cloud computing, the internet of thing, big data and smart manufacturing. Additionally, EU countries are facing Industry 4.0 challenges dividing the level between Big Data maturity and the Industry 4.0 infrastructure; some countries as Luxembourg, Czech Republic, Estonia, Portugal, Slovakia, Slovenia, France and Italy presents the optimal balance between both concepts (Castelo-Branco I., 2019).

Hermann et al. (Hermann M., 2016) stated four design principles that help to understand and define the Industry 4.0 main covertures: (a) Interoperability: Connexions between machines, devices, sensors and people in a flexible manner; giving rise to Smart Factories. (b) Information transparency: elaborate a virtual copy of the physical word to spread the information of the different processes. There is an increase of sensors to acquire higher quantity of information to enrich the digital plant. (c) Technical assistance: user-friendly interfaces to support operators with visual assistance and facilitate making decisions and solving urgent problems quickly. (c) Decentralized decisions: development of cyber physical systems to make decisions decentralized and autonomously, reducing human and technological resources. With the aim of defining the potential of this environment, Figure II.35 gathers a digital compass with the choices of this philosophy divided into eight basic value drivers and 26 practical levers in order to orientate the manufacturing sector and analyse the application areas (D. Baur, 2015).



Figure II.35 Digital compass for Industry 4.0 philosophy application (D. Baur, 2015)

Concurrently, linked with the Industry 4.0 it could be found a promotion for sustainability, more environmentally friendly process and circular economy. The circular economy main objectives is change the “end-of-life” concept, opting for restoration, recycling, remanufacturing, reusing and refurbishing, eliminating resources wastage. Here is where the hybrid manufacturing (AM/SM) acquires great importance providing opportunities to repair damaged parts instead of discarding them (Yang S., 2018). Additionally, it brings extra benefits as reducing material waste, high flexibility for complex geometries and materials and reducing machines and human resources. To contribute to the state of the art related to hybrid manufacturing, Flynn et al. (Flynn J.M., 2016) studied the developments of AM/SM from an industrial and scientific point of view, analysing future challenges and opportunities related to material, process, software and industrial requirements; presenting numerous fields of applications for AM/SM hybrid manufacturing systems.

### ***II.5.2. Process integration and digitalization: Digital twins***

The digitalization of manufacturing processes is still in a critical stage of development; the number of variables involved, the difficulties of communication between machine and designing software and, finally, the post-processing and standardization have become a handicap studied for recent researches (Rosen R., 2015) (Abramovici G., 2016). Derived from this idea of digitalization and smart manufacturing, the concept *digital twin* (DT) came up with the aim of developing a more autonomous and competitive process (Schleich A., 2017). The DT concept is described as a digital representation of any product, service or production system and all parameters or characteristics involved in them, in order to evaluate and improve the real process reducing resources. The beginning of this concept was the virtual prototyping that present simulation of functional behaviour, virtual validation and prediction (Stark K., 2017). With the purpose of understanding deeper the DT environment, (Stark R., 2019) presented a structured approach for planning the scope and the type of DT, named as “digital twin 8-dimension model” shown in Figure II.36. This model is divided into 8 different dimensions of application; inside each dimension, there are found multiple target levels to support business and industries individually and serve as guidance for new product/service definition and extend existing products with DT knowledge. Moreover, it should be mentioned that DT is constantly learning from the past data and the present process. The main objectives for the Smart Factory and the DT could be grouped into the following points:

- Condition monitoring: Sensors play an important role in this objective; every single step inside the manufacturing chain is monitored: consumption, transports, movements, etc.
- Control: for this purpose, simulations and modelling reproduce the individualized manufacturing process, this point aligned with real manufacturing information feed the DT to be closer to the reality. One application is the avoidance of collisions or intrusions that would stop the process before any production issue.
- Real-time simulation: the information about the actual status of the process and the situation of every object/parameter involved in the process continuously updated for the DT real time simulation. They are directly connected to the machines and robots to interact as quickly as required.





Figure II.36 Digital twin 8-dimension model (Stark R., 2019)

One of the first DT in the industry was presented by NASA; in that case it was monitored and analysed the behaviour of one satellite and it was performed a simulation showing how different changes in the setting could affect to that behaviour (Grieves M., 2017).

## II.6. Repairing processes

Industries dedicated to manufacture high-added value components are betting on innovative processes and the trend of remanufacturing and repairing these components, looking for more financial and sustainable solutions or alternatives to conventional manufacturing processes. Among those innovative processes, laser based technologies are gaining more importance day by day due to the fact that they are easy to automate, the absence of cutting forces and the rapid processing.

The additive of material is the one that presents more versatility, extending its application from coatings generation to complete component direct fabrication. These technologies consist on depositing a thin layer of metal on a moving substrate. This deposition could be performed by powder injection or wire feeding; comparing both depositing methods, the

powder injection is the most flexible and extended one. In this process, the laser beam melts both, the substrate and the powder particles, depositing a track of the metallic powder on the substrate (Toyserkani E. K. A., 2005). When the tracks are overlapped, a layer is presented and then, layer-by-layer strategies are used for producing complex geometries and freeform design. The process presents high flexibility and reducing material waste, obtaining near-net-shape geometries (Y. Tian, 2016) (Ewald A., 2018). Thus, it is possible to reduce the elevated material consumption by machining processes and, additionally, the thermal affected area is reduced compared with conventional welding processes. Non-laser additive technologies have been used for years to repair high-added value components; traditionally conventional welding techniques have been applied manually. Thereby, in recent years *laser cladding* or *laser metal deposition* has steadily gained importance thanks to the main advantages related to cost saving and process flexibility.

The study of laser application as material additive processes went along with CO<sub>2</sub> high power laser development in 70s. Gnanamuthu (Gnanamuthu, 1980) performed researches dated from that period and analysed the feasibility of pre-deposited additive material to perform ceramic coatings on the top of metallic surfaces. Nevertheless, coatings are not the only laser application; W.M. Steen presented a contribution about the use of a 2kW continuous wave CO<sub>2</sub> laser for surface heat treatments (Steen W.M., 1979). At the same time, Mazumder et al. studied the process modelling and the application to improve different materials in terms of wear and corrosion resistance (J. Mazumder, 1986) (J. Singh, 1986).

During early 80s, the industrial sector started to consider the additive manufacturing using laser technologies as an alternative to conventional coating processes. The first aeronautical application consisted of high strength coating for a blade, developed by Rolls Royce in 1981. Pratt & Whitney also successfully tested this technology in 1983 (Doran, 1987) what drove aeronautical turbomachinery manufacturers to initiate this technology development to be implemented in their production processes; this is the case of General Electric. Therefore, many aeronautical companies developed diverse repairing systems for aeronautical, naval and industrial turbomachinery components, improving those products effective life (Macintyre, 1983). Automotive industry was another strong sector that bet for this technology; manufacturers as Fiat or Toyota coated, with high strength materials, valve seats in combustion motors to improve surfaces subject to extreme wear (A.G. Blake, 1988) (K. Tanaka, 1993).



In the 90s, additive manufacturing was oriented to components direct fabrication. It was developed the first semi-industrial additive manufacturing system denominated *direct metal deposition* (DMD) capable to create 2D and 3D parts reducing considerably manufacturing times and costs (J.L. Koch, 1993). From the scientific point of view, Professor Steen from the University of Liverpool made important contributions for the deep understanding of this process (M. Murphy, 1993) (M. Murphy W. S., 1994). From this moment on, this researching field has been continued in three process application lines: coatings, repairing operations and direct fabrication, but these researches were focused more on the process optimization than the applicability. On the one hand, they are found pure experimental researches with the aim of obtaining process parameters for different materials and geometries; on the other hand, there are theoretical lines for process modelling and simulation to define previously process parameters reducing the commissioning costs.

In the years thereafter, Fraunhofer Institute become one of the leaders of the technological advances in this field developing new additive manufacturing nozzles, control systems and path programming software, among others. They reach to an agreement with Rolls Royce for turbomachinery components repairing operations, as blisk and impellers which geometrical complexity implies an extra difficulty for additive manufacturing process and those operations (Fraunhofer IPT, 2015). Figure II.37 shows the methodology proposed by Fraunhofer IPT for IBRs repairing processes.

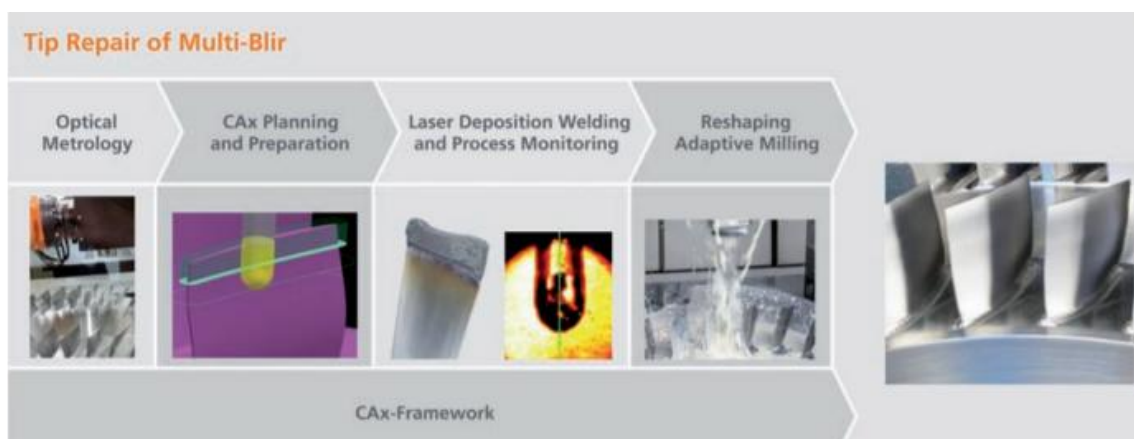


Figure II.37 Different steps for IBRs tips repairing operation (Fraunhofer IPT, 2015)

Moreover, following the same line, there are important researching groups at a national level; one example is the alliance between Danobat S.Coop-Ideko IK4 that installed a laser cladding system for Iberia maintenance department to repair aeronautical turbines blades. Another example is the High Performance Manufacturing Group from the University of the Basque

Country that contributes actively to this technology with scientific and experimental studies: Intelligent nozzle design for LMD (J. I. Arrizubieta, 2017), material behaviour and mechanical properties of nickel based alloys using laser cladding (I. Taberner, 2011), and process modelling and simulations (Ortega N., 2017).

In the recent years, there are some researches around the issues and results presented on hybrid manufacturing processes (M. Cortina, 2018). Some studies were performed around material properties, on the path of understanding the behaviour of repaired components using AM/SM processes. J.C. Heigel et al. (J.C. Heigel, 2018) analysed the impact of the residual stresses generated during the additive process (laser powder bed fusion) on the component and the distortion of that component during the machining process. A. Calleja et al. (Calleja A., 2018) studied material properties such as cutting forces, specific cutting energy, roughness and microhardness of three different material stages after turning and milling processes and a range of cutting parameters: deposited material with no heat treatment, deposited material with heat treatment and finally base material with heat treatment (not added material). Thereby, hybrid AM/SM technologies contribute to reducing the environmental impact of manufacturing Ni and Ti based alloys components up to 70% (N. Serres, 2011). This environmental efficiency is accentuated when the material to remove is much higher than the final part geometry. Besides that, AM advantages for moulds and dies manufacturing sector are deemed relevant in terms of process efficiency and defects or imperfections reduction (W.R. Morrow, 2007). Moreover, this process is very valuable for avoiding moulds discard that need some kind of redesign, something common in the automotive sector.

### ***II.6.1. Industrial Applications***

Laser cladding offers many advantages for high-added value components in sectors as aeronautic, aerospace, energy, medical or industrial. Even though these components are forged or casted to obtain a preform near to the final geometry, in many cases it is needed a machining process for small details as fixing lugs. This type of details implies bigger dimensions of the forged or casted component in order to manufacture the entire component with the details, so it leads to more material waste and machining times. Therefore, laser cladding is presented as a solution for these details generation over the forged/casted component, avoiding material waste and costs.

### **II.6.1.1 Moulds and dies sector**

The LMD or laser cladding process is mainly used for hard coatings generation over tool steel dies; however, these coatings have been extended to other materials, such as magnesium alloys. In this respect, this technology is presented as a feasible alternative to conventional methods for surface hardening treatments as the nitriding or electroplating (A. S. Khanna, 2008).

For moulds and dies sector, LMD is applied to repair worn areas in high value parts; extending these components service life; Figure II.38 shows a mould repairing process using this technology. In this field, the direct competitor is the manual welding process (W-T. Preciado, 2006). One of the main advantages presented by laser technologies against the manual welding consists on the automation capability. There are also some studies about entire mould fabrication; thus, it is presented a methodology to manufacture a near-net-shape geometry and machine to the final required tolerances. Thereby, Hu et al. (Y.P. Hu, 1998) proposed a stamping dies manufacturing process feasibility performing an analysis of microstructure and microhardness of alloyed steels added over structural steel AISI 1045. In this line, Schmidt et al. (M. Schmidt, 2010) performed an experimental study about this process applicability for coating the cutting corners in deep drawing dies, which are subjected to extreme wear. In so doing, the LMD process is considered to fabricate this type of dies made of low-alloyed steels coated by a wear resistant layer just in those areas expected to suffer from big efforts.

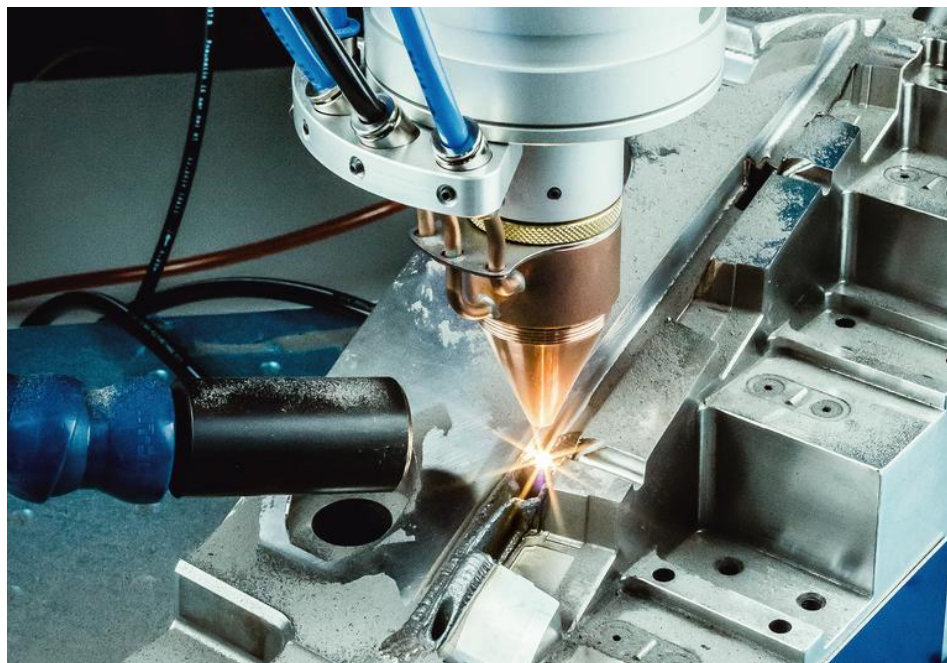


**Figure II.38** Mould repair operation using LMD process (OR Laser News, 2017)

### ***II.6.1.2 Aeronautical sector***

Regarding the application of this technology to the aeronautical sector, it is found some high-added value components with small thickness bodies with external details such as fixing lugs in the case of motor covers or blades mounted on rotary components. Accordingly, in a similar manner as for mould and dies sector, laser cladding is presented as an alternative to the manual welding TIG. Thus, there are many studies about this process application to Ti blades fabrication or theoretical methodologies for manufacturing these components using CAD modelling scheme, CAM programming and verification through reverse engineering (X. Cao, 2008).

These innovative repairing processes are crucial for this industry, turbomachinery manufacturers and turbine maintenance services which main common objective consists on enlarge turbomachinery components life cycle. Obviously, this repairing process is composed by a hybrid manufacturing processes combining laser cladding with machining. There are two main applications for laser cladding: (1) repairing high-added value components that present damage or local defects and (2) repairing some defects derived from the last stage of these components manufacturing chain. The comparison between conventional welding processes and multi-axis hybrid manufacturing processes resides on the clear limitations for conventional processes that are accentuated when high accuracy and reliability conditions are demanded by components specifications. These innovative hybrid manufacturing technologies allow the integration of almost every stage from the repairing process inside the same machine, becoming these technologies more flexible (S. Nowotny, 2001). These techniques application requires a complete study including hybrid process integration with the material deposition stage, the machining stage and the final surface measurements and control (L. Ren, 2010). Meanwhile, Richter et al. (K.-H. Richter, 2004) presented a detailed use of laser cladding process for Ti6Al4V blades fabrication.

A clear example of this repairing process at industrial level is conducted at General Electric (GE) facilities in Singapur where they are dedicated to aeronautical turbomachinery reparation since more than 30 years. Some of the components they are in charge of repairing are compressor blades from the GE90-115B integrated into Singapore Airlines Boeing 777-300ER. Despite of being the aeronautical sector the main target for this repairing process, as part of their business it is found industrial and marine motors components. Similarly, Iberia Maintenance disposes of a blades repairing cell for aeronautical turbomachinery components developed by Danobat-Ideko. These components work under extreme environment and

functioning conditions, so these are the main reasons why this damage leads to require repairation (Fraunhofer Institute for Laser Technology ILT, 2019). Blades are prone to suffer from two different wear types that may be repaired, the leading edge wear and the tip wear. In the first instance, derived from the elevated cost of repairing operations, if the number of affected blades is low, they could be replaced for new ones; while in the second case, the repairing operation is presented as a feasible solution.



**Figure II.39** Repair of turbomachinery components (Fraunhofer Institute for Laser Technology ILT, 2019)

### ***II.6.2. Repairing strategies and process control***

In those cases that the geometry is considered complex (free-form surfaces), as impeller or blisks, the repairing strategies are considered an extra challenge for laser cladding; this is due to the necessity of using 5-axis simultaneous. The properties of the added material are directly influenced by the additive strategies or tool-paths programming. The optimal tool-path definition is critical in order to reduce the harmful effect over the material mechanical and metallurgical properties. Apart from the possible damage as cracks or elevated porosity, one of the main determining factors to evaluate added clad quality consists on the residual stresses presented in the final component; therefore, it is possible to reduce these stresses optimising additive strategies. Overall, many factors may affect to laser cladding strategies cited hereafter:

- Additive manufacturing strategies must be robust to ensure the geometry generation even when the geometries are extremely complex.

- It should be avoided that the same tool-path passes more than once over the same point in order to reduce the risk of suffering from unnecessary overheating or excessive material built up at that point.
- Additionally, defined tool-paths should be as continuous as possible to reduce porosity and avoid undesired gaps.

Both from industrial and scientific point of view, many researches were developed with the aim of optimal tool-paths and parameters definition for laser cladding and hybrid manufacturing processes. Moreover, the application of these processes to any free-form surface implies more challenges but attract the interest of many sectors. Initially, some authors promoted the *slicing* strategy that consist on dividing the solid into different 2D layers and building up the desired geometry layer by layer (Toyserkani E. K. A., 2005). Nevertheless, the geometrical complexity led to perform repairing operations with non-uniform layers (L. Ren, 2008). With the aim of understanding the influence of laser cladding tool-paths, Tabernero et al. highlighted how they affected to the stress-strain diagram. Besides that, mechanical properties presented on this process depend on the concrete directionality of the additive strategy. Moreover, it was demonstrated that these properties presented high anisotropy; a factor to be considered in the choice of the most adequate deposition strategy (I. Tabernero A. L., 2011).

It should be considered that the generation or reparation using laser cladding requires an additional stage of material removing, leading to a hybrid manufacturing that combines additive and subtractive manufacturing processes (K. Eiamsa-ard, 2005). The LMD process is commonly performed using 3 or 3+2 axes strategies, this is due to the fact that 5-axis continuous strategies programming are still a challenge to be faced: great complexity derived from process characteristics and the lack of specific CAM software for programming these tool-path according to the process (S. Nowotny, 2001). Therefore, the adequate tool-path programming has direct influence on the final obtained results related to mechanical and physical properties.

A. Calleja et al. studied the feasibility of five continuous axes for LMD process, proposing a criterion to determine optimal conditions and strategies. For this purpose, a series of experiments were performed for coating a sphere geometry combining zig, zig-zag and contour strategies; with this defined geometry it was leaded to the conclusion that the combination that offered better results was a combination of horizontal zig-zag with 45° zig-zag and vertical zig-zag; shown in Figure II.40 (A. Calleja, 2014). In the same line, Laura Arregui et al. 2018 (Arregui L., 2018) studied the geometrical limitation for inclined walls, concluding to



good results for angles between  $90^\circ$  (vertical walls) and  $60^\circ$ . Moreover, related to LMD process parameters, it was presented a feed rate calculation algorithm in order to maintain the laser feed rate constant according to the most restrictive axis and homogenize 5-axis LMD process on a blisk (Calleja A. T. I., 2014).

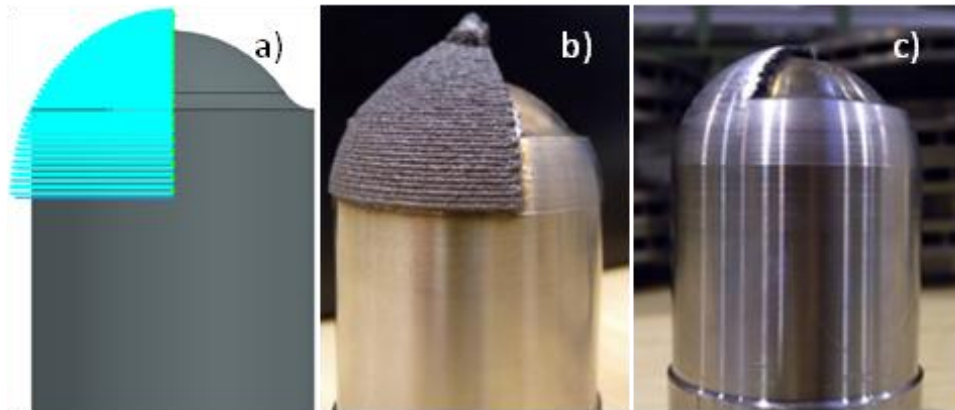


**Figure II.40** Different multi-axis LMD strategies applied to a spherical geometry: a) Programmed strategies, b) coated part, c) final part (A. Calleja, 2014)

On the one hand, the residual stresses accumulation is considered one of the limiting factors for the quality of the parts manufactured by laser cladding, so this factor is directly related to the optimal selected strategies. For those cases that the strategies follow the workpiece contour with a defined offset between trajectories, it is possible the appearance of residual stresses relaxation before performing the following contour trajectory (L. Ren, 2010). On the other hand, thermal stresses are derived from an imbalance in the surface warming during the process. Therefore, if the additive strategy is asymmetric, it will have an unfavorable effect on the final surface. Thus, the number of laser switch on and off should be reduced to the maximum and defined additive strategies should be robust to generate any surface independently from the geometric complexity.

Consequently, as it is expected from a growing process at early stages, LMD presents many challenges to be faced related to the high number of factors involved in the process such as laser integration, material properties, powder flux, feed rate, and strategies definition. After presenting this process applicability for aeronautical components, the first step to be faced is the optimal additive parameters definition for each concrete application. Process parameters vary depending on the used materials; many researchers analysed these parameters for different materials as stainless steels (A. J. Pinkerton, 2004), aluminium alloys (Chryssolouris G., 2002), titanium alloys (K.-H. Richter, 2004) or nickel based alloys (C. Paul, 2007). Additionally, material properties requirements should be satisfied, so some works are cited focus on the microstructures and mechanical properties using LMD for Tungsten alloys (L.

Chun, 2018), Ti/TiAl structural gradient material (H.P. Qu, 2010), and microhardness and thermodynamics in molten pools (S. Cao, 2017).

## **II.7. Specific CAD/CAM systems for IBRs manufacturing**

In the market, it is found a variety of CAD/CAM commercial software developed for 5-axis complex surfaces machining and tool-path definition. These environments are divided into two main machining operations groups: general and specific modules. On the one hand, general multi-axis operations what allow more flexibility to configure and personalize the tool-paths generation by the user. On the other hand, the growing industrial interest in optimising the manufacturing processes for turbomachinery monolithic components led to CAM software suppliers to develop specific manufacturing modules for these complex and demanded components. These specific modules stand out for the user-friendly environment for these components geometry definition generating, in an user-friendly environment, complex machining operations. Notwithstanding, they are under developing process, so there are some concrete machining operations that still offer better results programmed with the generic multi-axis software in return for higher design and computational costs.

Among some of the most specific CAD/CAM software, it is found the NX® from Siemens. This software includes a multiblade module for the complete manufacturing processes of IBRs, including roughing and finishing for the blades, splitters, hub, shroud and blinds. However, this module presents tool geometries limitations for some strategies (Siemens, 2018). SPRIT® is another software that performs trochoidal roughing strategies for 5-axis full slotting the space between blisk blades. This strategy results more productive in terms of material removal rates, being possible to eliminate the semifinishing strategy (ESPRIT, 2019). Moreover, there are CAM software exclusively oriented to manufacture turbomachinery components (impellers, blisks, rotors, etc.) as MAX-PAC™ from NREC Concepts (Concepts NREC, 2019). This software develops tool-path generation algorithms specially designed for turbomachinery components. Hypermill from Open Mind Technologies is also strongly committed to fabricate difficult components related to the aerospace sector (hyperMILL, 2019). Finally, Gibbs CAM® is a software that includes some options for manufacturing turbomachinery components (3D Systems, 2018).

Nevertheless, this last decade, with the emergence of hybrid manufacturing processes (AM/SM), it started a new researching line and industrial demand related to CAD/CAM software for complex geometries generation, addressed in the following subsection.



Moreover, process digitalization is still in a critical stage of development; the number of variables involved in the process, the difficulties of communication between machine and designing software and, finally, the post-processing and standardization of the process have become a handicap studied for recent researches (M.K. Thompson, 2016).

### ***II.7.1. CAD/CAM systems for hybrid manufacturing (AM/SM)***

In line with defined hybrid manufacturing challenges, one of the most critical stages is based on the CAM software solutions. Robert W. Hedrick et al. (Hedrick, 2015) divided AM oriented CAM software into two principal functions: Backplot and Machine simulation. On the one hand, the machine simulation covers machine components, limitations and represents the real movements that will be performed by the machine. On the other hand, the Backplot is focused on tool-path programming and verification, considering the contact between the tool and the manufacturing part; thus predicting intermediate and final results, geometries and errors derived from selected strategies so for AM and SM.

Related to the Backplot, there are defined different AM strategies: 2 ½ axis, 3-axis translational, 2 ½ + 2 rotary positions and finally 5-axis motion simultaneously. This last 5-axis motion allows maintaining the perpendicular position between the nozzle and the surface to be added, obtaining optimal results and more control of process performance (A. Calleja, 2014). With the new trend to “3D printers”, layer-by-layer software providers are increasingly growing; however, the demand for 5-axis AM programming is an actual need for building up more complex surfaces.

Many CAM software suppliers are developing solutions for AM/SM tool-path definitions and process verification. AIXpath GmbH developed a CAM module (ibeRep) specific for gas turbine blade repairing operations; it is a closed solution for laser micro-cladding, milling and measuring processes for this critical aeronautical components. Furthermore, this module offers the possibility of machine virtualization (ibeRep AIXpath GmbH, 2018). In the same line, The Fraunhofer Institute designed a process chain for LMD, supporting tool path programming layer by layer called LMDCAM2 (Acunity, 2018). AUTODESK developed a software solution (PowerMill Additive) that offers the option of tool path definition in a plane, layer by layer and previewing the built-up material (Powermill additive, 2018). With the idea of giving a solution for hybrid manufacturing combining LMD and machining, Siemens developed a full solution for hybrid manufacturing to be used with Lasertec 65 3D from DMG MORI. It contains the digital twin for that machine and a LMD module to program tool-paths, including

AM, layer by layer, and SM programming inside the same software (Siemens NX – DMG MORI, 2018).

### II.7.2. Virtual verification systems

Regarding Machine simulation, due to the similarities with conventional processes as milling or turning, software providers brought some solutions to the market. This is the case of CGTech Ltd. Company with the software VERICUT®; this software offers the possibility of machine virtualization, detecting collisions between involved components and detection of over-travel errors importing a NC code and machine components design (CGTech Ltd. , 2018). MachineWorks developed a software to simulate a full machine, detecting collisions, considering machine kinematics and with no limit for axes number to virtualize any CNC machine (MachineWorks , 2018). Among others, the CAD/CAM/CAE software NX from Siemens also presents a module called Machine Tool Builder, where machine components and kinematics are defined and capable to run a NC code to predict collisions and axes limitations, see Figure II.41 (Siemens NX, 2018). At this point, the accuracy of the simulation will be limited by the precision of the machine components design, the correct implementation of components correlation and axes limits definition.

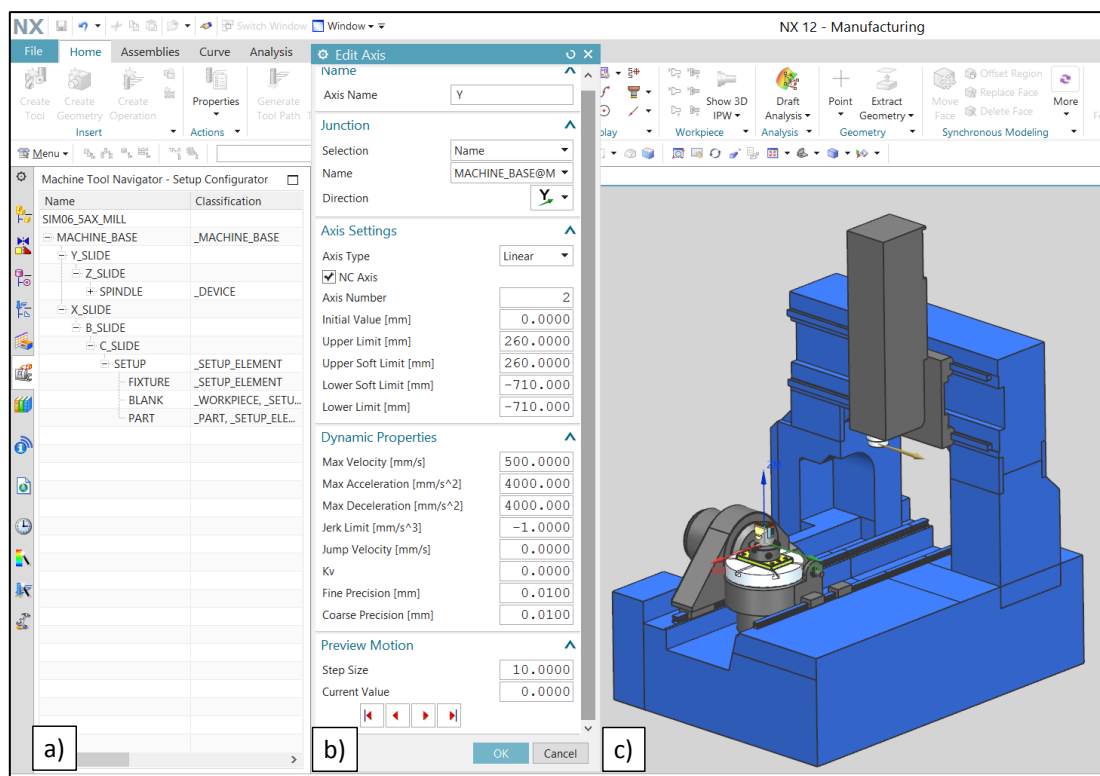


Figure II.41 Machine tool simulation module from NX® Siemens, a) machine kinematics, b) axis definition window and c) machine design

## II.8. Summary of the manufacturing and repair methods for turbomachinery integral rotary components

As set out along this chapter IBRs components were described. They are located in the critical areas of the aeronautical engines (so in the high pressure and low pressure turbines as in the compressors) and imply a manufacturing cost over 100 thousand €/piece, and at the present time they are only produced in 5 countries around the world, including Spain. Nevertheless, these components manufacturing and repairing processes imply a high number of scientific-technological challenges described hereafter:

1- Complex design requirements and geometries: IBRs are classified as sculpted or free-form surfaces, being non-developable surfaces. For these geometries generation they are used different methods as B-Splines or NURBS. Therefore, additionally to the complexity of these geometries manufacturing, in some cases (as closed-type IBRs) the accessibility for the tool along with the tough dimensional requirements are a handicap for manufacturers. Moreover, these geometries require from 5-axis simultaneous CAM programming solutions.

2- Difficult-to-cut materials: The hottest parts of the engine are composed of Ni-based superalloys, at this moment Inconel®718 (Ni-Fe) and in a short period of time new grades of Ni-Co Hastelloy®X, Udimet 720, Astroloy, Waspaloy among others. These alloys present machining difficulties due to elevate cutting forces, high temperatures, limited cutting conditions and the excessive tool wear.

3- High-cost production processes: Inside the IBRs manufacturing chain many stages are presented; such as, roughing, intermediate semifinishing, finishing and abrasive final operations in order to achieve desired tolerances. These stages suppose higher machining times and tool wear.

On the one hand and with the aim of giving a solution to described challenges, there were considered different manufacturing processes used for manufacturing IBRs. First, the conventional milling process evolved with different algorithms and tool geometries to face IBRs issues. However, the global competitiveness led to the search for new alternative processes more productive, in terms of quality, timing and costs. At this point, SAM is considered one of these alternatives in the last decade; because it could achieve higher removal rates and surface finishing quality closed to grinding processes.

On the other hand, the new trend of integral components instead of assembled components implies that IBRs, which are very high-added value components, require repairing solutions to avoid direct discard of them when the damage is located in a small area of the component. The LMD process is presented as a great solution for Ni-based alloys repairing strategies. Nonetheless, there is still a demand of CAD/CAM environments for 5-axis AM and optimal process parameters definition.

---

**Chapter III. Complete methodology for hybrid  
manufacturing and repairing of turbomachinery  
rotary components**

---



## Chapter III. Complete methodology for hybrid manufacturing and repairing of turbomachinery rotary components

*This chapter proposes a comprehensive methodology for hybrid manufacturing of turbomachinery components. Firstly, it is addressed the design of components differing into new part or part that requires a repairing process. Afterwards, additive and subtractive manufacturing stages are implemented. Finally, it is added a measuring and control stage after each process with the aim of encompassing a feasible methodology for hybrid manufacturing.*

### III.1. Introduction

Hybrid manufacturing (AM/SM) is presented as a great solution to manufacture and repair high-added value components, such as moulds and dies or IBRs; the great flexibility for complex geometries, as a near-net-shape process, and the reduction of material waste are some of the main advantages. By contrast, this process implies many steps and sub-steps inside the manufacturing chain: entire component design or damaged area location to be repaired, AM process with tool definition and additive parameters, SM process with tool definition and cutting parameters, measuring and control accomplishing quality requirements, etc.

Therefore, aligned with the fourth industrial revolution, Industry 4.0, it is proposed a methodology for manufacturing and repairing IBRs considering the importance of processes integration and digitalization. Therefore, the hybrid manufacturing process of turbomachinery IBRs is divided into four main stages, integrated inside the same environment, with the aim of ensuring, to the extent possible, that the followed methodology is reliable, and so the obtained part accomplishes final manufacturing requirements.

### III.2. Design process

With the aim of performing an adequate design process, it is important to consider machining process limitation, the demand of final tolerances and material requirements; obtaining the CAD file of the part to be manufactured.

The proposed diagram (Figure III.1) distinguishes the design process into two different paths, differing new part conception (direct manufacturing) from a part that needs to be repaired. In the second case, it should be pointed out that there is an intermediate sub-stage to achieve an adequate design. The use of hybrid manufacturing for repairing is a reality, due to the fact that this kind of parts are high added value components, and there is a real necessity of reducing manufacturing costs and material waste, as well as avoiding part discarding. Nevertheless, it is important before designing the area to be reconstructed, revising and measuring the extend of the damage. Once the damaged area is recognised, it is needed a subtractive manufacturing process in order to remove affected zone, so leading to determine the real area that needs to be hybrid manufactured. At this point, the design is carried out around this last manufacturing sub-stage. In most of cases, after that sub-stage, the part is scanned with optical or contact measuring systems attempting to get closer to the real geometry and, thereby, facilitate the processes of the following stages.

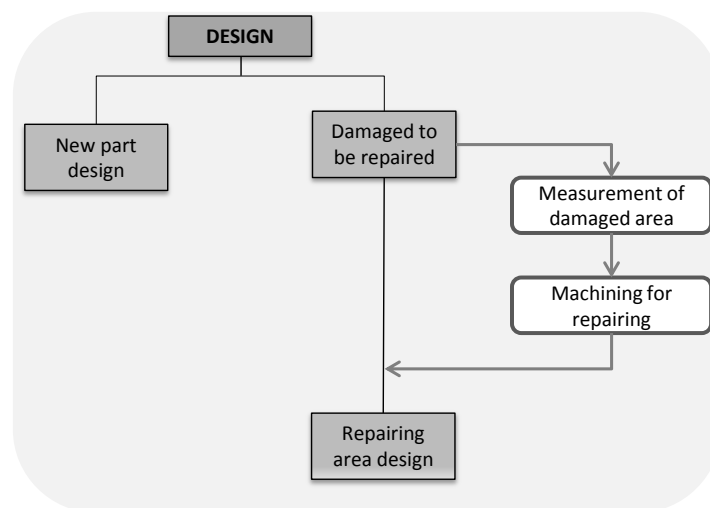


**Figure III.1** Diagram of the methodology for turbomachinery integral rotary components design in hybrid manufacturing

### III.3. LMD process integration

The next stage inside the hybrid manufacturing chain is the AM. In this case, among the different AM processes, LMD was selected thanks to the adjustability of repairing this kind of turbomachinery components. Furthermore, this technique is commonly used not only for repairing tasks, but also for coating or a near-net-shape new part generation. This integration to the proposed methodology is shown in Figure III.2.

As mentioned in the literature, LMD is considered to be at early stages, so there are still many challenges to be faced in order to obtain optimal results for the entire process. The first step



defined in this methodology consists of a CAM module integration for LMD process. Due to the complexity of these components, the control of process parameters and optimal tool-path programming are crucial to achieve optimal results at this intermediate stage. In a similar manner as in machining process, it is important to ensure the correct tool definition; in this case the type of laser nozzle (coaxial or discrete) and laser parameters (i.e. focal distance and spot size). Additionally, LMD tool-path programming was studied to offer a reliable solution. The AM strategy definition could be considered the border between acceptable parts (free of defects in material properties and geometrical deviation reduction) and a part to be discarded. It is worth stressing that the process knowledge is critical to define the parameters related to the process itself and the material used to be added or as a material base.

On top of that, it is proposed a geometrical model with the aim of obtaining a final part prediction. This predictive model allows to estimate the final geometry obtained applying defined tool-path and parameters. Thus, it is possible to calculate approximately the quantity of material needed to build up the desired geometry. Moreover, derived from the insufficient dimensional accuracy of AM processes, this stage requires, in all cases, a SM process. So, the predicted geometry is converted into the blank/bulk for the machining stage.

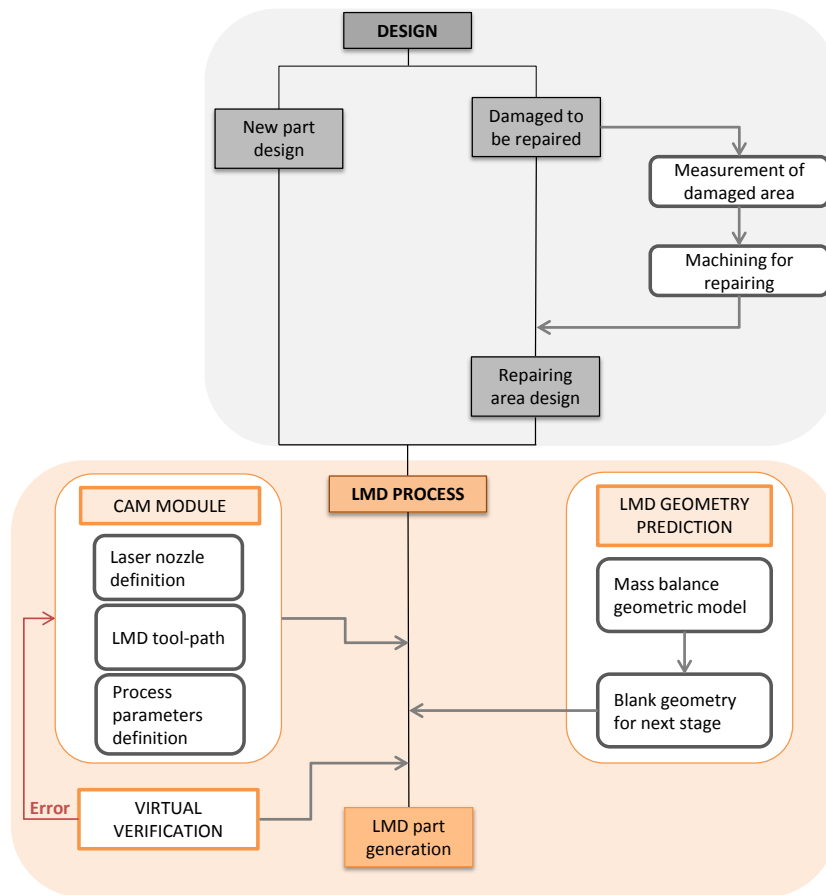


**Figure III.2** Integration of additive manufacturing process into turbomachinery integral rotary component hybrid manufacturing methodology

Finally, the complexity of this kind of components leads to require 5-axis continuous movements, so here is where the virtual verification plays a significant role. Inside the LMD process, the machine digitalization is defined as the last step, with the aim of predicting collisions between different machine components involved in the process or those machine components with the part to be manufactured. Additionally, it analyses the feasibility of machine kinematics to perform defined strategies. As it is shown in the diagram, this is the previous step to run the real process, so if it is found any error or problem at this step, it should be go back to the CAM module and re-program process parameter/strategies.

### III.4. Machining process integration

With the aim of completing the concept of hybrid manufacturing, the last principal stage in this chain is the machining process. For this stage, the first step is the geometry definition; so the blank/bulk is defined from the additive process and the final geometry comes from the designing stage. Figure III.3 shows the integration and correlation between these different stages.

Firstly, it is important to analyse different subtractive manufacturing options to select the most adequate process relying upon final part requirements (i.e. roughness, dimensional deviation, material properties) and process requirements (cost, tool, time, etc.). As mentioned before, turbomachinery integral rotary components are commonly made of difficult-to-cut thermo resistant superalloys; additionally, the complexity presented in their geometry implies manufacturing challenges related to tool path strategies. Therefore, among subtractive processes, this methodology works around one conventional process (milling process) and a non-conventional process (Super Abrasive Machining) that is addressed in chapter V.

Following the diagram flux and in accordance with the proposal for the additive stage, the next step is using the CAM module to define process parameters. Cutting tool (i.e. dimensions, cutting length, tool type, number of teeth), tool-path strategies (i.e. 2 + ½ axis, 3-axis, 5-axis), tool-path patterns (i.e. zig, zig-zag, helical) and cutting parameters (i.e.  $a_p$ ,  $a_e$ , feed, speed) are defined at this step.

The last step before machining is the virtual verification. This verification helps to predict collisions, inadequate tool engages and machine kinematic limitations. It should be pointed out that one of the characteristics inside turbomachinery IBRs is the existence of a small area between blades, implying tool accessibility limitations. Moreover, to obtain optimal results it is required the use of 5-axis simultaneously. This step is the one that gives green light to proceed with the machine, if any error is found, it is needed to go back to the CAM module and re-program the entire process avoiding any collision risk and reducing the possibility of obtaining a part to be rejected.

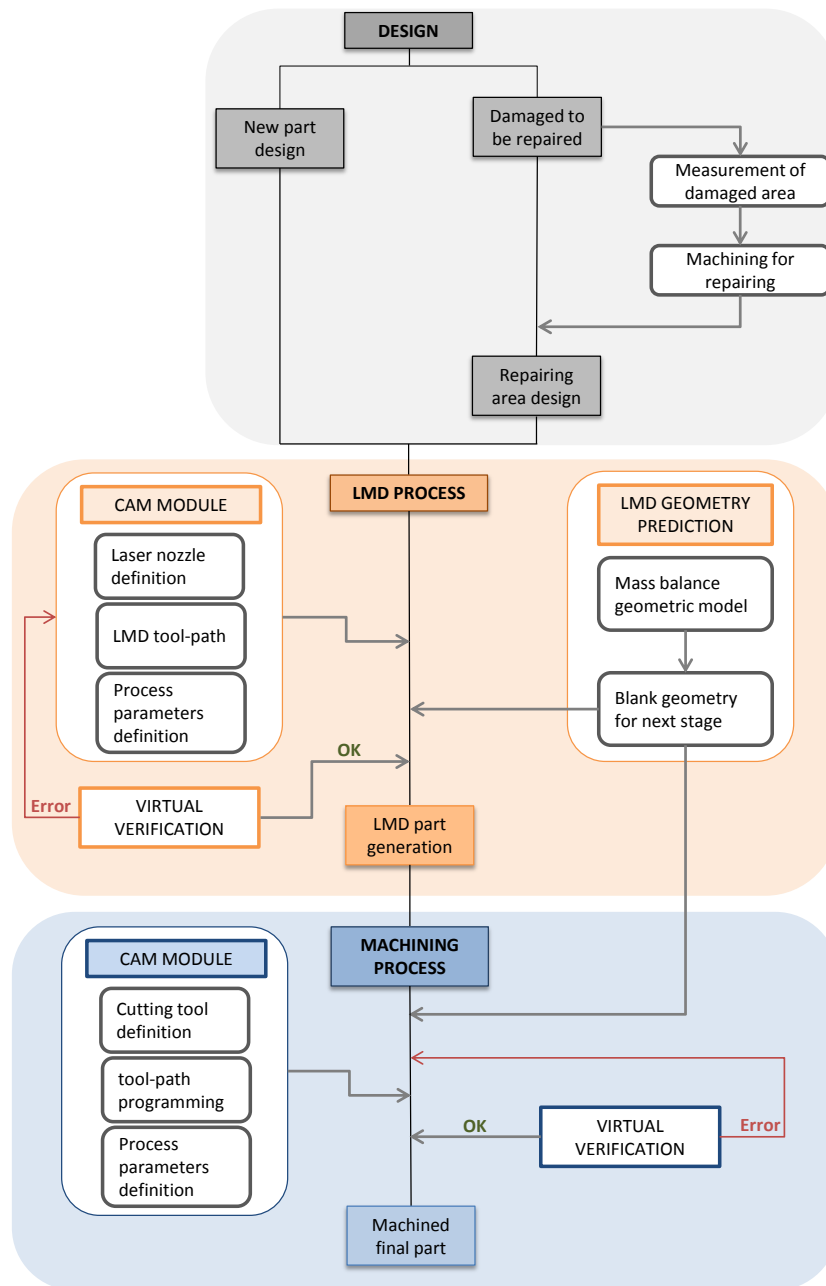


Figure III.3 Integration of subtractive manufacturing process into turbomachinery integral rotary component hybrid manufacturing methodology

### III.5. Measurement and control

In order to complete the methodology loop, after both main processes it was added a sub-stage of measuring and control. Ensuring the correct process performance before moving to the next stage; implying a better control of final results allowing early detection and correction of process issues. Figure III.4 shows control points implemented into the methodology.

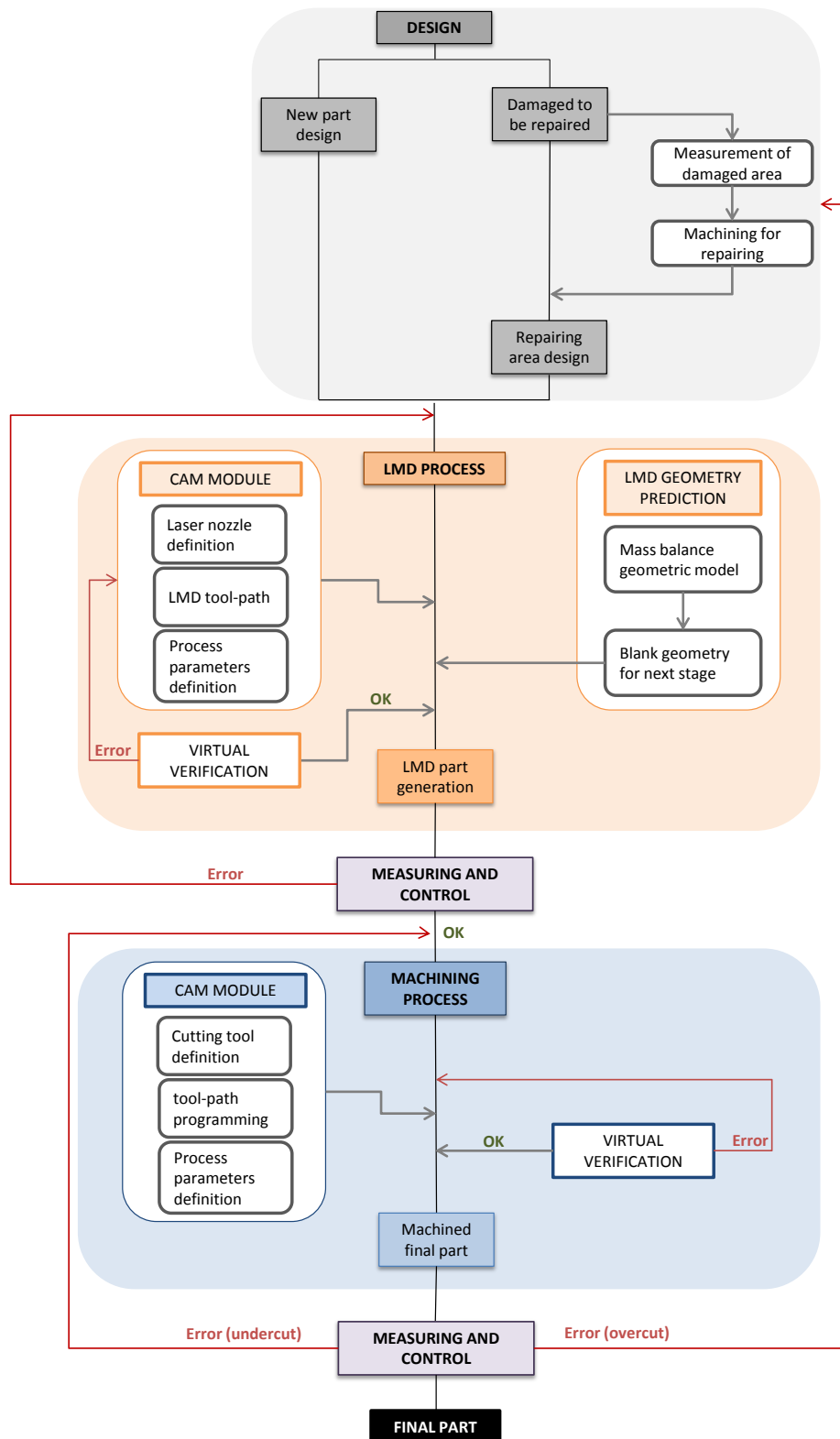


Figure III.4 Integration of measurement and control stages into turbomachinery integral rotary component hybrid manufacturing methodology

With the aim of ensuring the reliability of any manufacturing process, there are many measurements to be considered, such as dimensional deviation, surface roughness and integrity and material properties. Moreover, in the case of hybrid manufacturing combining

AM and SM, this quality control acquires special relevant derived from the interdependency between involved processes. The proposed methodology includes two internal control stages related to programmed tool-paths and two global process control stages to perform the entire process efficiently.

On the one hand, the internal control stages are defined after the virtual verification of each process; programmed strategies are tested with the virtual environment performing a control stage to evaluate the adaptability of defined tool-paths and collisions avoidance or redefine the strategies in case of necessity, so for AM and SM processes. This control is performed just with the virtual verification. On the other hand, a global control stage was defined after each process denominated “measuring and control” to analyse previous detailed quality requirements, such as dimensional deviation or material properties. If there is a mismatch found after LMD process, it could be solved readjusting the process parameters and selected strategies. In the case of machining, there are two possible errors, undercut and overcut. The undercut implies extra material compared with the final desired geometry, so it is needed to repeat the SM process. On the contrary, the overcut implies insufficient material to achieve required dimensions, so it is needed to return to the design stage and restart the hybrid process.

### **III.6. Main benefits of process stages co-integration**

Many authors studied the involved processes inside hybrid manufacturing, parameters and results in a separate manner, however, considering the co-integration inside the same methodology implies main benefits detailed hereafter:

- Direct connexion between different processes: It is important to consider the relation between different the different processes involved in the hybrid manufacturing. Furthermore, they are co-related so each one has a direct impact on the rest. This leads to the necessity of a methodology that defines feedback and control loops so for each process as for the co-relation. i.e. IBR repairing operation starts from the damage detection (control), warm areas removal (SM) and definition of the area to be repair (design), after that the entire process chain is performed as defined in the methodology: LMD, SM and control. In addition, the co-integration inside the same machine tool implies mainly the reduction of positioning errors, due to the fact that the performance of the entire process is run inside the same machine so it is not necessary clamping and unclamping operations.

- Consequent use of material and human resources: The advances in machine tools and the capability of unifying more than one process inside the same machine imply a considerable resources reduction in terms of machines and human resources. Moreover, the AM offers the possibility of material waste reduction being a near-net-shape technology. Therefore, the initial shape to be machined to the final size requires less material volume and less machining time and costs. Moreover, the co-integration of all processes inside the same CAD/CAM/CAE environment simplifies the constant change between them, avoiding the use of different software for each stage.

Thus, the development of a complete methodology for turbomachinery IBRs hybrid manufacturing leads to the disposal of a reliable and powerful tool to face the challenge of obtaining a final part that fulfils product requirements. Additionally, a powerful tool (CAM module for LMD) is implemented at the intermediate stage offering a user-friendly interface to program process parameters and tool-paths. This interface facilitates the control of the process definition embracing just specific parameters related to this technology. Moreover, each stage presents its own virtual verification with the aim of reducing unnecessary material waste and machine using time. Finally, the measuring and control closes the loop and defines the final part acceptance.





---

**Chapter IV. API development for hybrid  
manufacturing using Laser Metal Deposition**

---



## Chapter IV. API development for hybrid manufacturing using Laser Metal Deposition

*In this chapter, API developments are presented for a complete CAD/CAM module oriented to hybrid manufacturing processes (AM/SM) using LMD. These API offers a support for LMD strategies programming including a geometrical prediction model inside the same environment. The geometrical predictive model could be used as the initial blank for the following manufacturing stage (machining) inside the hybrid manufacturing chain, so becoming an effective predictive tool for the selection of process parameters and strategies.*

*This solution presents a user-friendly interface for different AM strategies. As a novelty, this development makes special emphasis on complex geometries and 5-axis tool-paths programming, integrating inside the same machining CAD/CAM/CAE software (NX™ from Siemens). With the aim of validating the developed solution, an IBR made of Hastelloy®X was selected to be hybrid manufactured over a core disk, building up 18 blades using 5 continuous axes.*

### IV.1. Introduction

The API (Application Programming Interface) concept is defined as a group of functions and procedures with a fixed objective presenting the peculiarity of being run by independent or external software. It is considered a strong weapon due to the flexibility offered allowing to different applications/software to keep a communication understanding each other. The use of API's is much extended inside manufacturing sector, for example to implement cutting forces models into CAD/CAM environments. In line with this idea, the specific module for LMD programming presented in this chapter is a combination of two APIs integrated in the commercial CAD/CAM/CAE software NX™ from Siemens. Furthermore, NX™ offers a programming assistant tool denominated NX Open that facilitates to customize APIs for this software, personalizing different procedures or complex tasks; even integrating third party applications through an open architecture using different programming languages as C/C++, C#, Visual basic, Java or Python.

The first developed API is related to LMD process programming, tool definition and mainly tool-path programming. This API could be applied for 3-axis and 5-axis simultaneous tool paths, so this is required for the generation of complex geometries. The second developed API

consists on a mass-balanced algorithm to predict the LMD clad dimension and the entire generated surface according to the selected material and process parameters. Both of them are integrated in a new defined module at the software initial window.

Figure IV.1 shows the flowchart followed by the LMD process through both APIs to generate the LMD added geometry. This solution could offer important data for hybrid manufacturing processes (AM/SM), such as the effects of different LMD strategies on the final added geometry and the new blank generation for the next step (SM) defined in the proposed methodology.

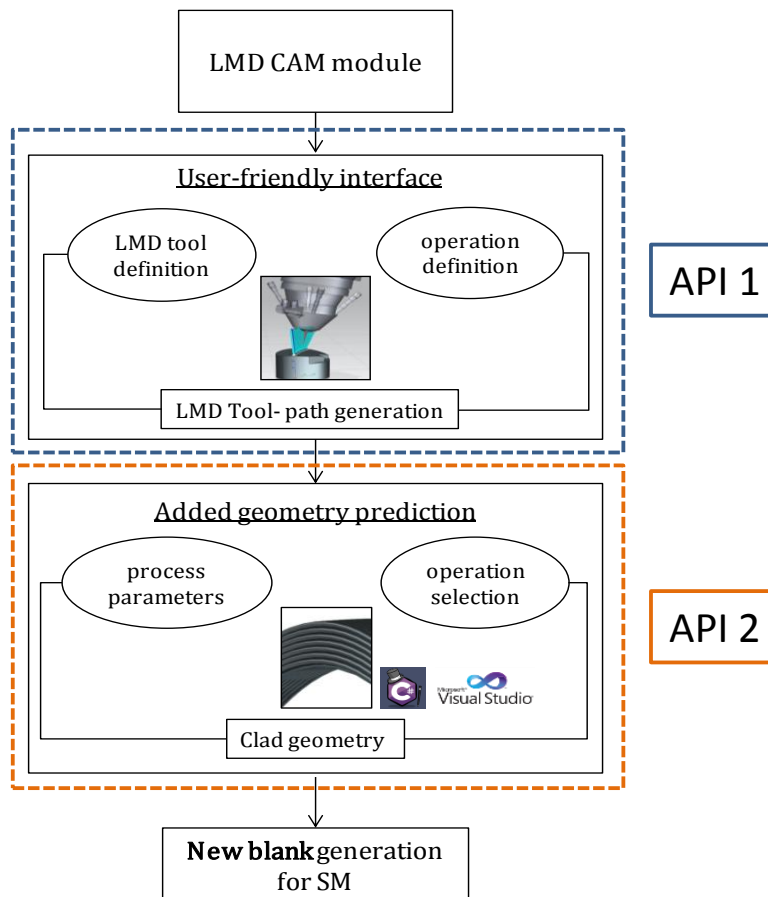


Figure IV.1 Flowchart for developed APIs integration for LMD CAM solution

## IV.2.API 1: CAM module for LMD

On the basis of a powerful tool for manufacturing processes as CAD/CAM/CAE software for SM and with the aim of giving a solution for LMD tool-path programming, a CAM module was developed to be implemented as a new module. In order to integrate the LMD CAM module in the same environment, a commercial CAD/CAM/CAE system was selected. In this case, NX®9.0

from Siemens was used; however it should be pointed that this methodology could be applied, with small modifications, within any CAD/CAM system.

This LMD module considers critical process parameters, such as powder flux, laser power and focal distance, among other. The main objective consists on unifying tool-path programming and SM inside the same environment, not only for 3-axis but also for 5-axis simultaneous. The user-friendly interface is implemented at each software stage, in a similar manner as machining module, including the API for clad geometry.

### IV.2.1. User-interface

The presented solution for LMD CAM module contains a user-friendly interface with the aim of facilitating the user operability. For this purpose, the first step consists on creating the access to the specific module. Afterwards, it is completed with the different templates related to the process parameters, the tool definition and the definition of LMD operations. Figure IV. 2 shows the two created possibilities to access to the programmed LMD module: directly from the initial window (Figure IV.2.a) and jumping into the LMD inside the machining environment (Figure IV.2.b). These alternatives are directly related to the selected process between LMD or hybrid manufacturing, thus to build up a geometry from the beginning the first option moves into the LMD process, however for repairing operations, the second option gives more flexibility to jump from different manufacturing processes in a second (from machining to LMD and vice versa).

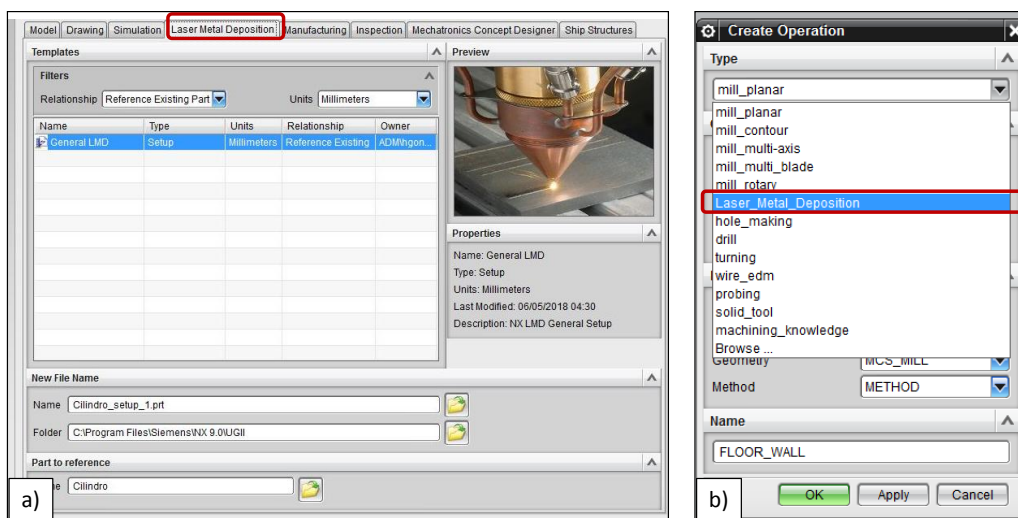


Figure IV.2 Accessibility to LMD CAM module: a) software initial window, b) inside machining module

It is worthy to mention that the main module is contained in both options, so the initial window makes an internal call to the customized LMD manufacturing set-up template. In order to program the LMD manufacturing template the following steps need to be performed.

#### IV.2.1.1 LMD CAM Module label at the initial window

The first step is creating a new template inside the corresponding NX® internal folders. The templates location is *C:\Program Files\Siemens\NX 9.0\UGII\templates*, where three different types of palettes are found (.prt, .sim and .pax). In this case, the extension related to the initial window labels is .pax, so it was created a new template named *ugs\_LMD\_templates.pax*; Figure IV.3 shows the programmed code inside the template and the relation with the terminology appeared in the initial LMD created window, i.e. label (red), metrics (green), master model (purple), description (yellow) and image (orange). The image (orange) requires a .jpg format, a resolution of 96 ppp and dimensions of 247x185 mm; and being inserted in the following route: *C:\ProgramFiles\Siemens\NX9.0\MACH\resource\template\_part\english*.

At this point, the initial window label is created. However, the most important line inside this code is the call to the specific LMD CAM template, because this archive contains the entire programmed API.

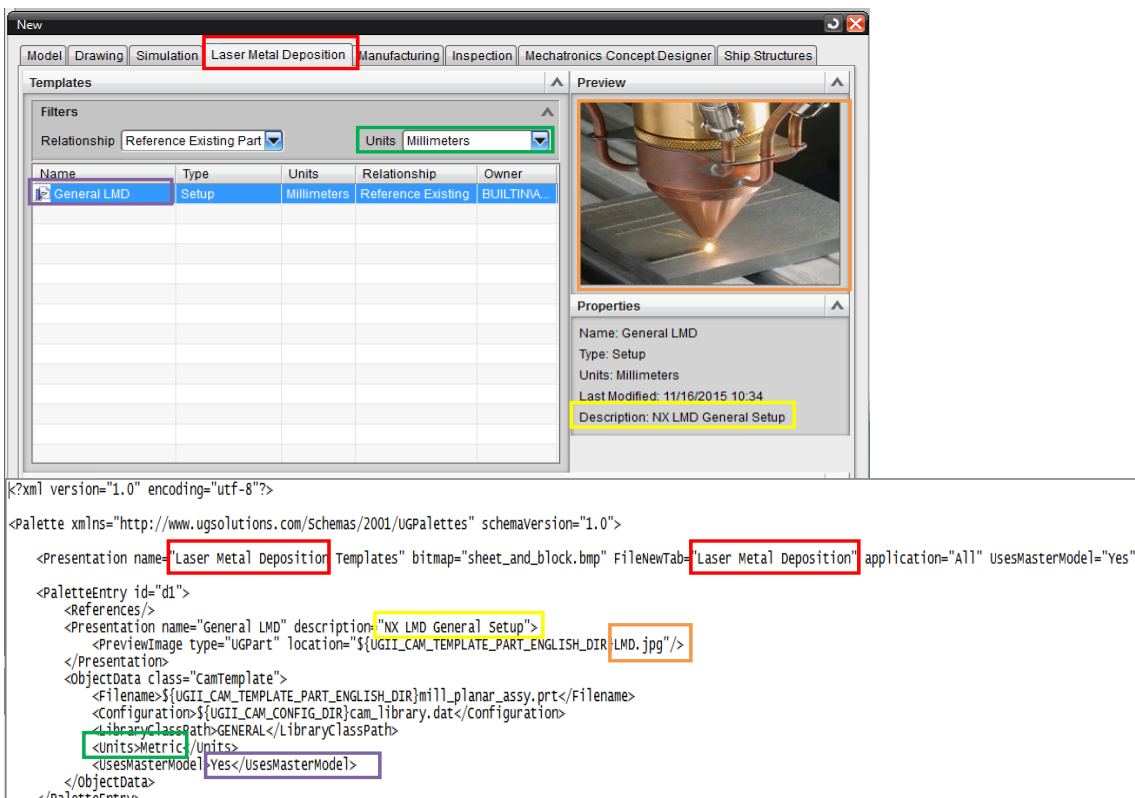


Figure IV.3 LMD module template and the relation with the code of the installed archive ugs\_LMD\_template.pax

Finally, the template needs to be included in another route to create the tab in the initial window. For this purpose, the archive *NXFileNewDialogTabOrder.dat*, located in *C:\Program Files\Siemens\NX 9.0\UGII*, needs to be modified including the programmed *ugs\_LMD\_templates.pax*.

#### IV.2.1.2 Specific LMD CAM template

The specific LMD CAM template contains the programmed API templates related to the LMD process, such as tool definition and LMD operations. In order to generate this template, Figure IV. 4 shows the different archives that need to be created and the existing co-relation between them. These files are described below more in detail.

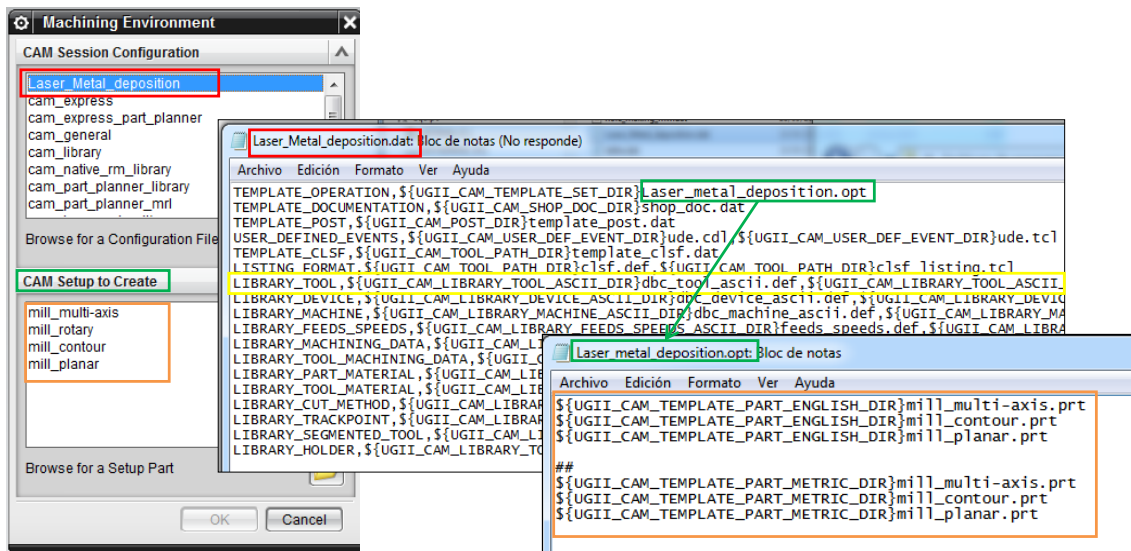


Figure IV.4 Required archives and their co-relation to implement the defined LMD module in the CAM environment

- **Laser\_Metal\_deposition.dat**: This archive consists on the CAM session configuration related to the LMD process; thus, it is required to recognise the created LMD template as a CAM session inside the software. The code provided calls different subroutines that contain the data from LMD operations, tool definition and the access to the different libraries to be used. Figure IV.4 shows the code written inside this file, emphasising the call to the CAM setup (green) and the specific LMD tool defined in the library (yellow).

This archive is located in *C:\ProgramFiles\Siemens\NX9.0\MACH\resource\configuration*

- **Laser\_Metal\_deposition.opt**: This file is related to the CAM setup and contains the set of .prt files with the different predefined machining operations. The number of

components inside this file depends on the final application. For example, for large batches of similar components, this offers the possibility of automating different set of components. In the case of LMD application, it contains one .prt file with LMD templates.

This archive is located in `C:\ProgramFiles\Siemens\NX9.0\MACH\resource\template_set`

- **Laser Metal deposition.prt**: This file extension matches with the files generated by NX® CAM software. It is the most intuitive file shown in Figure IV.5; on the left side is presented the operational tree, distinguishing 3-axis and 5-axis LMD operations, in the middle it is found an example of operation menu and, finally, on the right side it is found the master model. When this entire template is applied to a new component/geometry, the master model is replaced by this geometry, keeping the defined operations and origins. However, it is possible to make any modification of the origins or operations in case of necessity. The components programming of this file are described more in details in the following sections.

This archive is located `C:\ProgramFiles\Siemens\NX9.0\MACH\resource\template_part\metric`

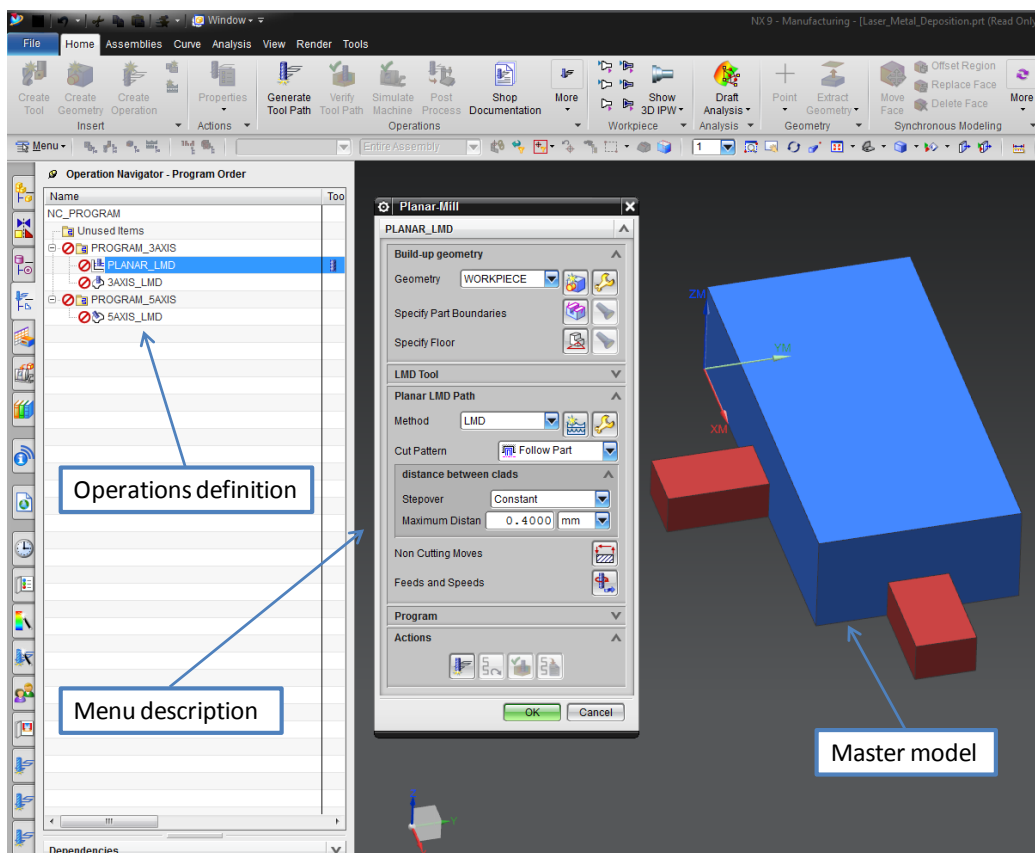


Figure IV.5 Laser\_Metal\_deposition.prt: Operations definition, Menu description and Master model



### ***IV.2.2. Process parameters and tool definition***

Along this chapter, a CAM solution is presented for the AM process known as LMD. This process is based on using a laser beam to generate a located and controlled melting pool onto the substrate or material base. Inside the melting pool, material particles (powder in this case) are injected creating a material layer or clad; thus, layer by layer the desired geometry is created. In order to adapt the API to the process, it is necessary to identify the main process parameters to be considered and defined in the API user windows, so introduced by the final operator. There are some fundamental parameters related to the process, to the clad geometry generation and for modelling the laser tool.

On the one hand, the considered parameters relative to the process to be implemented into the API are listed below:

- Power [W]: This is one of the principal parameters of process control, due to the fact that an excessive power could imply thermal damages on the workpiece and insufficient power could lead to a non-quality clad generation or even a non-existent clad.
- Nozzle feed rate [mm/min]: This parameter is the nozzle feed relative to the workpiece. It is directly related with the time that the laser beam interacts with the substrate, affecting to the final clad geometry. In the case of using a very slow feed, it could provoke over-built material, being stressed for small corners or radius. On the contrary, if the feed is defined elevate, there is a risk of not providing or melting enough material for the clad generation.
- Powder flux [g/min]: It is the material powder mass to be added by time unit. It determines the quantity of material injected into the melting pool, affecting to the clad height. The higher powder flux value, the bigger clad height is presented.

On the other hand, Figure IV.6 shows selected parameters for laser nozzle and beam modelling, such as the focal distance, the spot size and the cone angle. On the left side, it is presented the coaxial nozzle developed at the UPV/EHU (Figure IV.6.a) and on the right side, it is shown the nozzle modelling and the definition of the involved parameters to be defined at the API tooling menu (Figure IV.6.b).

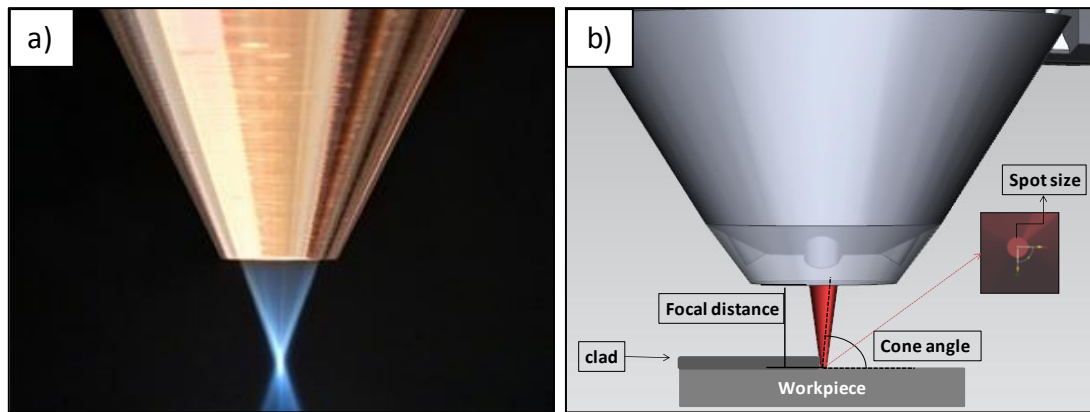


Figure IV.6 UPV/EHU Coaxial nozzle and beam modelling for the LMD CAM module

These parameters and their influence on the process performance and the generated clad geometry are listed below:

- Focal distance [mm]: The focal distance is located at the plane that the powder concentration is maxim; therefore, the laser beam is focalized at the same plane generating the spot size to be considered for the process. This distance represents the position where the adhesion of material is performed in optimal conditions. Moreover, in those cases that the laser beam is not well aligned at the focal plane, the powder concentration that arrives to the substrate is insufficient, leading to a low-quality clad or even non-existing clad formation. Furthermore, this parameter acquires special relevance for 5-axis LMD operations.
- Spot size [mm]: The spot size defines the area where the power is distributed. It is related with the energy that arrives to the substrate. This parameter depends on the laser beam characteristics and it is adjusted using laser optics. Thus, it has direct influence on the clad geometry.
- Cone angle (degrees): This parameter is created to facilitate geometrical definition for the tool generation internally for the CAM software, representing the laser beam and the powder concentration as a cone ending on the focal plane.

Finally, the file *Laser\_Metal\_deposition.prt* from the LMD CAM module was modified limiting the tool creation to LMD nozzles. Figure IV.7 shows the LMD tool definition menu and the steps to be followed. The first step is opening the “Create Tool” window, where the type “Laser\_Metal\_Deposition” presents only one option. After that, pushing the “Tool Subtype” the programmed menu appears. The yellow square shows the laser beam and the nozzle definition demanded by the API to create the tool.

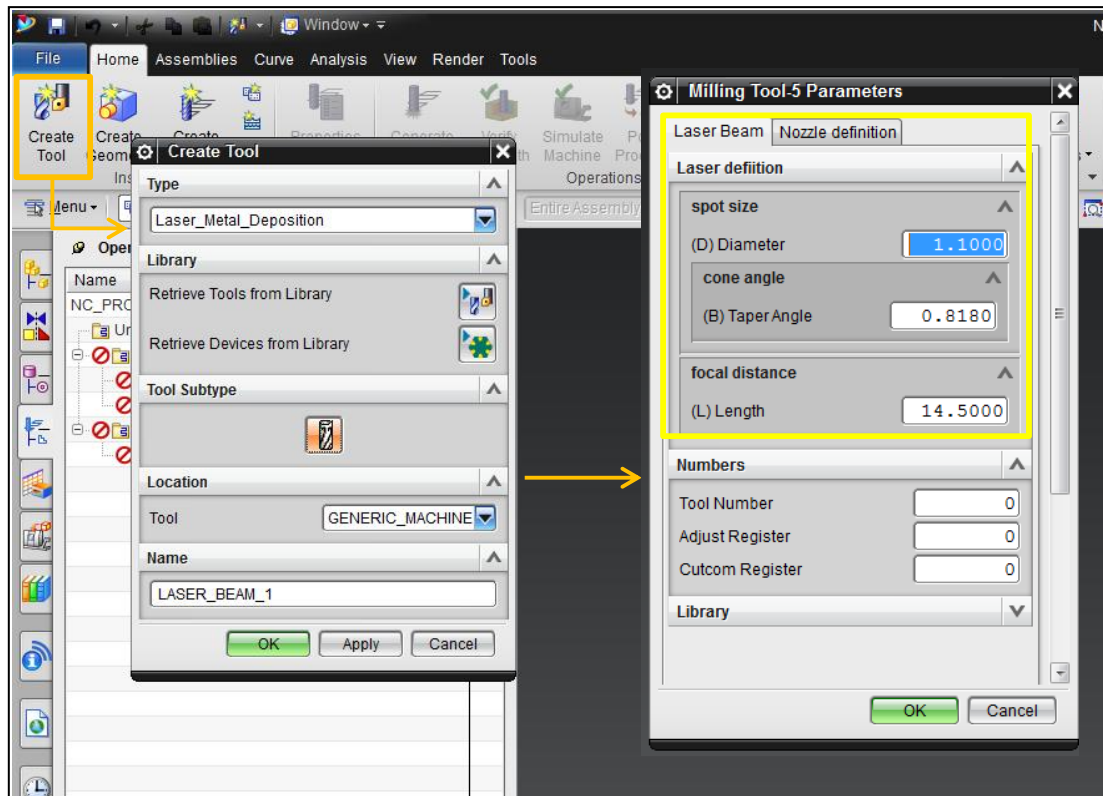


Figure IV.7 Implementation of LMD tool definition menu in the programmed CAM module for LMD

### IV.2.3. Tool-paths generation

The LMD process is increasingly widespread at the industrial sectors, but the growing complexity of the components geometries to be dealt with, leads to the necessity of 5-axis machine kinematics. This implies that one of the main challenges for this technology resides on the optimal tool-path definition and CNC code programming. The selected operation would affect not only to the geometrical results, but also to the mechanical properties and process quality. Besides, it should be distinguished the 3-axis operations from the 5 axis operations requirements, due to the differences at the tool-paths programming.

Therefore, it is important to determine the adequate CAM programming algorithms aligned with LMD process. Afterwards, these algorithms are considered in the LMD operations definition, reducing the inputs options at the operations menus to the minimum expression in order to facilitate the programming to the user and enclosing the LMD specific and non-changeable requirements internally. First of all, it should be pointed out that, opposed to conventional machining processes, the AM processes start the building up of the desired geometry from the bottom to the top; so the first and most important limitation implemented internally is related to the geometry growing direction.

Figure IV.8 contains different parameters and concepts included in the tool-paths internal programming, which are described more in details hereunder.

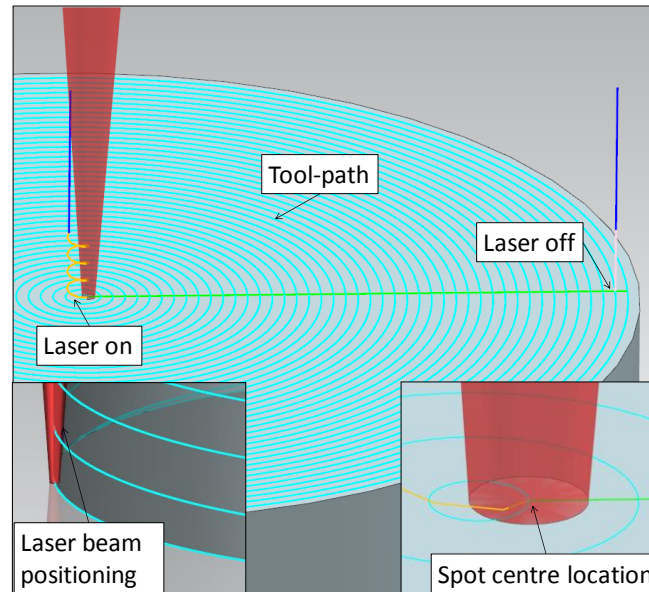


Figure IV.8 Parameters considered for LMD tool-paths generation

- Laser on/ Laser off: At the end of the approach path, it is included a *start of path event* to switch on the laser (M04) once the spot arrives to the focal plane. In a similar manner, at the beginning of the retract path an *end of path event* is included to switch off the laser (M05).
- Tool-paths stepover: This parameter depends on the material to be added and the process parameters. The user defines this parameter as the distance between adjacent clads; determining also the desired overlap between clads.
- Spot centre location: The CNC code, generated by the programmed strategies, positions the centre of the laser spot in the middle of the tool-path. In such a way that the generated clad distribution is controlled in location. Hence, for a profile coating it is ensured the extra material generation to be machined to the final size, reducing the material waste and facilitating the prediction of LMD created geometry.
- Laser beam orientation: Maintaining the laser beam normal to the substrate to be added in each position is considered critical for the optimal performance of the process. This leads to keep the focal distance as constant as possible, following the criteria of the perpendicularity principle. Thus, material waste is reduced and the continuity is preserved following the desired design.

### IV.2.4. Main LMD operations definition

Following the criteria established for LMD tool-paths generation, the next step inside the API is the CAM operations programming, defining different operations, strategies and designing the user environment. In the search for optimal LMD strategies and based on the most commonly LMD strategies studied in the literature, the developed module offers 3 different operations to be applied according to the selected geometry to be added and the LMD process requirements.

#### IV.2.4.1 Planar LMD

The first LMD operation is defined on the basis of 3D printer functioning, layer by layer strategy. This operation adds material in planar levels normal to a fixed axis, generating layer by layer a new geometry inside a user-limited area. It is recommended for general use in LMD for planar, single layers and multi-clads strategies. Figure IV.9 shows the Planar LMD menu at the user environment, the operation description and an example of application.

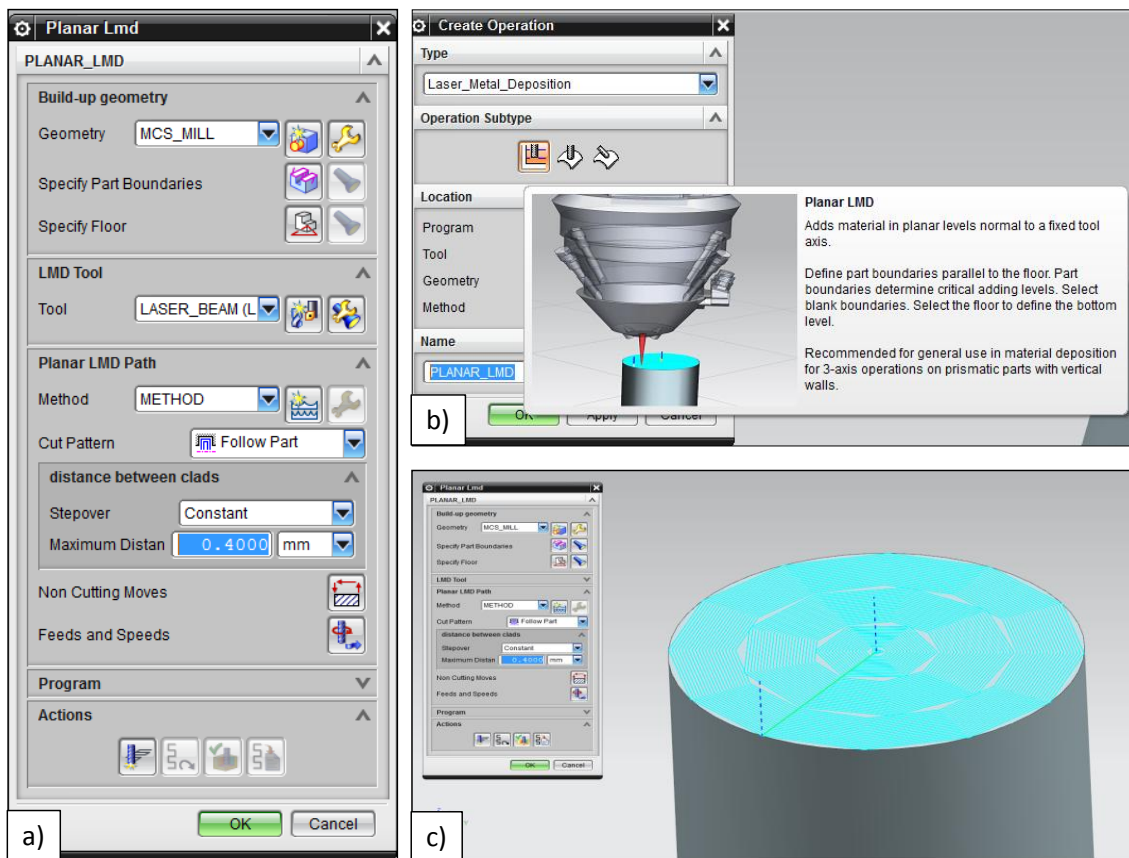


Figure IV.9 API Planar LMD operation: a) User menu, b) description and c) example of complete layer generation

The Planar LMD operation definition is divided into three main groups (shown in Figure IV.9.a):

- Build-up geometry: Inside this group, the user should define the geometry to be created, specify the boundaries to enclose the area for each layer and the location of the initial layer.
- LMD Tool: At this group, the laser tool to be used is selected. This tab is directly connected with the tool definition from the previous subsection.
- Planar LMD Path: At this group the patterns to be followed is defined (zig, zig-zag, helical, follow part, follow periphery...) depending on the expected clad formation direction. Additionally, the distance between clads is required in order to generate the desired overlap and obtain an adequate filled layer.

#### IV.2.4.2 3-axis LMD

The 3-axis LMD operation was designed oriented to a basic surface coating operation which requires 3-axis simultaneously movements. A continuous single clad is generated along the entire selected surface. It is recommended for general simple coatings or one-clad surfaces. Figure IV.10 shows the operational menu, the description and an example of application.

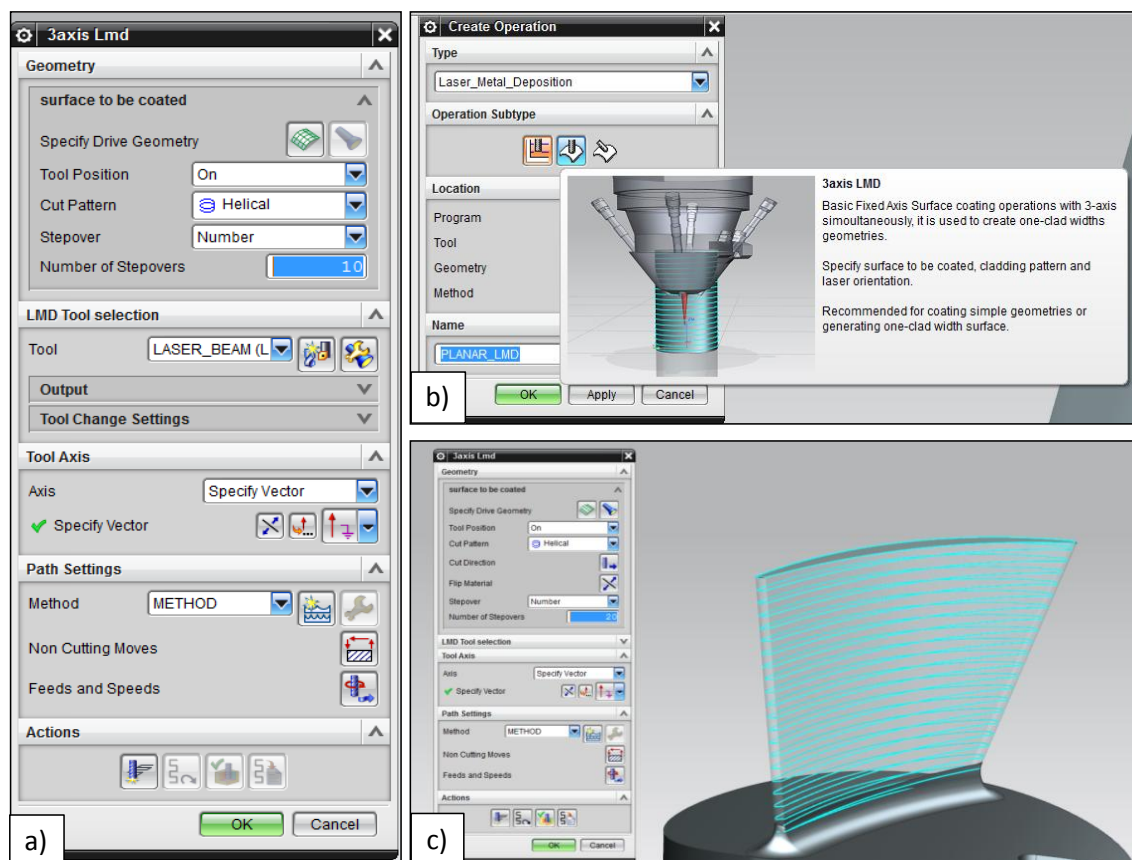


Figure IV.10 API 3-axis LMD operation: a) User menu, b) description and c) example of a developable single blade generation



In a similar manner as for the previous operation, there are some inputs requires to the user in order to generate the tool-path. The LMD tool selection tab is maintained equal for the three proposed operations.

- Geometry: For 3-axis strategy, this tab requires different sub-tabs to be fulfilled. The first one is defining the continuous surface to be built-up. After that, the tool position is determined to ensure that the clad is located centred at the tool position. Then, the common pattern used for this operation (helical) is predefined but it is offered the possibility to be modified according to the users' wishes.
- Tool axis: As it is explained in the description window, the tool axis is maintained along a specific vector defined by the user at this tab.

#### **IV.2.4.3 5-axis LMD**

The last programmed operation consists on a 5-axis LMD strategy. It is proposed for building up complex surfaces that require 5-axis continuous movements; such as IBRs or complex moulds and dies. The main target for this operation resides on following the principle of perpendicularity between the laser beam and the surface to be added. Figure IV.11 shows the operational menu, the description and an example of application.

Related to the inputs required from the user interface, the main difference compared with 3-axis LMD operation is the laser tool orientation. At this point, the laser tool axis orientation varies during the complete path for each tool tip coordinate. The predetermined option is *Normal to Part* according to defined specifications in the tool-paths generation. Notwithstanding, for experienced operators this tab offers other possibilities for tool axis orientation, such as *Swarf Drive* or *Interpolate Vector*. Both of them are commonly used for extreme complex surfaces with accessibility tool limitation. On the one hand, at the *Swarf Drive* the tool axis orientation is selected relative to the surface and completed with a range of tilt angle values. On the other hand, the *Interpolate Vector* allows the user to specify each tool path point with the corresponding tool axis position, however this programming process is tedious and time consuming.

Finally, it should be pointed out that in those cases where the elevated height of the geometry implies parameters control loosing, any of the two strategies, 3-axis LMD and 5-axis LMD, it is recommended to split the height in different sections in order to obtain an optimal temperature gradient in the material due to the process; implying more controlled geometrical

deformations. The main inconvenience of this sectioning is that some misalignments are observed between defined sections.

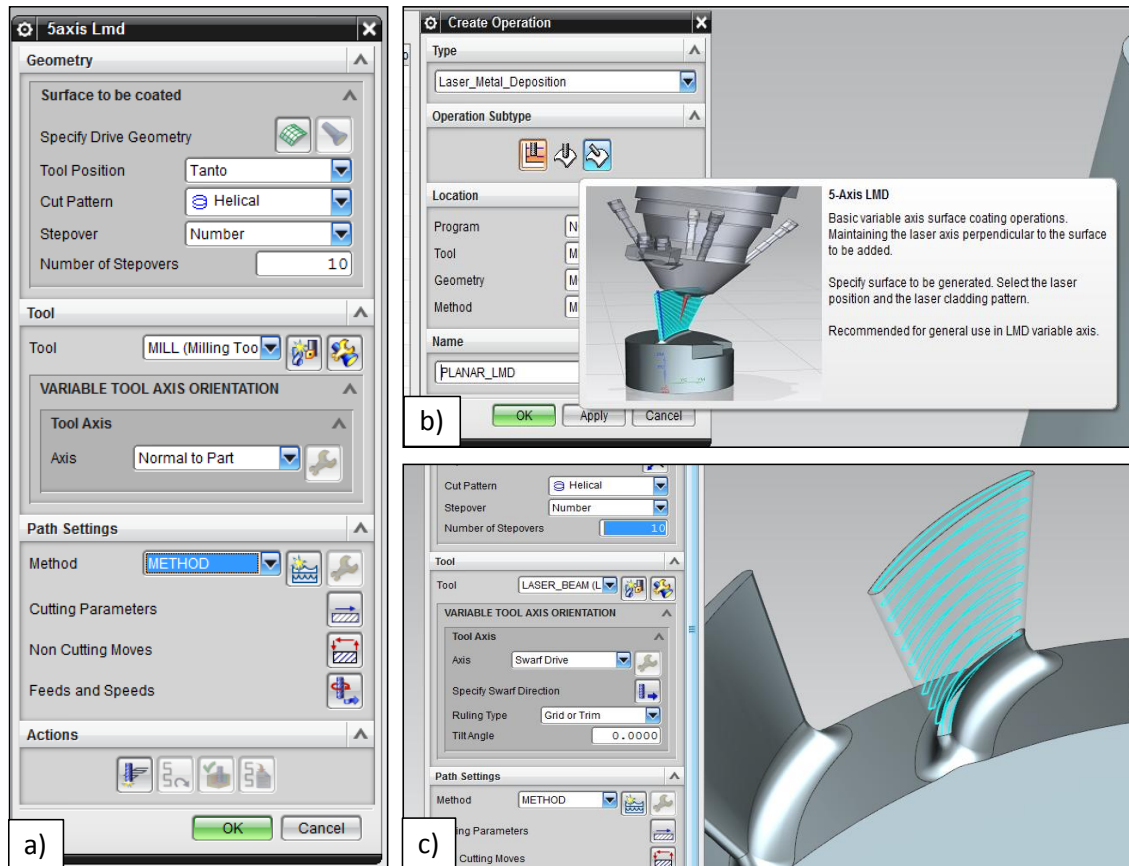


Figure IV.11 API 5-axis LMD operation: a) User menu, b) description and c) example of a blisk blade generation

### IV.3. API 2: development for added material geometry generation

Hitherto, the LMD CAM module is constructed in a similar manner as the common machining CAM modules, enabling the user to define process parameters, laser additive tool and tool-path to be used. Hence, once the programmer introduces the necessary input data (tool definition, AM conditions, nozzle feed, powder flux, laser power, etc.), it is performed the virtual verification of the programmed trajectory, avoiding collisions between the laser nozzle and the part to be generated and obtaining approximately the additive time expected for the selected tool-path.

It should be highlighted that using AM processes, the obtained geometry is unknown for SM leading to unexpected data, increasing manufacturing time in terms of oversizing the safety factor to avoid collisions, overcuts, undercuts, etc. For this reason, what the API 2 proposed at



this stage is directly related with the prediction of the expected added geometry. It is aligned with the surface finishing prediction offered by the machining CAM module, which compares the surface obtained after machining with the original part design and shows the dimensional deviation within a colour scale. For the case of LMD process, this API calculates the added material and generates the final obtained geometry displaying the clad generation along each layer and surface. Figure IV.12 shows the obtained outputs from each API: (a) generated tool-path and (b) the display of the clad and the final surface generation.

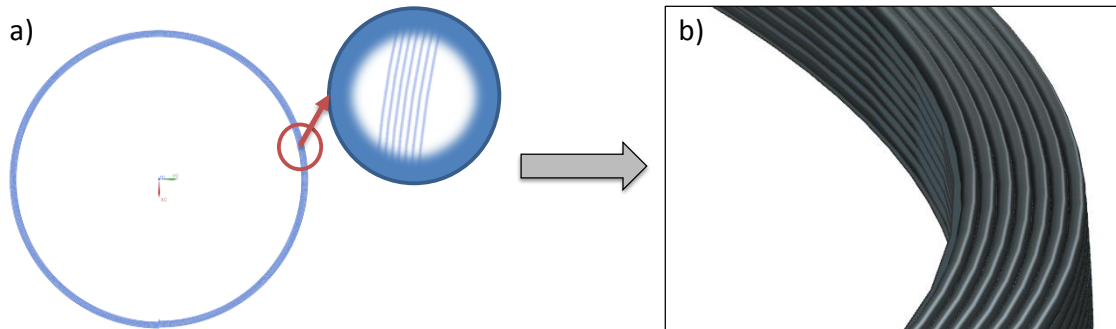


Figure IV.12 a) API 1 resulting tool-paths, b) API 2 resulting added geometry

Concerning the API code programming, a series of steps must be performed schematized at Figure IV.13. First of all, it is needed the input data from the API 1 NC code; this data is integrated in Visual Studio 2010® to be integrated in the algorithm for clad generation. At the same time the input related to the clad dimension is required (two options explained in the following sections).

After that, the clad generation model is implemented in Visual Studio 2010®, divided into three subprograms creating a library to be called from the CAM software. The programming language used for the algorithm implementation is C#, also available and understandable for NX Open, so the library is implemented inside the NX® software as the original libraries from this software.

The implementation of the developed solution was performed for the NX9.0® version environment. Notwithstanding, it should be highlighted that the developed API could be applied to any subsequent CAD/CAM software versions or adapted to any other CAD/CAM software with minor modification to avoid any programming language misunderstandings.

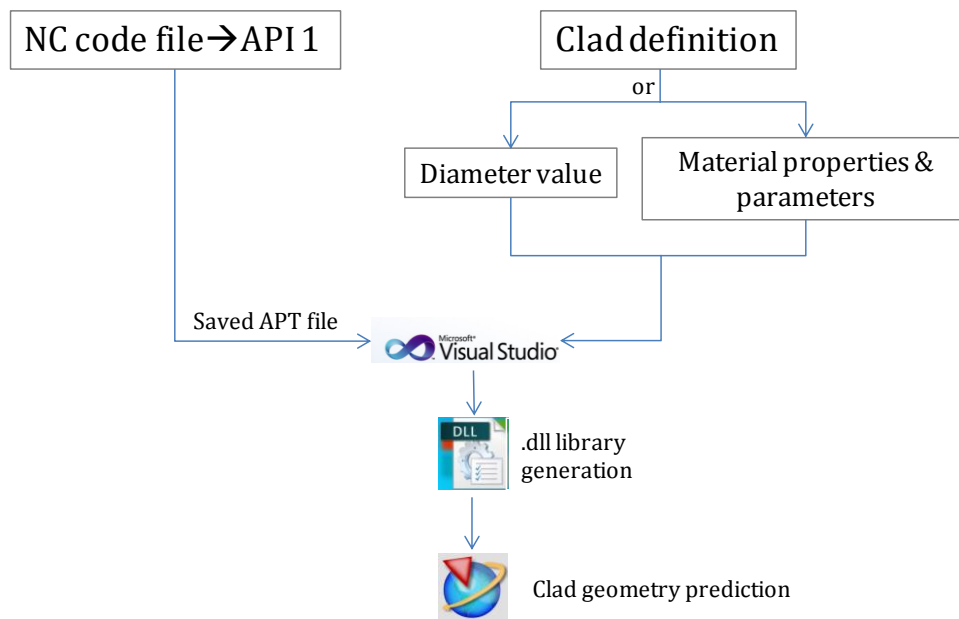


Figure IV.13 API 2: flowchart for final added geometry generation

### IV.3.1. Added material resulting solid

With the aim of running a more effective process, the implemented algorithm offers an approximation of expected geometry, so the blank that needs to be machined to a final size is known. For this purpose as it was mentioned previously, this API offers two different alternatives. The first one consists on introducing the clad diameter as a constant value determined by the user and the other one is based on a mass balance algorithm, where some equations are applied to calculate the added material according to the programmed tool-path strategy, considering material specifications and process parameters in order to predict the final geometry.

This new geometry estimation command is grouped into the analysis tools provided by CAM environments for manufacturing process optimization. In the specific case of this application, previous knowledge related to LMD adequate strategies and material behaviour for different LMD conditions, so the programmer could evaluate the adequacy of the obtained geometry for the machining process or the necessity of additional clad generation for the last finishing operations.

The programming of the API requires different steps to be performed internally once the command of LMD clad generation is activated. The programmed tool-paths are imported to Visual Studio 2010® to be implemented, later on, in the API code file. At the same time, all programmed steps for this API are performed supported by NXOpen functions. The following points describe the steps to generate the final growth part:

1. Primarily, the application performs an information storing process; that is, picking up the input data from the API 1 introduced by the user to be utilized in the model calculus. This model requires process information as the programmed tool path and the needed to choose which method will be used for clad generation. In the case that the user programmed more than one operation, this step offers the possibility of one by one. In this manner, each time that he user modifies LMD parameters; the algorithm recalculates the obtained added geometry.
2. In the second step, the API accesses to the *apt* file from the CNC ISO program. This file is composed of six columns of data with information related to tool-path points (the first three columns) and the tool orientation for each point (the second three columns). Therefore, at this step the file is cleaned up to be adapted to an adequate format for the following steps. In order to plot the different points and generate a spline, the tool orientation is removed and the coordinates format is modified to  $[x,y,z]$ .
3. In the third step, a spline is generated using the option *points from file*, the new coordinates file is implemented and plotted into the solid, creating the tool-path projection, representing the tool-tip coordinates from the post-processed LMD CNC program. This step is performed internally in Visual Studio 2010® to be considered the guide curve for the clad generation.
4. The fourth step corresponds to the clad diameter definition. Two different options are offered for the clad section definition, the first one is defined directly as an input based on the operator experience and, the other one, is calculated through a mass-balanced algorithm described in detail in the subsection IV.3.2. Once the clad section is determined, the circle is positioned at the beginning of the spline from the previous step. The main difference between the two clad diameter introduction options resides on the computational cost. The first one jumps directly into the circle design, the second option, however, makes a call to the subprogram that contains the mass-balanced algorithm and performs the needed calculus (this implies higher computational times). With the aim of facilitating the results obtained with the algorithm, the API pops-up a message window showing the obtained diameter value. Thus, this information could be considered by the user to determine the influence of selected parameters in the clad diameter.

5. In the last step, for the added geometry generation, the clad section is swept along the spline from the point 2. The combination of the different clads is converted into a new entire solid. Besides, this solid becomes the blank for the machining stage.

Once this application is run completely, important information is obtained for AM; additionally, this acquires special importance for hybrid manufacturing processes to optimise the machining process in terms of reducing non-cutting movements, so machining times.

### IV.3.2. Mass-balance based algorithm for the estimation of the added clad geometry

As a basis for programming the geometrical estimation algorithm, (I. Tabernero A. L., 2012) proposed a geometric modeling of added layers which data was supported from other developed models as powder flux model, attenuation model and thermal model. Establishing this geometric model as a reference, and including data by the user from experimental tests, such as powder flux and material density, Figure IV.14 shows the simplification performed by this algorithm to calculate clad diameter through stated equations:

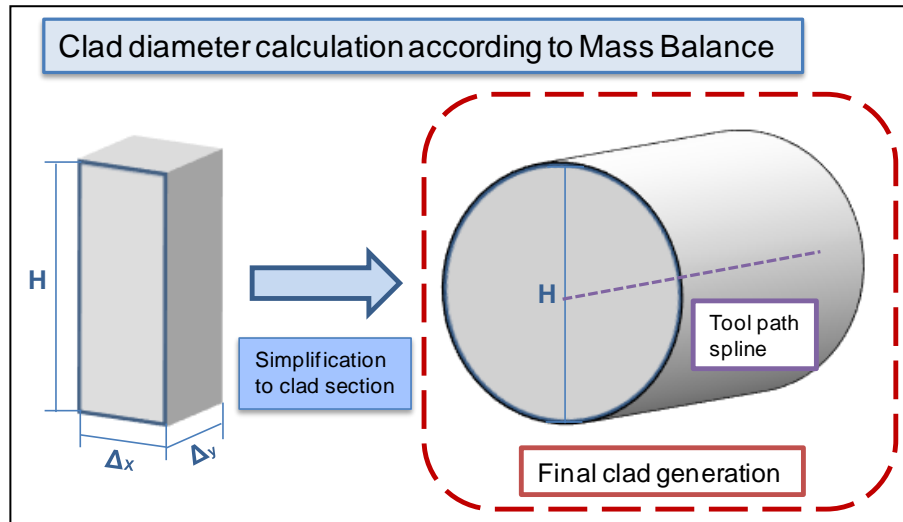


Figure IV.14 Calculation of LMD clad diameter according to Mass Balance algorithm

Figure IV.14 shows the parallelepiped generated in the control point where the material will be added. So the **Eq.1** determines the clad volume for defined parallelepiped:

$$Clad_{volume} = \Delta x * \Delta y * H \quad (Eq. 1)$$

This geometric model consists of a balance between the powder mass injected material in the point  $i$  and the parallelepiped added mass in the same point  $i$ . See **Eq.2**.

$$m_i^i = m_p^i \quad (\text{Eq. 2})$$

Added mass on  $i$  point depends on the powder flux in  $i$  point ( $\phi_i$ ) along the time spent for that addition in that point ( $t_{iny}$ ).

$$m_i^i = \phi_i * \Delta x * \Delta y * t_{iny} \quad (\text{Eq. 3})$$

Injection time in turn depends on tool-path discretization length ( $\Delta s$ ) divided by nozzle feed rate ( $v_f$ ).

$$t_{iny} = \Delta s / v_f \quad (\text{Eq. 4})$$

Besides, parallelepiped mass depends on material density ( $\rho_{mat}$ ) and generated volume.

$$m_p^i = \rho_{mat} * \Delta x * \Delta y * H_i \quad (\text{Eq. 5})$$

In this way, it is possible to calculate clad height for each point using **Eq.2** and replacing values with **Eq.3**, **Eq.4** and **Eq.5**:

$$m_i^i = m_p^i \rightarrow \phi_i * \Delta x * \Delta y * \Delta s / v_f = \rho_{mat} * \Delta x * \Delta y * H_i \rightarrow$$

$$H_i = \frac{\phi_i * \Delta s}{\rho_{mat} * v_f} \quad (\text{Eq. 6})$$

Finally, in this case it was assumed that clad diameter has the same value as clad height for the geometrical calculation.

$$Clad_{Diameter} = H_i \quad (\text{Eq. 7})$$

**Eq.6** presents the relation of the clad diameter with four different LMD process parameters. As initial assumption and according to the process, value of tool-path discretization length ( $\Delta s$ ) is defined during operations parameters definition, in a similar manner as in machining operations. Thus, at this point the API demands to the user the powder flux ( $\phi_i$ ), material density ( $\rho_{mat}$ ) values and the feed rate ( $v_f$ ); calculating internally the final clad section before generating the added geometry.

### IV.3.3. API 2 integration into API 1

For this API 2 integration into the API 1, it should be remarked that external software is needed to perform the algorithm calculus, in this case Visual Studio 2010®. Moreover, some data from the API 1 is demanded by the API 2, so the accessibility from one to the other must

be direct. For this purpose, Figure IV. 15 shows the access that is created through a button named *LMD Clad Generation* or pressing *F11* key.

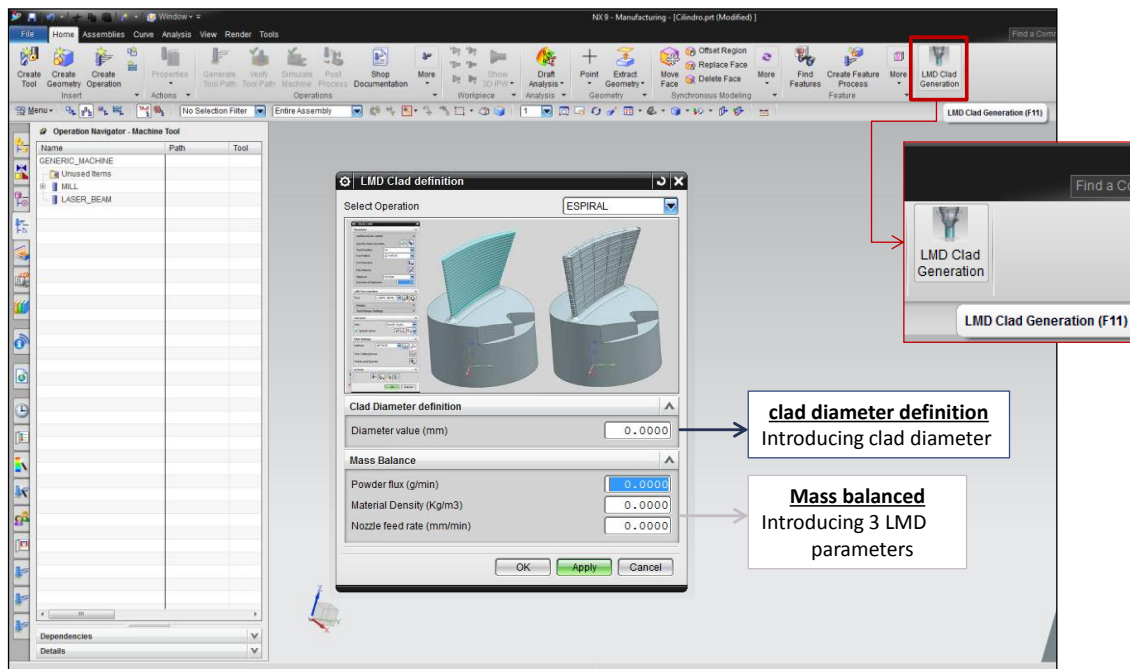


Figure IV.15 Developed API menu for LMD clad generation and LMD operation selection

Once more, in order to create this direct access some steps needs to be followed and described in detail hereafter.

1. **Programming a specific Menu for NX environment:** for this purpose, NX® contains a module denominated *Block UI Styler* (the access to this module: *File//All Aplications//Block UI Styler*). Inside this module, an editor is found that allows creating and personalising user menus. Figure IV. 16 shows different options for the menu, the generated menu for the application and the window with different parameters to determine menu names and images. Additionally, there is a tab named *Code generation* where the programming language is selected to implement the created menu inside the external software and complete it within the same programming language. In this case, C# was selected for the entire code programming, and the menu was divided into three main groups: (a) operation selection with explicative image, (b) clad diameter definition and (c) Mass balance parameters.

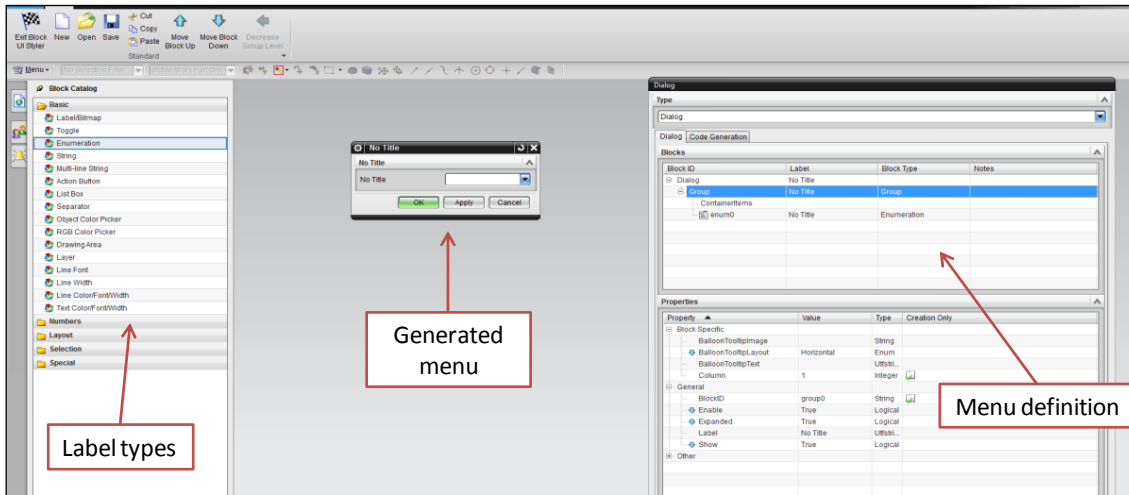


Figure IV.16 Block UI Styler and menu editor

Once the menu is completed and saved, two different files are generated with .cs and .dlx extensions. The first extension is the one implemented into the Visual Studio 2010® and the .dlx is related to internal NX® libraries.

2. **New project generation:** Inside the Visual Studio 2010®, new Class Library (.dll) is created to implement the created menu and different steps/algorithms to obtained API results. Figure IV. 17 shows the programming window with three sections: program code, project tree and the error/warning section. Firstly, the .cs file from the menu generation is included into the project. It should be mentioned that the menu is empty of code that will be completed afterwards.

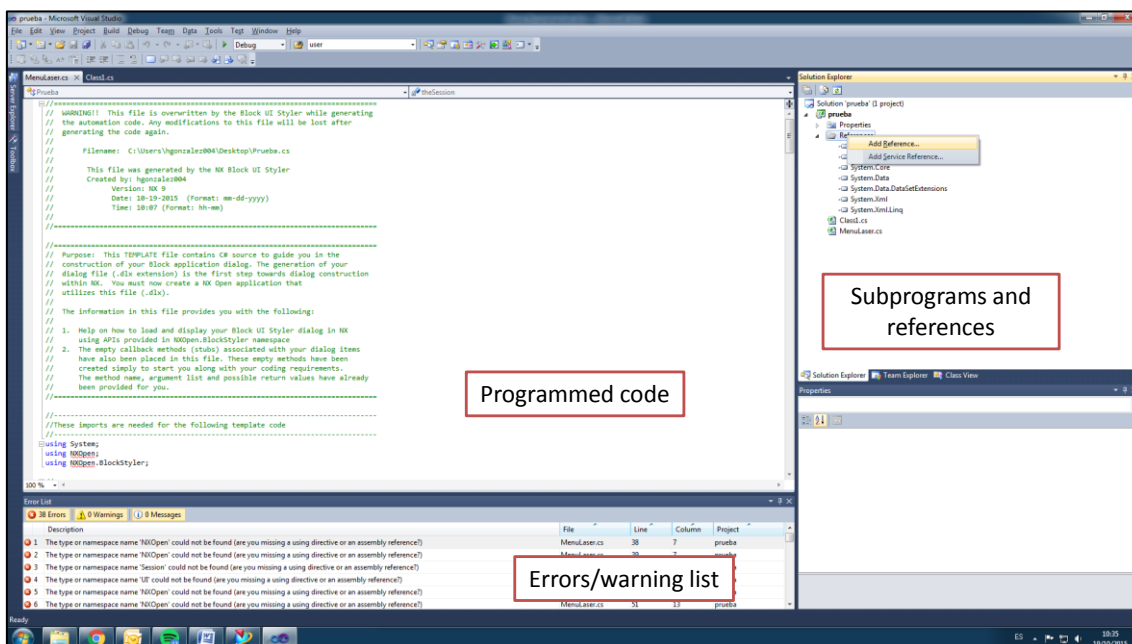


Figure IV.17 Visual Studio 2010® programming window

At this point, the error list claims some references from NXOpen for the library compilation to be understood by the CAD/CAM software. The required references are: NxOpen, NxOpen.UF, NxOpen.utilities and NxOpen.UI, all of them found in the following route: *C:\Program Files\Siemens\NX 9.0\UGII\managed*.

Now, the inserted menu is completed with different subprograms to perform the API steps described in previous sections. Figure IV. 18 shows a fragment of one of the subprograms for the additive operation selection. Once the code is completed with the needed subprograms and saved, a folder is generated with a main file *.sln* that contains the code to be modified, and different subfolders are found, where the file of the external library *API\_LASER.dll* is located.

```
{
  //1.SELECT THE OPERATION TO BE ANALYZED//
  int cont = 0;
  Session theSession = Session.GetSession();
  UI theUI = UI.GetUI();
  Part dispPart = theSession.Parts.Display;
  NXOpen.CAM.OperationCollection opers = dispPart.CAMSetup.CAMOperationCollection;
  IEnumerator en = opers.GetEnumerator();
  en.Reset();

  while (en.MoveNext())
  {
    cont++;
  }
  string[] listaop = new string[cont];

  en.Reset();
  cont = 0;
  while (en.MoveNext())
  {
    Operation oper = (Operation)en.Current;
    listaop[cont] = oper.Name;
    cont++;
  }
  enum0.SetEnumMembers(listaop);
}
```

Figure IV.18 Operation selection C# fragment from the API code

3. **Button design and API call:** In order to call the programmed API, there are two options. The first one is executing the *.dll* file directly from *File/Execute/NxOpen* and the second one consists on linking the *.dll* file to a customized button. Figure IV. 19 presents the customization window for the button definition. It is defined the type of library file (NxOpen), the file route and the image to be shown representing the API. Additionally, this button is included in the command bar as a quick access.



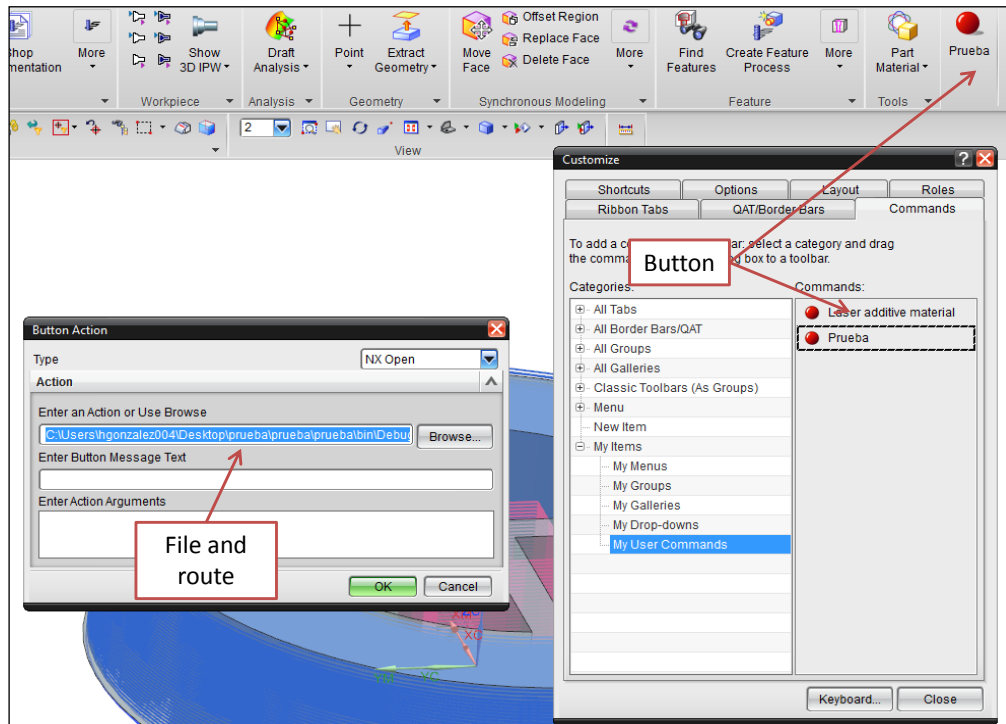


Figure IV.19 Operation selection C# fragment from the API code

## IV.4. Integration of the virtual machine for a complete simulation of the process

The virtual verification is one of the stages inside the manufacturing chain, currently integrated for machining processes. This stage offers the possibility of machining process verification related to possible collisions, elevated material removal rates, surface finishing, cutting speed optimization and non-cutting movements reduction. There are some commercial software available in the market oriented to give a solution for this challenge, such as Vericut® or the *Machine Tool Builder* module from NX®. In this manner, it is possible to work through every manufacturing stage inside the same digital environment for a part fabrication: Designing, machining, virtual verification and NC code post-processing.

Nevertheless, more concretely for AM processes, it is an actual necessity in industry due to the lack of specific software for these processes. On this account, this chapter presents the integration of the LMD centre into the virtual verification module from NX®, as the final step for the developed CAM module. It should be pointed out that the main objective for this verification resides on the possible collisions detection during the process performance. Moreover, the LMD virtual verification is considered a great need due to the quantity of elements involved in the process *per se* (laser nozzles, clamping fixtures, additional

measurement devices...) and the risk of collisions during multi-axis movements. Furthermore, for complex geometries generation that requires 5-axis simultaneous movements to keep the laser beam perpendicularity, the tool-paths imply an elevated collisions risk compared to more simple strategies. Thus, the process virtual verification grants a quick preview of machine components movements and prevents the appearance of collisions.

At the present work, it was performed the virtual integration of the machine used at the following sections. The machine implemented into NX® environment consists on a 5-axis Aktinos 500 retrofitted machine (3 linear axes and 2 rotary axes on a tilting table), equipped with a fiber laser Rofin FL010 with a maximum power of 1kW. Additionally, the machine was equipped with a height measuring sensor (range from 50 mm to 210 mm) and a coaxial nozzle. Figure IV. 20 shows the real machine and different components/parameters considered to define the digital environment. It is important to highlight that the exact definition of the geometry related to these components, as well as machine tool base and tilting table are crucial for the preview collisions feasibility.

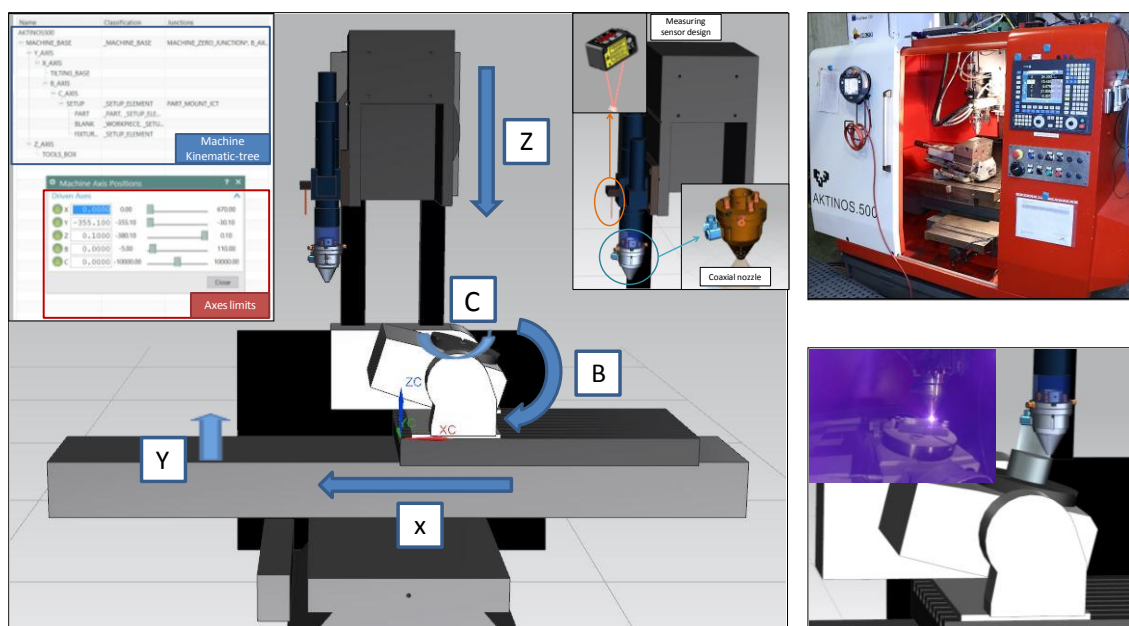


Figure IV.20 Digitalization of retrofitted Kondia B-500 and single-blade real process verification (UPV/EHU)

The virtual machine configuration process requires a serial of inputs to be run adequately. Firstly, it is needed to model different machine components involved in the process separately (machine base, tilting table, LMD nozzle and measuring sensor). In order to model the different machine components, CAD module from NX-Siemens is utilized. After designing each element individually, the machine is assembled considering the real position of each element and the co-relation between them.

Secondly, the machine kinematic three and the links between different machine elements needs to be introduced. In this case, the machine base and structure are defined as fixed components, so the rest elements are movable and mounted on the machine base. Directly over the machine base is located the Y axis, and depending on it is located the X axis. Mounted on the X axis it is situated the tilting table (B axis) and the rotary C axis. Finally, the Z axis is located along the machine structure where the nozzle and the height measuring device are integrated. Every axes travels are defined as a relative movement from the machine zero.

Finally, the postprocessor associated to the machine and the corresponding archive for the NC code transformation are required; in this case, it is the control Fagor 8070. Furthermore, this CNC needs to be completed with specific LMD code requirements, i.e. laser on and laser off commands. In addition, the laser beam is also virtualized with the objective of controlling the focal distance and the nozzle during every path movement.

## **IV.5. Validation of the defined methodology in single tracks**

### ***IV.5.1. Definition of used equipment***

The equipment used for the experimental tests for API validation is described in this section. In short, used equipment consists on a 5-axis kinematic machine with a high powered laser installed and a powder cladding nozzle. Finally, it is necessary the installation of a powder feeder system.

The experimental tests were performed with a conventional 3-axis milling machine Kondia B-500, that in 2010 was retrofitted to be converted into LMD machine with 3+2 continuous axes denominated Kondia Aktinos 500 (Table IV.1). This retrofitting process was carried out exclusively at the University of the Basque Country (UPV/EHU). Thus, it is the unique cell with this configuration; the X and Y axes are located in the machine base, where a tilting table is mounted with (B and C) or (A and C) depending on the process necessity. The complete virtualization of this machine with different axes configuration was described in the corresponding section (IV. 4) of this chapter.

On top of that, Table IV.2 contains the fibre laser cell with a power of 1 kW Rofin FL010 main characteristics.

Table IV.1 Kondia Aktinos-500 machine working characteristics



| <b><u>KONDIA AKTINOS-500</u></b>  |                              |                              |
|---|------------------------------|------------------------------|
|  | <b>Model</b>                 | Aktinos 500                  |
|   | <b>Numerical Control</b>     | FAGOR 8070                   |
|   | <b>Travels (X/Y/Z ; A/C)</b> | 600/400/380 mm ; 110°/± 360° |
|   | <b>Working area</b>          | 700 x 360 mm                 |
|   | <b>Feed</b>                  | Max. 24.000 mm/min           |
|   | <b>Positioning precision</b> | ± 0,01 mm                    |
|   | <b>Repeatability</b>         | ± 0,005 mm                   |
|   | <b>Resolution</b>            | 0,001 mm                     |

Table IV.2 Fiber laser Rofin FL010 characteristics

| <b><u>FIBER LASER ROFIN FL010</u></b>   |                     |                                      |
|---|---------------------|--------------------------------------|
|  | <b>Model</b>        | Rofin FL010                          |
|   | <b>Power</b>        | 1 Kw                                 |
|   | <b>Wavelength</b>   | Range of 1 µm                        |
|   | <b>Beam Quality</b> | 3-4 mm x mrad (using a 100 µm fiber) |
|   | <b>Kinematic</b>    | Kondia Aktinos-500                   |

The equipment used for feeding the powder is a SULZER Twin-10C feeder and its characteristics are shown in Table IV.3. This feeder allows the powder flux regulation through the rotation of a disc that distributes the powder to the nozzle.

**Table IV.3** Sulzer Twin-10C powder feeder characteristics

| <b>POWDER FEEDER SULZER TWIN 10-C</b> |                       |
|---------------------------------------|-----------------------|
| <b>Model</b>                          | SULZER TWIN 10-C      |
| <b>Powder flux</b>                    | 2 - 150 g/min         |
| <b>Powder size</b>                    | 2 - 200 $\mu\text{m}$ |
| <b>Gases</b>                          | Argon/Nitrogen        |
| <b>Gas pressure</b>                   | Max. 4 bar            |



The utilized nozzle consists on a continuous coaxial nozzle developed at the Department of Mechanical Engineering from the University of the Basque Country (UPV/EHU). The main characteristics and the design are exposed at the Table IV.4.

**Table IV.4** Continuous coaxial nozzle design and characteristics

| <b>POWDER FEEDER SULZER TWIN 10-C</b> |                       |                          |
|---------------------------------------|-----------------------|--------------------------|
|                                       | <b>Performance</b>    | Approx. 45%              |
|                                       | <b>Material</b>       | Stainless steel AISI 304 |
|                                       | <b>Powder flow</b>    | 2 - 150 g/min            |
|                                       | <b>Focal distance</b> | 14.5-15 mm               |

### IV.5.2. Material selection

The first step for the geometrical mass-balanced API verification consists on a serial of single tracks generated by LMD and controlled obtained clad diameters. The second step for this application is a complete blisk generation. For this purpose, two materials were selected common in the aeronautical sector, Inconel®718 for the core and Hastelloy®X for building up geometries.

On the one hand, related to Inconel®718 (Table IV. 5), it is one of the materials most widely used in the aeronautical sector in the last decades, representing more than the 30% of the engine total weight in commercial aircrafts (Schafrik R.E., 2001). A thermoresistant Ni based alloy that could achieve a working temperature up to 650 °C maintaining mechanical properties. Moreover, it is characterized by good resistance to fatigue and creep combined with high corrosion resistance under extreme working conditions at high temperatures. Despite of the relatively low thermal conductivity of Ni based alloys, the LMD process creates clad structures with fine grains and uniforms (Figure IV.21).



**Figure IV.21** Microstructure from LMD Inconel®718 clad generation (UPV/EHU)

Furthermore, this material is hardened by precipitation of the secondary phases ( $\gamma'$  and  $\gamma''$ ), what makes possible to be added without thermal treatment, so the treatment could be performed after the repairing operation to improve mechanical properties in those areas that are affected thermally during the process.

On the other hand, Hastelloy®X consists of a nickel-based superalloy that presents an excellent balance between resistance to oxidation and maintaining mechanical properties working under extreme temperatures, up to 1204°C (T. Sakthivel, 2012). Moreover, it is able to retain the protective oxide layer at high temperatures and consequently, retains the oxidation resistance (upmet, 2018). These are the reasons why this superalloy is considered to be used in aircrafts and turbine engines for combustion-zone components. It is worth mentioning that

this material has excellent weldability property, what suits with LMD process. Table IV. 6 shows Hastelloy®X chemical composition, mechanical and physical properties.

**Table IV.5** Inconel®718 composition, mechanical and physical properties (Kitagawa, Kubo, & Maekawa, 1997)

| <b>Chemical composition (%) of Inconel®718</b> |                  |                        |               |               |                 |      |      |      |      |    |     |    |
|--|------------------|------------------------|---------------|---------------|-----------------|------|------|------|------|----|-----|----|
| Ni   | Cr               | Fe                     | Mo            | Co            | Tg              | C    | Mn   | Si   | B    | Nb | Al  | Ti |
| 52.5   | 19               | 17                     | 3             | 1             | 0.6             | 0.08 | 0.35 | 0.35 | 0.01 | 5  | 0.6 | 1  |
| <b>Mechanical and physical properties</b>      |                  |                        |               |               |                 |      |      |      |      |    |     |    |
| Young's Modulus                                | Tensile Strength | Density                | Specific Heat | Melting Temp. | Thermal Conduct |      |      |      |      |    |     |    |
| 200 GPa  | 1.73 GPa         | 8470 kg/m <sup>3</sup> | 461 J/(kg·K)  | 1700 K        | 15 W/(m·K)      |      |      |      |      |    |     |    |

**Table IV.6** Hastelloy®X composition, mechanical and physical properties (International, 2018)

| <b>Chemical composition (%) of Hastelloy®X</b> |                  |                        |               |               |                 |     |           |           |               |             |             |              |
|--|------------------|------------------------|---------------|---------------|-----------------|-----|-----------|-----------|---------------|-------------|-------------|--------------|
| Ni   | Cr               | Fe                     | Mo            | Co            | Tg              | C   | Mn        | Si        | B             | Nb          | Al          | Ti           |
| 47   | 22               | 18                     | 9             | 1.5           | 0.6             | 0.1 | 1<br>max. | 1<br>max. | 0.008<br>max. | 0.5<br>max. | 0.5<br>max. | 0.15<br>max. |
| <b>Mechanical and physical properties</b>      |                  |                        |               |               |                 |     |           |           |               |             |             |              |
| Young's Modulus                                | Tensile Strength | Density                | Specific Heat | Melting Temp. | Thermal Conduct |     |           |           |               |             |             |              |
| 205 GPa  | 0.765 GPa        | 8220 kg/m <sup>3</sup> | 486 J/(kg·K)  | 1580 K        | 9.1W/(m·K)      |     |           |           |               |             |             |              |

### IV.5.3. API 2 estimation: single tracks and single blade

With the aim of analysing the viability of using the LMD process for Hastelloy®X and determining optimal LMD parameters for building-up Hastelloy®X over Inconel®718, 12 tests were performed with different LMD parameters combination: laser power, feed rate and



powder mass. Figure IV. 22 shows (a) the different added clads numbered according to each test and different clad geometrical parameters designation to be measured. In addition, Table IV. 7 shows the 12 tests and the measuring results of each generated clad. The main reason why those geometrical parameters were selected lies on the importance of the ratio between the height [H] and width [W] of the clad. This ratio is used as the key parameter to determine the optimum process conditions being directly related with the wetting angle of the clad, variable previously studied by (Y. Tian D. T., 2017).

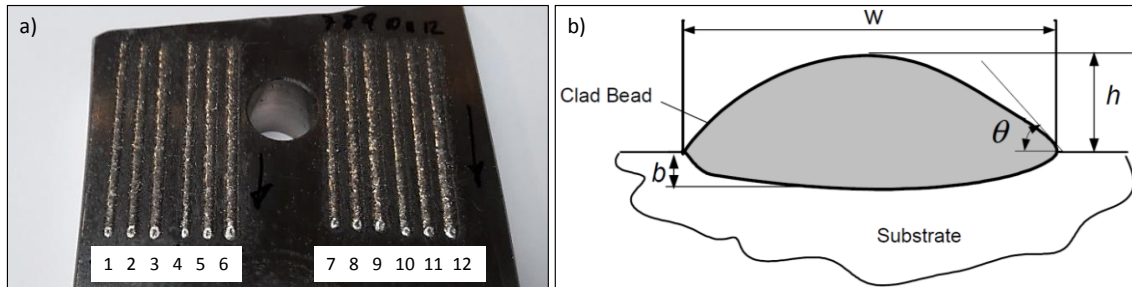


Figure IV.22 a) Hastelloy®X performed 12 test (UPV/EHU), b) clad geometrical parameters (Toyserkani E. K. A., 2004)

Table IV.7 Hastelloy®X experimental tests to obtain adequate LMD parameters

| Test | Laser Power [W] | Feed Rate [mm/min] | Powder Mass Flow [g/min] | Clad Dimensions [mm] |       |       |      |
|------|-----------------|--------------------|--------------------------|----------------------|-------|-------|------|
|      |                 |                    |                          | Height               | Width | Depth | H/W  |
| 1    | 500             | 500                | 4                        | 0.24                 | 1.38  | 0.66  | 0.18 |
| 2    | 600             | 500                | 4                        | 0.24                 | 1.57  | 0.69  | 0.15 |
| 3    | 700             | 500                | 4                        | 0.21                 | 1.73  | 0.67  | 0.12 |
| 4    | 400             | 400                | 4                        | 0.21                 | 1.29  | 0.65  | 0.16 |
| 5    | 500             | 400                | 4                        | 0.24                 | 1.53  | 0.93  | 0.16 |
| 6    | 600             | 400                | 4                        | 0.31                 | 1.66  | 0.76  | 0.19 |
| 7    | 500             | 500                | 6                        | 0.35                 | 1.62  | 0.98  | 0.22 |
| 8    | 600             | 500                | 6                        | 0.35                 | 1.68  | 0.98  | 0.21 |
| 9    | 700             | 500                | 6                        | 0.32                 | 1.72  | 0.96  | 0.19 |
| 10   | 400             | 300                | 3                        | 0.33                 | 1.41  | 0.75  | 0.23 |
| 11   | 500             | 300                | 3                        | 0.25                 | 1.71  | 0.95  | 0.14 |
| 12   | 600             | 300                | 3                        | 0.26                 | 1.85  | 1.07  | 0.14 |

After the analysis of obtained results, it was concluded that the test 10 presented the optimal ratio between the height and the width of the clad. Therefore, test 10 parameters are selected for the following entire blisk geometry generation.

With the aim of the developed API 2 validation and as it was mentioned in the geometrical model simplification, the height was selected to be compared with the calculus from the mass-

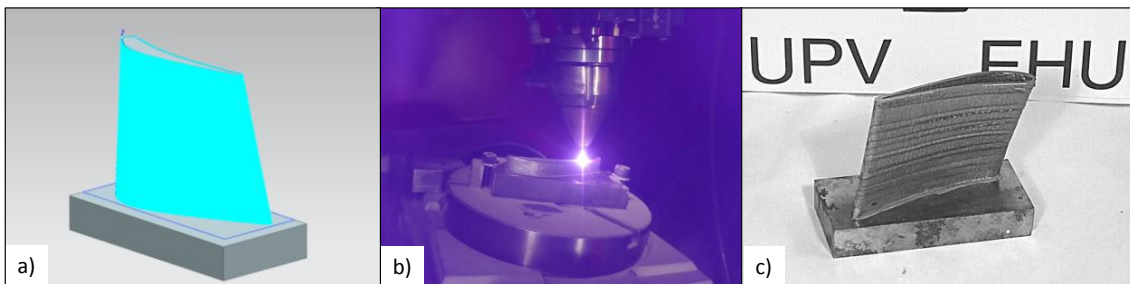


balanced algorithm (shown in Table IV. 8). It was selected the performed tests with those parameters that presented higher ratios between height and width (1, 6-10).

**Table IV.8** Validation of API 2 clad diameter calculation

| Test      | Laser Power [W] | Feed Rate [mm/min] | Powder Mass Flow [g/min] | Clad dimension H [mm] | API Clad diameter [mm] |
|-----------|-----------------|--------------------|--------------------------|-----------------------|------------------------|
| 1         | 500             | 500                | 4                        | 0.24                  | 0.25                   |
| 6         | 600             | 400                | 4                        | 0.31                  | 0.30                   |
| 7         | 500             | 500                | 6                        | 0.35                  | 0.36                   |
| 8         | 600             | 500                | 6                        | 0.35                  | 0.36                   |
| 9         | 700             | 500                | 6                        | 0.32                  | 0.36                   |
| <b>10</b> | <b>400</b>      | <b>300</b>         | <b>3</b>                 | <b>0.33</b>           | <b>0.30</b>            |

It should be mentioned that these expected results correspond to a single track mono-clad generation, which are slightly different from 5-axis generated geometries. In order to evaluate the LMD behavior for 5-axis continuous movements, a single blade with complex geometry was selected as a demonstrator (Figure IV. 23). Inconel®718 was selected for the single blade generation, selecting process parameters based on previous knowledge. Moreover, 5-axis helically growing was selected as the LMD strategy, maintaining the perpendicularly principle between the nozzle and the surface to be added. Therefore, the process behaviour of the virtual verification and complex LMD strategies could be evaluated.



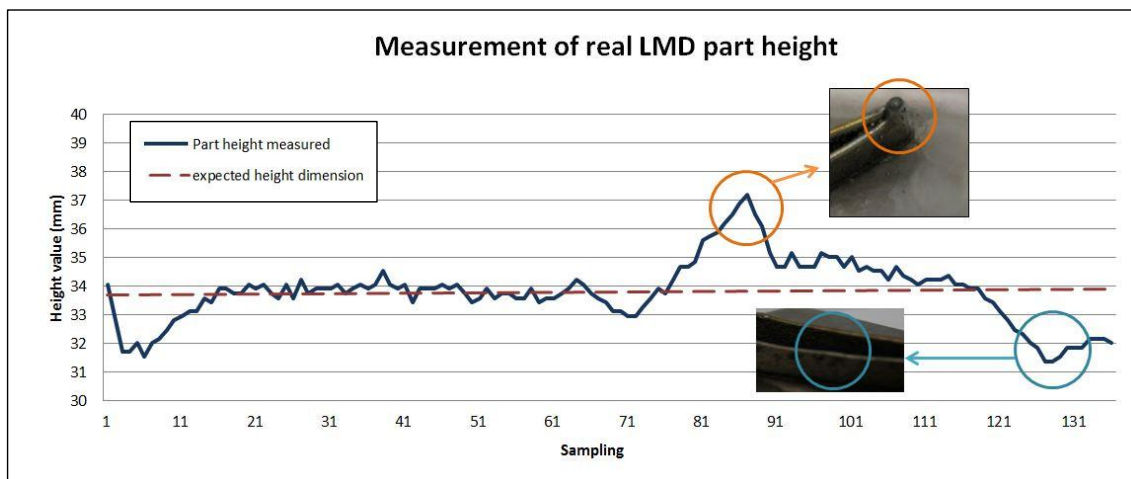
**Figure IV.23** a) single blade demonstrator and LMD strategy design, b) LMD process and c) final blade generated by LMD process

Table IV. 9 shows selected LMD process parameters for the single blade generation and the expected total height. With the objective of controlling the growing process and possible issues presented in 5-axis LMD strategies, the blade generation was interrupted at 34 mm (theoretically programmed) to be measured with the height sensor.

**Table IV.9** LMD process parameters for Inconel®718 single blade generation

| Laser Power [W] | Feed Rate [mm/min] | Powder Mass Flow [g/min] | Clad distance $\Delta z$ [mm] | API theoretical total height [mm] |
|-----------------|--------------------|--------------------------|-------------------------------|-----------------------------------|
| 650             | 500                | 5                        | 0.45                          | 34                                |

As it was mentioned before, a height measuring sensor was implemented aligned with the machine spindle. Hence, it is used the same tool-path programmed for LMD but relocated in X direction to be aligned with the micro laser remote sensor. This offers the possibility of measuring intermediate and final part height avoiding unclamping errors and optimising the process timing with not removing the piece for an inspection approach. Figure IV. 24 shows the obtained results at the intermediate height of 34 mm.



**Figure IV.24** a) LMD blade intermediate height measurements and different issues observed in 5-axis LMD process

Obtained results shown two main issues presented in the single blade LMD manufacturing. On the one hand, the orange circle shows the narrowest area presented in the designed geometry and presents undesired extra material. This issue is derived from the difficulties on the geometry that requires a completely change of direction in one point, so the machine spends more time adding material at that point that the optimal one. On the other hand, blue circle represents an area where the material did not grow as much as programmed. This issue is a consequence from 5-axis movements; it depends on the inclination angle at those points. Therefore, the clad height is reduced when the process is under 5-axis movements. The main reason for this issue is explained by the differences found in the Gaussian distribution compared with a flat substrate.

## IV.6. Case of study: Blisk LMD

As a final demonstrator, a blisk geometry was selected because it presents many challenges to be faced: (1) the necessity of repairing operations for these components, (2) the complexity found on the geometry definition and (3) the nozzle accessibility limitation for closed blades. Figure IV. 25 shows (a) the design of the blisk geometry with 18 Hastelloy®X blades built up over an Inconel®718 core and (b) the 5-axis LMD strategy definition using the API 1.

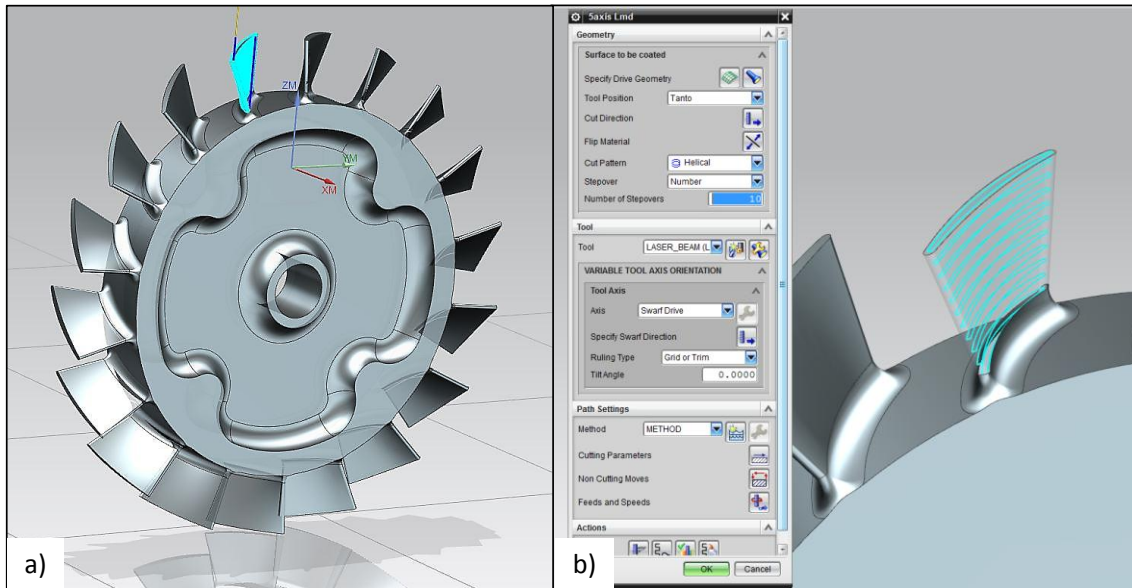


Figure IV.25 a) defined blisk geometry and b) API 1 LMD 5-axis strategy programming

Concurrently and according to the results from the performed tests in the previous subsection of Hastelloy®X over Inconel®718, LMD process parameters were selected as the test number 10 (Table IV. 10).

Table IV.10 LMD process parameters for Inconel®718 blisk generation

| Laser Power [W] | Feed Rate [mm/min] | Powder Mass Flow [g/min] | Protector gas flow rate [l/min] | Carrier gas flow rate [l/min] |
|-----------------|--------------------|--------------------------|---------------------------------|-------------------------------|
| 400             | 300                | 3                        | 13 (5bar)                       | 5.5 (1bar)                    |

The following step at the proposed methodology consists on the virtual verification and the clad/final obtained geometry estimation. Thus, Figure IV. 26 shows the virtual verification to ensure that using LMD with the programmed strategy avoids nozzle collisions with the consecutive blades and the expected final geometry introducing, into the mass-balanced algorithm (0.30 mm of clad diameter), the corresponding data related to defined process parameters.

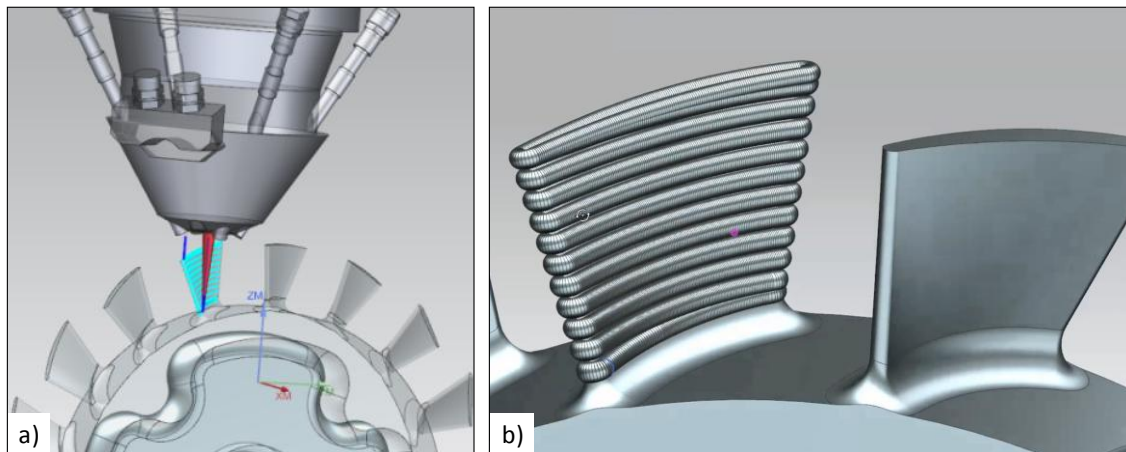


**Figure IV.26** a) LMD nozzle virtual verification and b) final geometry obtained with the mass-balance algorithm

It should be highlighted that an adequate tool-path selection is crucial to cover an optimal solution for such a complex geometry generation. Among the different strategies inside the performed interface, 5-axis LMD was selected, programming each blade with 5-axis helically and continuously movements, maintaining the perpendicular principle between the nozzle and the surface to be added. Notwithstanding, these kind of components presents an extra challenge due to the proximity between blades that leads to thermal issues (time to energy dissipation) so the necessity of stopping before the following blade generation. With the aim of optimising the blisk generation process, individual blades generation was programmed in alternation, following the order shown in Figure IV.27.

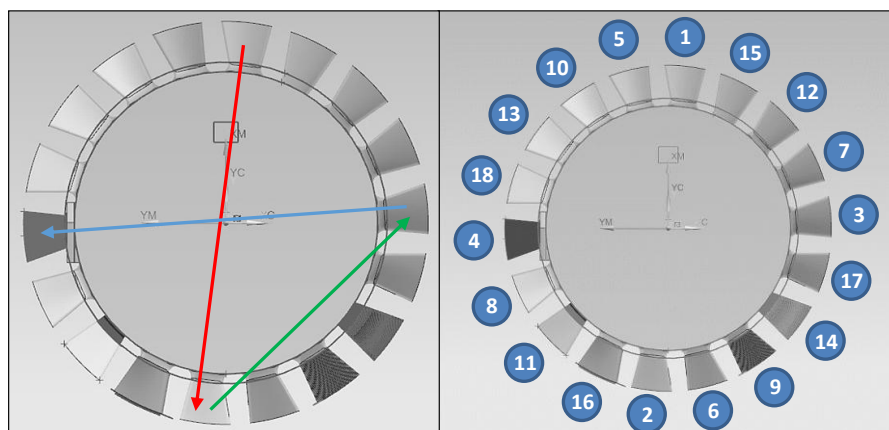


**Figure IV.27** Individual blades order of generation

Finally and with the aim of measuring dimensional deviation of the obtained part before the LMD process, an optical scanner (ATOS GOM®) based on blue light was used. The measurement generated a cloud of points to be compared with the original design of the final desired part. Figure IV. 28 shows on the top the process followed from (a) the entire blisk

generation, (b) unclamping finished added part and (c) the blue light scanning process; (d) and (e) shows obtained results from the LMD dimensional deviation.

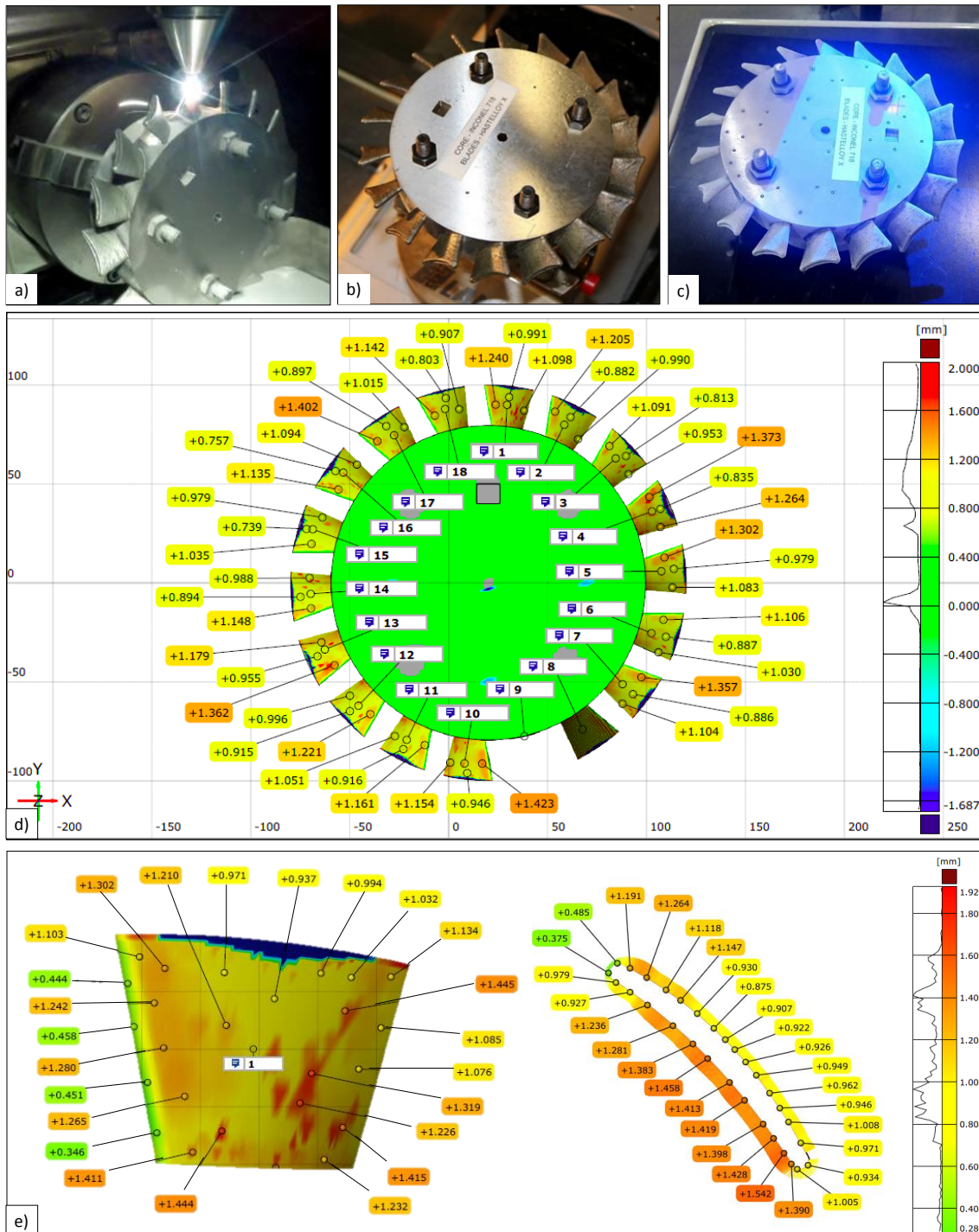


**Figure IV.28** a) LMD process for blisk generation, b) Obtained blisk geometry, c) Optical scanning process, d) General overview of dimensional deviation results, e) Blade 1 results from the front and the top point of view

Figure IV.28 (d) shows a general overview from the entire obtained blisk, it is appreciated the repeatability of the process tendency, presenting similar overbuilt and underbuilt material around each blades surfaces. The overbuilt material range varies from 0.5 and 1.5 mm to be



required and considered at the next step (machining) inside the proposed methodology. Furthermore, Figure IV. 28 (e) presents also the top view of the generated geometry, so it is shown, on the overbuilt (concave size) and underbuilt material (convex size), the change of orientation and inclination of the nozzle relative to the optimal flat substrate to maintain the perpendicularity to the surface to be added. Finally, at the blade two rounding corners are presented; however the extra material is different for each one. This difference is derived from the machine movements needed to change the direction, applying more time on the bottom side with higher and complex machine movements requirements (yellow to orange) than the time to change the direction on the top side (yellow to green) performing a more direct machine movement.

Regarding the blades height, a lack of material is presented on the top of blades (coloured in blue) what means that even though the expected blade height was 21 mm and it was achieved a height of 19 mm during the height measurements using the micro laser remote sensor (Figure IV. 29). Hence, similar behaviour at the previous section where single blade was presented related to 5-axis LMD issues (completely change of direction and inclination angles).

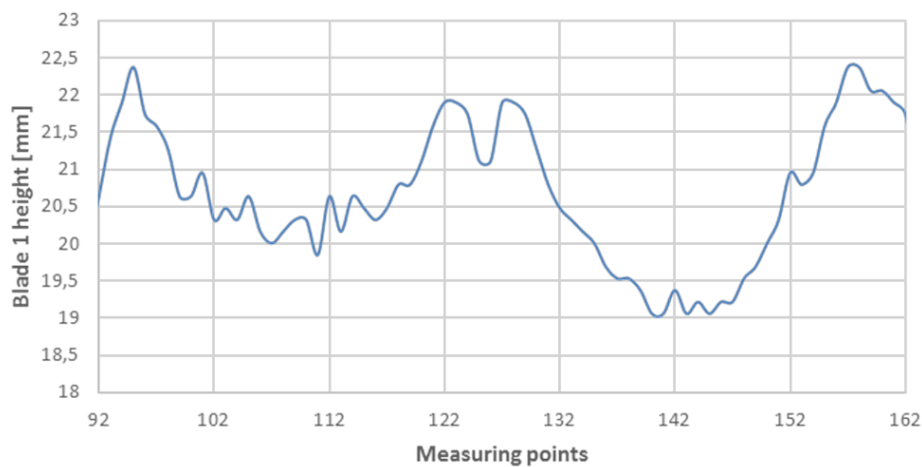


Figure IV.29 Blade 1 height measurements

After the LMD process was performed, a machining process was applied to obtain final part and accomplish dimensional requirements. For this purpose, a Kondia HS1000 machining center was used, with three linear axis (X, Y, Z) and two rotary axis mounted on a tilting table (B and C).The selected tool consisted on a ball nose milling tool with 2 flutes and a cutting length of 15 mm. Finally, selected parameters for the machining process are collected in the Table IV.11.

**Table IV.11** Machining process defined parameters

| Axial depth<br>$a_p$ [mm] | Radial depth<br>$a_e$ [mm] | Spindle speed<br>$S$ [rpm] | Machining feed<br>$F$ [mm/min] | Machining strategy                 |
|---------------------------|----------------------------|----------------------------|--------------------------------|------------------------------------|
| 0.45                      | 0.2                        | 2000                       | 200                            | Variable contour<br>– Surface area |

Related to machining operations selection, the same CAM software was used to design tool-path strategies and process verification. In a similar manner than the LMD process, according to the complexity of the geometry and in concordance with the strategy used to build up the blisk, a variable contour was selected. Therefore, this tool-path implied 5-axis simultaneous movements and virtual verification to avoid collisions and machine limitations. Figure IV. 29 shows on the right side the LMD obtained geometry and, on the left side, the machining process applied to two consecutive blades.

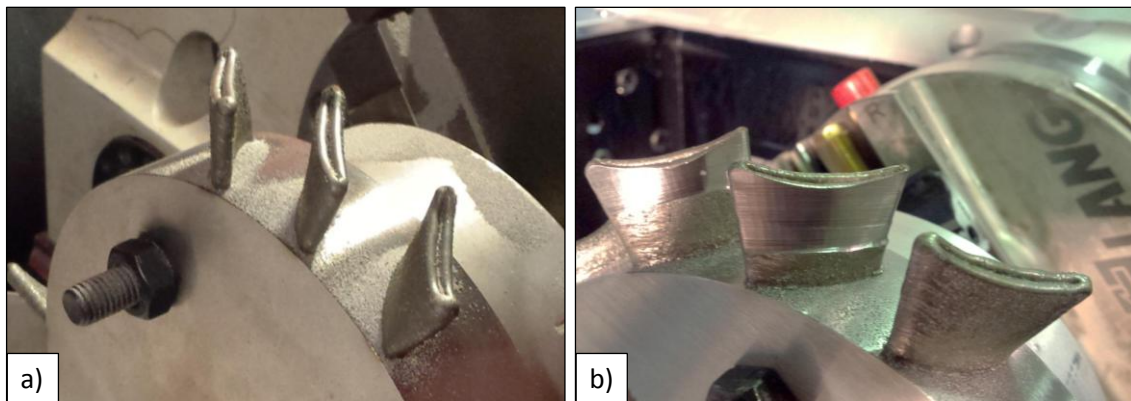


**Figure IV.30** a) LMD obtained blades and b) Machined blades





---

**Chapter V. New processes for manufacturing and  
repairing turbomachinery integral rotary  
components**

---



## Chapter V. New processes for manufacturing and repairing turbomachinery integral rotary components

*This chapter presents two scientific developments: the first one consists on an algorithm development and validation for the manufacturing of non-developable surfaces using flank milling strategy, optimising the tool resource using the total effective length of the cutting tool and reducing machining times requiring less cutting passes. For the developed algorithm validation, single blade was selected as the demonstrator. The results obtained, using the algorithm, were compared with the conventional process programmed using NX® CAD/CAM software.*

*The second development searches new manufacturing processes to be applied as a complement or alternative to conventional manufacturing processes for thermoresistant superalloys. Following this objective, the feasibility of the abrasive process known as Super Abrasive Machining applied to full slotting Inconel®718 was analysed.*

### V.1. Introduction

Free-form surfaces are designed using non-uniform rational B-splines (NURBS), being a popular tool for geometric modelling due to the easy control of the curves and surfaces definition; allowing the designers and modellers a straightforward tool towards the intended shape. In this line, designed surfaces could accomplish functioning requirements (i.e. fluid-dynamics requirements and specific physical constrains like force or pressure); hence, they are easily found in many industrial components, mainly in aerospace, automotive, die moulds, bio-medical and power sector. Nevertheless, complex geometries composed of free-form surfaces present different challenges for manufacturing processes: accessibility issues, elevated machining times and costs and clamping fixtures issues, among others.

Considering in particular the common manufacturing strategies used for the conventional milling process, free-form surfaces are usually machined using *point milling* strategy. As it was described previously, this strategy consists on a surface copy with a ball nose end milling tool, where the dimensional tolerance is defined by the height between the peaks derived from the selected machining passes number. Therefore, it implies elevated machining times (several passes to achieve dimensional tolerances) and high-localized tool wear because the cut is

performed with the same tool area. With the aim of improving process productivity and efficiency, there is a tendency of algorithm development to offer new solution to change from *point milling* to *flank milling* for complex geometries manufacturing reducing, in that way, manufacturing time, cost and a more regular finished geometry, avoiding peaks and valleys derived from the difference between tool passes.

Additionally, in relation to IBRs manufacturing processes, there is a research field regarding to different manufacturing processes in order to find new alternatives or complements to conventional manufacturing processes. Following this objective, this chapter presents an abrasive process known as *Super Abrasive Machining (SAM)* as a possible alternative to the conventional milling process. Moreover, this process offers the possibility to reduce machining steps inside the IBRs manufacturing chain; reducing the need of a final abrasive stage (commonly performed using *Abrasive Flow Machining* to achieve final desired tolerances).

Figure V.1 shows different steps inside the IBRs manufacturing chain and the application of presented developments in this chapter. On the one hand, it is presented the SAM process for roughing strategies with the aim of reducing roughing times, costs and optimising the material status before the following stages. On the other hand, it is shown an algorithm validation for complex geometries semifinishing and finishing *flank* strategies; because the dimensional tolerances and the material properties are mostly dependant on these stages, as well as presenting the highest manufacturing times (depending on the *point milling* strategies).

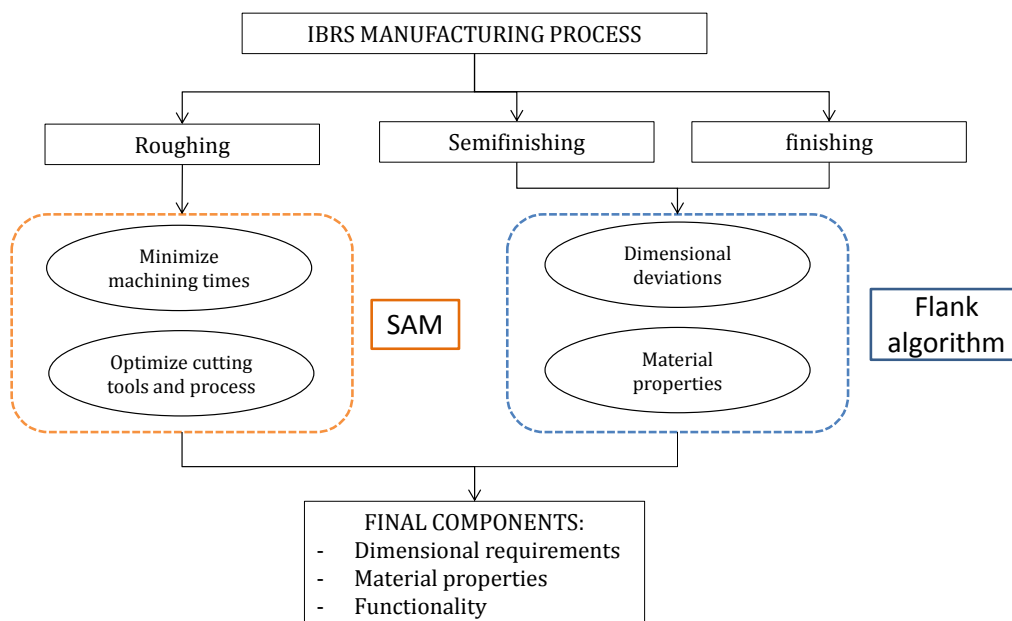


Figure V.1 IBRs manufacturing process and presented developments application

## V.2. Surface approximation algorithm for operations optimization

The use of different algorithms is presented as a real opportunity to improve manufacturing processes in terms of productivity and effectiveness. In this chapter, it is presented an algorithm for surface approximation with the aim of using flank milling instead of point milling, accomplishing finishing surface requirements.

The first step for the algorithm definition consists on analysing the surface to be machined. In the case of IBRs, those surfaces are commonly composed of non-developable complex surfaces. Once the surface is recognised, an auxiliary developable surface is calculated closely approximated to the desired surface; in a manner that accomplishes dimensional tolerances requirements using the total effective length of the cutting tool, minimizing the number of passes required by the process. These surface approximation algorithms are oriented to semifinishing and finishing processes because they are the ones that determine the accuracy of the final desired geometrical dimension, as well as the surface finish. Therefore, these operations are highly demanding tasks to achieve these components tough final requirements.

The basis for the development of these algorithms consists on adapting a cutting tool, generally toroidal or cylindrical geometry, so it is presented a superior order of the area in contact. Hence, the calculus for machining strategies is performed in a similar manner as for developable ruled surfaces. That is, those surfaces produced by the movement of a unique revolution parameter, being defined by the tangential contact with their generatrix in any instant of time. Therefore, the tool revolution surface slides tangentially over time, being the more adequate tools for *flank milling* operations.

Figure V.2 presents graphically the auxiliary surface and the calculus for a revolution cutting tool position along the surface to be machined (Bo P., 2016).

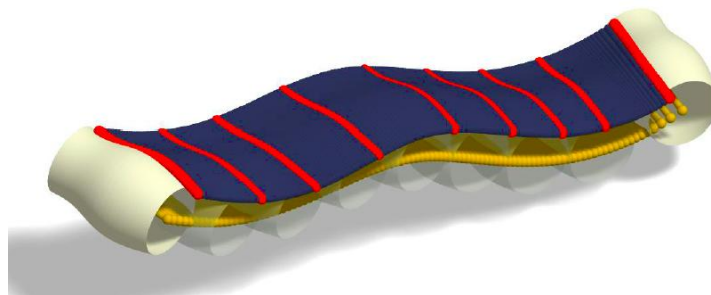


**Figure V.2** Graphical example for the auxiliary surface calculation (Bo P., 2016)

In the following subsection, it is presented a variant of this algorithm and the validation for specific tool geometry (conical tool) with the aim of adapting a non-developable surface to a flank millable surface within specific tolerances. For this purpose, the algorithm is developed with the basis stated on the algorithm presented by Bo P. in 2016.

### V.2.1. Conical tool flank approximation for surface finishing

Following this line of revolution tools for *flank milling* algorithms, conical tools are one of the most commonly used for IBRs manufacturing. One of the main advantages from conical tools is the adaptability to those areas with accessibility difficulties. In order to develop the algorithm for conical tool flank approximation, it is required different steps defined hereafter.

Firstly, the selected cutting tool needs to be modelled. For this purpose, the conical tool was considered as a truncated cone with the total tool effective length. Thus, Figure V.3.a shows the motion of the conical axis represented by  $pq$ , along the auxiliary proposed ruled surface  $R$  (yellow) calculated from the desired final surface (green). Aligned with the cutting tool model and the ruled surface definition, it needs to be considered the tangential movability (Figure V.3.b) of the cutting tool related to the surface to be manufactured.

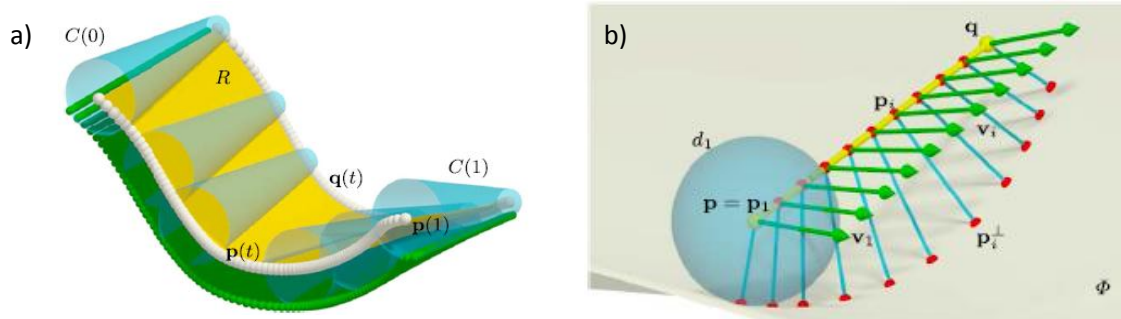
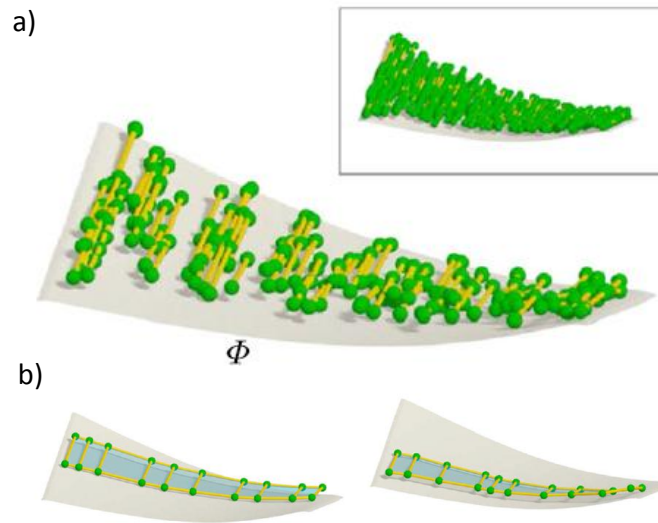


Figure V.3 Auxiliar surface calculation for the conical tool and the tangential movability definition

The following step consists on analysing the complete geometry to be manufactured in order to divide the surface in the minimum number of flank millable surfaces. In this case, it was selected a curved surface (similar to impellers blades or splitters) as an example to show the way that different conical envelopes are fitted. Figure V.4 shows the first surface analysis and how the surface is covered by different conical tool positions; with green points, it is shown the initial and final tool axis and the yellow lines represent the tool axis orientation. This distribution is covering the entire surface in an ideal and theoretical calculus (Figure V.4.a). Nevertheless, this tool positioning is not possible for the real manufacturing process.

Therefore, this needs to be adapted in order to perform the minimum quantity of passes in a feasible manner (Figure V.4.b).



**Figure V.4** Fitting conical envelopes to the final desired surface: a) random tool positioning for covering entire surface and b) feasible motion position for the tool to be adapted to the final surface

Finally, the algorithm performs a serial of iterations to optimise the cutting tool motion. This iterative calculus defines the final tool path to be performed considering various factors such as collisions between tool and part, overcuts and final dimensional tolerances ranges. Therefore, the different tool positions, that present better mobility, are selected and joined to generate the final tool path. Figure V.5 shows the optimization for the conical tool motion represented for a one parameter family of spheres ( $d_i$ ) centred along the axis, preserved throughout the motion ( $t \in [1,0]$ ).

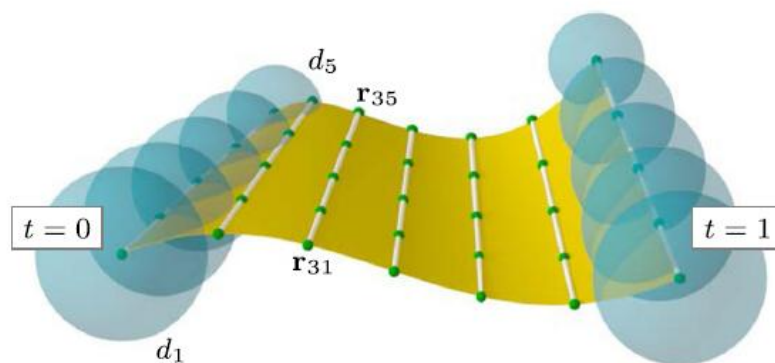


**Figure V.5** Motion optimization for the conical tool

As a result from the application of this algorithm, it is generated a .txt file with six columns, the first three represent the tool tip position ( $x, y, z$ ) and the second three are related to the directors cosines from the tool axe position. Furthermore, the use of this algorithm is needed to obtain surface dimensional requirements in those complex components where section

breaks/jumps between different tool paths along blade surface are not allowed. These applications occur frequently and this algorithm offers a solution to perform the machining operations just minimizing tool path passes.

The equations that control this algorithm are stated in Equations (1)–(5). In particular, taking  $\mathbf{p}$  and  $\mathbf{q}$  as the two boundary cubic B-spline curves, Equation (1) represents the whole objective function to obtain this approximation where  $\mu_1 = 1$ ,  $\mu_2 = \mu_4 = \mu_5 = 0.1$ , and  $\mu_3 = 0.001$ ; Equations (2) and (4) correspond to the two components of the objective function that represent the point-surface proximity. Equation (3) is the fairness of the two boundary curves to achieve a fair motion, Equation (5) controls the rigidity and Equation (6) maintains the tool motion as orthogonal to the conical axis as possible.

$$F_{motion}(\mathbf{p}, \mathbf{q}) = \mu_1 F_{plane}(\mathbf{p}, \mathbf{q}) + \mu_2 F_{fair}(\mathbf{p}, \mathbf{q}) + \mu_3 F_{point}(\mathbf{p}, \mathbf{q}) + \mu_4 F_{rigid}(\mathbf{p}, \mathbf{q}) + \mu_5 F_{ortho}(\mathbf{p}, \mathbf{q}) \quad (1)$$

where,

$$F_{plane}(\mathbf{p}, \mathbf{q}) = \frac{1}{mn} \sum_{j=1}^n \sum_{i=1}^m ((r_{ij} - r_{ij}^\perp, n_{ij}) - d_j)^2 \quad (2)$$

$$F_{fair}(\mathbf{p}, \mathbf{q}) = \frac{1}{m} \sum_{i=2}^{m-1} (p(t_{i-1}) - 2p(t_i) + p(t_{i+1}))^2 + \frac{1}{m} \sum_{i=2}^{m-1} (q(t_{i-1}) - 2q(t_i) + q(t_{i+1}))^2 \quad (3)$$

$$F_{point}(\mathbf{p}, \mathbf{q}) = \frac{1}{mn} \sum_{j=1}^n \sum_{i=1}^m \| r_{ij} - (r_{ij}^\perp + d_{ij} n_{ij}) \|^2 \quad (4)$$

$$F_{rigid}(\mathbf{p}, \mathbf{q}) = \langle p(t_i) - q(t_i), p(t_i) - q(t_i) \rangle - L^2 = 0 \quad (5)$$

$$F_{ortho}(\mathbf{p}, \mathbf{q}) = \frac{1}{m} \sum_{i=1}^{m-1} \left\langle \frac{p(t_{i+1}) - p(t_i)}{\|p(t_{i+1}) - p(t_i)\|}, d_i \right\rangle + \frac{1}{m} \sum_{i=1}^{m-1} \left\langle \frac{q(t_{i+1}) - q(t_i)}{\|q(t_{i+1}) - q(t_i)\|}, d_i \right\rangle \quad (6)$$

In this way, the full effective length is constantly in contact with the non-ruled surface designed and machining passes are confined to a single one if tool dimension covers all of the surface height. The accuracy of the process is controlled by the objective function (see Equation (1)).



### V.2.2. Validation of developed algorithm

With the aim of validating the developed algorithm, it was selected a single blade geometry made of aluminium to be manufactured. Figure V.6.a shows the defined demonstrator, where it could be distinguished the concave and convex sides from the geometry; each side will be manufactured with different tool-paths. Moreover, each side will be divided into 3 patches to be performed using flank milling because the total tool effective length is not able to cover the entire blade in a single patch (they are denominated for validation results as concave/convex 1, 2, and 3 from the bottom to the top, respectively).

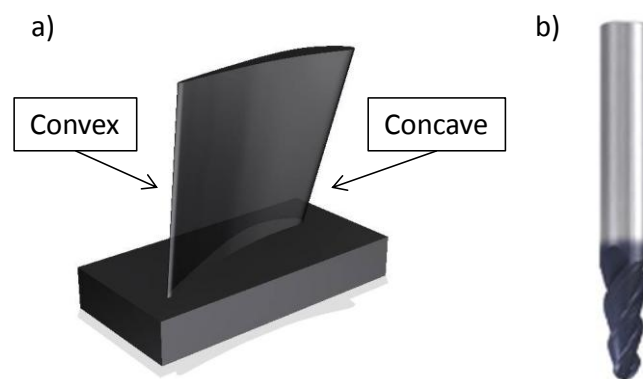


**Figure V.6** a) Demonstrator single blade design for algorithm validation and b) selected cutting tool

Related to the cutting tool (Figure V.6.b), three conical tools with different parameters were selected to validate the developed algorithm; defined as  $T_i (r_1, r_2, l)$ , where  $r_1$  and  $r_2$  are the cone radius at the top and the bottom, respectively, and  $l$  is the cutting length. Thus, they are designated as  $T_1 = (1.5, 3, 24)$ ,  $T_2 = (3, 5, 31)$  and  $T_3 = (2, 5, 30)$ .

Finally, the algorithm validation consists on comparing obtained results applying the algorithm with the tool-paths obtained using a commercial CAD/CAM software. Moreover, in order to compare both tool-paths avoiding external errors, the tool-paths format generated by the algorithm are imported into the same CAD/CAM software to compare both of them using the same post-processing system. Therefore, each side of the blade was divided into 3 patches and, for each tool, it was generated 300 points and 600 points tool-paths (Figure V.7).

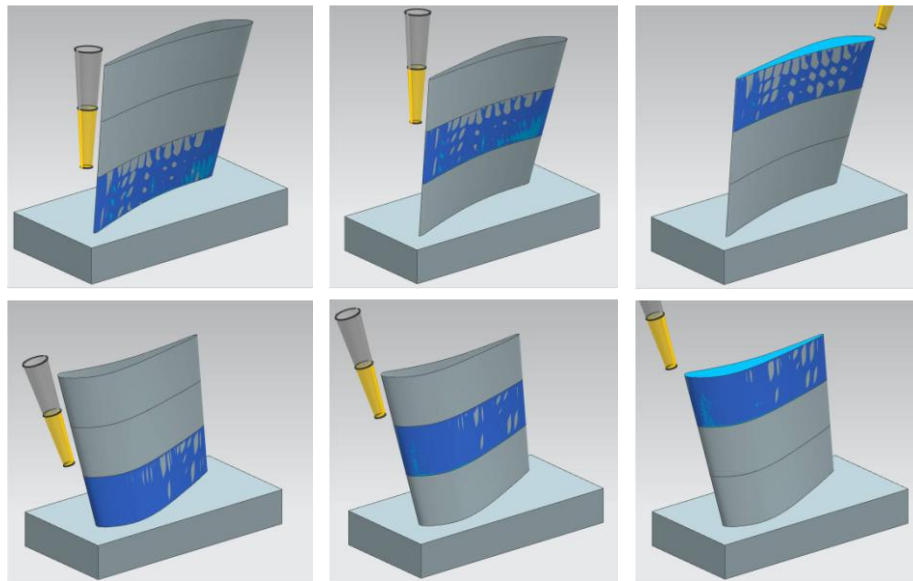


**Figure V.7** concave (top) and convex (bottom) 3 patches division for algorithm validation

The following tables (Table V.1, Table V.2 and Table V.3) show the comparison of obtained results with the maximum undercut and overcut values. For this purpose, the CAD/CAM software performs an internal calculus subtracting the tool-paths obtained geometry (considering the tool geometry) and the final desired geometry.

**Table V.1** Tool 1 comparison of the obtained results

|         |   | TOOL 1 (1.5,5,24)                 |                                    |   |   |
|---------|---|-----------------------------------|------------------------------------|---|---|
|         |   | ALGORITHM                         |                                    | CAM software                                |   |
|         |   | 300                               | 600                                | 300   | 600   |
| CONCAVE | 1 | patch0_CLF300<br>[0.0890,-0.0570] | patch0_CLF600<br>[0.0935,-0.0555]  | 1_concave_300<br>_tool1<br>[0.1357,-0.0125] | 1_concave_600<br>_tool1<br>[0.1280,-0.0125] |
|         | 2 | patch1_CLF300<br>[0.0890,-0.0740] | patch1_CLF600<br>[0.0935,-0.0732]  | 2_concave_300<br>_tool1<br>[0.1038,-0.0527] | 2_concave_600<br>_tool1<br>[0.1241,-0.0527] |
|         | 3 | patch2_CLF300<br>[0.0935,-0.0443] | patch2_CLF600<br>[0.08905,-0.0504] | 3_concave_300<br>_tool1<br>[0.1344,-0.0171] | 3_concave_600<br>_tool1<br>[0.1140,-0.0135] |
| CONVEX  | 1 | patch0_CLF300<br>[0.0890,-0.0574] | patch0_CLF600<br>[0.0935,-0.0574]  | 1_convex_300<br>_tool1<br>[0.1091,-0.0256]  | 1_convex_600<br>_tool1<br>[0.1091,-0.0172]  |
|         | 2 | patch1_CLF300<br>[0.0890,-0.0504] | patch1_CLF600<br>[0.0890,-0.0504]  | 2_convex_300<br>_tool1<br>[0.1322,-0.0164]  | 2_convex_600<br>_tool1<br>[0.1322,-0.0164]  |
|         | 3 | patch2_CLF300<br>[0.0935,-0.0739] | patch2_CLF600<br>[0.0935,-0.0731]  | 3_convex_300<br>_tool1<br>[0.1705,-0.0118]  | 3_convex_600<br>_tool1<br>[0.1716,-0.0118]  |

**Table V.2** Tool 2 comparison of the obtained results

| <b>TOOL 2 (3,5,31)</b> |   |                                   |                                   |   |   |
|------------------------|---|-----------------------------------|-----------------------------------|---|---|
|                        |   | ALGORITHM                         |                                   | CAM software                                |   |
|                        |   | 300                               | 600                               | 300   | 600   |
| CONCAVE                | 1 | patch0_CLF300<br>[0.0890,-0.0504] | patch0_CLF600<br>[0.0935,-0.0363] | 1_concave_300<br>_tool2<br>[0.0956,-0.0191] | 1_concave_600<br>_tool2<br>[0.1011,-0.0189] |
|                        | 2 | patch1_CLF300<br>[0.0935,-0.0564] | patch1_CLF600<br>[0.0935,-0.0659] | 2_concave_300<br>_tool2<br>[0.1246,-0.0168] | 2_concave_600<br>_tool2<br>[0.1070,-0.0168] |
|                        | 3 | patch2_CLF300<br>[0.0935,-0.0325] | patch2_CLF600<br>[0.0935,-0.0325] | 3_concave_300<br>_tool2<br>[0.1768,-0.0162] | 3_concave_600<br>_tool2<br>[0.1147,-0.0050] |
| CONVEX                 | 1 | patch0_CLF300<br>[0.0935,-0.0325] | patch0_CLF600<br>[0.0935,-0.0325] | 1_convex_300<br>_tool2<br>[0.1801,-0.0209]  | 1_convex_600<br>_tool2<br>[0.1801,-0.0209]  |
|                        | 2 | patch1_CLF300<br>[0.0890,-0.0682] | patch1_CLF600<br>[0.0890,-0.0663] | 2_convex_300<br>_tool2<br>[0.1297,-0.0211]  | 2_convex_600<br>_tool2<br>[0.1297,-0.0211]  |
|                        | 3 | patch2_CLF300<br>[0.0935,-0.0472] | patch2_CLF600<br>[0.0935,-0.0451] | 3_convex_300<br>_tool2<br>[0.0965,-0.0250]  | 3_convex_600<br>_tool2<br>[0.1035,-0.0250]  |

**Table V.3** Tool 3 comparison of the obtained results

| <b>TOOL 3 (2,5,30)</b> |   |                                   |                                   |   |   |
|------------------------|---|-----------------------------------|-----------------------------------|---|---|
|                        |   | ALGORITHM                         |                                   | CAM software                                |   |
|                        |   | 300                               | 600                               | 300   | 600   |
| CONCAVE                | 1 | patch0_CLF300<br>[0.0935,-0.0358] | patch0_CLF600<br>[0.0935,-0.0331] | 1_concave_300<br>_tool3<br>[0.1551,-0.0193] | 1_concave_600<br>_tool3<br>[0.1551,-0.0193] |
|                        | 2 | patch1_CLF300<br>[0.0935,-0.0449] | patch1_CLF600<br>[0.0935,-0.0441] | 2_concave_300<br>_tool3<br>[0.1946,-0.0190] | 2_concave_600<br>_tool3<br>[0.1428,-0.0190] |
|                        | 3 | patch2_CLF300<br>[0.0935,-0.0415] | patch2_CLF600<br>[0.0935,-0.0410] | 3_concave_300<br>_tool3<br>[0.1238,-0.0336] | 3_concave_600<br>_tool3<br>[0.1495,-0.0195] |
| CONVEX                 | 1 | patch0_CLF300<br>[0.0935,-0.0325] | patch0_CLF600<br>[0.0935,-0.0325] | 1_convex_300<br>_tool3<br>[0.0859,-0.0351]  | 1_convex_600<br>_tool3<br>[0.0859,-0.0351]  |
|                        | 2 | patch1_CLF300<br>[0.0935,-0.0325] | patch1_CLF600<br>[0.0935,-0.0325] | 2_convex_300<br>_tool3<br>[0.1756,-0.0216]  | 2_convex_600<br>_tool3<br>[0.1771,-0.0216]  |
|                        | 3 | patch2_CLF300<br>[0.0935,-0.0325] | patch2_CLF600<br>[0.0935,-0.0325] | 3_convex_300<br>_tool3<br>[0.1607,-0.0254]  | 3_convex_600<br>_tool3<br>[0.1619,-0.0254]  |

In order to select the optimal option for the single blade real manufacturing, it was established a dimensional criterion of 50  $\mu\text{m}$ , according to (F.Klocke, 2013) for these type of components. Hence, tool 3 was selected because it presents undercuts smaller than 50  $\mu\text{m}$ , considering undercuts the limiting machining defect, being overcuts easy to be controlled by remanufacturing those surfaces.

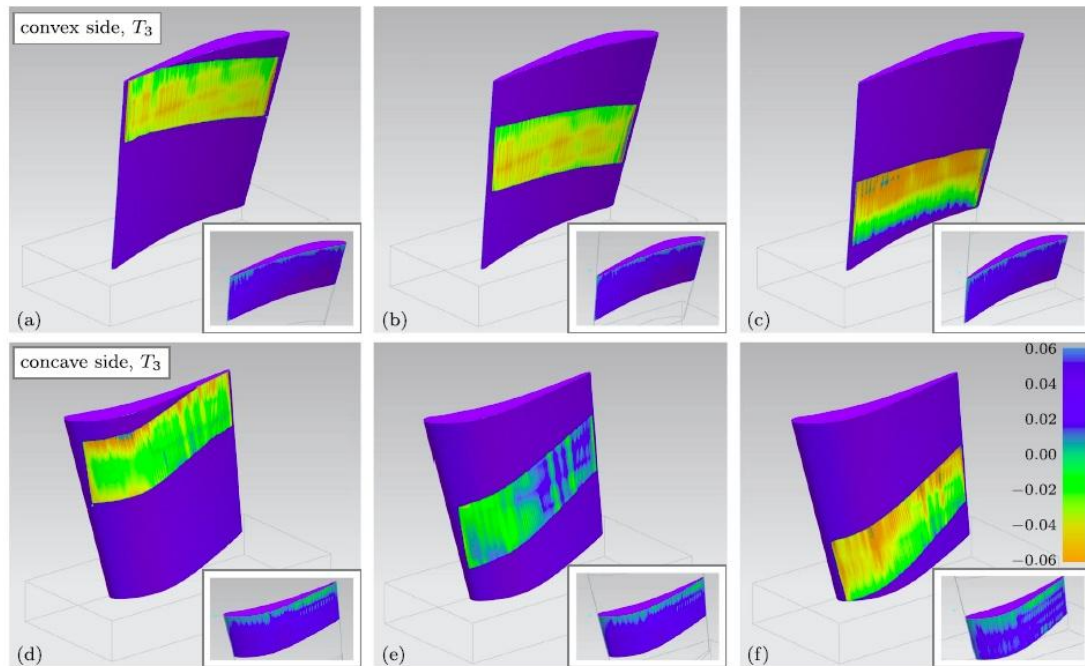


**Figure V.8** Surface finishing approximation for T3 comparing the results obtained with the algorithm (blades) with CAM software results (bottom of each picture)

The last step of this validation consisted on conducting physical experiments using a 5-axis machining centre KONDIA® HS1000. Machining parameters were selected according to the material to be machined:  $V_c = 157$  m/min,  $V_f = 1000$  m/min and  $N = 3000$  rpm. Figure V.9 shows final components obtained by the commercial CAM software (left part) and the algorithm application (right part). It was observe that the algorithm approach minimizes the distance between different patches, appreciating a perfectly smooth solution (observed at the surface light reflexion). Nevertheless, the final component obtained by the commercial software present tiny imperfection even though it fulfils dimensional deviation tolerances.



Figure V.9 Final obtained components using the default (left) and the algorithm (right)

### V.3. New manufacturing processes: Super Abrasive Machining (SAM)

As it was mentioned previously regarding IBRs manufacturing processes, the complexity of these components and the industrial need of more productive processes led to investigate new alternative or complement processes to the conventional one. The conventional milling process (Figure V.10) consists of different roughing, semifinishing and finishing operations. Firstly, roughing operation is performed in two steps, one consists of straight full slotting with a great diameter cutting tool, and the second one is the roughing of the remaining corner with smaller cutting tool to facilitate the accessibility to semifinishing strategies avoiding collisions risks. Secondly, for the semifinishing operation, each blade is divided into three sections (top, middle and bottom) and then the blisk platform (machining the surface between blades, letting a slight excess of material compared with the final size) is semifinished at this stage. Thirdly, at the finishing stage it is expected to achieve final dimensional requirements. This stage is divided into 4 main groups: blades, hub, fillet radius and pockets. For the finishing of blades surfaces, it is used a 6mm of diameter ball-end mill and it is changed each two blades. For the platform finishing, it is used a conical tool with small diameter and it is changed after 14 blades. As an extra part of the platform, it is machined with the same conical tool the fillet radius of all blades being replaced each 6 blades. Finally, pockets between each blade, 68 in total, are machined with the same cutting tool, being replaced after 14 blades.

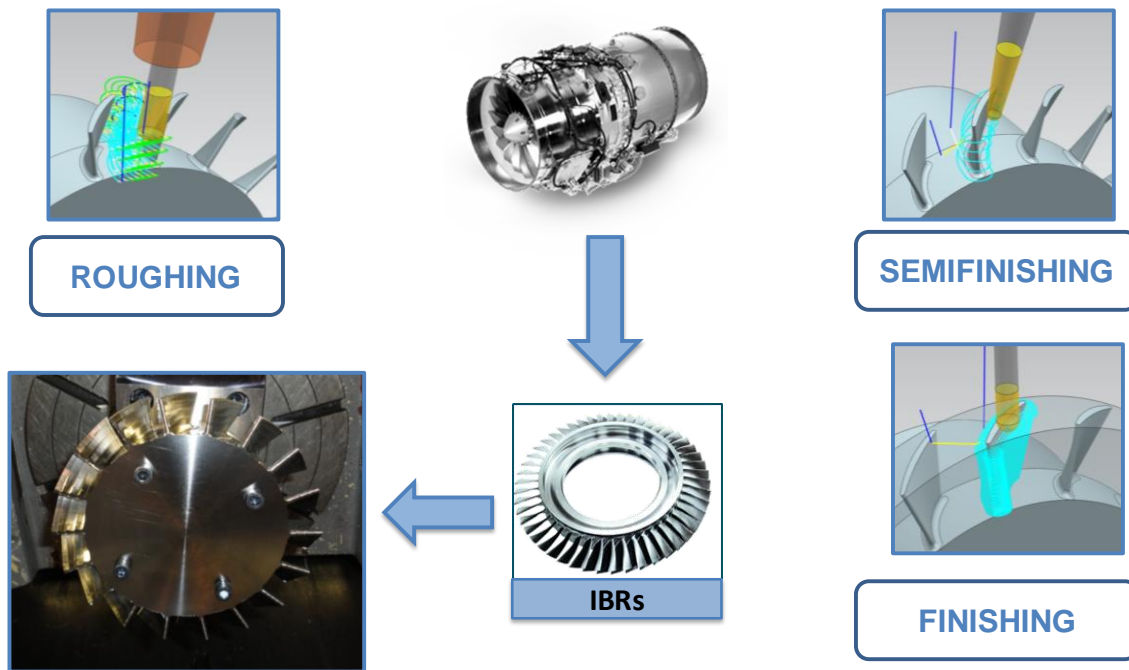


Figure V.10 Medium-sized IBRs conventional manufacturing process

Finally, once the blades achieve final desired tolerances, it is performed a surface finishing process known as *Abrasive Flow Machining (AFM)*. This non-conventional abrasive technology is characterized by good performance for complex geometrical cavities achieving great dimensional accuracies and finishing surface quality requirements. Therefore, the *AFM* has influence on the final geometry obtaining a surface roughness closer to abrasive processes instead of milling processes.

According to the idea of using abrasive processes to achieve final roughness and tolerances, this chapter presents the analysis of the feasibility for the *Super Abrasive Machining (SAM)* process as an alternative or compliment to the conventional milling process. This process is defined as “grinding at machining rates”. Therefore, this technology provides, under similar cutting conditions of single point machining, a finishing precisions closer to grinding technology, what makes this process more versatile than grinding or milling. Nevertheless, one of the main limitations presented by this process is the equipment requirements of high-speed spindles (60,000-90,000 rpm) for optimal performance; what makes this process unachievable to the most of the current machining centres whose spindles rotary speed capacity are below 24,000 rpm.

With the aim of analyzing the adequacy of flank SAM compared to flank milling in terms of surface quality applied to thermo-resistant super alloys, a serial of experiments were designed. These experiments were performed as full slotting with the total effective tool length for flank




SAM and flank milling; considered some of the hardest and extreme manufacturing conditions. Additionally, this work is performed to give an opportunity and feasibility to this technique in conventional machining centres, so the tests were performed with a conventional machining centre presented at the following subsection.

### V.3.1. Description of the equipment


The equipment used for the experimental set-up is described in this section. In short, used equipment consists on a 5-axis kinematic conventional machining centre Ibarmia® ZV-25/U600. Thus, at this cell configuration the X, Y and Z axes are located in the machine spindle and the A and C rotary axes are mounted on a tilting table; additionally, the spindle speed capacity is 18,000 rpms. On top of that, Table V.4 contains the 5-axis conventional machining centre Ibarmia® ZV-25/U600 main characteristics.

Table V.4 Ibarmia® ZV-25/U600 main characteristics

| <b><u>IBARMIA® ZV-25/U600</u></b>   |                              |                                    |
|---|------------------------------|------------------------------------|
|  | <b>Model</b>                 | Ibarmia® ZV-25/U600                |
|   | <b>Numerical Control</b>     | HEIDENHAIN® iTNC-530               |
|   | <b>Travels (X/Y/Z ; A/C)</b> | 600/428/410 mm ; ± 120°/± 360°     |
|   | <b>Working area</b>          | ∅ 400 mm                           |
|   | <b>Feed</b>                  | Max. 40,000 mm/min;<br>Max. 20 rpm |
|   | <b>Positioning precision</b> | ± 0.005 mm                         |
|   | <b>Repeatability</b>         | ± 0,005 mm                         |
|   | <b>Turning speeds</b>        | 18,000 rpm                         |


In order to measure the surface roughness, the microscope Leica® DCM 3D was used, so for topographies and surface profiles (Table V.5).

**Table V.5** Optical confocal microscope characteristics

| <b>OPTICAL CONFOCAL MICROSCOPE</b>  |                  |                                    |
|---|------------------|------------------------------------|
|  | <b>Model</b>     | Leica® DCM 3D                      |
|   | <b>Zoom</b>      | 5x - 10x – 20x –<br>50x – 150x     |
|   | <b>Trails</b>    | X: 100 mm<br>Y: 300 mm<br>Z: 40 mm |
|   | <b>Precision</b> | ~0.1 μm                            |

For analysing the microstructure, the cross-section and the appearance of white layer a microscope Mitutoyo® TM505 was selected.


**Table V.6** Mitutoyo® TM-505 microscope main characteristics

| <b>MITUTOYO MICROSCOPE</b>  |                  |                     |
|---|------------------|---------------------|
|  | <b>Model</b>     | MITUTOYO®<br>TM-505 |
|   | <b>Zoom</b>      | 30x - 75x           |
|   | <b>Trails</b>    | 0 - 50 mm           |
|   | <b>Precision</b> | ~1 μm               |



For analysing the microhardness, the microhardness tester<sup>®</sup> FM-800 was selected.

**Table V.7** Microhardness Tester FM-800 main characteristics

| <b>MICROHARDNESS TESTER<sup>®</sup> FM-800</b>                                     |                         |  |
|--|-------------------------|--|
|  | <b>Model</b>            | Future-Tech Corp. <sup>®</sup><br>FM-800 |
|  | <b>Zoom</b>             | 50x & 10x                                |
|  | <b>Dimensions</b>       | 100 x 100 mm                             |
|  | <b>Test load</b>        | 0.5 – 2 kg                               |
|  | <b>Diamond Indenter</b> | Vickers Indenter (HV)                    |
|  | <b>Measurement unit</b> | 0.01 μm                                  |

### V.3.2. Material

According to turbomachinery industry necessities, Inconel® 718 was selected as a challenging material for these processes. This superalloy constitutes one of the most common materials in the aeronautic industry, more concretely for engines and turbines. This material consists of a nickel-based hardened alloy through the precipitation of its metallic matrix secondary phases; Figure V.11 shows the microstructure of selected material. It was observed a fine grained structure (ASTM6) with a discrete carbide phase scattered inside the grains, usually presented in Inconel® 718. In this case, the material achieved an average value of hardness 42 HRc.

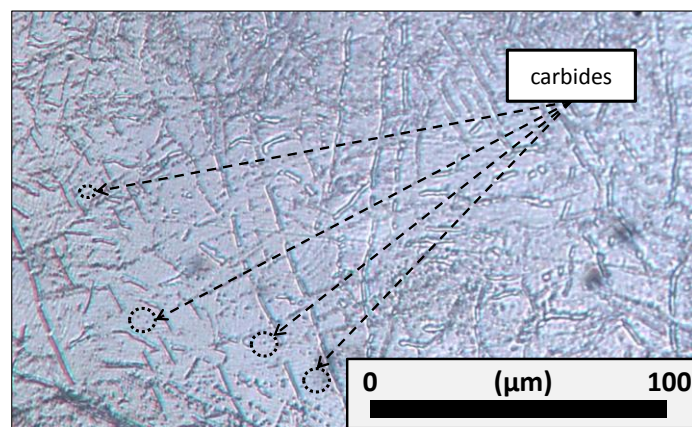


Figure V.11 Microstructure of selected material Inconel® 718

This thermo-resistant super alloy is characterized by good resistance to fatigue and creep combined with high corrosion resistance under extreme working conditions at high temperatures. Nevertheless, it is considered a difficult-to-cut material due to the magnitude of cutting forces, low material removal rates, built-up edges, and extreme tool wear during machining.

The chemical composition, mechanical, and physical properties of this material are shown in Table V.8.

Table V.8 Inconel 718 chemical composition (%), mechanical and physical properties

| Ni       | Cr | Co              | Fe | Nb               | Mo | Ti                     | Al  | B             | C    | Mn            | Si   | Others          |
|----------|----|-----------------|----|------------------|----|------------------------|-----|---------------|------|---------------|------|-----------------|
| 52.5     | 19 | 1               | 17 | 5                | 3  | 1                      | 0.6 | 0.01          | 0.08 | 0.35          | 0.35 | 1.79            |
| Hardness |    | Young's Modulus |    | Tensile Strength |    | Density                |     | Specific Heat |      | Melting Temp. |      | Thermal Conduct |
| 42 HRc   |    | 206 GPa         |    | 1.73 GPa         |    | 8470 kg/m <sup>3</sup> |     | 461 J/(kg·K)  |      | 1550 K        |      | 15 W/(m·K)      |

Therefore, this material was selected for experimental trials in order to provide data for both manufacturing techniques (flank SAM and flank milling), showing their behavior working with difficult-to-cut materials and under aggressive machining conditions.

### ***V.3.3.Slotting strategy: experimental set-up***

Related to manufacturing strategies, flank milling and flank SAM were selected in order to remove the highest amount of material according to the tool limitations, using the total cutting effective length (shown in Figure V.12). One of the main advantages of using the total effective length consists of increasing material removal rates combined with a reduction of machining times, since also machining cost. Moreover, this strategy implies extreme cutting conditions with lubricating, refrigerating and chip evacuation issues.

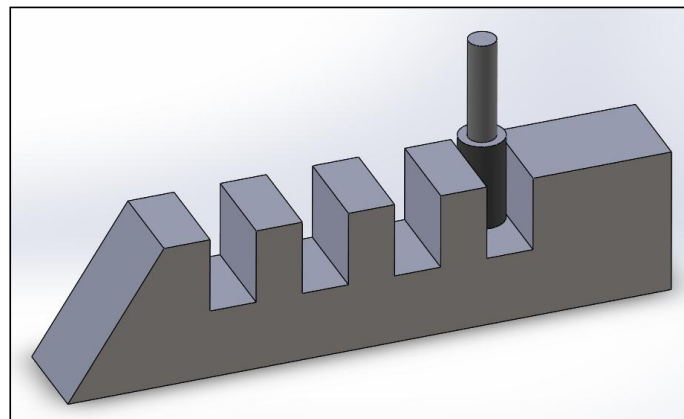


**Figure V.12** Full slotting definition

Related to the cutting tools, on the one hand, and for the case of flank milling, the selected tool (Figure V.13) consisted of a 16 mm diameter, with 20 mm of cutting length and four-tooth; made of carbide coated with AlTiN, commonly used for these applications. This coating was selected because the presence of aluminum implies higher surface hardness and resistance to oxidation (Barthelmä F., 2016).



**Figure V.13** Selected milling cutting tool

On the other hand, for flank SAM it was selected a monolayer electroplated CBN grinding tool, with a grain size of 300  $\mu\text{m}$ , 16 mm of diameter and a total effective length of 20 mm. Figure V.14 shows the grinding tool, analysing the grain distribution and the tool surface profile. In these tools, the abrasive grains distribution is randomly located along the entire surface, what leads to ensure better surface quality of manufactured components, even when the wear at grinding tools is considered elevated before discarding.

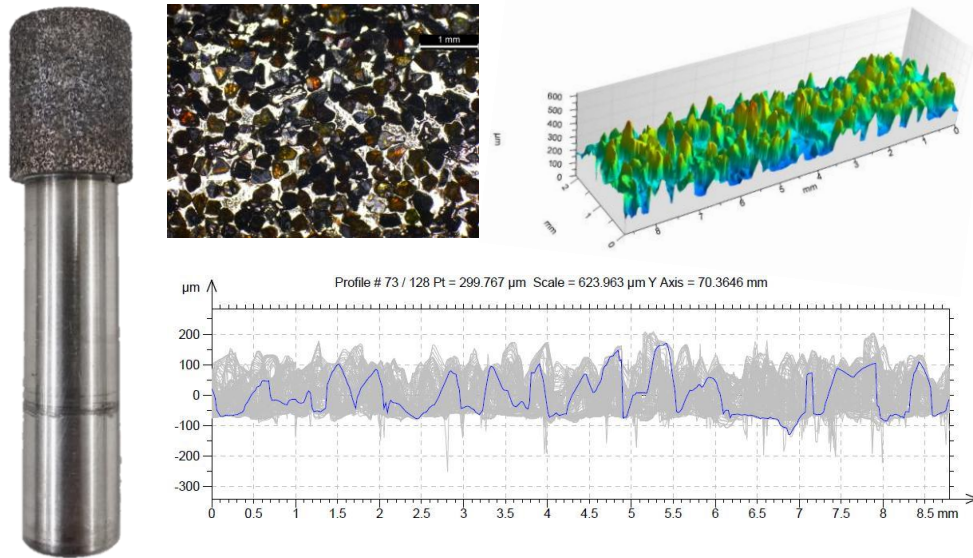


Figure V.14 Selected grinding tool and grain distribution pattern and profile

Finally, Table V.9 contains the selected cutting conditions for the tests performance according to recommended industrial conditions and previous knowledge on manufacturing Inconel® 718 using conventional processes.

Table V.9 Definition of the cutting conditions for the experiments

| Cutting Conditions | Flank Milling                           | Flank SAM                               |
|--------------------|---|---|
| Feed Rate          | 0.01 mm/tooth                           | 45 mm/min                               |
| Cutting Speed      | 20 m/min                                | 900 m/min                               |
| $a_p$              | 20 mm                                   | 20 mm                                   |
| $a_e$              | 16 mm                                   | 16 mm                                   |
| Cutting Fluid      | Synthetic oil emulsion Houghton®<br>20% | Synthetic oil emulsion Houghton®<br>20% |

One of the main characteristics of the presented experiments resides on the spindle speed limitation from the used machining centre. In spite of not being the optimal spindle speed for the SAM technique; in this case, cutting conditions were limited to machine capacities. The main objective from the presented work related to selected equipment consists of analysing the allowance of performing this SAM technique with conventional machining centres (in this case limited up to 18,000 rpms). Hence, the selection of cutting conditions is limited, from one side by the machine maximum rotational speed and, from the other side, the cutting parameters recommended by cutting tools providers for conventional milling techniques.

Notwithstanding, it is important to evaluate these cutting conditions to consider the productivity of the performed process. For this purpose, there are two parameters commonly used for comparing different grinding process and evaluate their efficiency. These parameters are the equivalent chip thickness ( $h_{eq}$ ) and the specific material removal rate ( $Q'$ ) (Vidal G., 2018). Figure V.15 shows the definition of the grinding parameters involved in the process and the  $h_{eq}$  and  $Q'$  calculus.

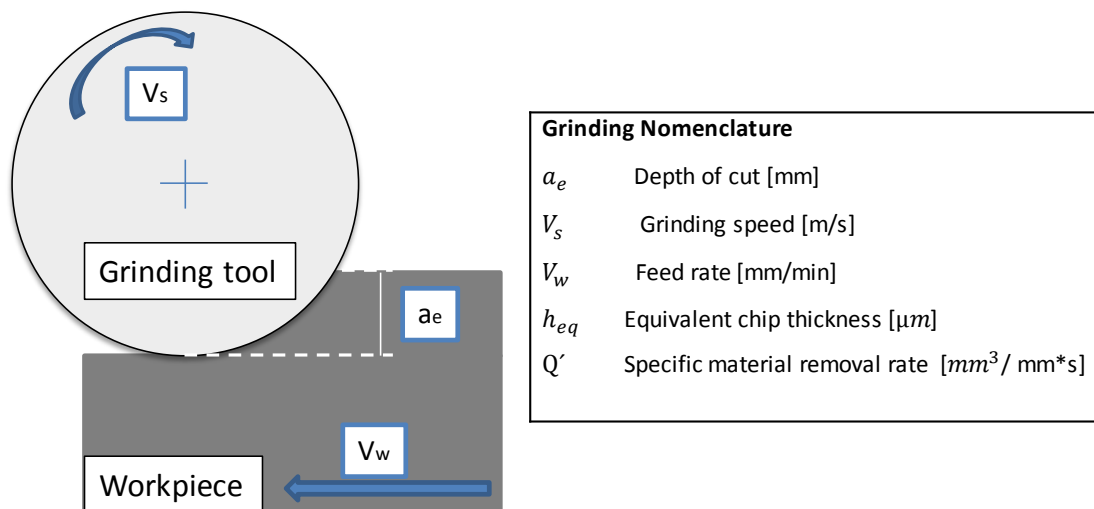


Figure V.15 Grinding process parameters definition

Therefore, Equations (1) and (2) show the equivalent chip thickness and specific material removal rate calculus. These two concepts depend on the following parameters: cutting depth ( $a_e$ ), feed ( $v_w$ ), and cutting speed ( $v_s$ ).

$$Q' = a_e v_w, \quad (1)$$

$$h_{eq} = a_e \frac{v_w}{v_s}, \quad (2)$$

The main difference between the proposed roughing strategies compared with conventional grinding conditions is found in the depth of cut since, in this case, the whole tool diameter was used. Consequently, the equivalent chip thickness obtained was  $0.8 \mu\text{m}$  and the specific material removal rate was  $12 \text{ mm}^3/\text{mm s}$ . Hence, this value was compared with the obtained values for creep feed grinding by Marinescu et al. (Marinescu I.D., 2004) of  $13 \text{ mm}^3/\text{mm}^*s$  for Inconel® 989 and Inconel® 718. It was compared with this productive process because it is characterized by high stock-removal rates with deep depths of cut as the presented case. Accordingly, selected cutting conditions could open new opportunities to implement SAM process in conventional machining centres.

### ***V.3.4. Obtained results***

With the aim of evaluating the feasibility of SAM process and the comparison with the conventional milling process for roughing operations (concretely for full slotting), surface quality was measured; obtained results and discussion are presented in the following subsections. Related to the obtained surface, roughness, the cross-section, the appearance of white layer and microhardness were analysed. Finally, the tool wear for the abrasive tool was studied.

#### ***V.3.4.1 Roughness***

During the tests performance, the roughness was measured *in-situ* in order to obtain the surface irregularities depending on the manufacturing process used for each trial. For this purpose, a Surtronic Duo portable roughness tester from Taylor Hobson® (Ultra Precision Technologies Division of AMETEK Inc., Berwyn, PA, USA) was used. For the measuring process, the direction of measurements was perpendicular to the cut. This was carried out in order to obtain the peaks and valleys of the tool teeth, considered the most unfavourable case. Table V.10 shows obtained  $R_a$  and  $R_z$  roughness obtained values for the five manufactured slots and both manufacturing processes (flank SAM and flank milling).

**Table V.10** In-situ obtained roughness values for FSAM and Fmilling

| ROUGHNESS VALUES ( $\mu\text{m}$ ) |   |           |       |               |       |
|------------------------------------|---|-----------|-------|---------------|-------|
| Manufacturing processes            |   | Flank SAM |       | Flank milling |       |
|                                    |   | $R_a$     | $R_z$ | $R_a$         | $R_z$ |
| SLOT Number                        | 1 | 2.66      | 36.03 | 4.85          | 49.79 |
|                                    | 2 | 2.92      | 38.75 | 4.9           | 50.2  |
|                                    | 3 | 2.98      | 39.45 | 4.82          | 49.2  |
|                                    | 4 | 2.88      | 37.72 | 4.95          | 50.87 |
|                                    | 5 | 3.05      | 39.81 | 5.2           | 51.11 |
| Average value                      |   | 2.90      | 38.35 | 4.94          | 50.23 |

Comparing obtained values, the flank milling process presents an average roughness ( $R_a$ ) of  $4.94 \mu\text{m}$ . This value is drastically reduced using flank SAM technique, obtaining an average of  $2.90 \mu\text{m}$ . That is, approximately an improvement of  $\approx 45\%$ . This behaviour is preserved in the mean values of five consecutive maximum heights between peak-valley ( $R_z$ ). In particular, the values obtained were  $50.23 \mu\text{m}$  and  $38.35 \mu\text{m}$  in the case of flank milling and FSAM machining, respectively. This represents a reduction of  $\approx 28\%$  when SAM is used.

Additionally, after manufacturing all slots, the confocal microscope Leica DCM 3D was used to obtain the profile and the 2D topography for the slot 1 produced by both manufacturing processes. According to the standard of ISO 4288 (ISO, 1996), measuring setting in this case was established as  $0.8 \text{ mm}$  cut-off length and  $4 \text{ mm}$  of evaluation length. Figure V.16 shows both profiles and surface 2D topography. It is appreciated that, under similar cutting conditions, the flank SAM produces a surface characterized by lower roughness values in relation with flank milling. Moreover, the 2D patterns observed coincide with typical milling and grinding processes respectively. In particular, in the first case the pattern is directional due to the milling cutting edge, and in the second one, the pattern is non-directional due to the fact that grinding tools are composed of small grains distributed randomly over the tool surface.



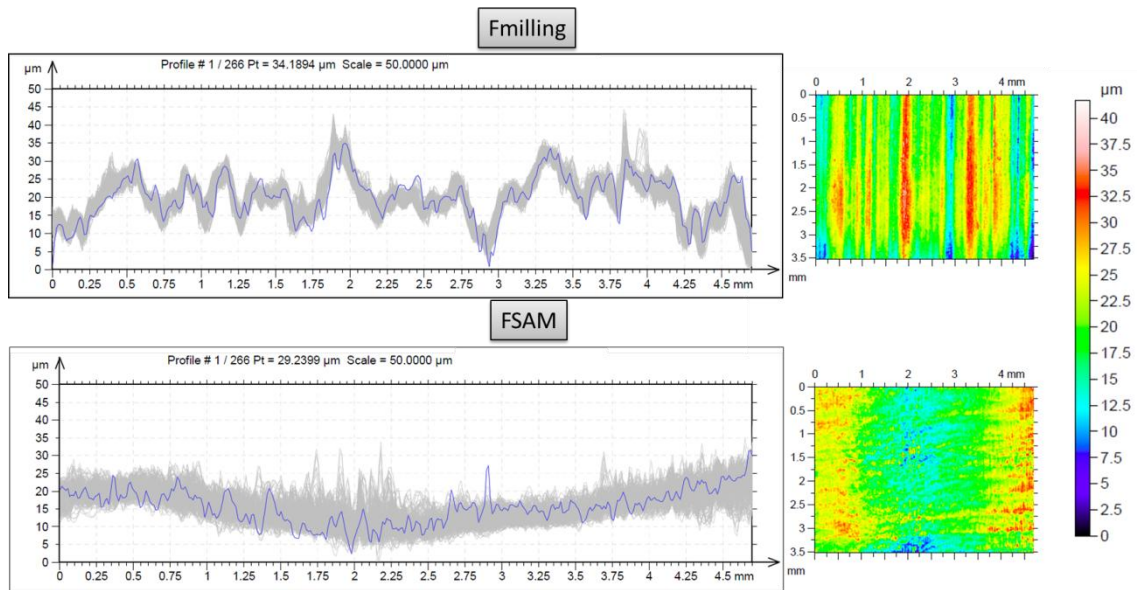


Figure V.16 Slot 1 surface profile and 2D topography

Finally, a slot 1 3D topography was plotted for both processes (Figure V.17). This offers an easy view to the surface finishing and peaks and valleys. Moreover, for the milling process different teeth passes are appreciated. Nevertheless, SAM process shows a more regular and random finishing surface.

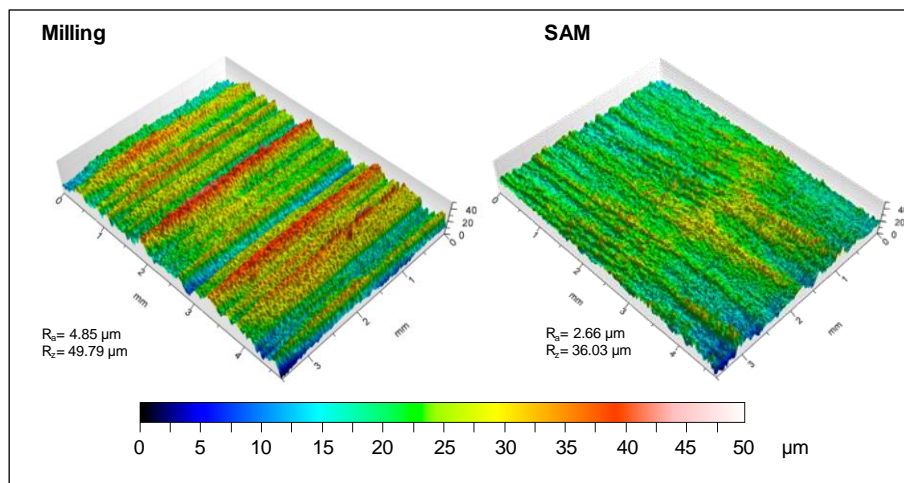


Figure V.17 3D topography for flank milling and flank SAM respectively

These results lead to consider flank SAM technique as an alternative, in terms of roughness, for roughing strategies applied to these difficult-to-cut materials. Furthermore, obtained results showed the possibility of using this technique for replacing intermediate manufacturing stages as semifinishing strategies.



### V.3.4.2 Cross-section and white layer

In line with the previous results, Figure V.18 shows the slot 1 cross-section perpendicular to the workpiece cutting direction for both processes. Flank milling presented some irregularities on the machined surface with a macroscopic deviation. This is a result of aggressive cutting conditions with thermo-resistant superalloys. Furthermore, opening full slots is an extra difficulty in the designed tests. Thus, this implies inadequate space for chip removal and refrigeration, leading the cutting tool to be more prone to suffer from tooth breakage. On the contrary, the flank SAM top layer presented a more regular finished surface with a minimal deviation. This is the consequence of using grinding tools instead of milling tools because these tools have a wear type more regular even in the case of grain detachment. These results explained roughness obtained values. Regarding surface finishing, flank SAM offered a more stable behaviour comparing with conventional technique. This is aligned with the possibility of reducing machining steps in real components.

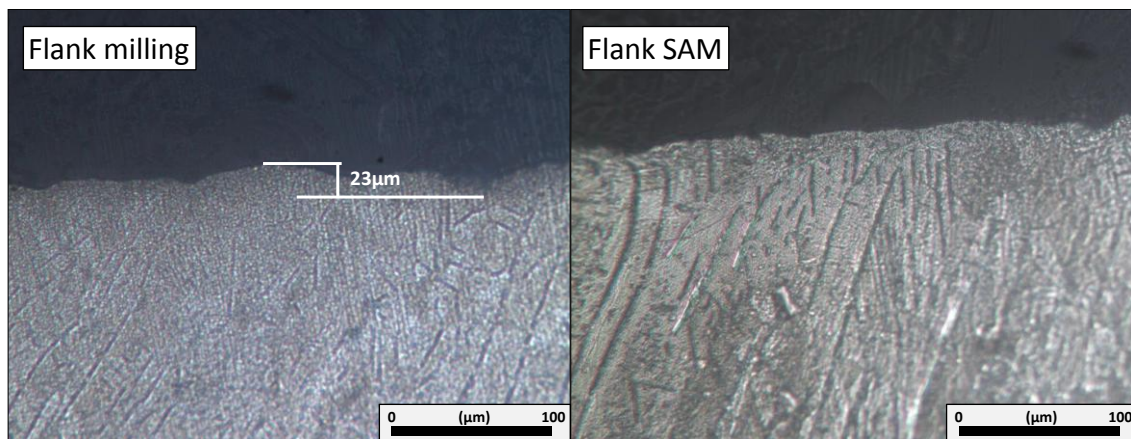


Figure V.18 Cross-section of the Inconel<sup>®</sup> 718 surface after flank milling and flank SAM

Besides that, another important aspect to be analysed is the formation of white layer. This white layer consists of a hard surface layer formed by ferrous materials whilst using high cutting temperatures that can modify the surface integrity. This white layer is produced by the rapid heating during machining over the austenitizing temperature, followed by a quick cooling of this surface. Furthermore, some experts related the existence of this white layer for nickel-based superalloys not only to the high heat during the process but to the low thermal conductivity property of these materials (Herbert C.R.J., 2012). In order to detect this layer, it appears in the microscope as a thin white layer. It should be mentioned that the existence of the white layer implies a direct discard of technique or conditions if the size overpass is 2  $\mu\text{m}$  (Smith S., 2007). In this line, considering roughing strategies for flank SAM and flank milling as

hard cutting conditions and suffering considerable thermal changes, it is important to point out that no white layer was found for any of these processes.

### V.3.4.3 Residual stress

With the aim of measuring residual stress in the manufactured surfaces and analysing differences between both processes, hole-drilling strain gage method was selected. According to the selected material, properties for determining residual stresses were established as Young's modulus (206 GPa), Poisson's ratio (0.294), and yield stress (550 MPa). The rosette type selected was 062 UL with a mean diameter of 5.13 mm, the hole diameter was 1.94 mm and a limit depth of 0.75 mm. The relation between hole diameter and maximum depth is  $0.75/1.94 = 0.386$ . In line with ASTM standard E837 (Standard, 2013), when applying blind-hole drilling residual stress analysis the relation between hole diameter (D) and maximum hole depth (Z) is specified as  $Z/D = 0.4$ .

Figure V.19 and Figure V.20 show obtained results of principal stresses and each axis stress for flank SAM and flank milling, respectively.

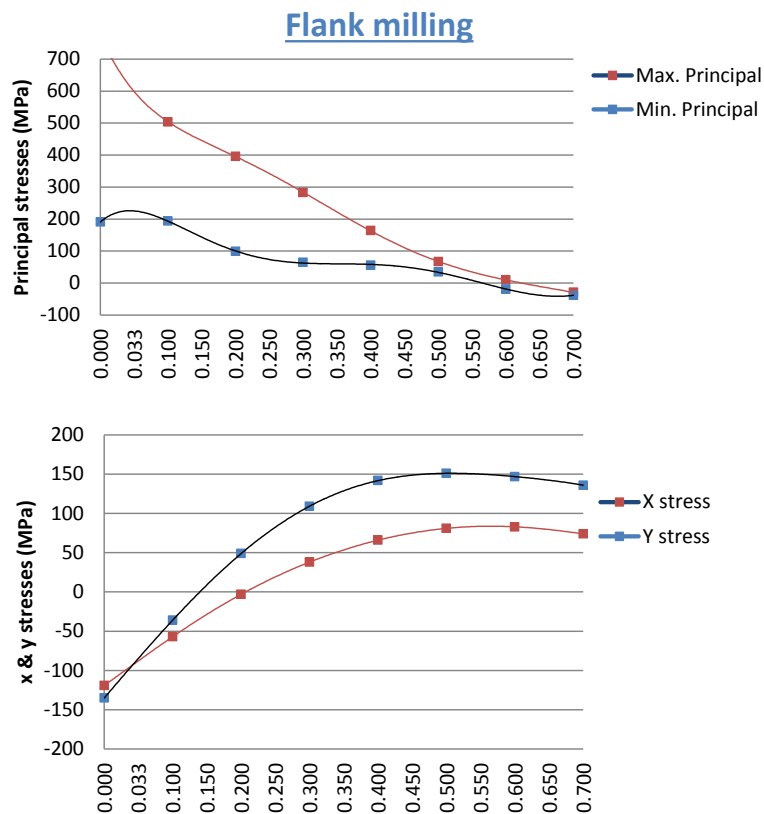


Figure V.19 Residual stresses obtained for flank milling on Inconel<sup>®</sup> 718

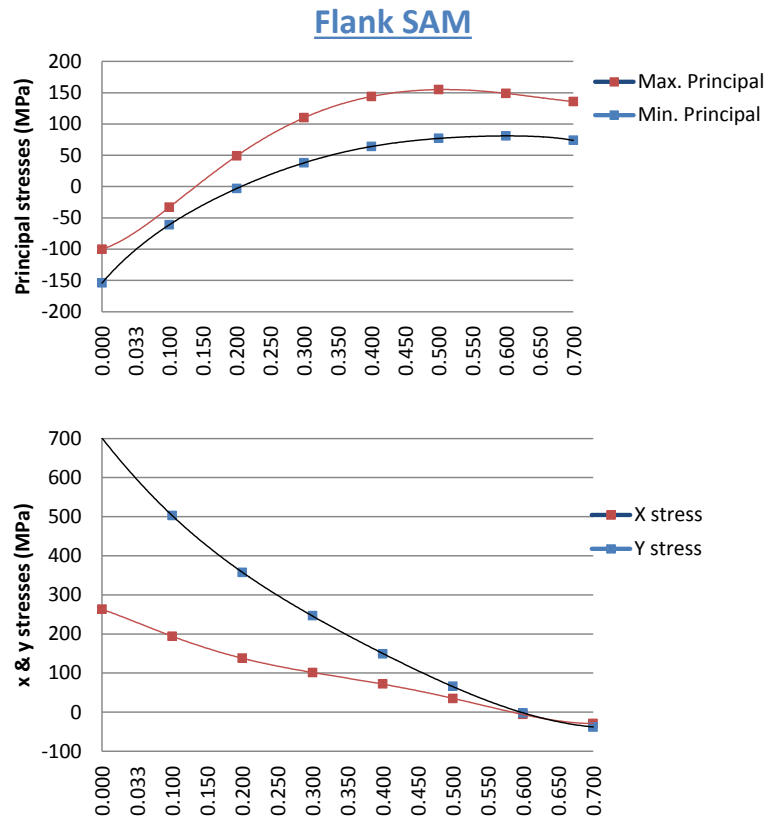


Figure V.20 Residual stresses obtained for flank SAM on Inconel® 718

Analysing obtained residual stresses, for flank milling technique it was appreciated a tensile residual stress near to machined surface common in this process. On the contrary, flank SAM measurements showed a compressive pattern of residual stress near to the manufactured surface. Therefore, the most remarkable aspect is that flank SAM values are compressive values, usual for grinding processes. This is presented as an advantage because it could imply better behaviour to fatigue failure and prevents brittle fracture.

#### V.3.4.4 Microhardness

Related to material properties, microhardness was measured for material base, flank milling, and flank SAM. Following the ASTM standard E384 (E384, 2017) that covers micro-indentation hardness testing, Vickers test was selected. According to the ASTM standard E140 (E140, 2012), these values were converted internally into Rockwell hardness and presented in the plot at the most commonly used units for these materials. Figure V.21 shows the different measuring planes/points definition for obtaining microhardness values, representing the cutting direction, the cross-section to be cut and two main areas: the depth machined surface

(the surface that was manufactured by different processes) and the depth undeformed material (also denominated material base which did not suffer any manufacturing process).

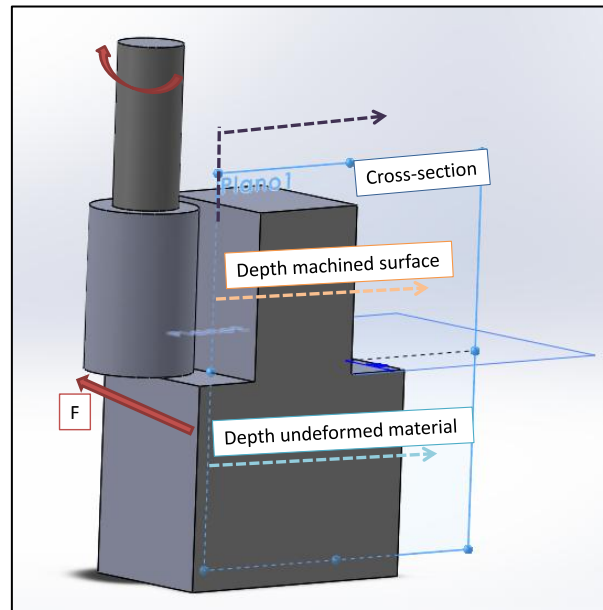


Figure V.21 Measuring sections and slot performance direction definition

Figure V.22 shows the Vickers indenter used and obtained results, determining a measuring length along the first 1 mm of 0.1 mm and over this value of 0.5 mm. This measurement was carried out in order to obtain more information close to the machined surface. The results presented for undeformed material (material base) a microhardness value with an average of 52 HRc (with a minimum of 49 HRc and a maximum of 55 HRc). These values were set as the reference for the study of material property variation in both manufacturing processes.

Regarding the machined areas, main differences were observed at the first 0.8 mm, aligned with the depths where residual stresses were stabilized. In the case of flank milling, microhardness values were situated within 46.5 HRc and 53 HRc. Conversely, for flank SAM an increase was observed in microhardness values up to 58 HRc. These values are considered a direct consequence of the appearance of compressive residual stresses on the machined surface due to the fact that compressive stresses implied a rise in hardness values. This behavior is in concordance with the study carried out by Hua et al. (Hua J., 2005) in which the increase of hardness was related with the maximum hardness value.

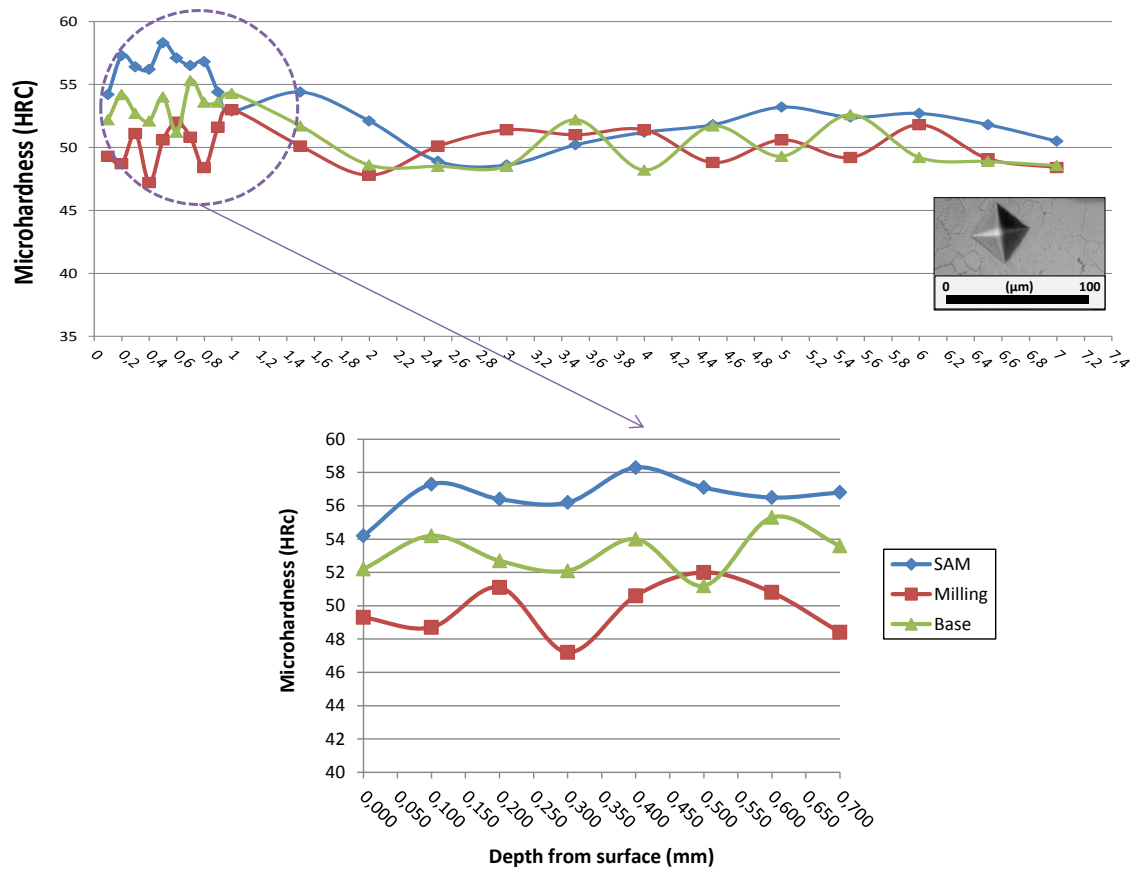


Figure V.22 Microhardness obtained values for material base, flank milling and flank SAM

### V.3.4.6 Tool wear

Tool wear presented in conventional milling tools is irregular and pronounced in some of the cutting edges, what could imply an unpredictable and uncontrolled tool breakage. Abrasive tools present commonly a competitive advantage related to the tool wear, because the grain wear distribution is random but more uniform, what leads to ensure better surface quality of the manufactured components, even though it appears grinding tool heavy wear.

Furthermore, in this case full slotting implies two main issues that could provoke extreme tool wear: no place for chip evacuation and elevated temperatures achieved during the processes. Moreover, the SAM process was performed under the same lubri-cooling techniques as the conventional milling process, using coolant as the cutting fluid. Therefore, it should be pointed out that coolant presents two benefits: lubrication and refrigeration.

Figure V.23 shows, on the top left side, the augmented image of the abrasive tool remarking a dark area where the heat generated a burned area. On the top right side, it is presented the

3D topography of the two main tool wear types found in the abrasive tool: grain detachment and heavy loadings. Finally, at the bottom side it is presented the tool surface profile to evaluate the magnitude of both types of tool wear.

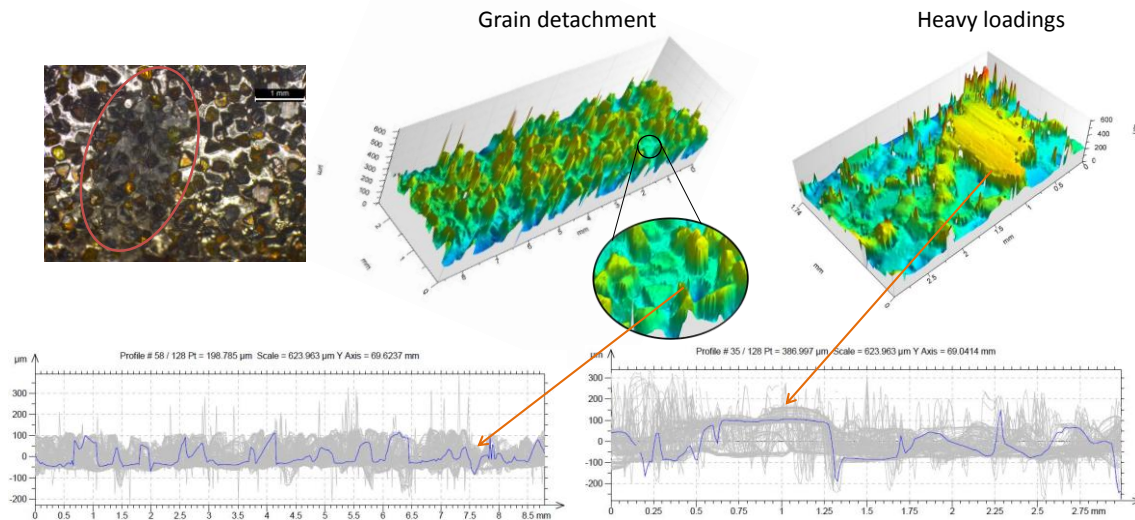


Figure V.23 Abrasive tool wear types presented during the performed tests

Regarding tool wear types, on the one hand, heavy loadings of manufactured material over the grinding tool was considerably presented in the areas closest to the bottom of the slot and the size was 0.6 mm along the tool length and 1.75 mm along cutting direction. Moreover, this area was coincident with the one that presented the superficial burned section; considering this area of the tool where the most critical contact between the tool and the workpiece appeared, with the highest limitation for chip removal and temperature control. On the other hand, it was found some grain detachment, but in this case, this type of wear was no critical for tool life. These issues could be derived from the insufficient lubrication-refrigeration ability of the process under those extreme cutting operations.

#### V.3.4.6 Summary of obtained results and conclusions

In this section, full slots were manufactured in Inconel® 718 with the main objective of comparing flank milling and flank SAM techniques in conventional machining centres. This new concept of using SAM as a roughing technique leads to consider this process as a feasible alternative for traditional milling. Additionally, the possibility of adapting a conventional machine to the use of both processes simultaneously fits with the trend of multitasking machines. Therefore, the main conclusions obtained from performed tests are listed below:

1. **Flank SAM** technique applied to roughing operations presented **elevated material removal rates**, reaching  $240 \text{ mm}^3/\text{s}$ . This means that the process has been optimised in terms of manufacturing time and costs.
2. Regarding the surface roughness, the topography obtained with both techniques presents a regular pattern that is associated to each technology. However, the surface roughness values present high differences between them. Specifically, the use of **SAM** process **implies a reduction of  $\approx 45\%$  and  $\approx 28\%$  in  $R_a$  and  $R_z$** , respectively.
3. Concerning the cross-section, it was observed that conventional milling process generated irregularities on the machined surface. This is directly related to the differences presented on roughness values. The reason why **surface irregularities were avoided with flank SAM is derived from the tool type**. In this case, the use of grinding tools maintained a more constant tool wear. Additionally, it needs to be pointed out that **no white layer was found** in any case.
4. Related to the residual stresses, considering the importance of the appearance of residual stress (both tensile and compressive), it should be highlighted that **compressive residual stresses** and tensile residual stresses arose on the machined surface by **flank SAM** and flank milling respectively. Furthermore, compressive residual stresses in some processes **add value to the material properties**, such as better behaviour to fatigue failure.
5. Finally, the **microhardness** showed **higher values** for the **flank SAM** surface. This improvement of the material property is a direct consequence of compressive residual stresses.

Therefore, from a technical point of view related to surface integrity in terms of surface roughness, residual stresses, microstructure and microhardness, the obtained results in these experiments showed that flank SAM did not present a limitation for being used with conventional machines; as long as cutting conditions were adequately adapted to spindle rotary capacity.





---

## **Chapter VI. Contributions and future research lines**

---



# Chapter VI. Contributions and future research lines

*This chapter presents a summary of the principal thesis contributions and future research lines derived from it.*

## VII.1. Introduction

This work presents an integrated methodology for hybrid manufacturing combining additive and subtractive manufacturing processes to fabricate and repair high-added value components, concretely aeronautical turbomachinery integral rotary components. The main application of this methodology was focused on those types of components; however, it could be generalized to other components that present high geometrical complexity and tough finishing requirements.

The following sections cover the thesis scientific contributions, the main formats and environments to spread the obtained knowledge and future research lines derived from this work.

## VII.2. Thesis contributions

The most relevant results of this work are summarized in the following scientific contributions.

1. **Complete methodology for manufacturing and repair hybrid manufacturing (AM/SM) for high-added value components:** It was established a full methodology over different stages inside hybrid manufacturing (design, AM, SM and measuring & control), integrating all stages in the same CAD/CAM environment. This methodology was developed for high-added value components, more concretely for monolithic turbomachinery components. Inside the proposed methodology, it was implemented in the AM stage a CAM module for the AM with the prediction of the obtained added geometry and the process virtual verification. For the material removal stage, it is considered a new manufacturing process (SAM) and an algorithm development for optimising manufacturing process.

2. **Complete LMD module development for AM tool-paths programming and generated geometry prediction:** It was developed an entire CAM module for LMD strategies programming layer by layer, 3-axis planar and 5-axis strategies following LMD process principles and requirements. Additionally, this CAM module was completed with a geometry estimation model based on a mass-balance analysis. The implementation of this model implies the final generated geometry prediction to be used as the blank for the next step inside the manufacturing chain. This model ask to the user some inputs related to the material, the defined LMD process parameters, and the selection of the defined tool path to predict the final geometry to be generated, so the quantity material needed for that purpose is also calculated.
3. **LMD module integration inside a commercial CAD/CAM software:** The developed LMD module was implemented inside a commercial CAD/CAM software for SM (Siemens NX®) with the main objective of completely integrating every hybrid manufacturing stage in the same environment to facilitate the rapid change from one stage to another one. Moreover, the use of predictive models inside the same environment allows a quick response to error detection and correction (tool-paths, process parameters, and non-cutting movements, among others) before using the real machine.
4. **LMD process analysis for 5-axis strategies through case studies:** it was presented two case studies for Inconel®718 5-axis complex geometries generation (single blade and complete blisk) according to some objectives inside the industrial sector, analysing the geometry final size generation.
5. **Virtual verification of the LMD process:** It was performed the 5-axis tool-paths programming verification inside the CAD/CAM commercial software. In this manner, the machining process was inverted to analyse the additive process using the module initially oriented to subtractive operations. Additionally, the LMD machine entire geometry was implemented for tool-paths virtual verification in order to validate designed strategies; concretely for 5-axis complex operations avoiding and predicting collisions between different machine elements.
6. **Mathematical algorithms for flank milling/flank SAM non-developable surfaces:** Development of an algorithm to approximate a non-developable surface to a ruled surface in order to facilitate the application of the flank milling technique instead of the conventional point milling technique used for those type of surfaces. Moreover, a

complex blade geometry was selected to evaluate the adequacy of this algorithm to complex industrial applications. Thus, the experiment shown as a result the comparison between the flank milling programming using a commercial CAM software and the tool-path generated using the algorithm. Furthermore, the first verification was performed inside the virtual environment comparing final dimension estimations; afterwards, the real component was manufactured using both techniques achieving better surface finishing quality for the one manufactured by the algorithm. This mathematical algorithm opens a new opportunity to optimise machining times and cost, reducing the needed passes for final tolerances requirements.

- 7. Evaluation of SAM adequacy for industrial applications as an alternative or compliments to conventional milling process:** It was performed some full-slotting experiments comparing SAM process and the conventional milling process under the same cutting conditions. Additionally, those tests were performed with the same machining centre, usually presented in most of industrial workshops. Even those machines are not the optimal ones for this SAM process performance, this work presents the opportunity to spread this technology to support the conventional process. SAM offers better finishing results, so it could be presented as an alternative to intermediate semifinishing processes or even to avoid the actual required abrasive post-processes.

## VII.3. Publications

During the period covered by this research activity, which has given rise to this doctoral thesis, the obtained results and knowledge spread across a number of publications in diverse formats and environments.

### VII.3.1. Indexed publications

- **Optimised methodology for aircraft engine IBRs five-axis machining process.** E. Artetxe, H. González, A. Calleja, A. Fernández-Valdivielso, R. Polvorosa, A. Lamikiz, L.N. López de Lacalle. (2016) Int. J. Mechatronics and Manufacturing Systems, Vol. 9, pp. 385 - 401. DOI: <https://doi.org/10.1504/IJMMS.2016.082873>
- **Multitasking machines: evolution, resources, processes and programming.** A. Calleja, H. González, R. Polvorosa, L.N. López de Lacalle. (2017) DYNA, Vol. 92, Issue 6, pp. 637 - 642. DOI: <http://dx.doi.org/10.6036/8237>

- **Super Abrasive Machining of Integral Rotary Components Using Grinding Flank Tools.** H. González, A. Calleja, O. Pereira, N. Ortega, L.N. López de Lacalle, M. Barton. (2018) Metals, MDPI, pp. 8 - 24. DOI: <https://doi.org/10.3390/met8010024>
- **A reliable machining process by means of intensive use of modelling and process monitoring: Approach 2025.** H. González, I. Cascón, J.A. Ealo, F. Santos, T. Ostra, M. Cuesta, A. Madariaga, P. Arrazola, L.N. Lopez-De LaCalle. (2018) DYNA, Vol. 93, Issue 6, pp. 689-696. DOI: <http://dx.doi.org/10.6036/8841>
- **Turbo engine components repair methodology by laser material deposition.** J. Ruiz-Salas, H. González, A. Calleja, E. Ukar, A. Lamikiz. (2018) DYNA, Vol. 93, Issue 6, pp. 643-648. DOI: <http://dx.doi.org/10.6036/8838>
- **Highly-accurate 5-axis flank CNC machining with conical tools.** A. Calleja, P. Bo, H. González, M. Barton, L.N. López de Lacalle. (2018) International Journal of Advanced Manufacturing Technology, Springer, Vol. 97, Issue 5-8, pp 1605-1615. DOI: <https://doi.org/10.1007/s00170-018-2033-7>
- **Comparison of Flank Super Abrasive Machining vs. Flank Milling on Inconel® 718 Surfaces.** H. González, O. Pereira, A. Fernández-Valdivielso, L.N. López de Lacalle, A. Calleja. (2018) Materials, MDPI, Vol. 11, Issue 9 - 1638, pp. DOI: <https://doi.org/10.3390/ma11091638>

### *VII.3.2. National and international congresses*

- **Solución combinada para la fabricación y reparación de turbocomponentes.** E. Artetxe, A. Calleja, H. González, A. Lamikiz, L.N. López de Lacalle. (Noviembre 2016) XXI Congreso Nacional de Ingeniería Mecánica. Elche, España. ISBN: 978-84-16024-37-7.
- **Componentes de turbomaquinaria mediante mecanizado súper abrasivo: enfoque global.** H. González, A. Calleja, H. Bravo, M. Barton, N. Ortega, L.N. López de Lacalle. (Octubre 2017) XXI Congreso de Máquina-Herramienta. Donosti, España.
- **CAM aplicado a la fabricación aditiva de un blade en 5 ejes de Inconel®718.** H. González, A. Calleja, M. Renderos, J.E. Ruiz, A. Lamikiz, L.N. López de Lacalle. (Octubre 2017) XIII Congreso Iberoamericano de Ingeniería Mecánica. Lisboa, Portugal. ISBN: 978-989-95683-4-1.

- **CAM development for Additive Manufacturing in turbo-machinery components.** H. González, I. Arrizubieta, A. Calleja, J.E. Ruiz, A. Lamikiz. (Junio 2017) Manufacturing Engineering Society International Conference 2017 (MESIC). Vigo, España. ISBN: 978-84-697-3077-5
- **Super abrasive machining Technology for manufacturing turbomachinery rotary components.** H. González, A. Calleja, O. Pereira, L.N. López de Lacalle. (December 2017). Electrophysical machining in modern industry congress. Perm, Rusia. ISBN: 978-5-398-01932-2.
- **Global approach to IBR manufacturing process with Super Abrasive Machining.** H. González, A. Calleja, O. Pereira, N. Ortega, M. Barton, L.N. López de Lacalle. (March 2018). High Speed Machining 2018 (HSM 2018). Donosti, España.
- **Digital twin of the LMD process: CAM and Process virtualization.** H. González, A. Calleja, J.E. Ruiz, A. Lamikiz. (September 2018), International Conference on Industrial Internet of Things and Smart Manufacturing. London, United Kingdom.
- **Mecanizado superabrasivo para superaleaciones termorresistentes.** H. González, O. Pereira, A. Calleja, H. Bravo, N. Ortega, A. Fernández-Valdivielso, L.N. López de Lacalle. (Septiembre 2018) XXII Congreso Nacional de Ingeniería Mecánica. Madrid, España. ISSN: 0212-5072.
- **Desarrollo de estrategia y sensorización en proceso de LMD para reparación de geometrías tipo blisk.** J.E. Ruiz, H. González, M. Cortina, J.I. Arrizubieta, A. Lamikiz. (Septiembre 2018) XXII Congreso Nacional de Ingeniería Mecánica. Madrid, España. ISSN: 0212-5072.
- **IBR manufacturing by hybrid combination of laser metal deposition and machining process.** J.E. Ruiz, H. González, M. Cortina, J.I. Arrizubieta, A. Lamikiz. (Octubre 2018) 26th International Conference on Advanced Nanotechnology. Moscow, Rusia. DOI: 10.21767/2471-9838-C5-020.
- **General methodology for manufacturing complex geometries in turbo-machinery components.** H. González, A. Calleja, O. Pereira, E. Artetxe, A. Lamikiz, L.N. López de Lacalle. (Octubre 2018) 26th International Conference on Advanced Nanotechnology. Moscow, Rusia. DOI: 10.21767/2471-9838-C5-020.

- **Digital Twin in manufacturing. An application following the Industry 4.0 philosophy.** G. Gómez, P. Fernández-Lucio, H. González, A. Calleja, O. Pereira, L.N. López de Lacalle. (December 2018). II Electrophysical machining in modern industry congress. Perm, Rusia. ISBN: 978-5-398-02132-5.
- **Blisk blades machining on heat-resistant alloys.** A. Calleja, H. González, R. Polvorosa, O. Pereira, L.N. López de Lacalle. XXVII Processing and Fabrication of Advance Materials. Jönköping, Sweden.
- **Slotting strategies for Super Abrasive Machining (SAM) in Inconel®718.** H. González, O. Pereira, A. Calleja, P. Fernández-Lucio, A. Fernández-Valdivielso, G. Urbikain, L.N. López de Lacalle. Madrid, Spain. ISBN: 978-84-09-10387-4

## VII.4. Future research lines

The presented dissertation opens new lines of interest for future researching works among which should be highlighted the following ones:

- Development and optimization of the CAM module specifically oriented to LMD operations in order to spread the use of 5-axis operations for AM. The use of 5-axis operations for LMD is considered a new line of R&D.
- Spread the hybrid technology to a higher variety of materials, characterizing and analysing those materials commonly used for high-added value complex components.
- Development of an specific software to virtual verification of the complete AM/SM process, supported by AM/SM simulation models (thermal, particles flux, geometric models, among others) in order to visualize the material clads growing process and the characteristics/quality of them and final geometry prediction.
- Applying the defined methodology for AM and SM in a combined and synchronized manner, manufacturing added layers at the same time that the geometry is generated layer by layer. At the present work separated machines were used for AM and SM respectively, but the new trend to hybrid manufacturing systems that combine both technologies inside the same machine, allow the combination of studied processes and proposed methodology.



- Analysing in depth the behaviour of the new SAM process related to the surface integrity for different materials and complex geometries. Moreover, it is needed to study the process as individual and as a compliment inside a hybrid manufacturing process for finishing AM generated components.



---

## Bibliography

(n.d.). Retrieved from [https://www.tedae.org/uploads/attachments/1461082017\\_retos-del-sector](https://www.tedae.org/uploads/attachments/1461082017_retos-del-sector)

3D Systems. (2018). *GibbsCAM, 5-Axis MultiBlade*. Retrieved 06 25, 2018, from [https://www.3dsystems.com/software/gibbscam/5-axis-multiblade?smtNoRedir=1&\\_ga=2.80879893.326713443.1561145052-963208895.1561145052](https://www.3dsystems.com/software/gibbscam/5-axis-multiblade?smtNoRedir=1&_ga=2.80879893.326713443.1561145052-963208895.1561145052)

A. Bhattacharjee, B. S. (2017). Titanium Alloys: Part 2-Alloy Development, Properties and Applications. In *Aerospace Materials and Material Technologies* (Vol. 1: Aerospace Materials). Springer Science+Business Media Singapore.

A. Calleja, I. T. (2014). Improvement of strategies and parameters for multi-axis laser cladding operations. *Optics and Lasers in Engineering* , 56, 113-120.

A. J. Pinkerton, L. L. (2004). Multiple-layer cladding of stainless steel using a high-powered diode laser: an experimental investigation of the process characteristics and material properties. *Thin Solid Films* , 453-454, 471-476.

A. Klink, M. H. (2018). Technological and Economical Assessment of Alternative Process Chains for Turbocharger Impeller Manufacture. *Procedia CIRP* , 77, 586-589.

A. Pleta, F. A. (2018). A comparative study on the cutting force coefficient identification between trochoidal and slot milling. In P. Manufacturing (Ed.), *46th SME North American Manufacturing Research Conference, NAMRC46*, 26, pp. 570-579. Texas, USA.

A. S. Khanna, S. K. (2008). Hard coatings based on thermal spray and laser cladding. *International Journal of Refractory Metals & Hard Materials* .

A.G. Blake, A. M. (1988). Laser coating technology: a commercial reality, Laser Beam Surface Treating and Coating. *G. Sepold* , *SPIE 957*, 56-65.

A.L. Cooke, J. S. (2010). Variability in the Geometric Accuracy of Additively Manufactured, Test Parts. *National Institute of Standards and Technology Gaithersburg, MD* , 1-12.

Abramovici G., D. (2016). Semantic Data Management for the Development and Continuous Reconfiguration of Smart Products and Systems. *CIRP Annals* , 65 (1), 185-188.

Acunity. (2018). Retrieved 12 08, 2018, from <http://acunity.de/en/technologies/laser-metal-deposition/#1156>

Air Force Technology. (n.d.). *Antonov An-70 Transport / Cargo Aircraft*. Retrieved from <https://www.airforce-technology.com/projects/antonovan70freighter/>

Airbus. (2017). *Global Market Forecast 2017-2036*. Retrieved 10 5, 2018, from <http://www.airbus.com/aircraft/market/global-market-forecast.html>

Åkerman, J. (2005). Sustainable air transport - on track in 2050. *Transportation Research Part D: Transport and Environment*, 10 (Issue 2), 111-126.

Allcock, A. (2015)., *WFL Millturn Technologies Open House underlines big developments*. Retrieved 12 06, 2018, from <http://www.machinery.co.uk/machinery-features/wfl-millturn-technologies-kyal-machine-tools-additive-manufacturing>

Arregui L., G. I. (2018). Study of the geometrical limitations associated to the metallic part manufacturing by the LMD process. *Procedia CIRP* 68 , 363-368.

Asociación Española de Empresas Tecnológicas de Defensa, A. y. (n.d.). *Retos del Sector Aeronáutico en España, Guía Estratégica 2015-2025*. Retrieved from [https://www.tedae.org/uploads/files/1461082425\\_retos-del-sector-aeronautico-en-espana-guia-estrategica-2015-2025-pdf.pdf](https://www.tedae.org/uploads/files/1461082425_retos-del-sector-aeronautico-en-espana-guia-estrategica-2015-2025-pdf.pdf)

Barthelmä F., F. H. (2016). Hard coatings to improve the machining of nickel based materials. *Procedia CIRP*, 46, 294-298.

Bellis, M. (n.d.). *Turboshaft engines, Different types of engines*. Retrieved 01 27, 2019, from [http://inventors.about.com/od/jstartinventions/ss/jet\\_engine\\_4.htm](http://inventors.about.com/od/jstartinventions/ss/jet_engine_4.htm)

Bo P., B. M. (2016). Towards efficient 5-axis flank CNC machining of free-form surfaces via fitting envelopes of surfaces of revolution. *Computer-Aided Design*, 79, 1-11.

Bo Pengbo, B. M. (2019). n initialization of milling paths for 5-axis flank CNC machining of free-form surfaces with general milling tools. *Computer Aided Geometric Design*, 71, 30-42.

Boddenberg, K. (1966). On the manufacture of impeller for turbocompressors. *Doctoral Thesis*

Boeing. (2017). *Current Market Outlook 2017-2036*. Retrieved 10 5, 2018, from <http://www.boeing.com/commercial/market/current-market-outlook-2017/>

- Brian J. Schwartz, B. D. (2006). *Patent No. US7101263B2*. United States.
- Brian J. Schwartz, D. F. (2006). *Patent No. US 7144307 B2*. United States.
- Brian J. Schwartz, D. F. (2011). *Patent No. US7896728B2*. United States.
- Brown & Sharpe Manufacturing Company. (1935). *Practical treatise on milling and milling machines*. la Universidad de Wisconsin - Madison.
- C. Kling, C. E. (2011). *How a Turbofan Engine Works*.
- C. Leyens, J. H. (2003). *Continuous Fiber Reinforced Titanium Matrix Composites: Fabrication, Properties and Applications*. WILEY-VCH Verlag GmbH & Co.
- C. Paul, P. G. (2007). Investigating laser rapid manufacturing for Inconel-625 components. *Optics & Laser Technology* , 39, 800-805.
- C. Robinson, M. C. (2012). Impeller-Diffuser Interaction in Centrifugal Compressors. *ASME Turbo Expo 2012: Turbine Technical Conference and Exposition, vol.8: Turbomachinery*.
- Caggiano A., T. R. (2009). CBN grinding performance improvement in aircraft engine components manufacture. *Procedia CIRP* , 9, 109-114.
- Calleja A., T. I. (2014). . Feed rate calculation algorithm for the homogeneous material deposition of blisk blades by 5-axis laser cladding. *Int. J. Adv. Manuf Technol* , 74, 1219-1228.
- Calleja A., U. G. (2018). Inconel 718 superalloy machinability evaluation after laser cladding additive manufacturing process. *The International Journal of Advanced Manufacturing Technology* , 97, 2873-2885.
- Calleja-Ochoa A., G.-B. H.-T.-R.-d.-L. (2017). Multitasking machines: evolution, resources, processes and scheduling. *DYNA* , 92, 637-642.
- Campbell, F. (2006). *Manufacturing technology for aerospace structural materials*. Great Britain: Elsevier Ltd.
- Castelo-Branco I., C.-J. F. (2019). Assessing Industry 4.0 readiness in manufacturing: Evidence for the European Union. *Computers in Industry* , 107, 22-32.
- CGTech Ltd. . (2018). *New VERICUT version on display at Advanced Engineering 2018*. Retrieved 12 07, 2018, from <http://www.cgtech.com/advanced-engineering-2018>

- Change, I. P. (1999). *Aviation and the Global Atmosphere*. Cambridge: A special report of IPCC Working groups I and III. Cambridge University Press.
- Cha-Soo Jun, K. C.-S. (2003). Optimising tool orientations for 5-axis machining by configuration-space search method. *Computer-Aided Design* , 35 (6), 549-566.
- Chen H.P., K. H. (2009). Removing tool marks of blade surfaces by smoothing five-axis point milling cutter paths. *Journal of Materials Processing Technology* , 209-217, 5810-5817.
- Chen Xuezhen, X. Z. (2016). Experimental research on electrochemical machining of titanium alloy Ti60 for a blisk. *Chinese Journal of Aeronautics* , 29 (1), 274-282.
- Chevrolet. (2016, September 22). *What is a turbocharger and how does it work?* Retrieved April 2019, 2019, from Eagle ridge Chevrolet Buick GMC:  
<https://www.eagleridgegm.com/what-is-a-turbocharger-and-how-does-it-work/>
- Choi B.K., K. D. (1997). C-space approach to tool-path generation for die and mould machining. *Computer-Aided Design* , 29 (9), 657-669.
- Chryssolouris G., Z. S. (2002). An experimental investigation of laser cladding. *CIRP Annals-Manufacturing Technology* , 51 (1), 145-148.
- Concepts NREC. (2019). *Specialized CAM Software MAX-PAC*. Retrieved 06 21, 2019, from <https://www.conceptsnrec.com/solutions/software/computer-aided-manufacturing/max-pac>
- Curtis D.T., S. S. (2009). Electrochemical superabrasive machining of a nickel-based aeroengine alloy using mounted grinding points. *CIRP Ann. Manuf. Technol.* , 58, 173-176.
- D. Baur, C. W. (2015, June). *Manufacturing's next act*. Retrieved 04 04, 2019, from McKinsey & Company: <https://www.mckinsey.com/business-functions/operations/our-insights/manufacturings-next-act>
- D. Y. Yang, F. G. (2013). Overview on Five-Axis Precision EDM Techniques. *Procedia CIRP* , 6, 192-198.
- D.E. Van Zante. (2016). *Advances in Turbofan Engines: A US Perspective*. Encyclopedia of Aerospace Engineering (eds R.Blockley and W. Sbyy).
- D.K. Aspinwall, S. S. (2007). Profiled Superabrasive Grinding Wheels for the Machining of a Nickel Based Superalloy. *Annals of the CIRP* , 53, 335-338.

D.K. Aspinwall, S. S. (2008). Workpiece surface roughness and integrity after WEDM of Ti-6Al-4 V and Inconel 718 using minimum damage generator technology. *CIRP Ann. —Manuf. Technol.* , 57 (1), 187-190.

Daniel F. Grady, J. C. (2010). *Patent No. US7789732B2*. United States.

Dawes, J. D. (1999). Computational fluid dynamics for turbomachinery design. *Proc Instn Mech Engrs* , 213 (Part C), 107-124.

Dehghan Ghadikolaei, A. V. (2014). Experimental study on the effect of finishing parameters on surface roughness in magneto-rheological abrasive flow finishing process. *Proc. Inst. Mech. Eng. Part B J. Eng. Manuf* , 229, 1517-1524.

Díez, V. S. (2002). *El motor de reacción y sus sistemas auxiliares*. Madrid: Thomson Editores Spain.

DMG MORI. (2014). *LasrTec 65 Additive Manufacturing – Additive manufacturing for exceptional finished part quality*. DMG MORI USA, IL.

do Carmo, M. (1976). *Differential Geometry of Curves and Surfaces*. Prentice-Hall, Englewood Cliffs, New Jersey.

Doran, S. (1987). The laser where flexibility ultimately means economy. *Production Magazine* .

E. Abele, C. H. (2017). Process design for rough machining of Ti6Al4V integral components. *Procedia Manufacturing* , 14, 118-127.

E. Artetxe, H. G.-V. (2016). Optimised methodology for aircraft engine IBRs five-axis machining process. *Int. J. Mechatronics and Manufacturing Systems* , 9 (4), 385-401.

E. Zorrilla, J. M. (1986). *Dibujo técnico I - Sistemas de representación*. Escuela técnica superior de ingenieros industriales y de ingenieros de telecomunicación.

E140, A. (2012). Standard Hardness Conversion Tables for Metals Relationship Among Brinell Hardness, Vickers Hardness, Rockwell Hardness, Superficial Hardness, Knoop Hardness, and Scleroscope Hardness. *ASTM Standard E140* . West Conshohocken, PA, USA.

E384, A. (2017). Standard Test Method for Microindentation Hardness of Materials. *ASTM International* . West Conshohocken, PA, USA.

Elb-Schliff. (2016). *MillGrind Adds Material Deposition Welding*. Retrieved 12 06, 2018, from <https://www.additivemanufacturing.media/products/-elb-schliff-millgrind-adds-material-deposition-welding>

El-Sayed, A. (2016). *Fundamentals of Aircraft and Rocket Propulsion*. London: Springer-Verlag London.

emuge high performance tools. (2017). *Circle segment cutters (5-axis milling tooling)*. Retrieved March 20, 2019, from <https://www.emuge.com/products/end-mills/circle-segment-cutters>

Erickson, R. (2011). *Patent No. US2011/0189924 A1*. U.S.

ESPRIT. (2019). *SolidMillTurn*. Retrieved 05 24, 2019, from Multi-Tasking Efficiency: <https://www.espritam.com/products/multi-tasking>

Ewald A., S. T. (2018). Evolutionary-based optimization strategy in a hybrid manufactured process using LMD. *Procedia CIRP 74* , 163-167.

F. Chiarello, L. T. (2018). Extracting and mapping industry 4.0 technologies using wikipedia. *Comput. Ind. , 100*, 244-257.

F. Klocke, A. K. (2014). Turbomachinery component manufacture by application of electrochemical, electro-physical and photonic processes. *CIRP Annals - Manufacturing Technology , 63*, 703-726.

F. Klocke, R. S. (2015). Technological and Economical Assessment of Alternative Process Chains for Blisk Manufacture. In P. CIRP (Ed.), *15th Machining Innovations Conference for Aerospace Industry, 35*, pp. 67-72.

F., K., Krämer, K., Sangermann, H., & Lung, D. (2012). Thermo-mechanical tool load during high performance cutting of hard-to-cut materials. *Procedia Fifth Conference on High Performance Cutting , (pp. 295–300)*.

F.Klocke, M. A. (2013). Technological and economical comparison of roughing strategies via milling, sinking-EDM, wire-EDM and ECM for titanium- and nickel-based blisks. *CIRP Journal of Manufacturing Science and Technology , 6 (3)*, 198-203.



- Fan H.Z., W. W. (2013). A novel five-axis rough machining method for efficient manufacturing of centrifugal impeller with free-form blades. *The International Journal of Advanced Manufacturing Technology* , 68 (5/8), 1219-1229.
- Flaño O., A. I. (2018). M. Improvement of EDM performance in high-aspect ratio slot machining using multi-holed electrodes. *Precis. Eng.* , 51, 223-231.
- Flynn J.M., S. A. (2016). Hybrid additive and subtractive machine tools – Research and industrial developments. *International Journal of Machine Tools & Manufacture* , 101, 79-101.
- Forrest, A. (1972). On coons and other methods for the representation of curved surfaces. *Computer Graphics and Image Processing* , 1 (4), 341-359.
- Fraunhofer Institute for Laser Technology ILT. (2019). *Laser Material Deposition*. Retrieved 05 20, 2019, from <https://www.ilt.fraunhofer.de/en/technology-focus/laser-material-processing/laser-metal-deposition.html>
- Fraunhofer IPT. (2015). Live presentations: Integrated process chains. *ICTM - International conference on turbomachinery manufacturing*, (p. 10). AACHEN.
- Fritz Klocke, S. L. (2015). Abrasive machining of advanced aerospace alloys and composites. *CIRP Annals - Manufacturing Technology* , 64, 581-604.
- G. Kappmeyer, C. H. (2012). Modern Machining of Advanced Aerospace Alloys - Enabler for Quality and Performance. *Procedia CIRP* , 1, 28-43.
- G. Lütjering, J. W. (2007). *Titanium, Engineering Materials and Processes*. Berlin: Springer-Verlag Berlin Heidelberg.
- G. Modgil, W. A. (2013). Design Optimization of a High-Pressure Turbine Blade using Generalized Polynomial Chaos. *gPC* , 1, 1-16.
- G. Srinivas, K. R. (2018). Recent developments in turbomachinery component materials and manufacturing challenges for aero engine applications. *IOP Conf. Series: Materials Science and Engineering* , 314.
- G. Urbikain, E. A. (2017). Numerical simulation of milling forces with barrel-shaped tools considering runout and tool inclination angles. *Applied Mathematical Modelling* , 47, 619-636.
- GE International Inc. (2013). *Patent No. EP 2 540 424 A2*.

- Gnanamuthu, D. (1980). Laser surface treatment. *Optical Engineering* , 19 (5), 783-792.
- Gong H., C. L. (2005). Improved positioning of cylindrical cutter for flank milling ruled surfaces. *Computer-Aided Design* , 37 (12), 1205-1213.
- Gong H., W. N. (2009). Optimise tool paths of flank milling with generic cutters based on approximation using the tool envelope surface. *Computer-Aided Design* , 41, 981-989.
- Gonzalez-Barrio, H. C.-M.-B.-B.-Z.-Z.-A.-D. (2018). A RELIABLE MACHINING PROCESS BY MEANS OF INTENSIVE USE OF MODELLING AND PROCESS MONITORING: APPROACH 2025. *Dyna* , 93 (6), 689-696.
- Grieves M., V. J. (2017). Digital Twin: Mitigating Unpredictable, Undesirable Emergent Behavior. *Complex Systems, Transdisciplinary Perspectives on Complex Systems* , 88-113.
- H. Gong, N. W. (2009). Optimise tool paths of flank milling with generic cutters based on approximation using the tool envelope surface. *Computer-Aided Design* , 45 (12), 981-989.
- H.D. Perkins, D. P. (2015). Advanced Engine Designs and Concepts Beyond the Geared Turbofan. *Encyclopedia of Aerospace Engineering* .
- H.P. Qu, P. L. (2010). Microstructure and mechanical property of laser melting deposition (LMD) Ti/TiAl structural gradient materia. *Materials and Design* 31 , 574-582.
- Han Z.L., Y. D. (1999). Iso-phot based tool-path generation for machining free- form surfaces. *Journal of Manufacturing Science and Engineering, ASME Transactions* , 121 (4), 654-664.
- Hedrick, R. W. (2015). Development considerations for an additive manufacturing CAM system. *IFAC-PapersOnLine* , 28 (3), 2327–2332.
- Heo E.Y., K. D. (2008). Efficient rough-cut plan for machining an impeller with a 5-axis NC machine. *International Journal of Computer Integrated Manufacturing* , 21 (8), 971-983.
- Herbert C.R.J., K. J. (2012). An evaluation of the evolution of workpiece surface integrity in hole making operations for a nickel-based super alloy. *J. Mater. Process. Technol.* , 212, 1723-1730.
- Hermann M., P. T. (2016). Design Principles for Industrie 4.0 Scenarios. *49th Hawaii International Conference on System Sciences (HICSS)* , 3928-3937.

- Hermle. (2016). *MPA - A Metal Powder Application Technique*. Retrieved 12 06, 2018, from [https://www.hermle.de/en/services/additive\\_manufacturing/technology\\_mpa/getPrm/entry/additive\\_manufacturing\\_and\\_milling\\_combined/](https://www.hermle.de/en/services/additive_manufacturing/technology_mpa/getPrm/entry/additive_manufacturing_and_milling_combined/)
- Hornsby, C. (2002). CFD – Driving pump design forward. *World Pumps* , 18-22.
- Hua J., S. R. (2005). Effect of feed rate, workpiece hardness and cutting edge on subsurface residual stress in the hard turning of bearing steel using chamfer+hone cutting edge geometry. *Mater. Sci. Eng. , 394*, 238-248.
- hyperMILL. (2019). *Milling of impellers and blisks made easy*. Wessling, Germany: OPEN MIND Technologies AG.
- I. Taberero, A. L. (2011). Evaluation of the mechanical properties of Inconel 718 components built by laser cladding. *International Journal of Machine Tools and Manufacture* , 51 (6), 564-470.
- I. Taberero, A. L. (2011). Evaluation of the mechanical properties of Inconel 718 components built by laser cladding. *International Journal of Machine Tools and Manufacture* , 51 (6), 456-470.
- I. Taberero, A. L. (2012). Geometric Modelling of Added Layers by Coaxial Laser Cladding. *Physics Procedia* (39), 913-920.
- I. Ayesta, B. J. (2016). Optimum electrode path generation for EDM manufacturing of aerospace components. *Robotics and Computer-Integrated Manufacturing* , 37, 273-281.
- Ian Gibson, D. R. (2015). Additive Manufacturing Technologies: 3D Printing, Rapid Prototyping, and Direct Digital Manufacturing. *Johnson Matthey Technol. Rev. , 59* (3), 193-198.
- IBARMIA® INNOVATEK. (2015). *Additive Manufacturing and Multitasking Machining in the Same Machine*. Retrieved 12 06, 2018, from <https://www.ibarmia.com/en/today/ibarmia-additive-manufacturing-multitasking>
- iBeRep AIXpath GmbH. (2018). Retrieved 12 08, 2018, from <http://www.aixpath.de/products/iberep.html>
- Iberia. (2014). Retrieved 10 5, 2018, from [www.iberia.com](http://www.iberia.com)
- International, H. (2018, 07 05). *Haynes International*. Retrieved from <http://www.haynesintl.com/>

- ISO, 4. (1996). Geometrical Product Specifications (GPS), Surface Texture: Profile Method, Rules and Procedures for the Assessment of Surface Texture. Geneva, Switzerland.
- J. Aschenbruck, R. A. (2014). Recent Progress in Turbine Blade and Compressor Blisk Regeneration. *Procedia CIRP* , 22, 256-262.
- J. I. Arrizubieta, J. E. (2017). Intelligent nozzle design for the Laser Metal Deposition process in the Industry 4.0. *Procedia Manufacturing* , 13, 1237-1244.
- J. Karlsson, M. N. (2014). Surface oxidation behavior of Ti-6Al-4V manufactured by Electron Beam Melting (EBM®). *Journal of Manufacturing Processes* , 4-10.
- J. M. de Monicault, J. G. (2008). *Issues and Progresses in Manufacturing of Aero Titanium Parts*. Safran Group, 24th ITA.
- J. Mazumder, J. S. (1986). Laser surface alloying and cladding for corrosion and wear. *NATO ASI Series, Series E: Applied Sciences* , 115, 297-307.
- J. P. Duncan, S. G. (1983). *Sculptured Surfaces in Engineering and Medicine*. Cambridge University press, Cambridge-London-New York.
- J. S. Anagnostopoulos, H. P. (2006). CFD Analysis and Design Effects in a Radial Pump Impeller. 1-7, 763-770.
- J. Senatore, Y. L. (2008). Analytical estimation of error in flank milling of ruled surfaces. *Computer-Aided Design* , 40 (5), 595-603.
- J. Singh, J. M. (1986). In-situ formation of Ni-Cr-Al-R.E. alloy by laser cladding with mixed powder feed. *Springer-Verlag* , 169-179.
- J. Spann, S. H. (2006). The evolution of pump design simulation. *World Pumps* , 32-35.
- J. Zhang, D. Z. (2016). Improvement of trailing edge accuracy in blisk electrochemical machining by optimising the electric field with an extended cathode. *Journal of Materials Processing Technology* , 231, 301-311.
- J.C. Heigel, T. P.-H. (2018). Experimental investigation of residual stress and its impact on machining in hybrid additive/subtractive manufacturing. *46th SME North American Manufacturing Research Conference, NAMRC 46* , 929-940.

- 
- J.D. Mattingly, K. B. (2016). *Elements of Propulsion: Gas Turbines and Rockets*. American Institute of Aeronautics and Astronautics.
- J.L. Koch, J. M. (1993). Rapid prototyping by laser cladding. *Laser material processing , Proceedings of ICALEO'93*, 882-891.
- J.P. Kruth, L. S. (1995). Study of the white layer of a surface machined by die-sinking electro-discharge machining. *CIRP Ann.—Manuf. Technol. , 44 (1)*, 169-172.
- Julien Chaves-Jacob, G. P. (2012). Optimal strategy for finishing impeller blades using 5-axis machining. *International Journal of Advanced Manufacturing Technology , 58*, 573-583.
- K. Eiamsa-ard, H. J. (2005). Part Repair using a Hybrid Manufacturing System. *SFF Symposium , 425-433*.
- K. Morishige, Y. T. (1997). 5-Axis Control Rough Cutting of an Impeller with Efficiency and Accuracy. *Proceedings of International Conference on Robotics and Automation , 2*, 1241-1246.
- K. Tanaka, T. S. (1993). New copper based composite for engine valve seat directly deposited onto aluminium alloy by laser cladding process. *Japan Institute of Metals , 57 (10)*, 114-1122.
- K.-H. Richter, S. O. (2004). Laser cladding of titanium alloy Ti6242 to restore damaged blades. *Proceedings of the 23rd International Congress on Applications of Lasers and Electro-Optics .*
- K.-H. Richter, S. O. (2004). Laser cladding of titanium alloy Ti6242 to restore damaged blades. *Proceedings of the 23rd International Congress on Applications of Lasers and Electro-Optics .*
- K.P. Rajurkara, M. S. (2013). Review of Electrochemical and Electrodischarge Machining. *The Seventeenth CIRP Conference on Electro Physical and Chemical Machining (ISEM), Procedia CIRP , 6*, 13-26.
- Kitagawa, T., Kubo, A., & Maekawa, K. (1997). Temperature and wear of cutting in high-speed machining of Inconel 718 and Ti-6Al-6V-2Sn. *Wear , 202*, 142-148.
- Koreis, & Robert, R. (2015). *Patent No. 20150064299*. United States.
- Kumar, B. R. (2013). A Review on Blisk Technology. *International Journal of Innovative Research in Science, Engineering and Technology , 2-5*.
- Kumar, B. R. (2013). A Review on Blisk Technology. *International Journal of Innovative Research in Science , 2-5*.

- Kyprianidis, K. (2011). Future Aero Engine Designs: An Evolving Vision. In *In Tech*.
- L. Chun, M. S. (2018). Microstructures and properties of 80W-20Fe alloys prepared using laser melting deposition process. *International Journal of Refractory Metals & Hard Materials* 77 , 113-119.
- L. I. Gang, Z. W.-S. (2007). A special CAD / CAM software for electrodischarge machining of shrouded turbine blisk. *Journal of Shanghai University* , 11 (1), 74-78.
- L. Ren, T. S. (2010). Integrated Process Planning for a Multiaxis Hybrid Manufacturing System. *Journal of Manufacturing Science and Engineering* , 132-2 (1006), 1-7.
- L. Ren, T. S. (2010). Integrated Process Planning for a Multiaxis Hybrid Manufacturing System. *Journal of Manufacturing Science and Engineering* , 132-2, 1006:1-7.
- L. Ren, T. S. (2008). Process planning strategies for solid freeform fabrication of metal parts. *Journal of Manufacturing Systems* , 27 (4), 158-165.
- L.N. López de Lacalle, A. L. (2011). *Advanced Cutting Tools, Machining of Hard Materials*. London: Springer-Verlag London.
- Lavernhe S, T. C. (2008). Optimization of 5-axis high-speed machining using a surface based approach. *Computer-Aided Design* , 40, 1015-1023.
- Lawrence E. Murr, S. M. (2012). Metal Fabrication by Additive Manufacturing Using Laser and Electron Beam Melting Technologies. *J. Mater. Sci. Technol.* , 28 (1), 1-14.
- Li C., M. S. (2007). Flank Millable Surfaces Generated via Polynomial Composition. *Computer-Aided Design and Applications* , 4 (1/4), 41-48.
- Lin R.S., K. Y. (1996). Efficient tool-path planning for machining free-form surfaces. *Journal of Engineering for Industry, ASME Transactions* , 118 (1), 20-28.
- Loney G.C., O. T. (1987). NC machining of free form surfaces. *Computer-Aided Design* , 19 (2), 85-90.
- M. Bußmann, E. B. (2009). Blisk Production of the Future Technological and Logistical Aspects of Future-Oriented Construction and Manufacturing Processes of Integrally Bladed Rotors. *19th ISABE International Symposium on Airbreathing*. Montreal.

- 
- M. Bußmann, E. B. (2013). *Market-Oriented Blisk Manufacturing - A Challenge for Production Engineering*. MTU Aero Engines.
- M. Bußmann, J. K. (2005). An Integrated Cost-Effective Approach to Blisk Manufacturing. *Proceedings of 17th Symposium on Air Breathing Engines, ISABE* .
- M. Cortina, J. A. (2018). Latest Developments in Industrial Hybrid Machine Tools that Combine Additive and Subtractive Operations. *Materials* , 11(12) (2583).
- M. Murphy, C. L. (1993). Studies in rapid prototyping by laser surface cladding. *Proceedings of ICALEO'93* , 882-891.
- M. Murphy, W. S. (1994). A novel prototyping technique for the manufacture of metallic components. *Proceedings of ICALEO'94* , 31-40.
- M. Schmidt, R. K. (2010). Direct laser deposition of Cu alloy on forming tool surfaces-Process window and mechanical properties. *CIRP Annals - Manufacturing Technology* , 59, 211-214.
- M.K. Thompson, G. M. (2016). Design for Additive Manufacturing: Trends, opportunities, considerations, and constraints. *CIRP Annals - Manufacturing Technology* , 65, 737-760.
- MachineWorks . (2018). *MachineWorks offers a software development toolkit that is ideally suited for complex simulation, verification and clash detection for any type of CNC machining*. Retrieved 12 07, 2018, from <https://www.machineworks.com/material-removal/>
- Macintyre, R. (1983). Laser hard surfacing of gas turbine blade shroud interlocks. *LIM-1* .
- Mantel, B. M. (2006). *Patent No. US7007382B2*. United States.
- Marc Lorenzo Campomanes, C. E.-M. (2007). *Patent No. US7303461B1*. United States.
- Marco Cherubini, G. F. (2014). *Patent No. EP2705926A1*. Italy.
- Marinescu I.D., R. W. (2004). Tribology of Abrasive Machining Processes. In W. Andrew. Norwich, NY, USA.
- Mateo, A. (2011). Blisk Fabrication by Linear Friction Welding. *Advances in Gas Turbine Technology* .
- Mateo, A. (2014). On the feasibility of Blisk produced by linear friction welding. *Revista de Metalurgia* , 50 (3), e023.

- Mazak. (2015). *Mazak Introduces New HYBRID Multi-Tasking Technology*. Retrieved 12 06, 2018, from <https://www.mazakusa.com/machines/integrex-i-400am/>
- Morishige K., T. Y. (1997). Collision-free tool path generation using 2- dimensional C-space for 5-axis control machining. *International Journal of Advanced Manufacturing Technology* , 13, 393-400.
- Moussaoui, K., Mouseigne, M., Senatore, J., Chieragatti, R., & Lamesle, P. (2015). Influence of milling on the fatigue lifetime of a Ti6Al4V titanium alloy. *Metals* , 5, 1148–1162.
- MTU Power. (2019). *Blisk (blade integrated disks)*. Retrieved from <https://power.mtu.de/engineering-and-manufacturing/aero-solutions/parts-manufacturing/rotating-components/blisks/>
- N. Serres, D. T. (2011). Environmental comparison of MESO-CLAD® process and conventional machining implementing life cycle assessment. *Journal of Cleaner Production* , 19, 1117-1124.
- N. SHOKROLLAHI, E. S. (2014). Experimental comparison of iso scallop, iso planar and iso parametric algorithms in machining sculptured surfaces. *Indian J.Sci.Res* , 1 (2), 475-481.
- Nagae A, M. T. (2012). History and Current Situation of Multi-Tasking Machine Tools. *SME-Japan* , 1-5.
- NASA. (2007). Pushing the Envelope: A NASA Guide to Engines. *National Aeronautics and Space Administration, John H. Glenn Research Center's Educational Programs Office* .
- Noble, D. F. (1984). *Forces of Production: A Social History of Industrial Automation*. New York, USA: Knopf.
- Onur Rauf Bingol, A. K. (2019). NURBS-Python: An open-source object-oriented NURBS modeling framework in Python. *SoftwareX* , 9, 85-94.
- OR Laser News. (2017). *Additive Manufacturing Enables Fast Modification of Molds*. Retrieved 02 25, 2019, from <https://www.or-laser.com/en/news/additive-manufacturing-enables-fast-modification-of-molds/?C=1>
- Ortega N., M. S. (2017). Computed tomography approach to quality control of the Inconel 718 components obtained by additive manufacturing (SLM). *Procedia Manufacturing* , 13, 116-123.
- P.P. Walsh, P. F. (2004). *Gas Turbine Performance*. Malden: Second ed., Blackwell Publishing.



- Pereira, O., Rodríguez, A., Barreiro, J., Fernández-Abia, A. I., & López de Lacalle, L. N. (2017). Nozzle design of combined use of MQL and cryogenic gas in machining. *International Journal of Precision Engineering and Manufacturing-Green Technology*, 4, 87-95.
- Petrilli, R. (2012). *Super abrasive machining for PM*. metal-powder.net. Elsevier Ltd.
- Powermill additive. (2018). Retrieved 12 08, 2018, from <https://knowledge.autodesk.com/support/powermill/learn-explore/caas/CloudHelp/cloudhelp/2019/ENU/PWRM-Additive/files/GUID-9733E2DD-7745-404F-8A13-652763AABE69-htm.html>
- pplc, R.-R. (1986). *the jet engine*. Derby, England: Renault Printing Co Ltd.
- Pranit M. Patil, D. R. (2013). An Overview of Effect of Splitter Blades on Centrifugal Pump Performance. *International Journal of Engineering Research & Technology (IJERT)*, 2 (11), 2249-2252.
- Qi R., L. W. (2009). Five-axis rough machining for impellers. *Frontiers of Mechanical Engineering in China*, 4 (1), 71-76.
- R. Biollo, E. B. (2011). State-of-Art of Transonic Axial Compressors. In *Advances in Gas Turbine Technology*. In Tech.
- R. F. Harik, H. G. (2013). 5-axis flank milling: A state-of-the-art review. *Computer-Aided Design*, 45 (3), 796-808.
- R.Padmanabhan, M. L. (2011). Lightweight metal alloy tailor welded blanks. *Tailor Welded Blanks for Advanced Manufacturing*, 97-117.
- Rao, N. (2011). Materials for Gas Turbines - An Overview. In *Advances in Gas Turbine Technology*. In Tech.
- Reed, R. (2006). *The Superalloys: Fundamentals and Applications*. Cambridge University Press.
- Roberts, K. D. (1994). *Eli Terry and the Connecticut Shelf Clock*. Ken Roberts Publishing.
- Rolls-Royce. (2019, February 29). *Rolls-Royce UltraFan one step closer as Advanced Low Pressure System (ALPS) testing gets underway*. Retrieved from <https://www.rolls-royce.com/products-and-services/civil-aerospace/future-products.aspx#/>

Rosen R., V. W. (2015). About the importance of autonomy and digital twins for the future of manufacturing. *IFAC-PapersOnLine* , 28 (3), 567-572.

S. Cao, D. G. (2017). Relation of microstructure, microhardness and underlying thermodynamics in molten pools of laser melting deposition processed TiC/Inconel 625 composites. *Journal of Alloys and Compounds* 692 , 758-769.

S. Nowotny, S. S. (2001). Integrated Laser Milling Center for Complete Machining. *Laser Materials Processing Conference* .

Sander, P. (2017, April 13). *First 3D printed hydraulic manifold successfully flies on Airbus A380 aircraft*. Retrieved March 19, 2019, from 3D Printing Media Network:  
<https://www.3dprintingmedia.network/first-3d-printed-hydraulic-manifold-successfully-flies-airbus-a380-aircraft/>

Sandvik Coromant. (2019). *Workpiece materials*. Retrieved April 23, 2019, from <https://www.sandvik.coromant.com/es-es/knowledge/materials/pages/workpiece-materials.aspx>

Schafrik R.E., W. D. (2001). Application of alloy 718 in GE aircraft engines: past, present and next five years. *Superalloys 718, 625, 706 and Various Derivatives*, Ed. E.A. Loria, Warrendale, PA , 1-11.

Schleich A., M. W. (2017). Shaping the Digital Twin for Design and Production Engineering. *CIRP Annals — Manufacturing Technology* .

ScottTech. (2017, June 21). *How does a centrifugal pump work?* Retrieved April 18, 2019, from mahan's thermal products: <http://mahans.com/how-does-a-centrifugal-pump-work/>

Senatore J., M. F. (2012). 5-Axis Flank Milling of Sculptured Surfaces. In *Machining of Complex Sculptured Surfaces*. London: Springer London.

Shanshan Yang, A. R. (2018). Opportunities for Industry 4.0 to support Remanufacturing. *Applied Science* , 8, 1177.

Shunyu Liu, Y. C. (2019). Additive manufacturing of Ti6Al4V alloy: A review. *Materials and Design* , 164 (107552), 1-23.

Siemens. (2018). *Digitally transform part production using NX for Manufacturing*. Retrieved March 25, 2018, from <https://www.plm.automation.siemens.com/global/en/products/nx/nx-for-manufacturing.html>

Siemens NX – DMG MORI. (2018). Retrieved 12 08, 2018, from <https://www.plm.automation.siemens.com/global/es/our-story/customers/hoedtke/17607>

Siemens NX. (2018). *Digitally transform part production using NX for Manufacturing*. Retrieved 12 07, 2018, from <https://www.plm.automation.siemens.com/global/en/products/nx/nx-for-manufacturing.html>

Sinha M.K., M. R. (2017). Application of eco-friendly nanofluids during grinding of Inconel 718 through small quantity lubrication. *J. Clean. Prod.* , 141, 1359-1375.

Smith S., M. S.-C. (2007). Effect of surface integrity of hard turned AISI 52100 steel on fatigue performance. *Mater. Sci. Eng.* , 459, 337-346.

Snecma. (2009). *Patent No. EP 2 257 409 B1*.

Spittle, P. (2003). Gas turbine technology. *Physics Education* , 38-6.

Springer, E. (2001). *Constructing a Turbocharger Turbojet Engine, Turbojet technologies*. Published by Turbojet Technologies PM B349 4676 Commercial St. SE Salem, OR 97302-1902 USA.

Standard, 8. (2013). Determining Residual Stresses by the Hole-Drilling Strain-Gage Method. *ASTM International* . West Conshohocken, PA, USA.

Stark K., N. (2017). Innovations in Digital Modelling for Next Generation Manufacturing System Design. *CIRP Annals* , 66 (1), 169-172.

Stark R., F. C. (2019). Development and operation of Digital Twins for technical systems and services. *CIRP Annals* , 1-4.

Steen W.M., C. C. (1979). Surface heat treatment of EnS steel using a 2kW continuous-wave CO2 laser. *Metals Technology* , 6 (1), 456-462.

T. Sakthivel, K. L. (2012). Effect of temperature and strain rate on serrated flow behaviour of Hastelloy®X. *Materials Science and Engineering: A* 534 , 580-587.

- T.D., T. (2014). Algorithms for collision detection and avoidance for five-axis NC machining: a state of the art review. *Computer-Aided Design* , 51, 1-17.
- T.-K. Yeh, H.-P. C. (2013). Corrosion of Nickel and Iron Based Superalloys in High Temperature Gas Environments. *ECS Trans.* , 50 (31), 33-49.
- Torres, A., Arbizu, I., & Pérez, C. (2017). Analytical Modelling of Energy Density and Optimization of the EDM Machining Parameters of Inconel 600. *Metals* , 7(5), 166.
- Toyserkani E., K. A. (2004). *Laser Cladding*. CRC Press.
- Toyserkani E., K. A. (2005). *Laser Cladding Toyserkani*. CRC Press LLC.
- Tung C., T. P. (2011). Tool Path Generation and Manufacturing Process for Blades of a Compressor Rotor. *World Academy of Science, Engineering and Technology* , 5, 154-159.
- upmet. (2018). *alloy-x*. Retrieved from <https://www.upmet.com/products/nickel-alloys/alloy-x>
- V. Roblek, M. M. (2016). A complex view of Industry 4.0. *SAGE Open* , 6 (2), 1-11.
- Vidal G., O. N. (2018). An Analysis of Electroplated cBN Grinding Wheel Wear and Conditioning during Creep Feed Grinding of Aeronautical Alloys. *Metals* , 8, 350.
- W.R. Morrow, H. Q. (2007). Environmental aspects of laser-based and conventional tool and die manufacturing. *Journal of Cleaner Production* , 15, 932-943.
- Włodzimierz Wilk, M. J. (2008). Modern technology of the turbine blades removal machining. *The 8 International Conference Advanced Manufacturing Operations*, (pp. 347-355). Kranevo, Bulgaria.
- Woodbury, R. S. (1972). *History of the Milling Machine*. Cambridge, Massachusetts, USA: MIT Press.
- W-T. Preciado, C. E. (2006). Repair welding of polymer injection molds manufactured in AISI P20 and VP50IM steels. *Journal of Materials Processing Technology* , 179, 244-250.
- Wu C.Y. (1995). Arbitrary Surface Flank Milling of Fan, Compressor, and Impeller Blades. *Turbo Expo: Power for Land, Sea, and Air* , Volume 5: Manufacturing Materials and Metallurgy; Ceramics; Structures and Dynamics; Controls, Diagnostics and Instrumentation; Education.

- Wu, C. Y. (2012). Arbitrary surface flank milling & flank SAM in the design and manufacturing of jet engine fan and compressor airfoils. *Proceedings of ASME Turbo Expo 2012*, (pp. 1-10). Copenhagen, Denmark.
- X. Cao, M. J. (2008). Optimization of bead spacing during laser cladding of ZE41A-T5 magnesium alloy castings. *Journal of Materials Processing Technology* , 205, 322-331.
- Xiaoming Kang, W. L. (2018). Maximum free distance method for electrode feeding path planning in EDM machining of integral shrouded blisks. *Precision Engineering* , 51, 514-520.
- Y. Cui, Z. L. (2019). Self-starting analysis of an OWC axial impulse turbine in constant flows:experimental and numerical studies. *Appl. Ocean Res.* , 82, 458-469.
- Y. Tian, D. T. (2017). Influences of processing parameters on surface roughness of Hastelloy®X produced by selective laser melting. *Additive Manufacturing* 13 , 103-112.
- Y. Tian, e. a. (2016). *Additive Manufacturing*.
- Y.P. Hu, C. C. (1998). Development of a new laser cladding process for manufacturing cutting an stamping dies. *Journal of Materials Science* , 33, 1287-1292.
- Yang S., R. A. (2018). Opportunities for Industry 4.0 to support Remanufacturing. *Applied Science* , 8, 1177.
- YingCui, Z. X. (2019). Review of CFD studies on axial-flow self-rectifying turbines for OWC wave energy conversion. *Ocean Engineering* , 175, 80-102.
- Yuan-Shin Lee, Y. M. (2000). Rolling-ball method and contour marching approach to identifying critical regions for complex surface machining. *Computers in Industry* , 41 (2), 163-180.
- Yuji Miki, J. K. (2011). *Patent No. US8014893B2*.
- Zelinski, P. (2015, April 24). *Highlighting Hybrid Manufacturing*. Retrieved April 20, 2019, from Additive Manufacturing: <https://www.additivemanufacturing.media/articles/highlighting-hybrid-manufacturing>